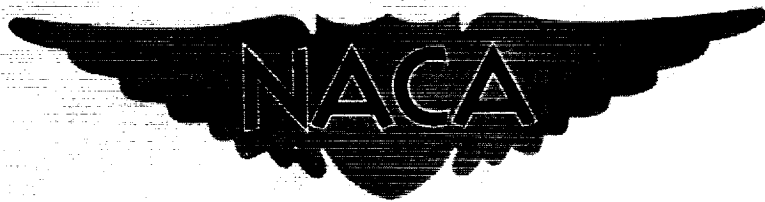


NACA RM 157D19

CASE FILE COPY

Copy
RM L57D19



RESEARCH MEMORANDUM

AERODYNAMIC CHARACTERISTICS OF MISSILE CONFIGURATIONS WITH
WINGS OF LOW ASPECT RATIO FOR VARIOUS COMBINATIONS OF
FOREBODIES, AFTERBODIES, AND NOSE SHAPES FOR
COMBINED ANGLES OF ATTACK AND SIDESLIP
AT A MACH NUMBER OF 2.01

By Ross B. Robinson

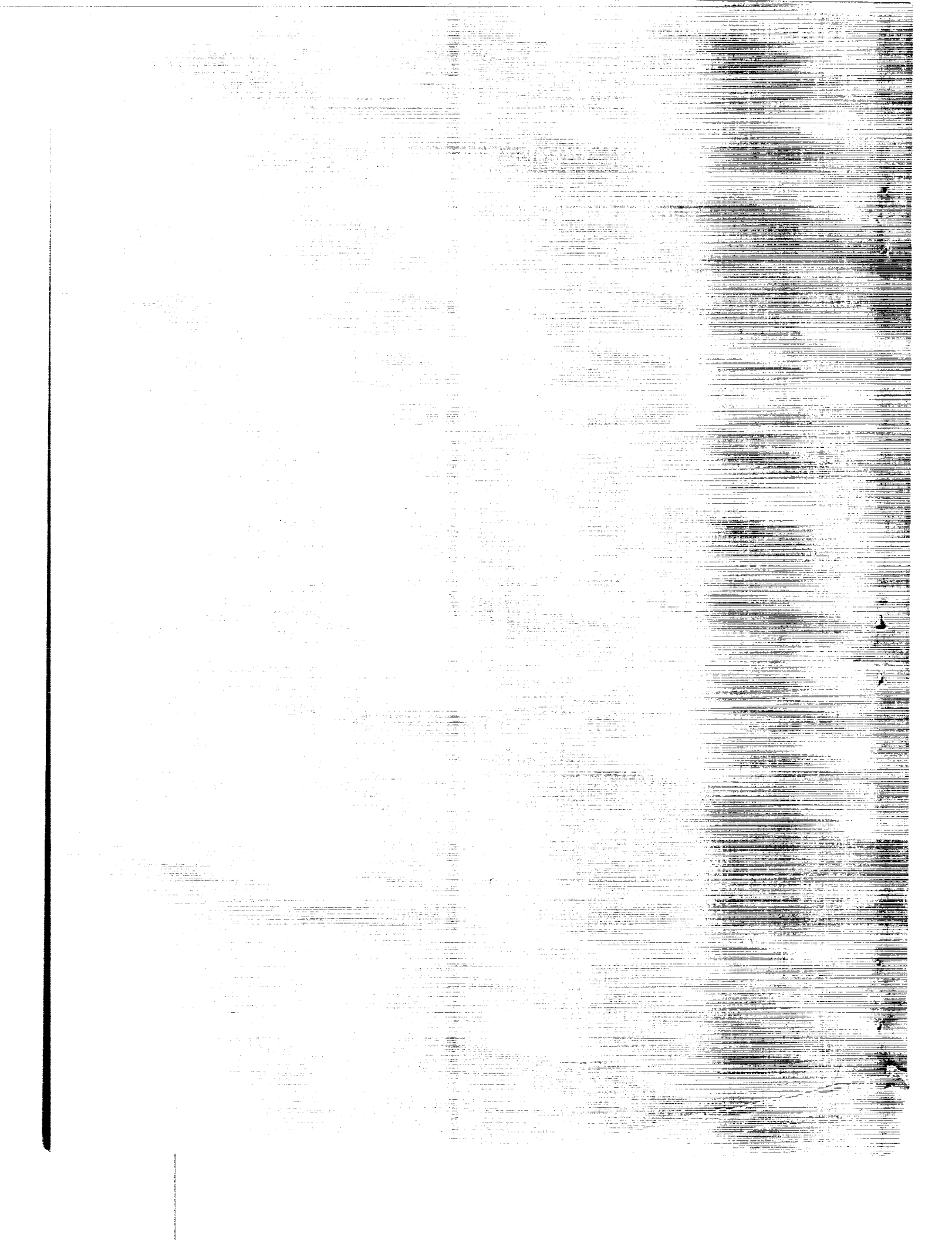
Langley Aeronautical Laboratory
Langley Field, Va.

NATIONAL ADVISORY COMMITTEE
FOR AERONAUTICS

WASHINGTON

June 25, 1957

Declassified January 12, 1961



NATIONAL ADVISORY COMMITTEE FOR AERONAUTICS

RESEARCH MEMORANDUM

AERODYNAMIC CHARACTERISTICS OF MISSILE CONFIGURATIONS WITH
WINGS OF LOW ASPECT RATIO FOR VARIOUS COMBINATIONS OF
FOREBODIES, AFTERBODIES, AND NOSE SHAPES FOR
COMBINED ANGLES OF ATTACK AND SIDESLIP
AT A MACH NUMBER OF 2.01

By Ross B. Robinson

SUMMARY

An investigation has been made in the Langley 4- by 4-foot supersonic pressure tunnel to determine the aerodynamic characteristics of a series of missile configurations having low-aspect-ratio wings at a Mach number of 2.01. The effects of wing plan form and size, length-diameter ratio, forebody and afterbody length, boattailed and flared afterbodies, and various nose shapes were determined. Six-component force and moment data are presented for combined angles of attack and sideslip to about 28° . No analysis of the data has been made in this report.

INTRODUCTION

A problem of increasing importance in missile design is the efficient utilization of internal stowage space in aircraft. The use of low-aspect-ratio lifting surfaces with small span-diameter ratios would result in more compact missiles occupying materially less volume than the same number of configurations with large-span lifting surfaces.

Another problem of missile design is the maneuverability required by the limited scanning angles of the missile seeking equipment. The missile should be capable of large attitude changes with minimum control deflections. A configuration with nonlinear lift and pitching-moment variations such that the values of static margin and lift-curve slope are low near zero angle of attack would satisfy this requirement.

Flow pressure measurements were performed on a configuration of the Boeing 727 aircraft at the NASA Langley Research Center in May 1970. The aircraft was in a clean configuration with no wing anti-torque fairings, no vertical stabilizer, and no horizontal stabilizer. The aircraft had a standard Boeing 727-100 airfoil, and a standard Boeing 727-100 tail section.

The aircraft had a standard Boeing 727-100 airfoil, and a standard Boeing 727-100 tail section. The aircraft had a standard Boeing 727-100 airfoil, and a standard Boeing 727-100 tail section. The aircraft had a standard Boeing 727-100 airfoil, and a standard Boeing 727-100 tail section.

The data are presented as distributions of moments at the leading edge of the wing. All the data are referred to the body centerline of the aircraft.

| | |
|-------|--|
| C_N | normal-force coefficient, $\frac{N}{qS}$ |
| C_A | axial-force coefficient, $\frac{A}{qS}$ |
| C_M | pitching-moment coefficient, $\frac{M_Y}{qSd}$ |
| C_P | rolling-moment coefficient, $\frac{M_Z}{qSd}$ |
| C_R | yawing-moment coefficient, $\frac{M_X}{qSd}$ |
| C_Q | side-force coefficient, $\frac{Q}{qS}$ |
| N | normal force |
| A | axial force |

— 1 —

Journal of Health Politics, Policy and Law, Vol. 36, No. 1, January 2011
DOI 10.1215/03616878-36-1 © 2011 by The University of Chicago

Recent acoustic recordings of noise

Figure 1. Mean daily energy intake (kJ) and energy density (kJ/g) of the diet consumed by each subject.

lengths of cylindrical

ch tripod tip

on tripod

cylinder with hemispherical nose

Additional reading

Afterbodies (fig. 2(d)):

| | |
|-----------------|-------------------------|
| A_0 | no afterbody |
| A_1, A_2 | cylindrical afterbodies |
| A_3, A_4, A_5 | boattailed afterbodies |
| A_6, A_7, A_8 | flared afterbodies |

Wings (fig. 2(f)):

| | |
|-----------------|-------------------|
| W_0 | wing off |
| W_1, W_2, W_3 | delta wings |
| W_4, W_5, W_6 | rectangular wings |

MODEL AND APPARATUS

Sketches of a typical complete model and of the model components are shown in figure 2. The geometric characteristics of the various components and combinations of forebodies, wings, and afterbodies are given in table I. Values of x/l and l/d for all the bodies are also given in table I. The models used in this investigation are shown in figure 3.

The various configurations were obtained by attaching combinations of forebodies, afterbodies, and wings to a cylindrical section W_0 having a diameter of 3.00 inches (this diameter is hereinafter referred to as 1 caliber in calculating body lengths) housing the internal strain-gage balance (fig. 2(f)).

The basic forebodies investigated were a series of 3.5-caliber ogive-cylinders with varying lengths of cylindrical section (fig. 2(b)). In addition, a 3.5-caliber ogive with a rounded nose (F_5 , fig. 2(c)) to which a slotted cage (F_6 , fig. 2(c)) or a 3-inch spike could be attached (F_4 , fig. 2(c)), and a flat-face cylinder with a tripod, with and without a wire mesh around the tripod (F_2 and F_3 , fig. 2(c)) were tested. The 3-inch spike was selected as a result of tests at a Mach number of 1.61 of a similar configuration (refs. 4 and 5) which indicated this spike length to be optimum for minimum drag at small angles of attack.

The afterbodies, shown in figure 2(d), consisted of the following configurations: A_0 , no afterbody; A_1 , a 1-caliber cylinder; A_2 , a 2-caliber cylinder; A_3 , a 1-caliber 6.50° boattail; A_4 , a 1-caliber 6.50° boattail attached to a 1-caliber cylinder; A_5 , a 2-caliber 3.25° boattail; A_6 , a 1-caliber 6.50° flare; A_7 , a 1-caliber 6.50° flare attached to a 1-caliber cylinder; and A_8 , a 2-caliber 3.25° flare.

Cruciform wings were mounted in slots in the balance housing. Three rectangular-wing and three delta-wing configurations were tested (fig. 2(f) and table 1). The wings were so designed that the exposed areas of the medium and large wings of each series were two and four times, respectively, those of the small wings. Areas of corresponding wings in each series were equal; for example, the exposed area of the large rectangular wing was equal to that of the large delta wing.

Two spoilers, one for each horizontal wing panel, were provided for the large delta wing (fig. 2(g)). Deflections of 45° and 90° were obtained by facing either the oblique or the perpendicular face of the spoiler forward. The length of each spoiler was 3.094 inches and the width of each spoiler was 0.625 inch. The height of each spoiler was 0.625 inch.

The models were mounted on a rotary sting to permit testing through ranges of combined angles of attack and sideslip. Six-component force and moment data were measured by an internal strain-gage balance. Base pressures were measured with a single tube well inside the model. A cylindrical wooden block approximately the same size as the base of the model and 1 inch long was attached to the sting about $1/8$ inch behind the model base.

TESTS, CORRECTIONS AND ACCURACY

Test Conditions

The tests were made at a Mach number of 2.01, a stagnation temperature of 100° F, and a stagnation pressure of 1,440 pounds per square foot absolute. The Reynolds number, based on the maximum diameter, was 0.62×10^6 (2.47×10^6 based on a length of 1 foot). Stagnation dewpoints of -25° or below were maintained to eliminate condensation effects. The angle-of-attack range for pitch tests was from -4° to about 28° at zero sideslip, and the angle-of-sideslip range was from -4° to a maximum of about 28° at angles of attack of about 0° , 4.1° , 8.2° , 12.3° , 16.4° , 20.5° , and 24.7° .

Precision and Accuracy

The angles of attack and sideslip were determined by the balance and sting after tests. The mean error in angle of attack was about $\pm 0.01^\circ$ and the standard variation in angle of attack for all the configurations did not exceed $\pm 0.02^\circ$. No corrections have been applied to the data to account for these variations.

The axial-force data were influenced by a large difference between static pressure at the unbalanced base and the free-stream static pressure. Since the unbalanced base was located at an angle of attack of about 30° , the free-stream static pressure is about 1.5 times the free-stream total pressure. Consequently, the free-stream total pressure is approximately constant pressure across the base of the model. Unfortunately, measurements for several of the configurations were discontinued because of instrument failure. The axial-force coefficients for the remaining configurations were computed by using half-pressure measurements taken at the configuration trailing edge location. The mean errors in angle of attack were about $\pm 0.02^\circ$.

The probable errors in the force and moment data for small angles of attack and sideslip are considerably larger for the body-wing configuration without wings than for the body-wing configuration. The unbalanced strake-base balance was not able to measure very small load coefficients with sufficient accuracy. Small increments of forces and moments could not be accurately measured in certain load ranges. Very probably, the largest instrument errors were about the same for all configurations. Comparison of tests made with and without the wooden biplane tail section in combination with large delta wings, no afterbody, and 30° angle of attack showed negligible effect of the tail on the force and moment.

Estimated probable errors in the force and moment data for small angles of attack and sideslip, zero shift, calibrated, and zero instrument errors are as follows:

| | | | | | | |
|-------|-------------|-------------|-------------|-------------|-------------|-------------|
| C_N | ± 0.005 |
| C_A | ± 0.005 |
| C_m | ± 0.005 |
| C_l | ± 0.005 |
| C_n | ± 0.005 |
| C_Y | ± 0.005 |

The angles of attack at zero sideslip and sideslip angles and zero angle of attack are estimated to be correct within $\pm 0.02^\circ$. The balance angles of attack and sideslip for angles are correct within $\pm 0.02^\circ$.

AERODYNAMIC DATA

The aerodynamic characteristics presented in figures 4 to 21 are the effects of delta wings with various nose shapes on the aerodynamic characteristics in pitch and in sideslip at various angles of attack with various cylindrical afterbodies. The results of these tests are found in figures 4 to 21. Figures 22 to 30 present the effects of forebody length on the aerodynamic characteristics in pitch and in sideslip for forebodies with various cylindrical afterbodies. The results of forebodies with various cylindrical afterbodies and with large delta wing at various angles of attack ($t/d = 10$) are presented in figures 22 to 25. The results of various boattailed and flared afterbodies with various nose shapes on the aerodynamic characteristics in pitch and in sideslip at various angles of attack are presented in figures 31 to 39. The results of the effect of the various special nose shapes on the aerodynamic characteristics in pitch and in sideslip at various angles of attack and with large delta wing are presented in figures 40 to 45 (all configurations have $t/d = 10$). The effects of spoiler deflection on a forebody with a small-diameter cylindrical afterbody and large delta wings are presented in figures 46 to 49. The aerodynamic characteristics in pitch and in sideslip at various angles of attack are presented in figure 46 ($t/d = 10$).

The axial-force coefficients for the following configurations were measured at Langley, pressures from similar configurations as described in the following table, were used.

| Configuration | Figure |
|--------------------------------------|--------|
| $F_{xW} A_0, F_{yW} A_0, F_{zW} A_0$ | 22 |
| $F_{xW} A_1, F_{yW} A_1$ | 23 |
| $F_{xW} A_2, F_{yW} A_2$ | 24 |
| $F_{xW} A_0$ | 40 |

No axial-force coefficients have been presented for configurations $F_{xW} A_3$ and $F_{xW} A_5$. The measured base pressures were not accurate and no base pressures for similar configurations were available.

CONCLUDING REMARKS

An investigation was made in the Langley 4- by 4-foot supersonic pressure tunnel to determine the aerodynamic characteristics on a configuration with various combinations of forebodies, afterbodies, nose shapes, and wings with low aspect ratio. Six-component force and moment

data were obtained for combined angles of attack and sideslip to about 28° . No analysis of the data has been made in this report.

Langley Aeronautical Laboratory,
National Advisory Committee for Aeronautics,
Langley Field, Va., April 3, 1957.

REFERENCES

1. Spearman, M. Leroy, and Robinson, Ross B.: Aerodynamic Characteristics of a Cruciform-Wing Missile With Canard Control Surfaces and of Some Very Small Span Wing-Body Missiles at a Mach Number of 1.41. NACA RM L54B11, 1954.
2. Katzen, Elliott D., and Jorgensen, Leland H.: Aerodynamics of Missiles Employing Wings of Very Low Aspect Ratio. NACA RM A55L13b, 1956.
3. Jorgensen, Leland H., and Katzen, Elliott D.: Wing-Body Combinations With Wings of Very Low Aspect Ratio at Supersonic Speeds. NACA RM A56G16, 1956.
4. Robins, A. Warner: Preliminary Investigation of the Effects of Several Seeker-Nose Configurations on the Longitudinal Characteristics of a Canard-Type Missile at a Mach Number of 1.60. NACA RM L53I18, 1953.
5. Gapcynski, John P., and Robins, A. Warner: The Effect of Nose Radius and Shape on the Aerodynamic Characteristics of a Fuselage and a Wing-Fuselage Combination at Angles of Attack. NACA RM L53I23a, 1953.

TABLE I.- GEOMETRIC CHARACTERISTICS OF MODELS

(a) Characteristics of model components

| | w_1 | w_2 | w_3 | w_4 | w_5 | w_6 |
|---|-----------|-----------|-----------|-----------|-----------|-----------|
| Wings: | | | | | | |
| Area, exposed, sq ft | 0.3611 | 0.1805 | 0.0903 | 0.3611 | 0.1805 | 0.0903 |
| Span, exposed, in. | 8.00 | 4.00 | 2.00 | 4.00 | 2.00 | 1.00 |
| Aspect ratio, exposed panel | 1.23 | 0.615 | 0.308 | 0.308 | 0.154 | 0.077 |
| Taper ratio | 0 | 0 | 0 | 1 | 1 | 1 |
| Root chord, exposed, in. | 13.00 | 13.00 | 13.00 | 13.00 | 13.00 | 13.00 |
| Root chord, center line, in. | 17.875 | 22.75 | 32.50 | 32.50 | 15.00 | 15.00 |
| Leading-edge sweep, deg | 81.5 | 72.9 | 85.6 | 85.6 | 0 | 0 |
| Ratio of total span to maximum body diameter | 3.667 | 2.333 | 1.667 | 2.333 | 1.667 | 1.333 |
| Ratio of exposed wing area to maximum body cross-sectional area | 7.35 | 3.68 | 1.84 | 7.35 | 3.68 | 1.84 |
| Balance section, w_0 : | | | | | | |
| Length, in. | • • • • • | • • • • • | • • • • • | • • • • • | • • • • • | • • • • • |
| Maximum diameter, in. | • • • • • | • • • • • | • • • • • | • • • • • | • • • • • | • • • • • |
| Length-diameter ratio, l/d | • • • • • | • • • • • | • • • • • | • • • • • | • • • • • | • • • • • |
| Maximum cross-sectional area, sq ft. | • • • • • | • • • • • | • • • • • | • • • • • | • • • • • | • • • • • |
| Forebodies: | | | | | | |
| Length, in. | • • • • • | • • • • • | • • • • • | • • • • • | • • • • • | • • • • • |
| Maximum diameter, in. | • • • • • | • • • • • | • • • • • | • • • • • | • • • • • | • • • • • |
| Length-diameter ratio, l/d | • • • • • | • • • • • | • • • • • | • • • • • | • • • • • | • • • • • |
| Maximum cross-sectional area, sq ft. | • • • • • | • • • • • | • • • • • | • • • • • | • • • • • | • • • • • |
| Special noses: | | | | | | |
| Length, in. | • • • • • | • • • • • | • • • • • | • • • • • | • • • • • | • • • • • |
| Maximum diameter, in. | • • • • • | • • • • • | • • • • • | • • • • • | • • • • • | • • • • • |
| Maximum cross-sectional area, sq ft. | • • • • • | • • • • • | • • • • • | • • • • • | • • • • • | • • • • • |
| Afterbodies: | | | | | | |
| Length, in. | A_1 | A_2 | A_3 | A_4 | A_5 | A_6 |
| Forward diameter, in. | 3.00 | 6.00 | 3.00 | 6.00 | 3.00 | 3.00 |
| Ratio of length to forward diameter | 3.00 | 3.00 | 3.00 | 3.00 | 3.00 | 3.00 |
| Half-angle of boattail or flare, deg. | 1.00 | 2.00 | 1.00 | 2.00 | 1.00 | 2.00 |
| Rear diameter, in. | 0 | 0 | 6.50 | 3.25 | 6.50 | 3.25 |
| | 3.00 | 3.00 | 2.52 | 2.52 | 3.68 | 3.68 |

TABLE I.- GEOMETRIC CHARACTERISTICS OF MODELS - Concluded.

(b) Body-component combinations

| Component combinations | Length, in. | Length-diameter ratio | Center-of-gravity location from base, calibers | Center-of-gravity location from nose, x/l | Alternate afterbodies used |
|--|-------------|-----------------------|--|---|---|
| F ₁ W ₀ A ₀ | 24.00 | 8 | 4.33 | 0.459 | None |
| F ₇ W ₀ A ₀ | 27.00 | 9 | 4.33 | .519 | None |
| F ₁ W ₀ A ₁ | 27.00 | 9 | 5.33 | .408 | None |
| F ₈ W ₀ A ₀ | 30.00 | 10 | 4.33 | .567 | None |
| F ₇ W ₀ A ₁ | 30.00 | 10 | 5.33 | .467 | A ₃ or A ₆ |
| F ₁ W ₀ A ₂ | 30.00 | 10 | 6.33 | .367 | A ₄ , A ₅ , A ₇ , A ₈ |
| F ₉ W ₀ A ₀ | 33.00 | 11 | 4.33 | .606 | None |
| F ₈ W ₀ A ₁ | 33.00 | 11 | 5.33 | .515 | None |
| F ₇ W ₀ A ₂ | 33.00 | 11 | 6.33 | .424 | None |
| F ₉ W ₀ A ₁ | 36.00 | 12 | 5.33 | .556 | None |
| F ₈ W ₀ A ₁ | 36.00 | 12 | 6.33 | .473 | None |
| F ₉ W ₀ A ₂ | 39.00 | 13 | 6.33 | .513 | None |
| F ₅ W ₀ A ₀ | 23.36 | 7.78 | 4.33 | .443 | None |
| F ₆ W ₀ A ₀ | 26.36 | 8.78 | 4.33 | .507 | None |
| F ₄ W ₀ A ₀ | 26.36 | 8.78 | 4.33 | .507 | None |
| F ₃ W ₀ A ₀ | 22.12 | 7.37 | 4.33 | .412 | None |
| F ₂ W ₀ A ₀ | 22.12 | 7.37 | 4.33 | .412 | None |

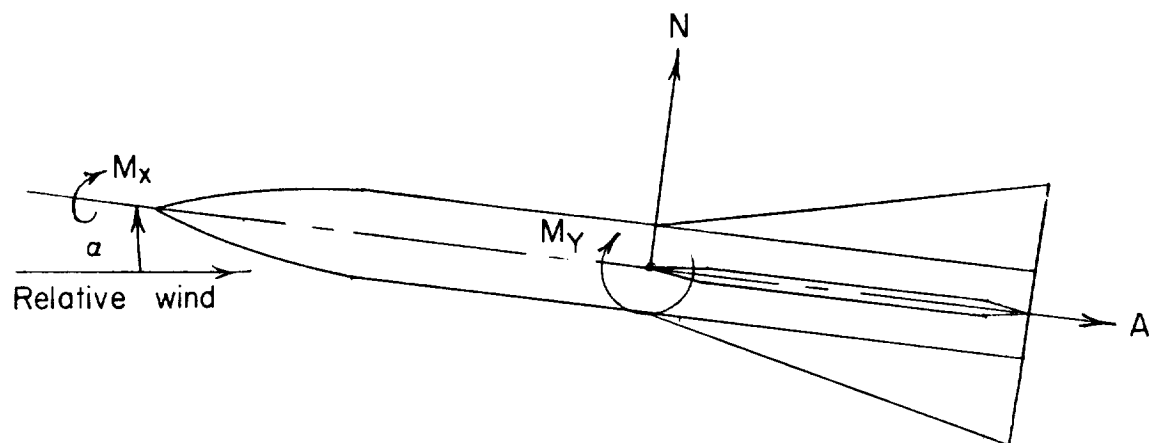
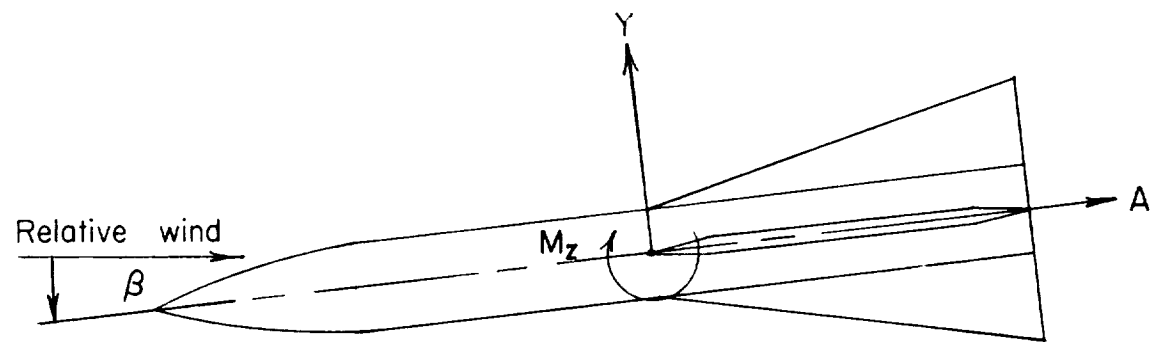


Figure 1.- Axis systems. Arrows indicate positive directions of forces, moments, and angles.

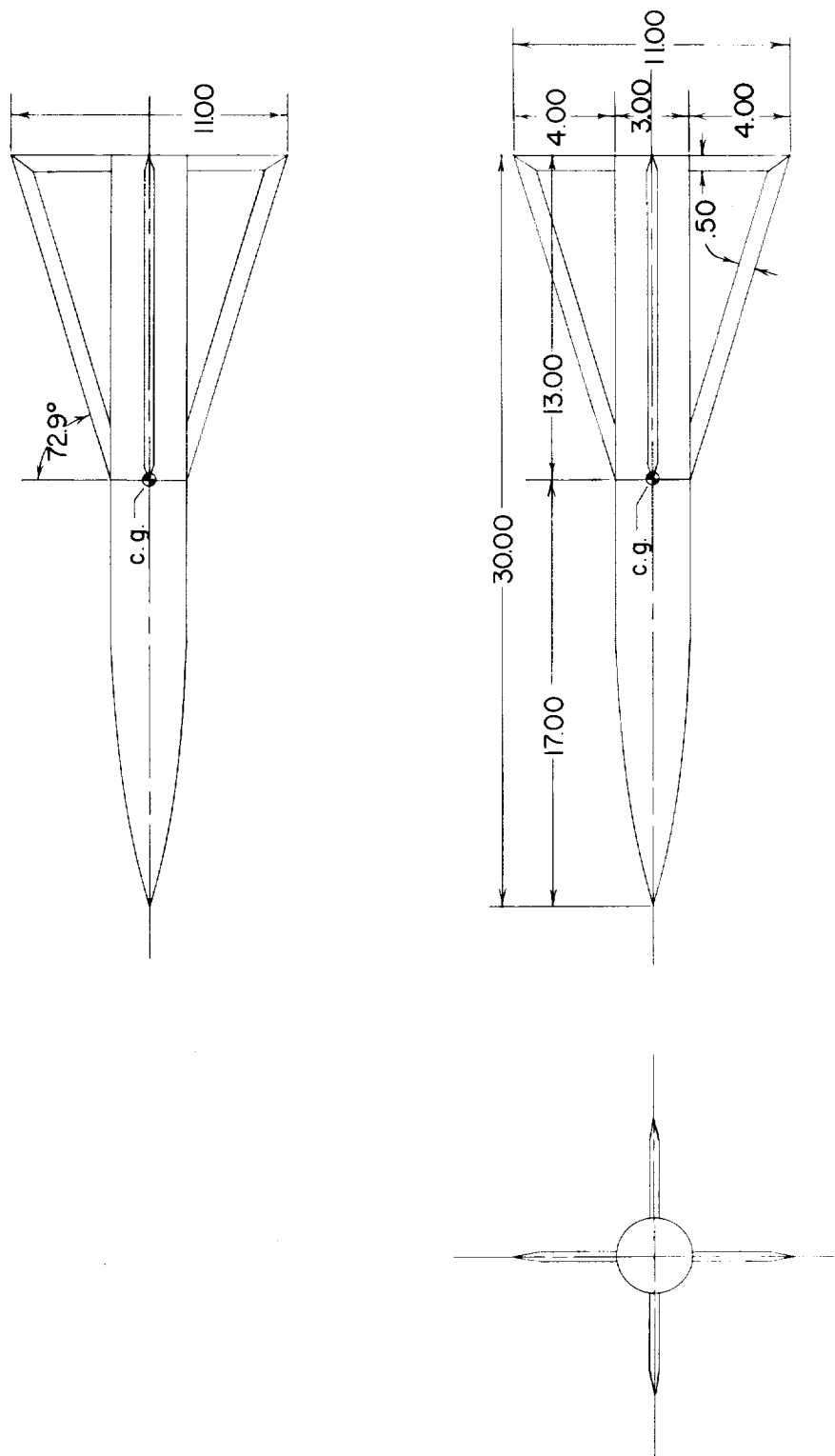
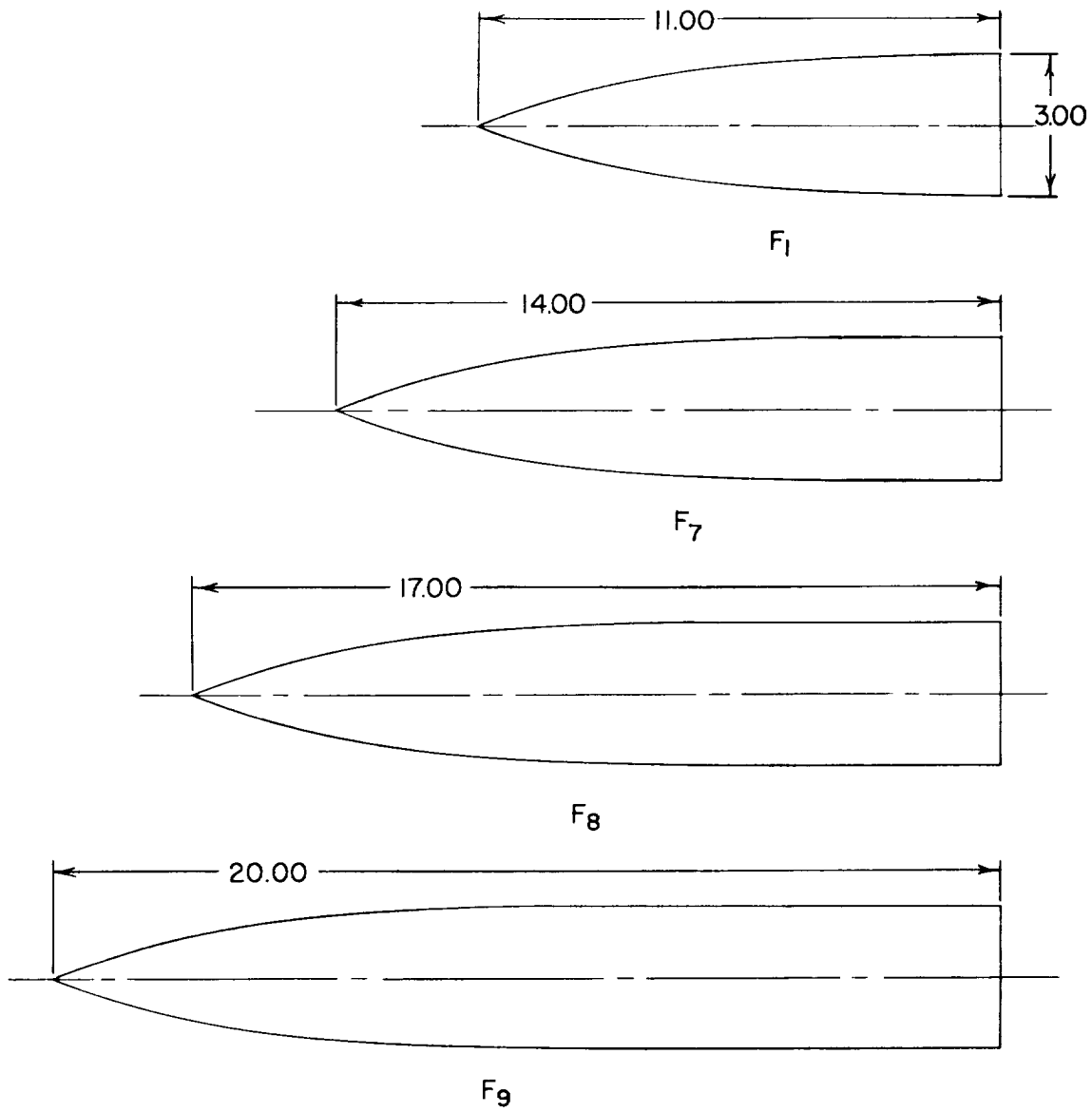
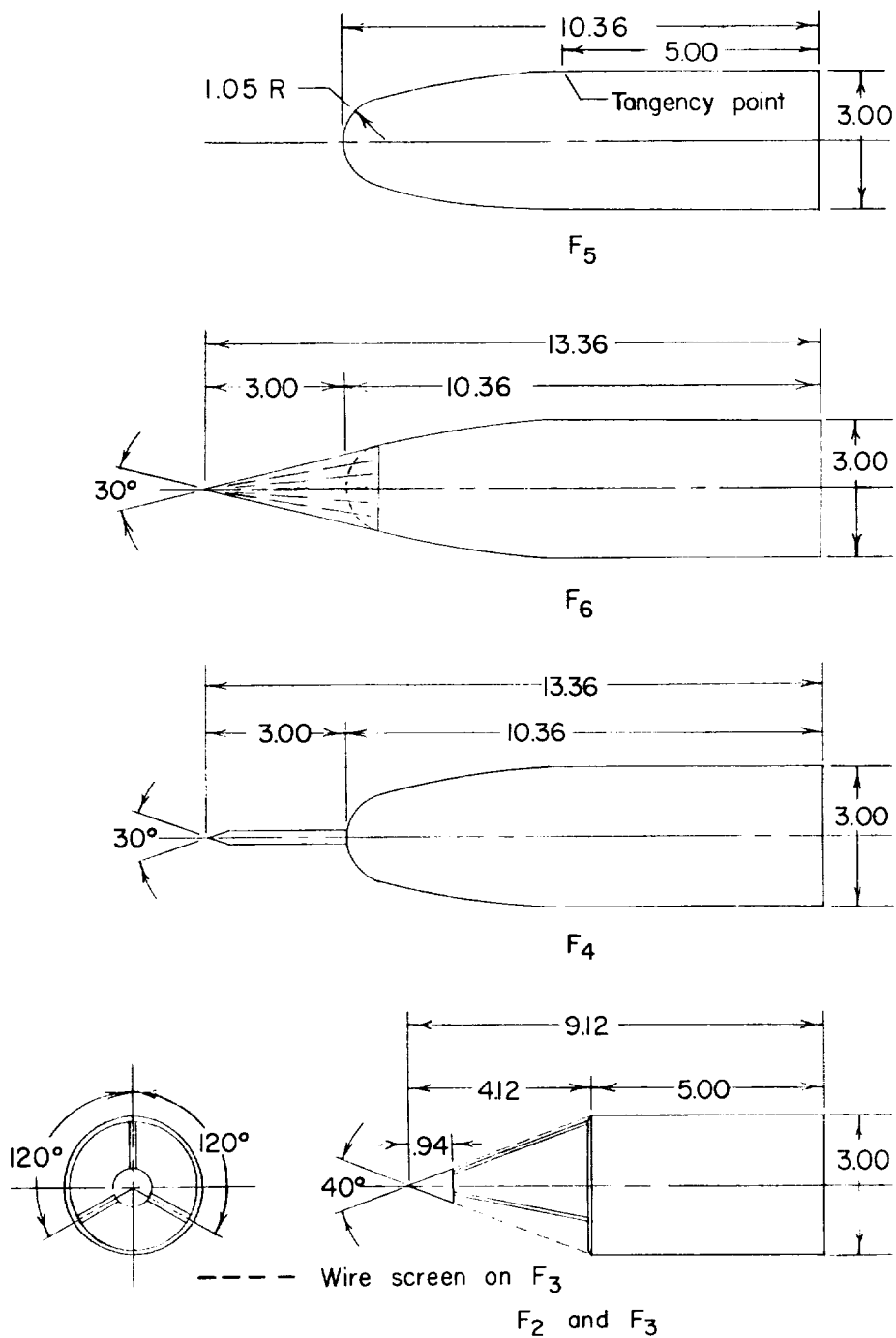
(a) Details of typical configuration, F₈W₁A₀.

Figure 2.- Details of models. All dimensions are in inches except as noted.



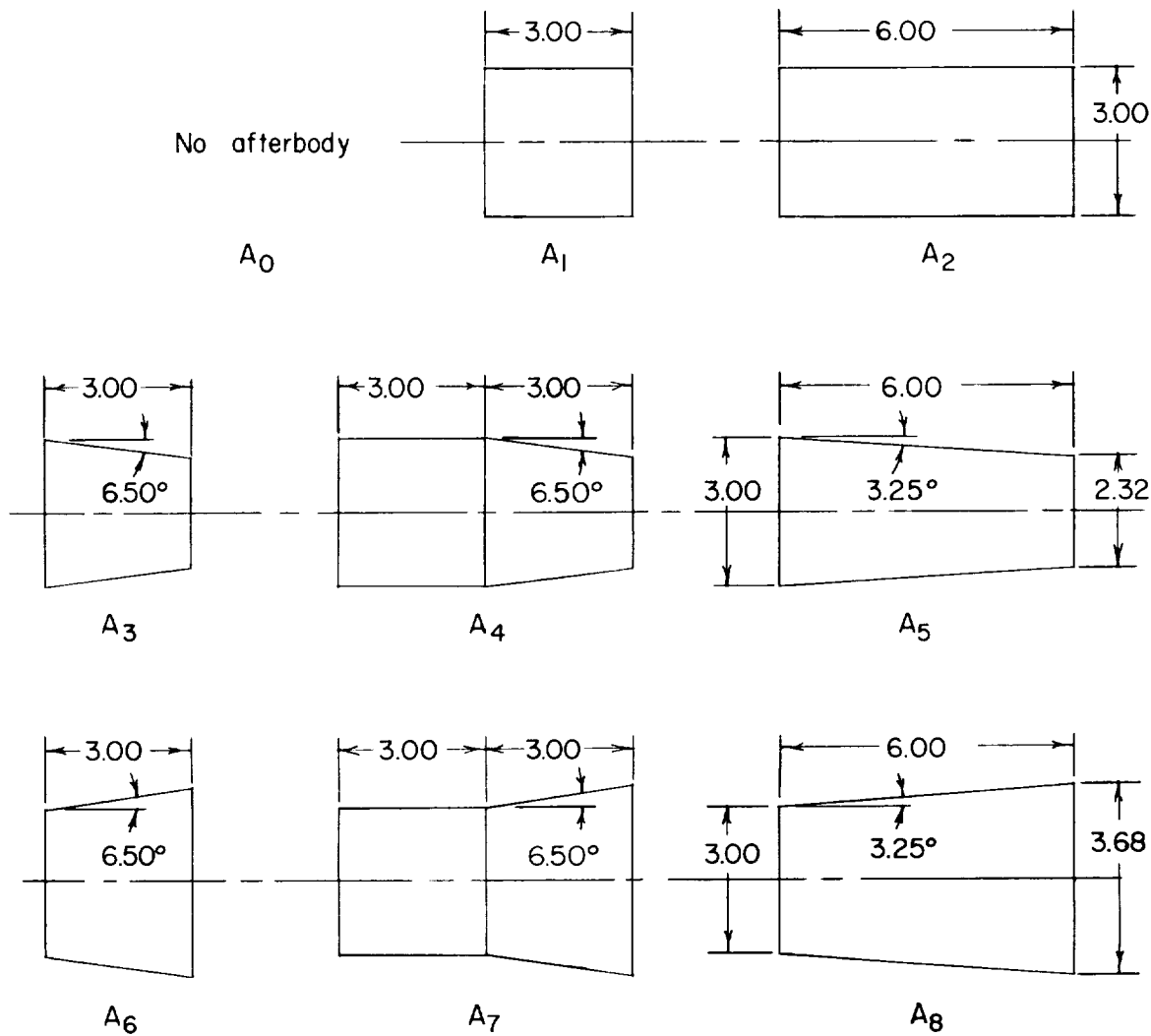
(b) Forebodies with 3.5-caliber-ogive cylinders and with constant rear diameter of 3.00 inches.

Figure 2.- Continued.



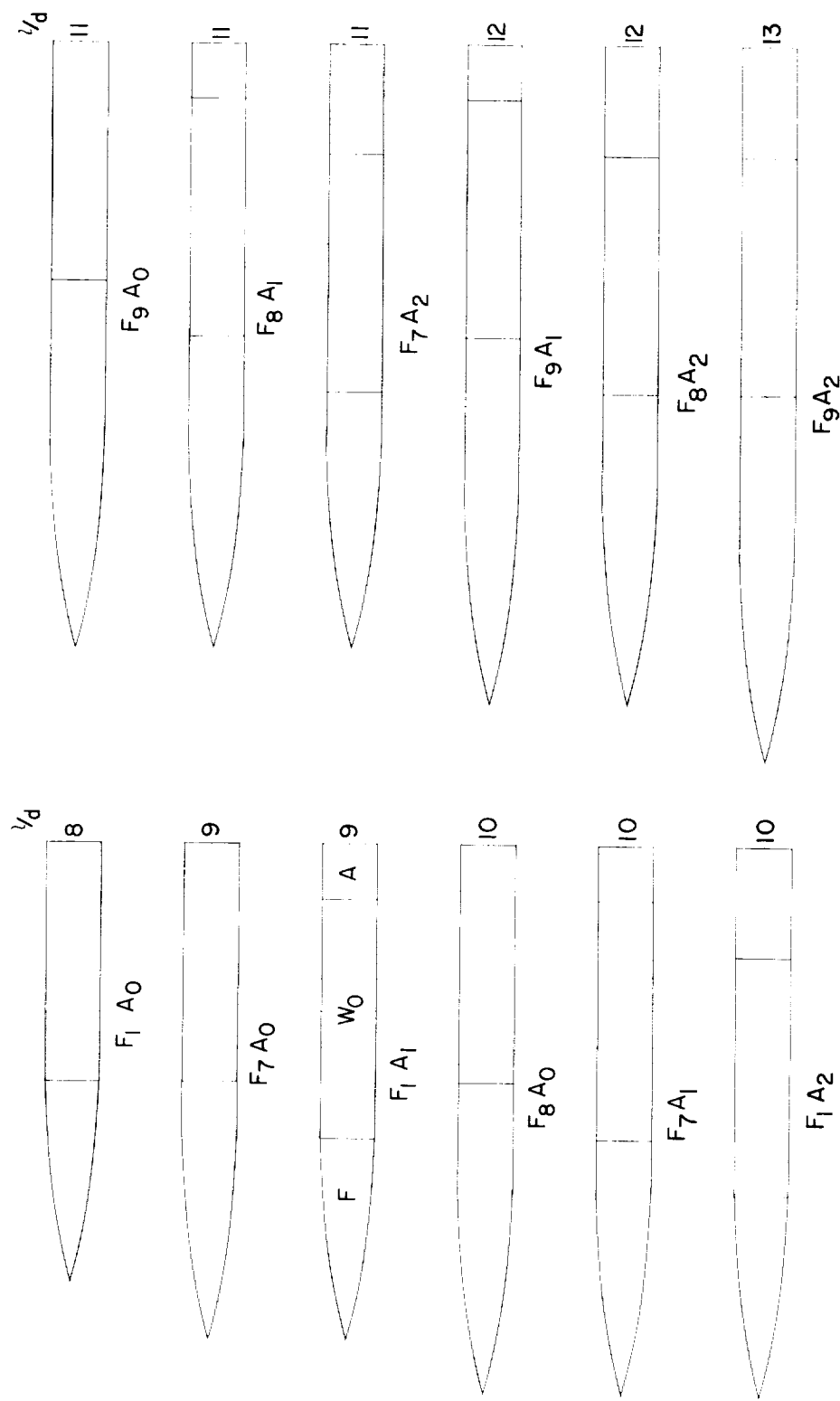
(c) Special nose shapes.

Figure 2.- Continued.



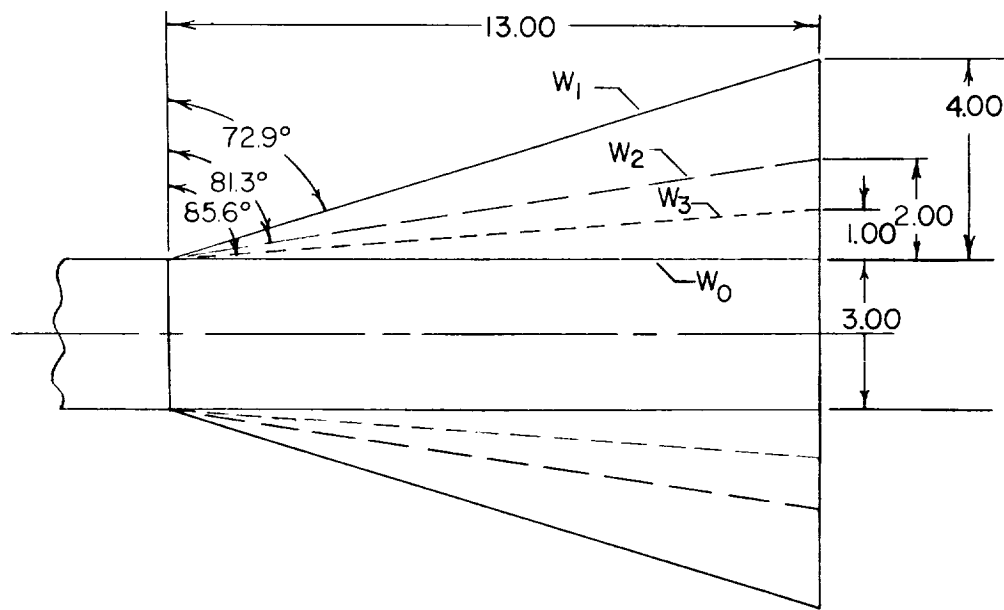
(d) Afterbodies. (All afterbodies are bodies of revolution.)

Figure 2.- Continued.

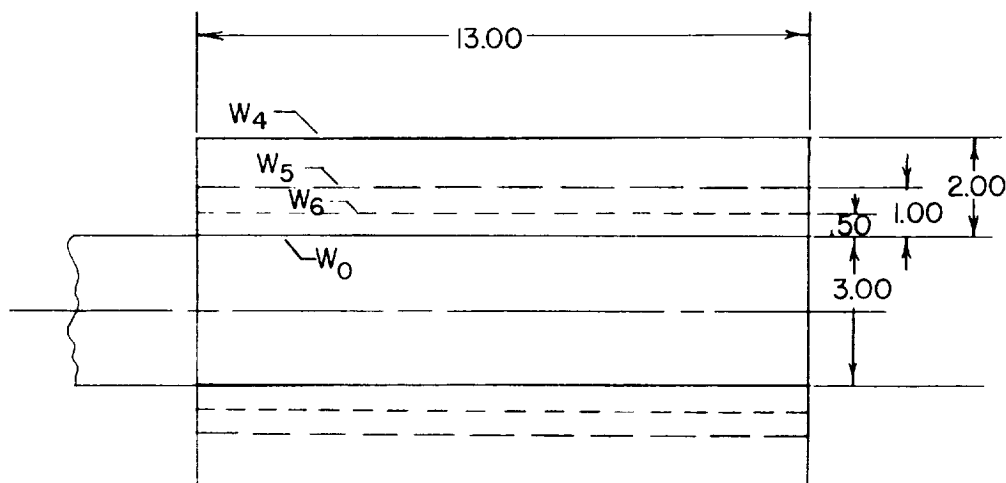


(e) Fuselage combinations. (All configurations include balance section W₀. See F₁A₁ and figs. 2(b) and 2(d) for details.)

Figure 2.- Continued.



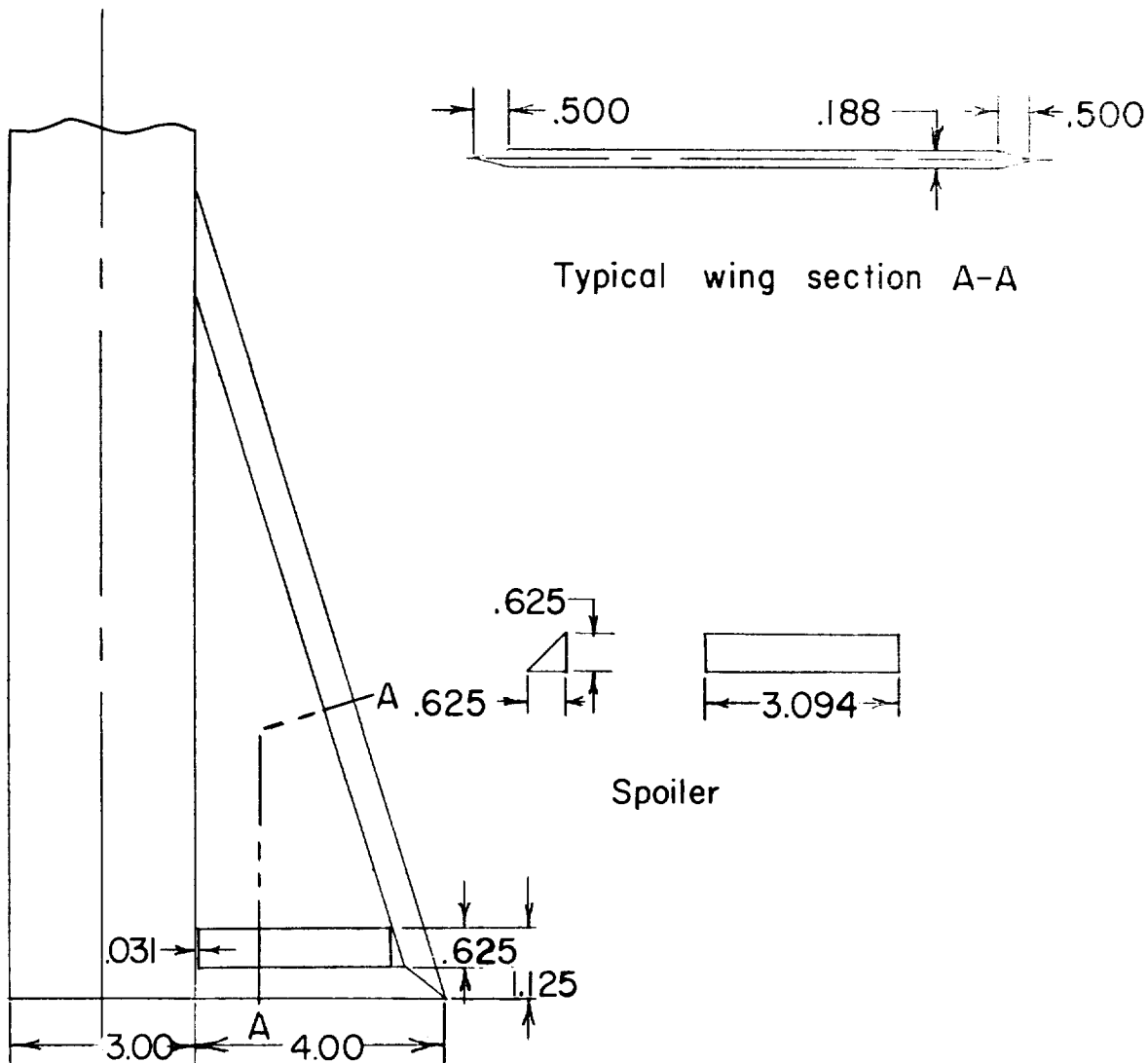
Delta wing series



Rectangular wing series

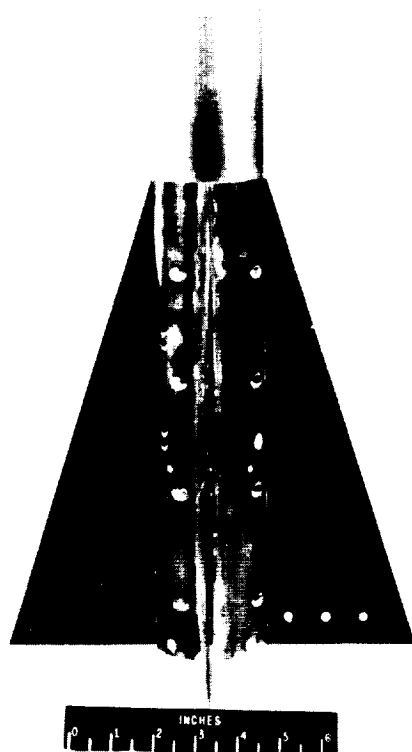
(f) Details of wings.

Figure 2.- Continued.



(g) Details of spoilers.

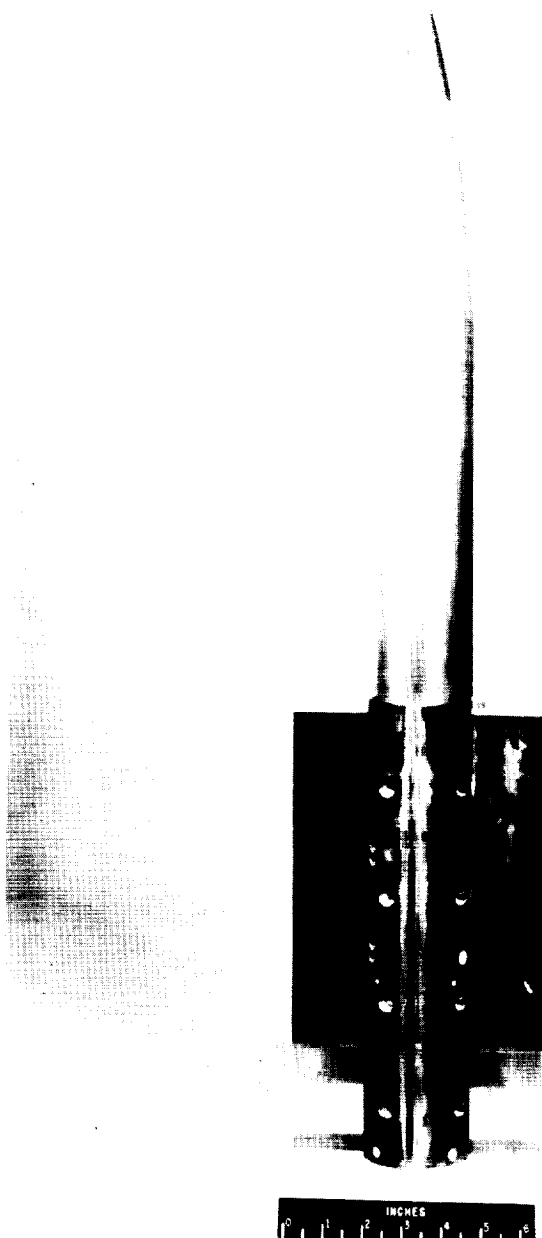
Figure 2.- Concluded.



(a) Typical delta-wing configuration.

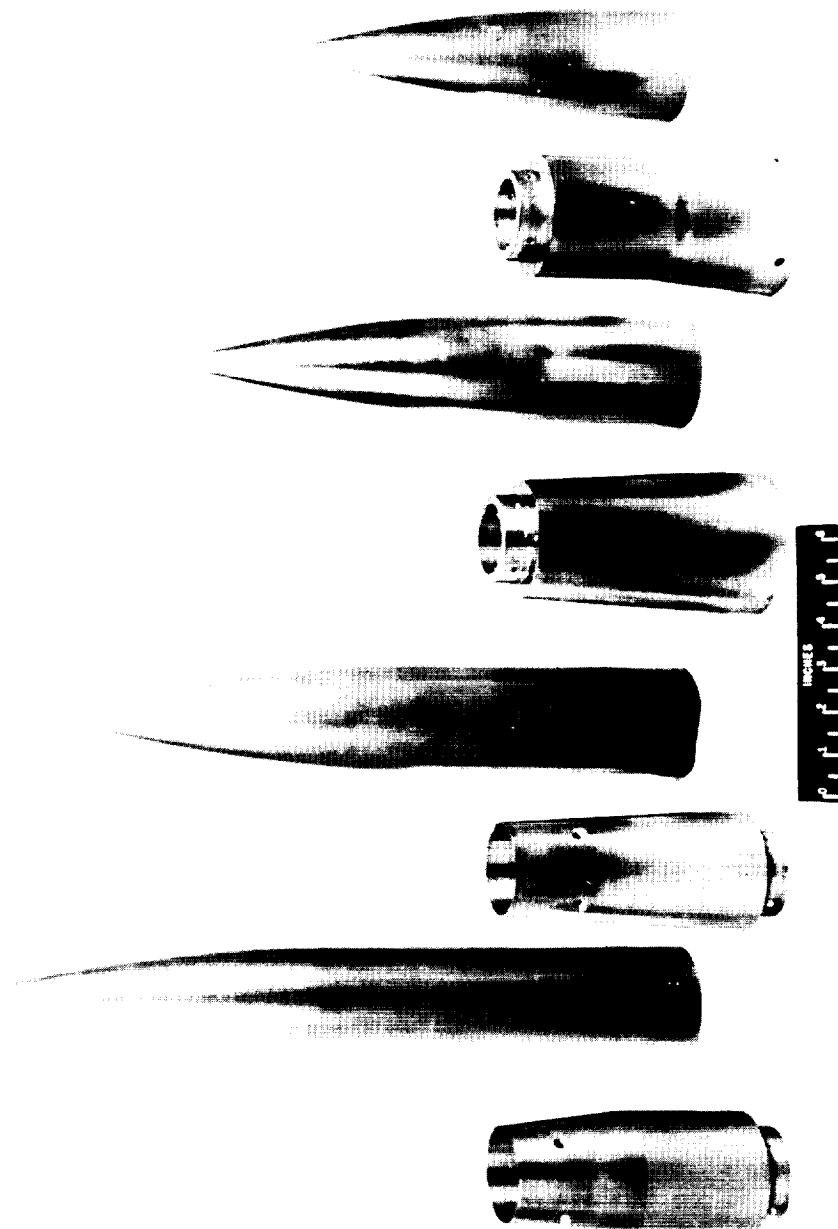
L-94318

Figure 3.- Models used in investigation.



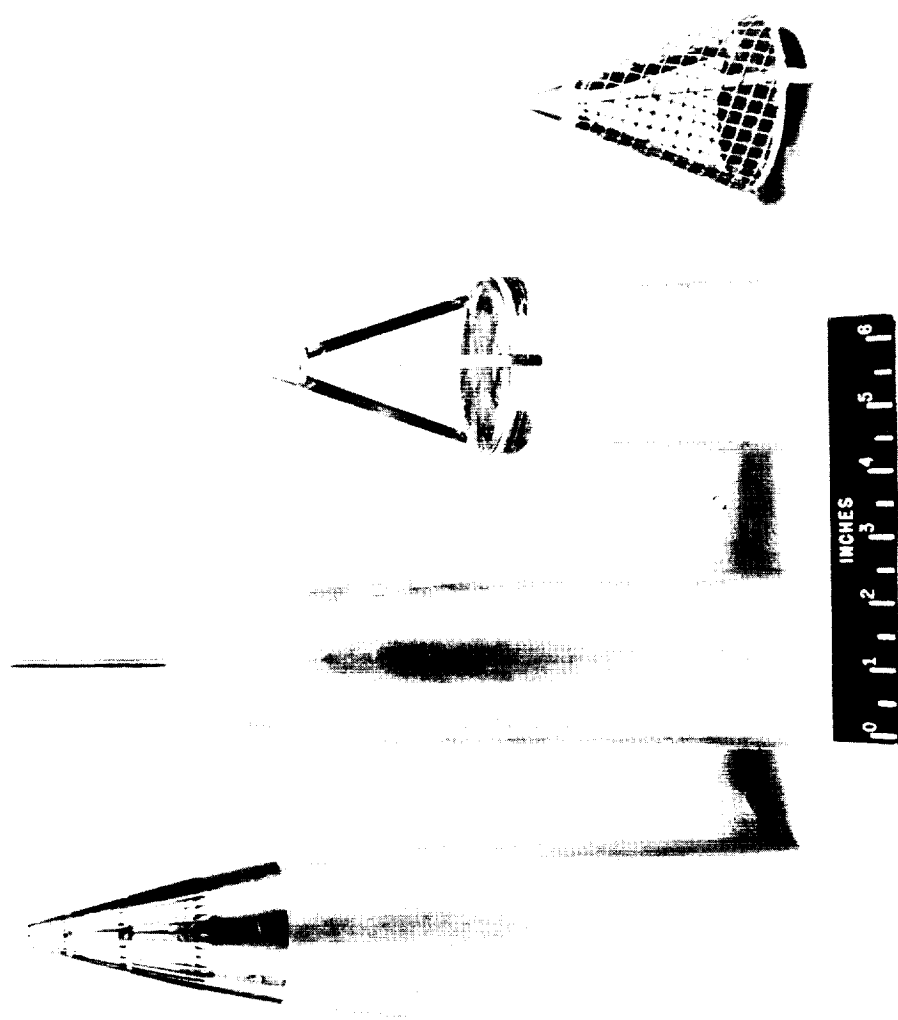
(b) Typical rectangular-wing configuration. L-94317

Figure 3.- Continued.



(c) Ogive cylinders and 2-caliber boattailed and flared afterbodies.
L-94320

Figure 3.- Continued.



(3) Fully assembled triped mine.

Figure 3.- Concluded.

L-94519

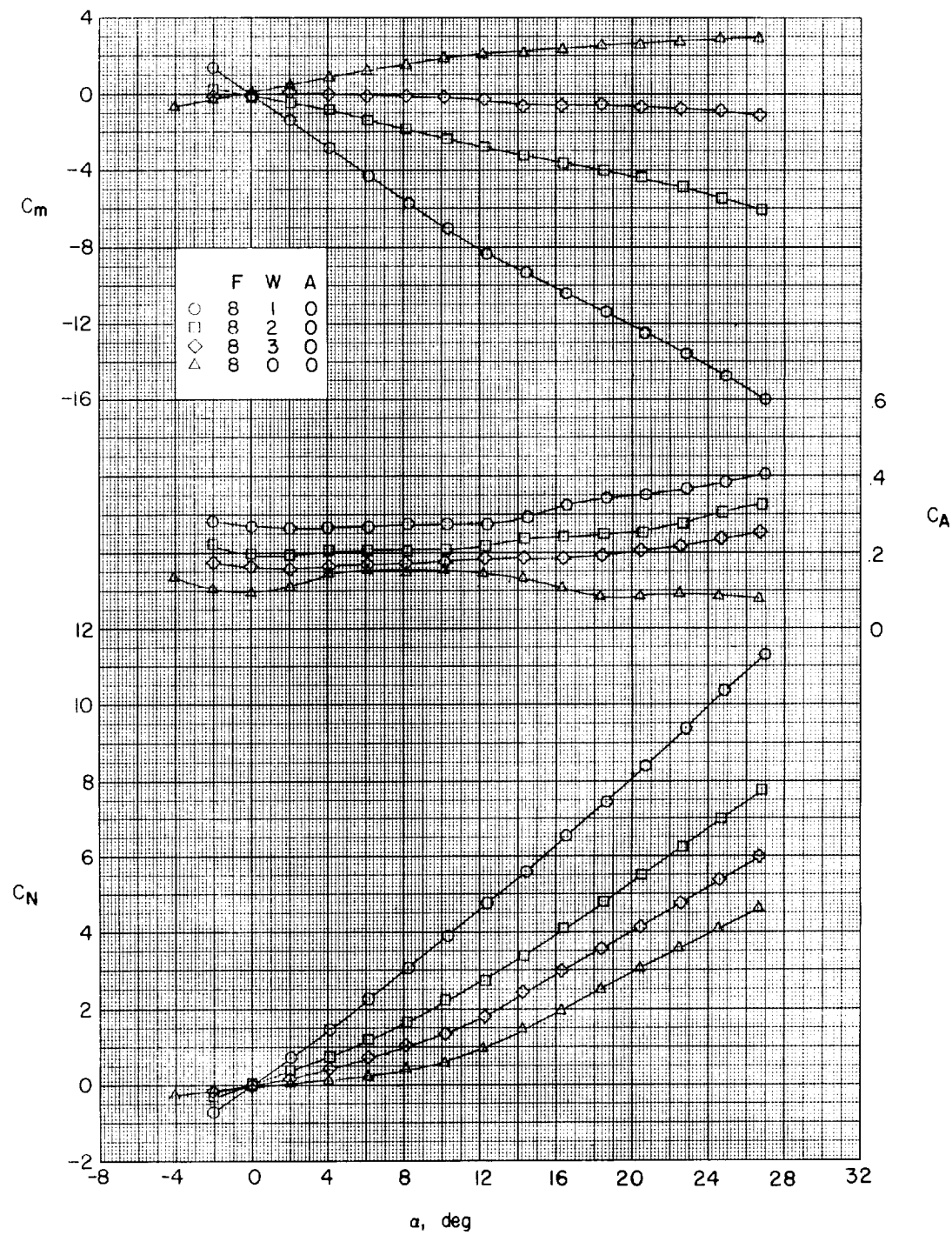


Figure 4.- Effects of delta wings on aerodynamic characteristics in pitch. No afterbody; $l/d = 10$.

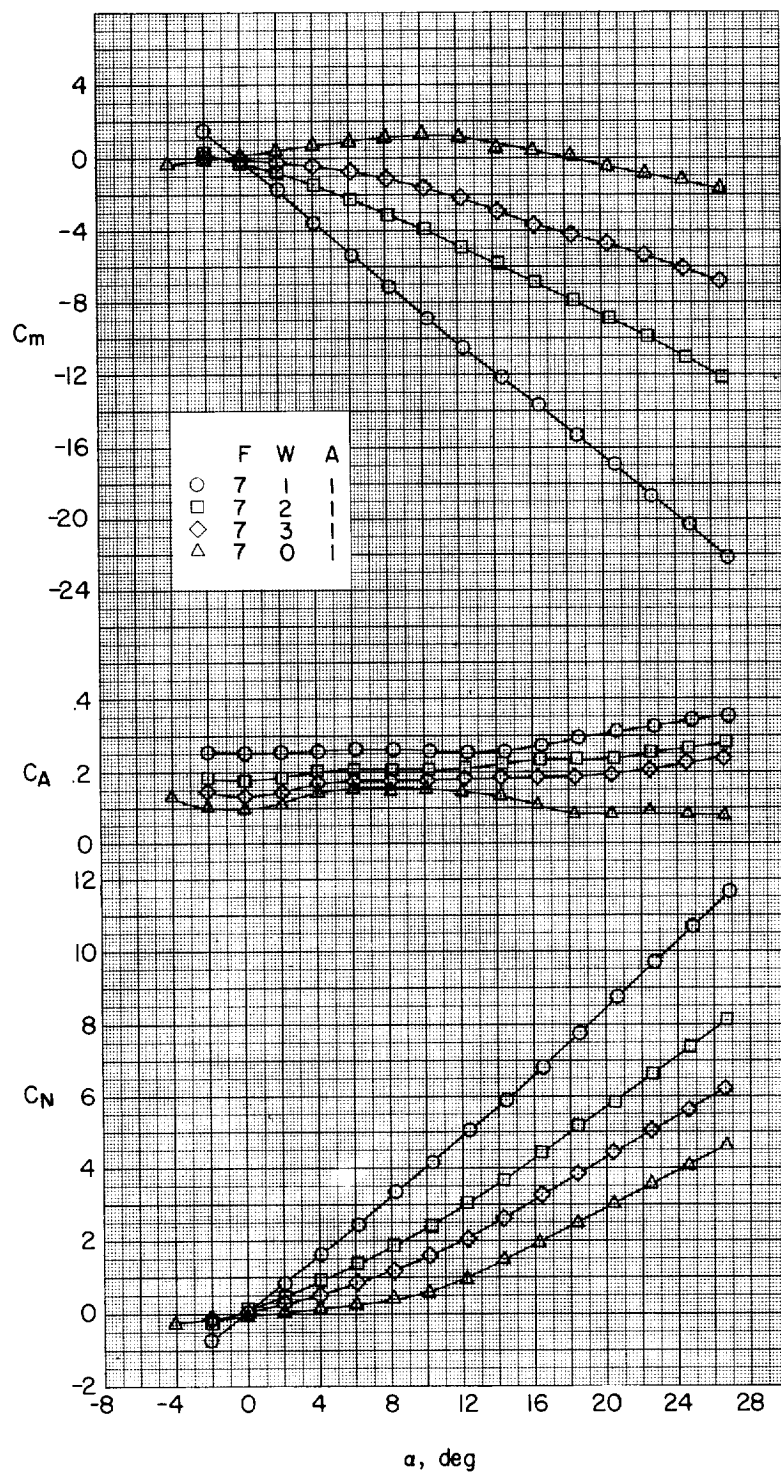


Figure 5.- Effects of delta wings on aerodynamic characteristics in pitch. One-caliber cylindrical afterbody; $l/d = 10$.

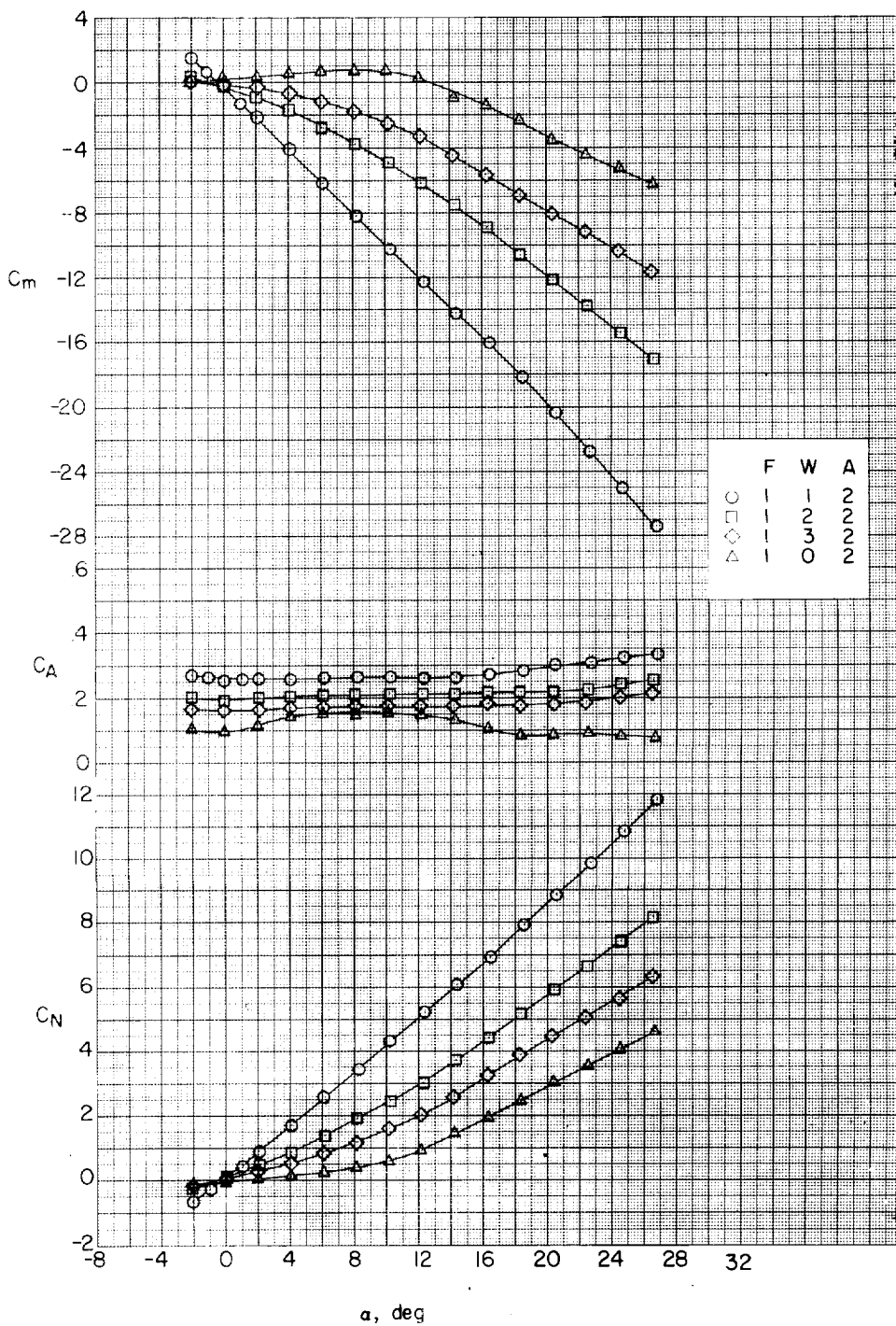
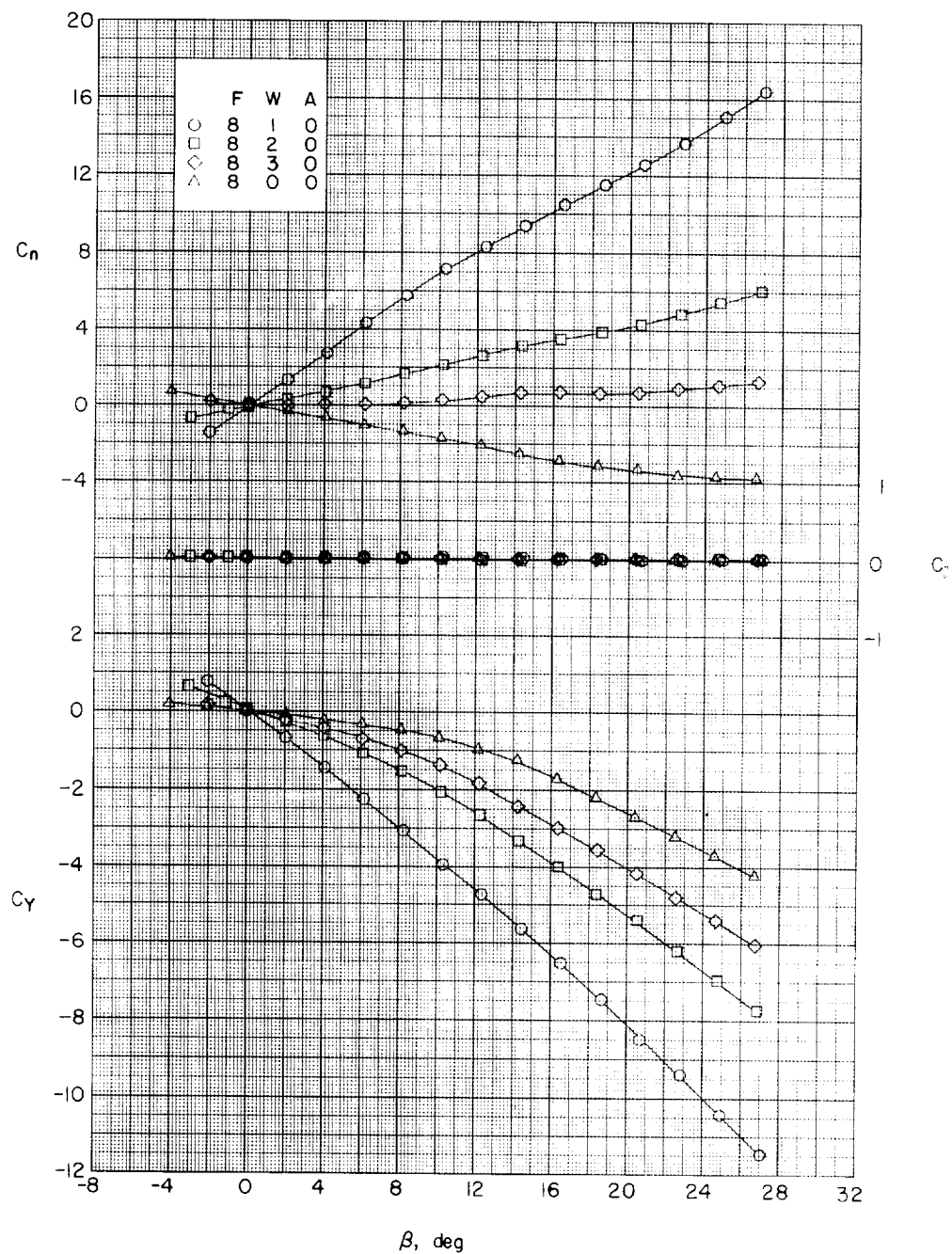


Figure 6.- Effects of delta wings on aerodynamic characteristics in pitch. Two-caliber cylindrical afterbody; $l/d = 10$.



(a) $\alpha = 0^\circ$.

Figure 7.- Effects of delta wings on aerodynamic characteristics in side-slip. No afterbody; $l/d = 10$.

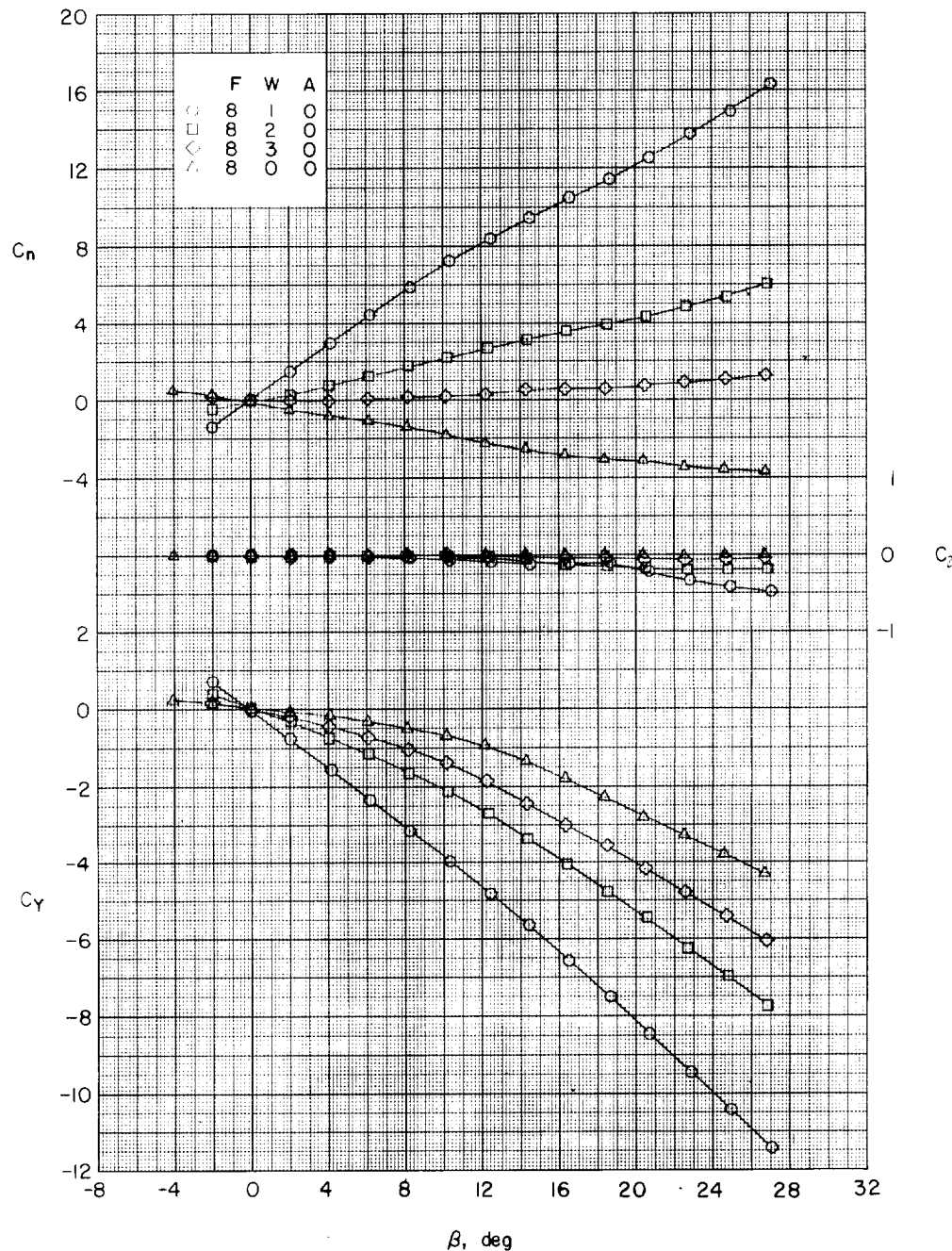
(b) $\alpha \approx 4.1^\circ$.

Figure 7.- Continued.

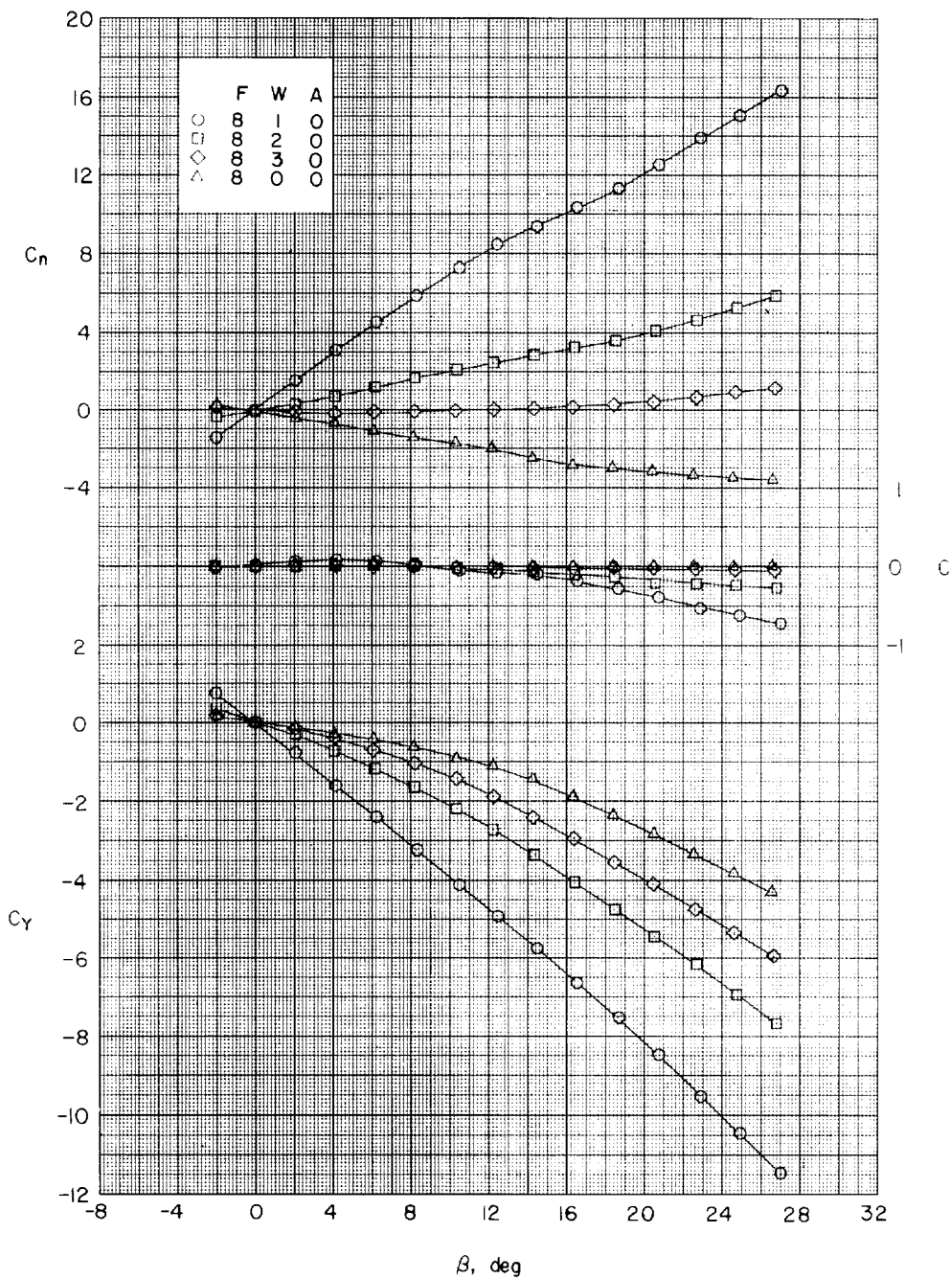
(c) $\alpha \approx 8.2^\circ$.

Figure 7.- Continued.

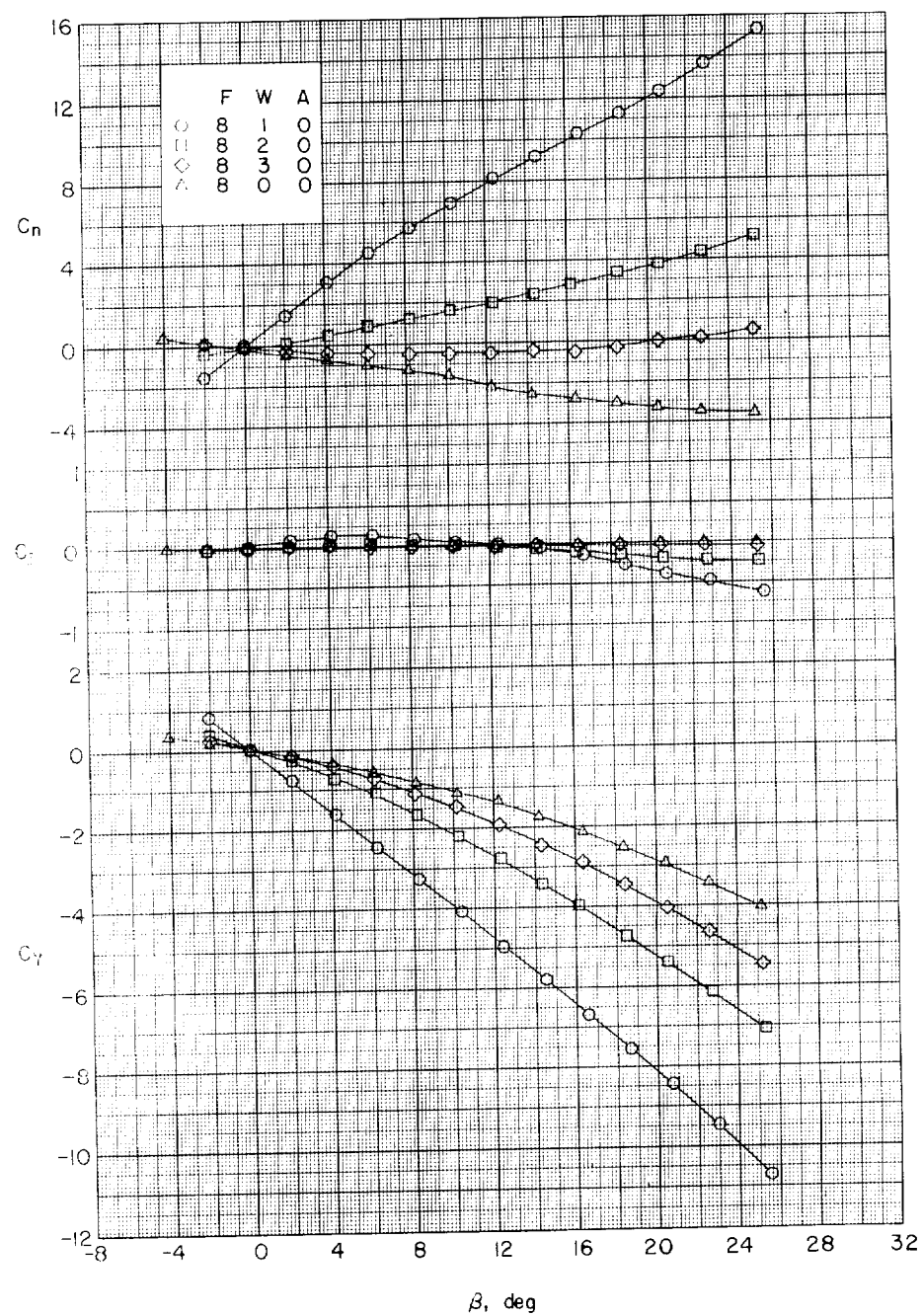
(d) $\alpha \approx 12.3^\circ$.

Figure 7.- Continued.

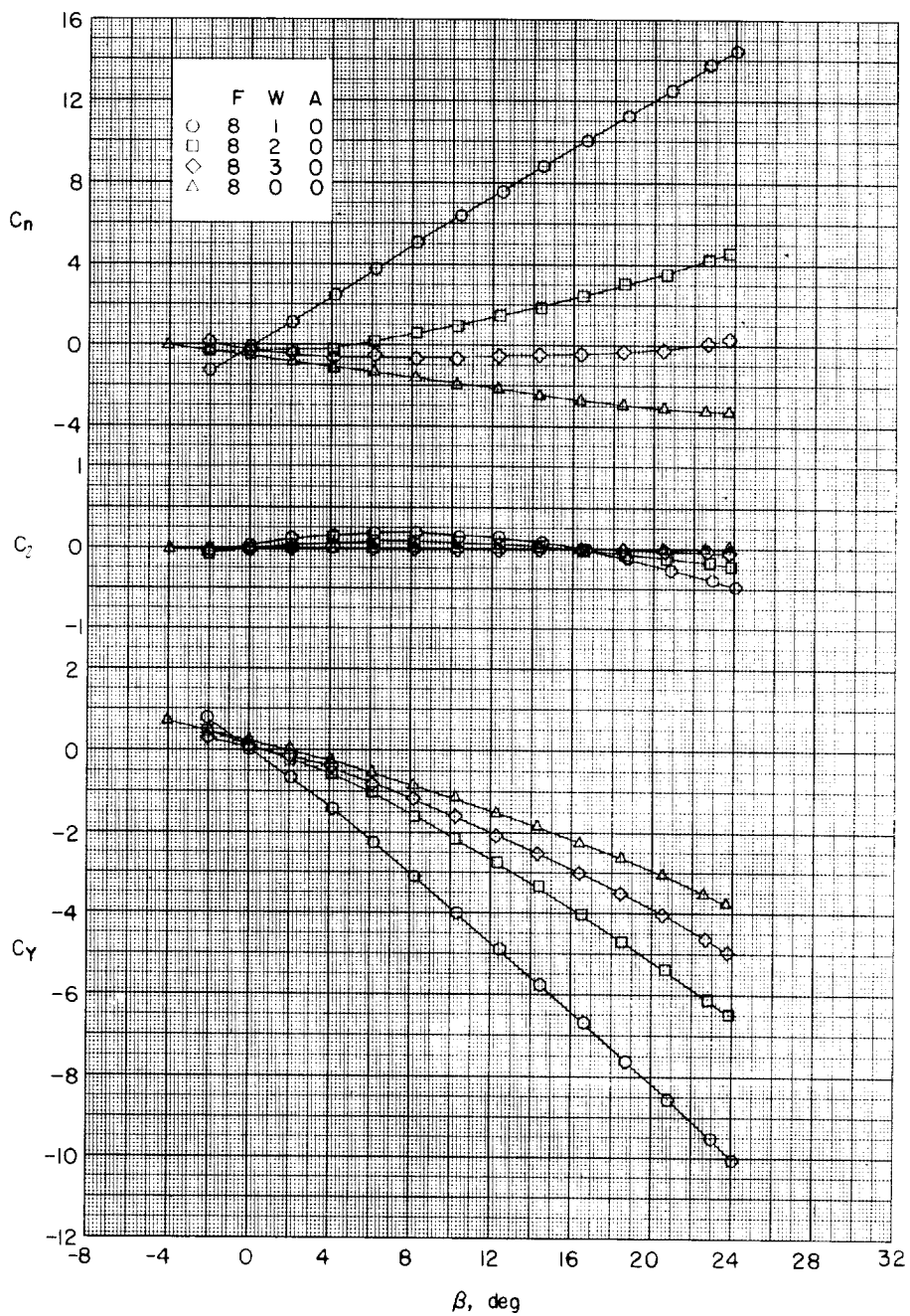
(e) $\alpha \approx 16.4^\circ$.

Figure 7.- Continued.

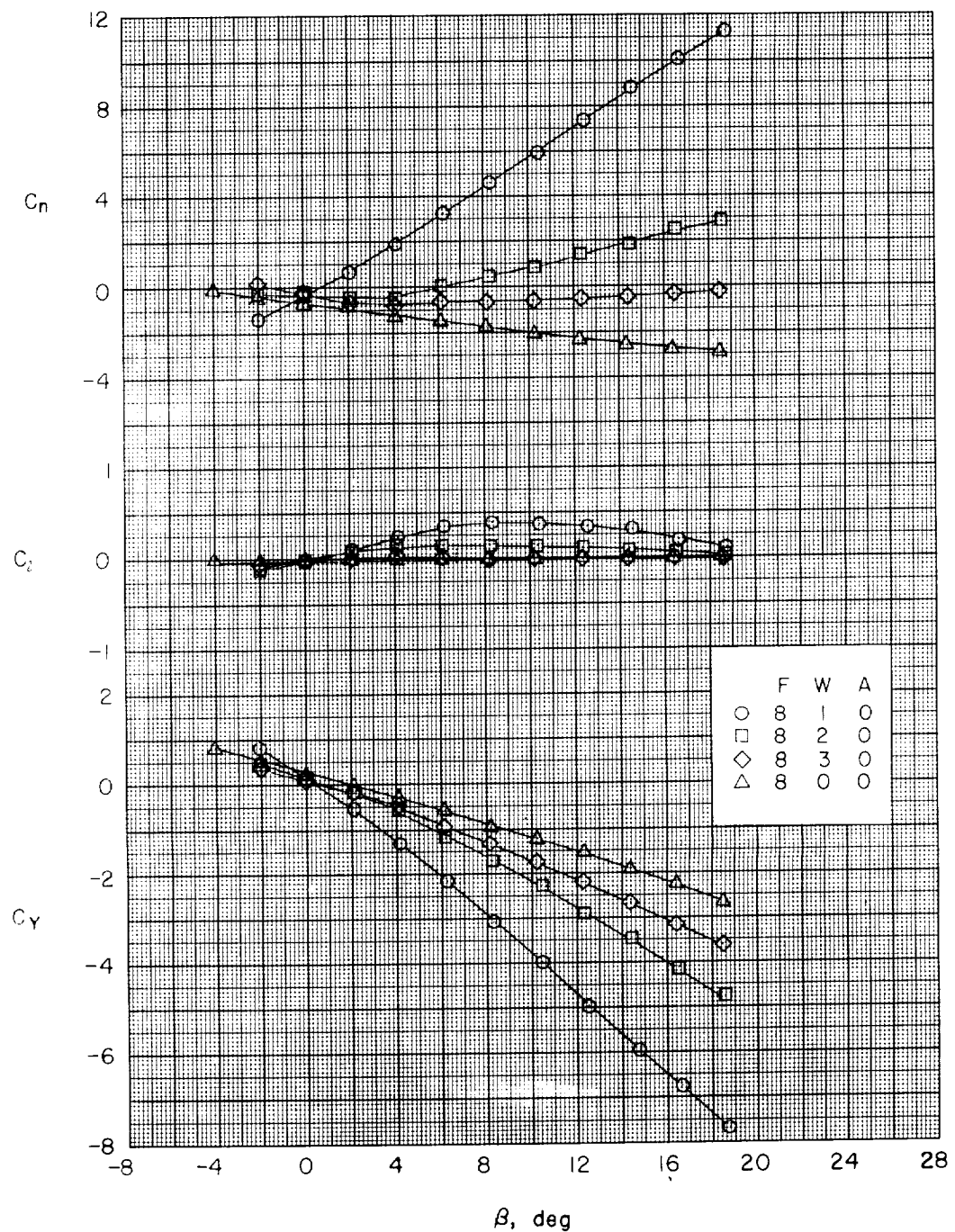
(f) $\alpha \approx 20.5^\circ$.

Figure 7.- Continued.

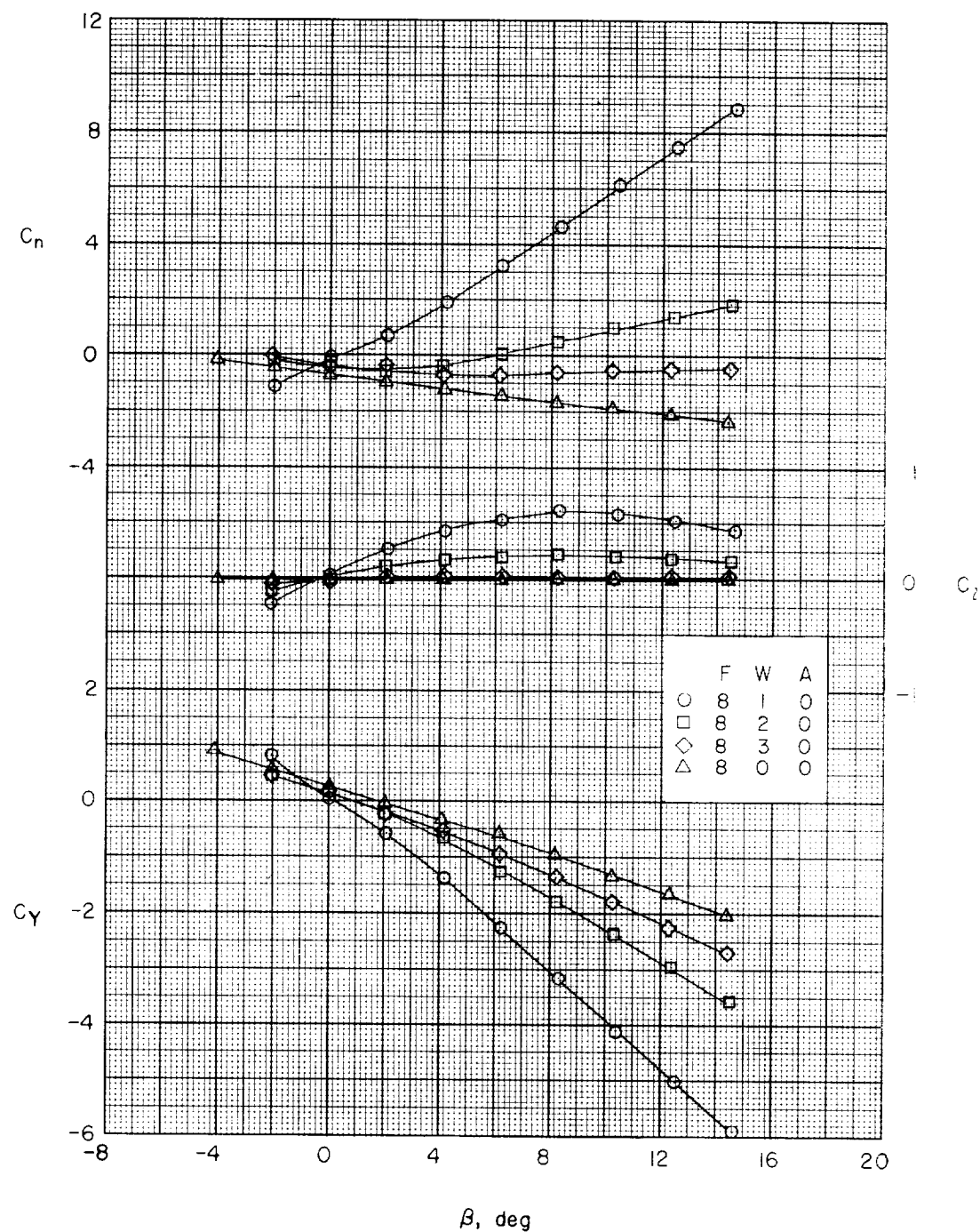
(g) $\alpha \approx 24.7^\circ$.

Figure 7.- Concluded.

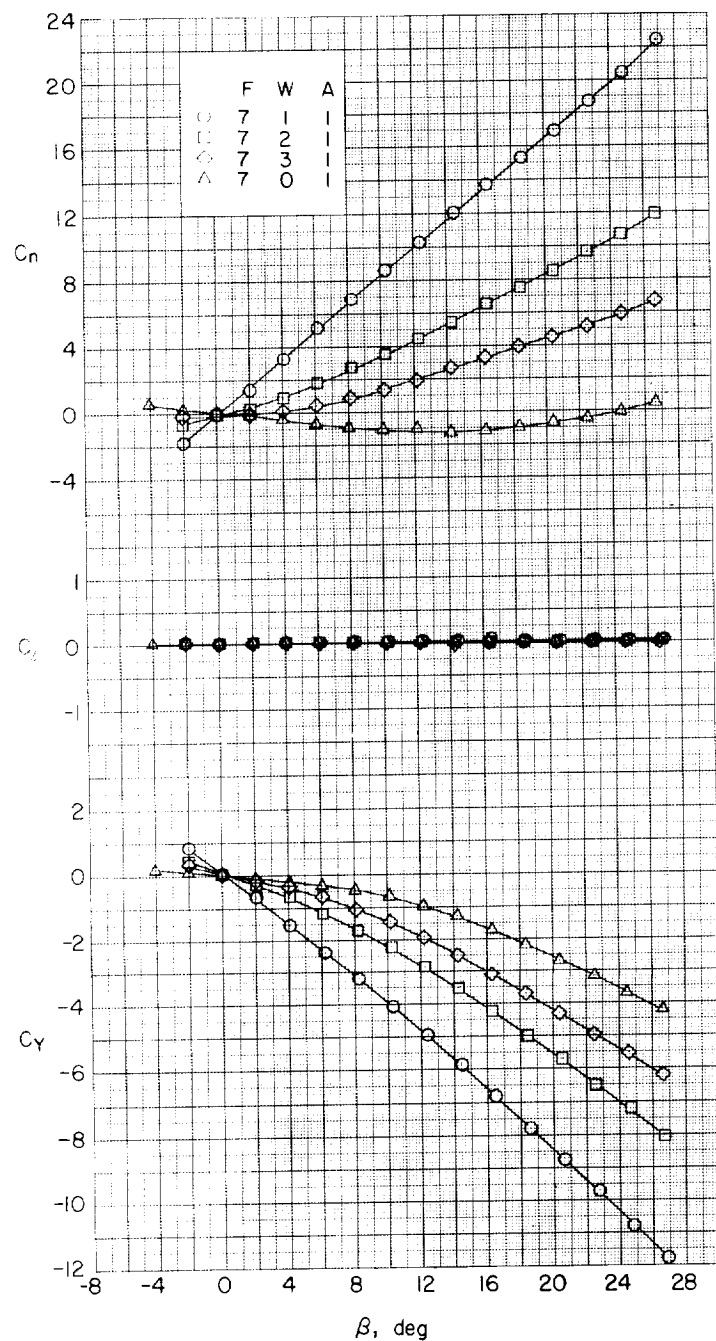
(a) $\alpha = 0^\circ$.

Figure 8.- Effects of delta wings on aerodynamic characteristics in side-slip. One-caliber cylindrical afterbody; $l/d = 10$.

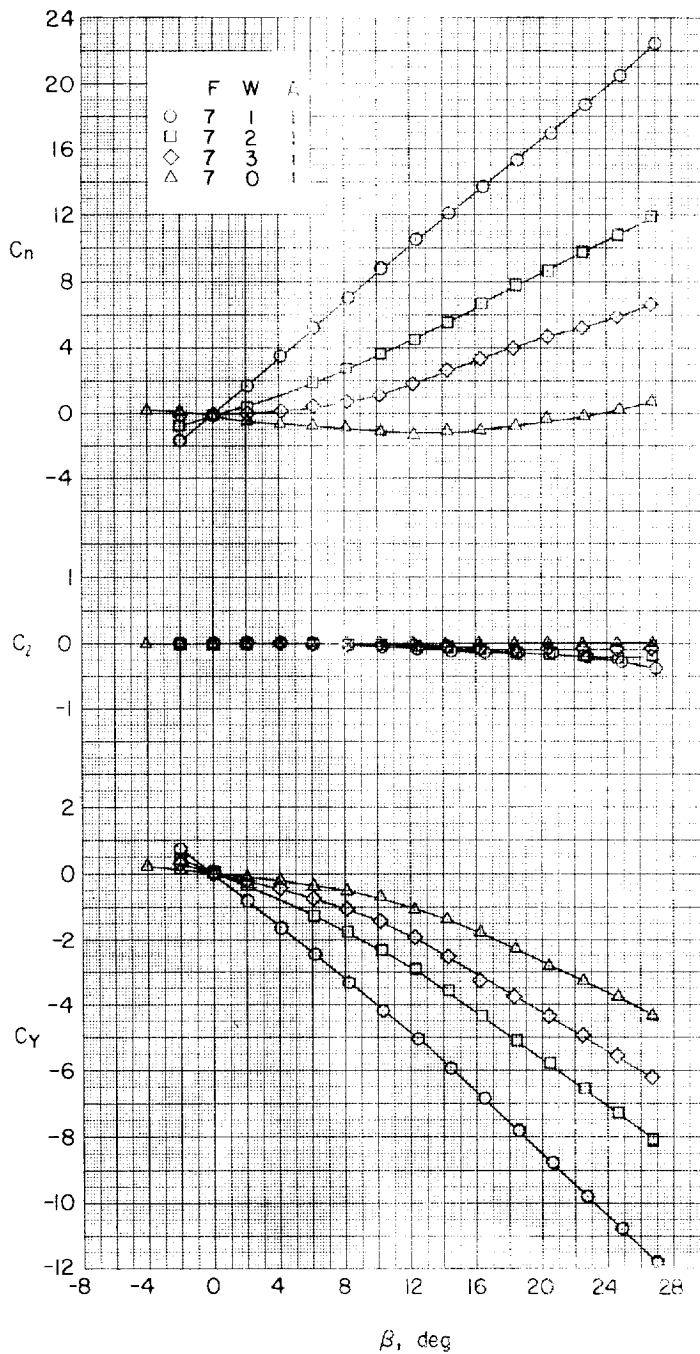
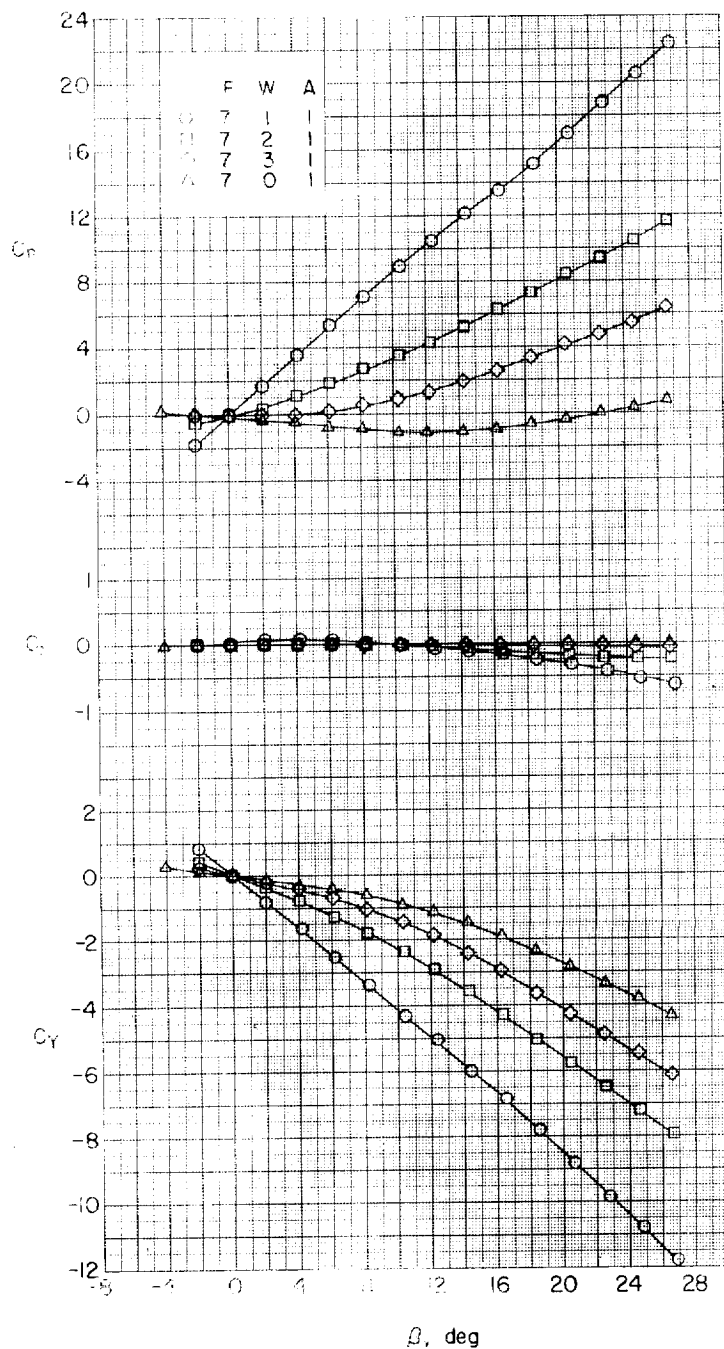
(b) $\alpha \approx 4.1^\circ$.

Figure 8.- Continued.



(c) $\alpha \approx 8.2^\circ$.

Figure 2. - Continued.

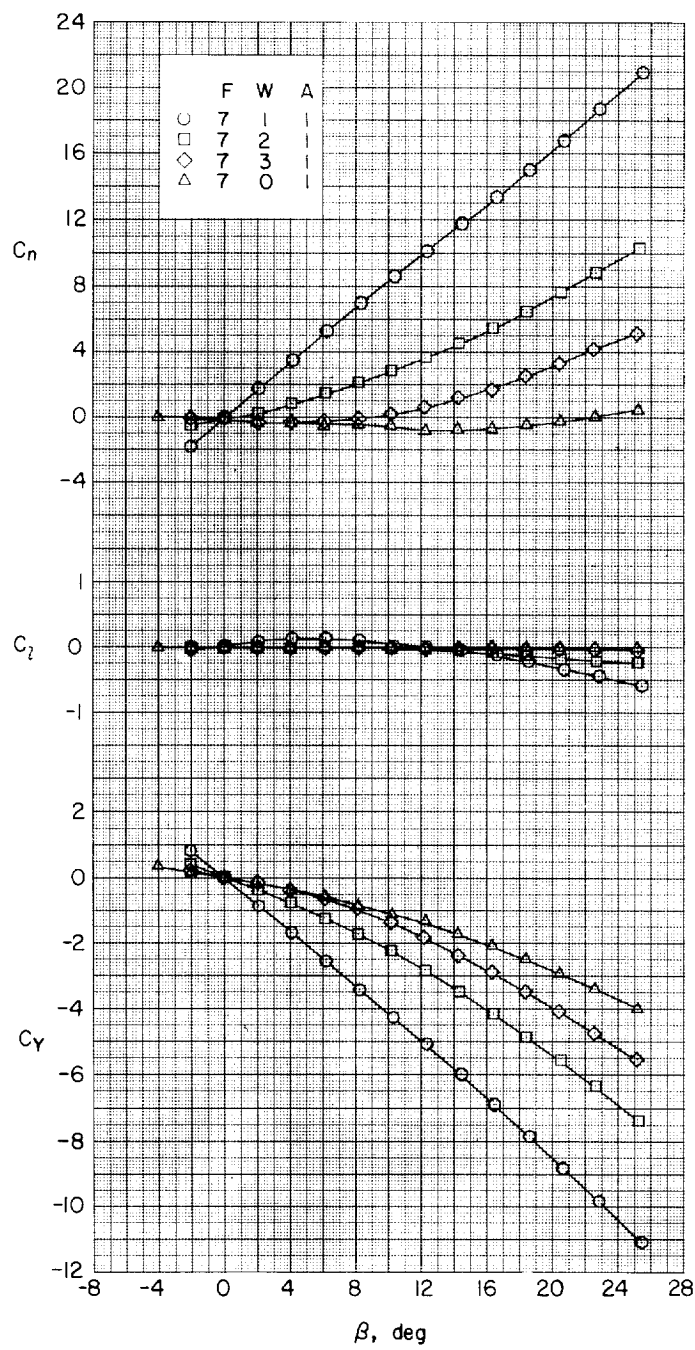
(d) $\alpha \approx 12.5^\circ$.

Figure 8.- Continued.

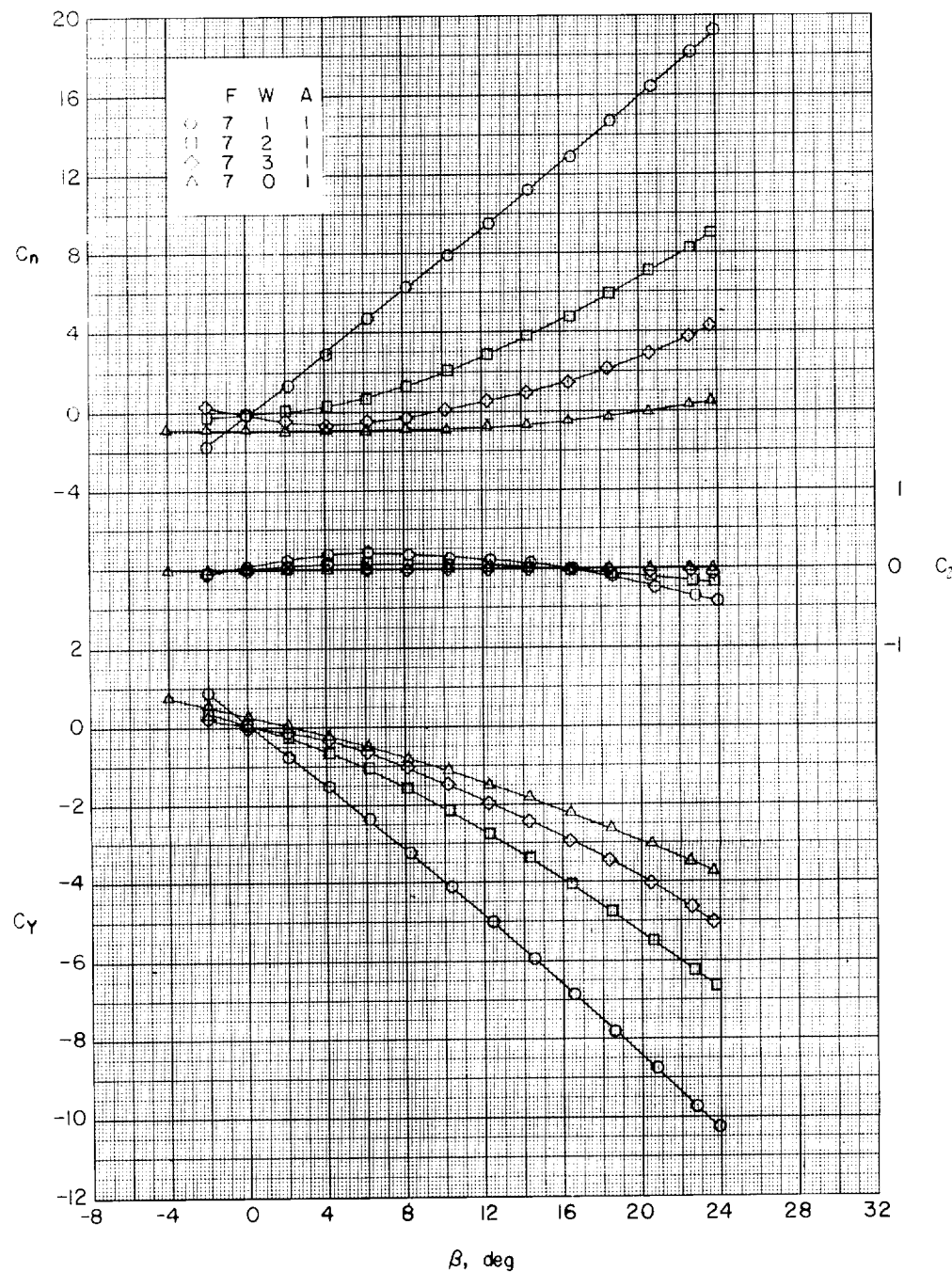
(e) $\alpha \approx 16.4^\circ$.

Figure 8.- Continued.

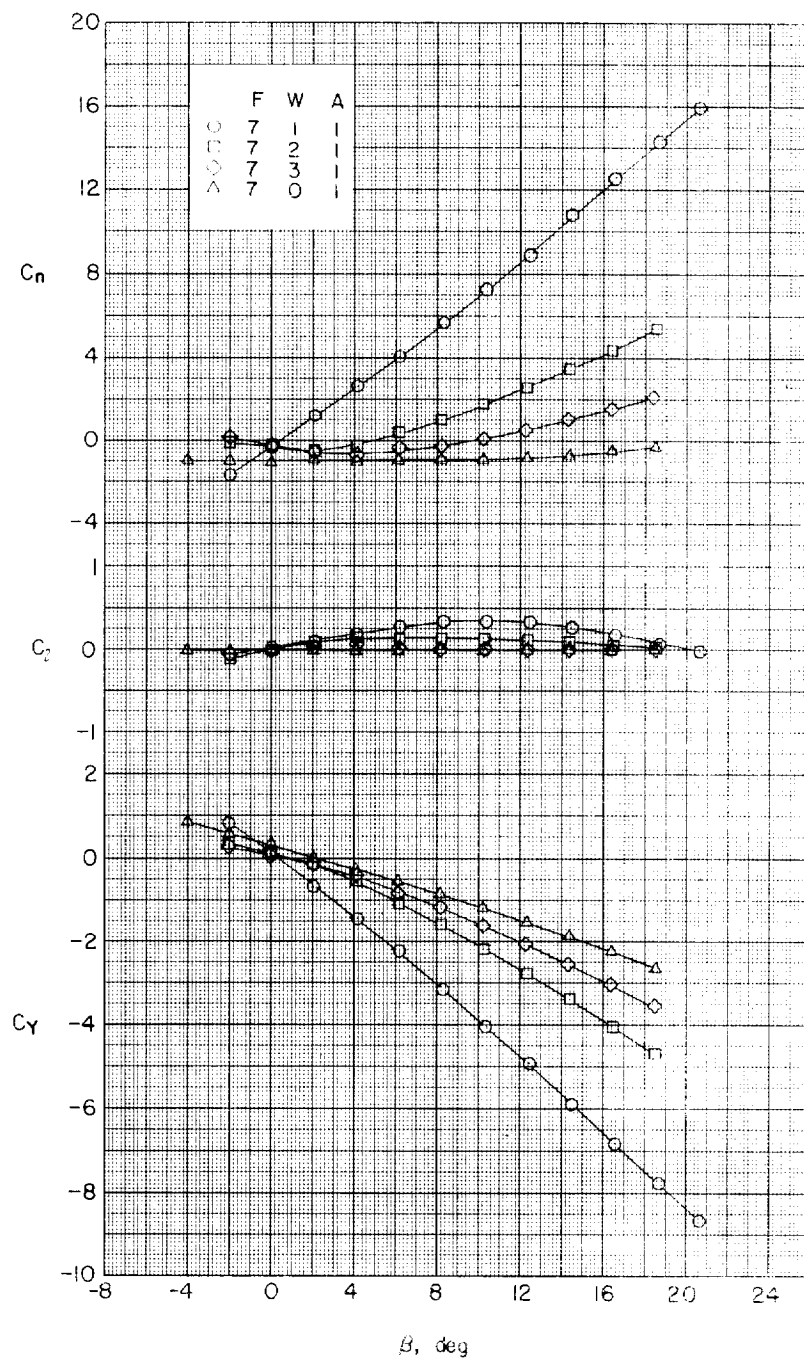
(f) $\alpha \approx 20.5^\circ$.

Figure 8.- Continued.

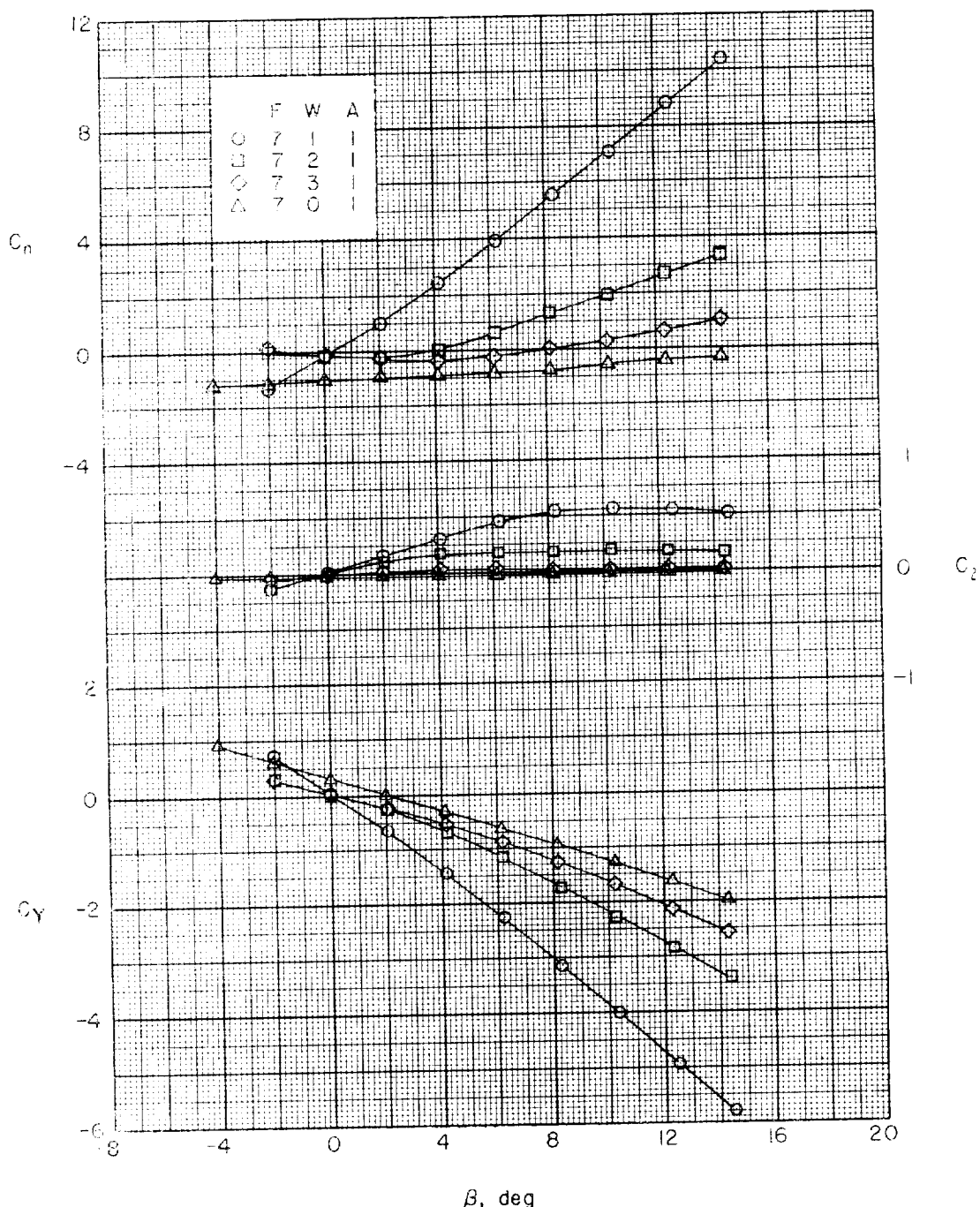
(g) $\alpha \approx 24.7^\circ$.

Figure 8.- Concluded.

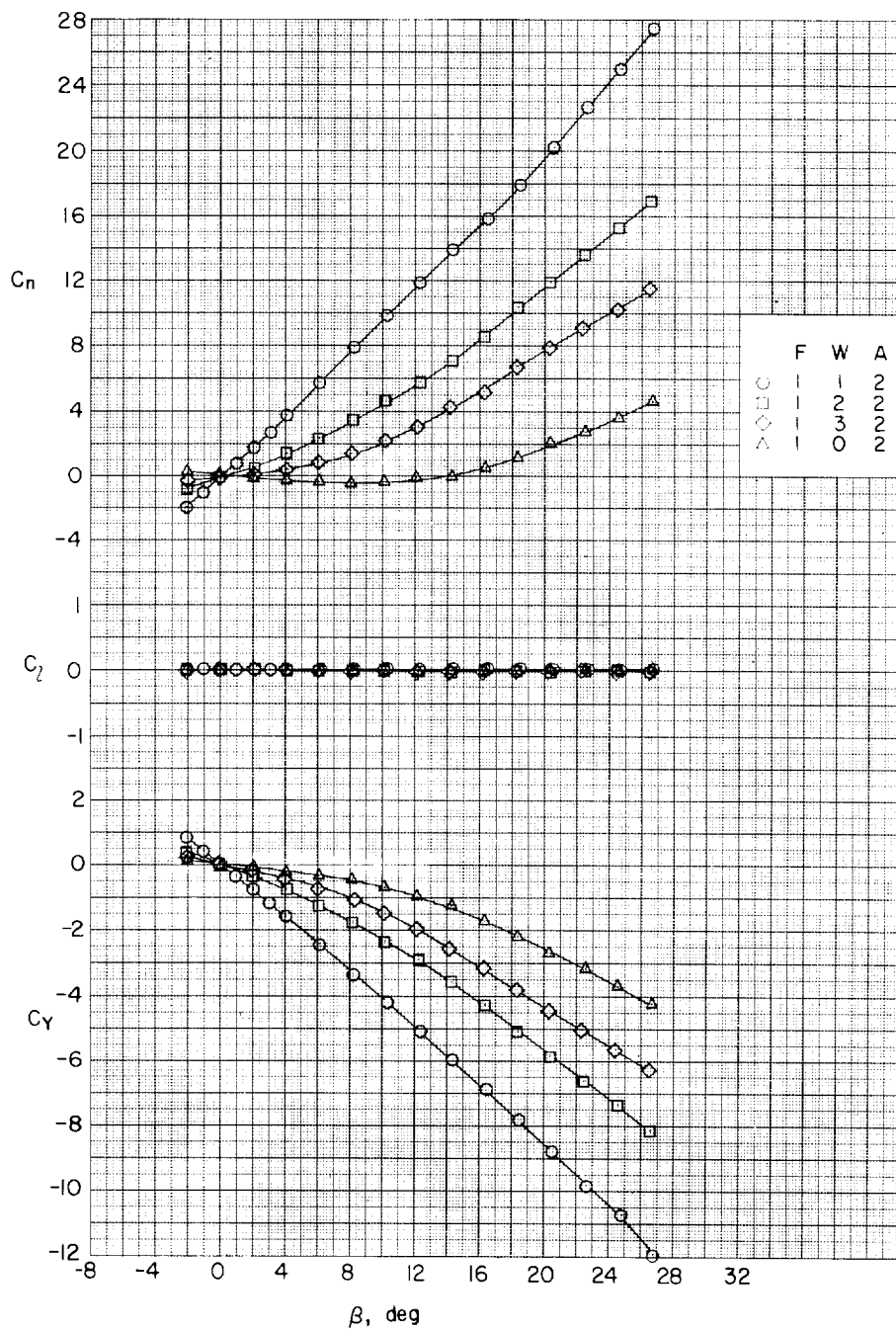
(a) $\alpha \approx 0^\circ$.

Figure 9.- Effects of delta wings on aerodynamic characteristics in side-slip. Two-caliber cylindrical afterbody; $l/d = 10$.

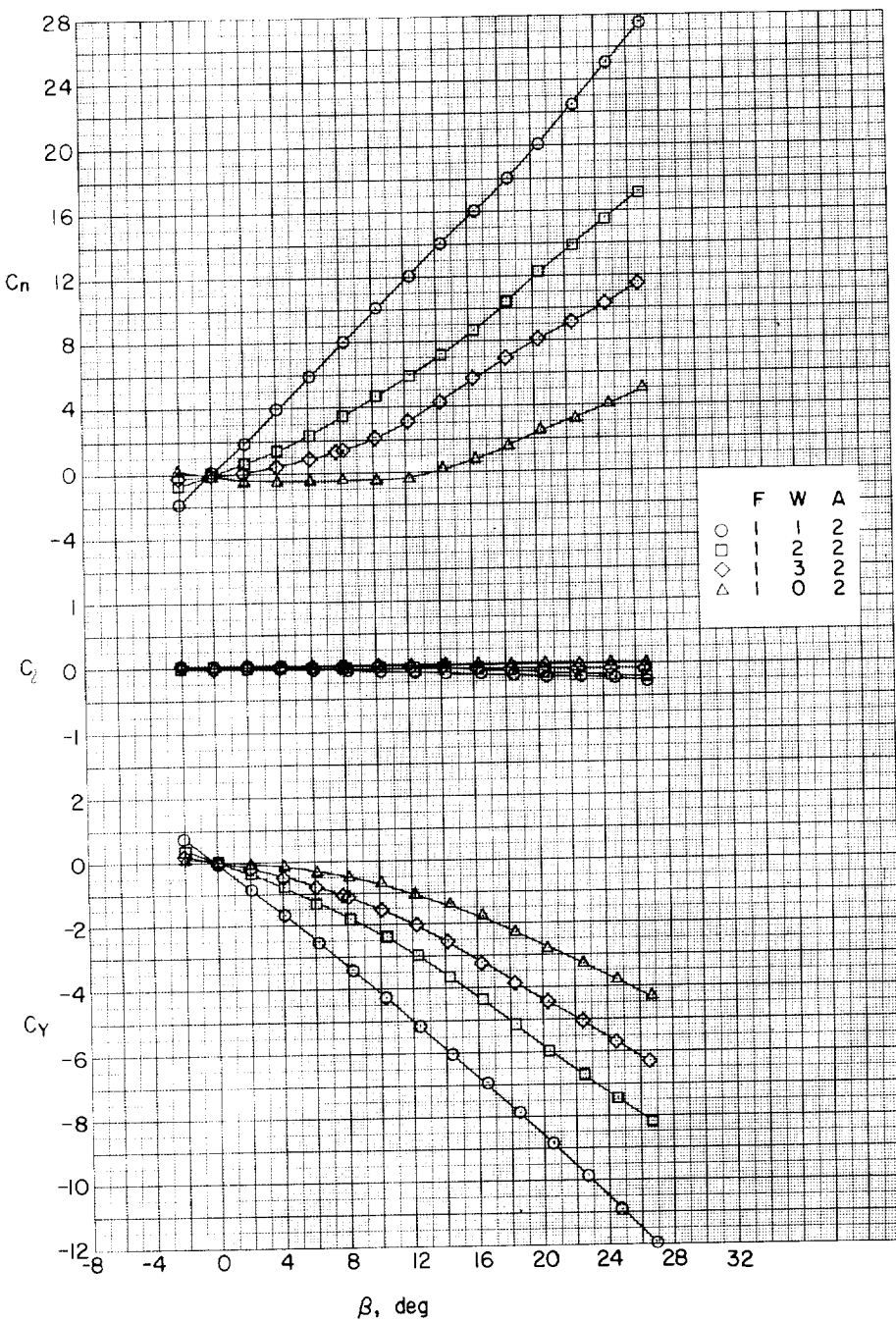
(b) $\alpha \approx 4.1^\circ$.

Figure 9.- Continued.

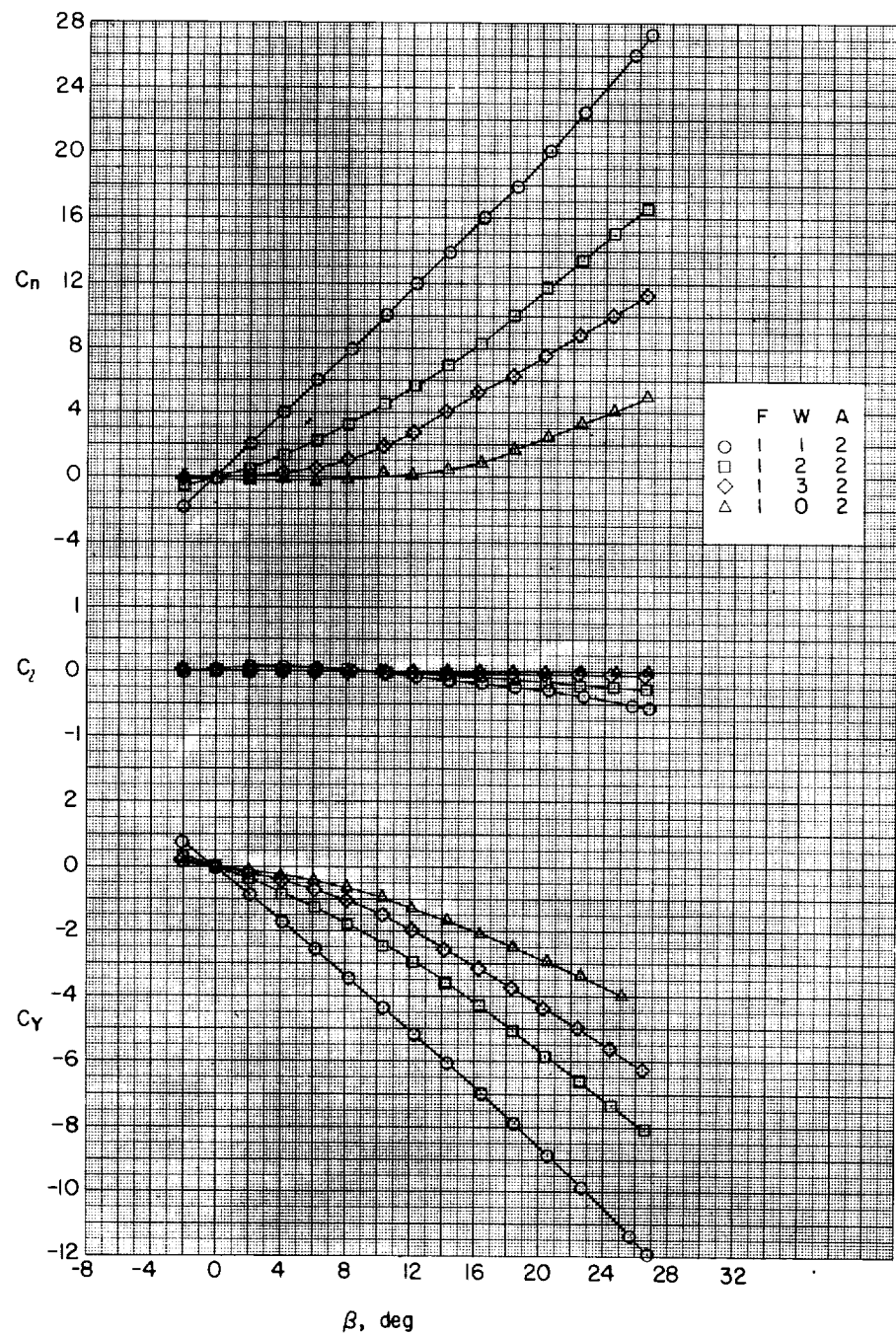
(c) $\alpha \approx 8.2^\circ$.

Figure 9.- Continued.

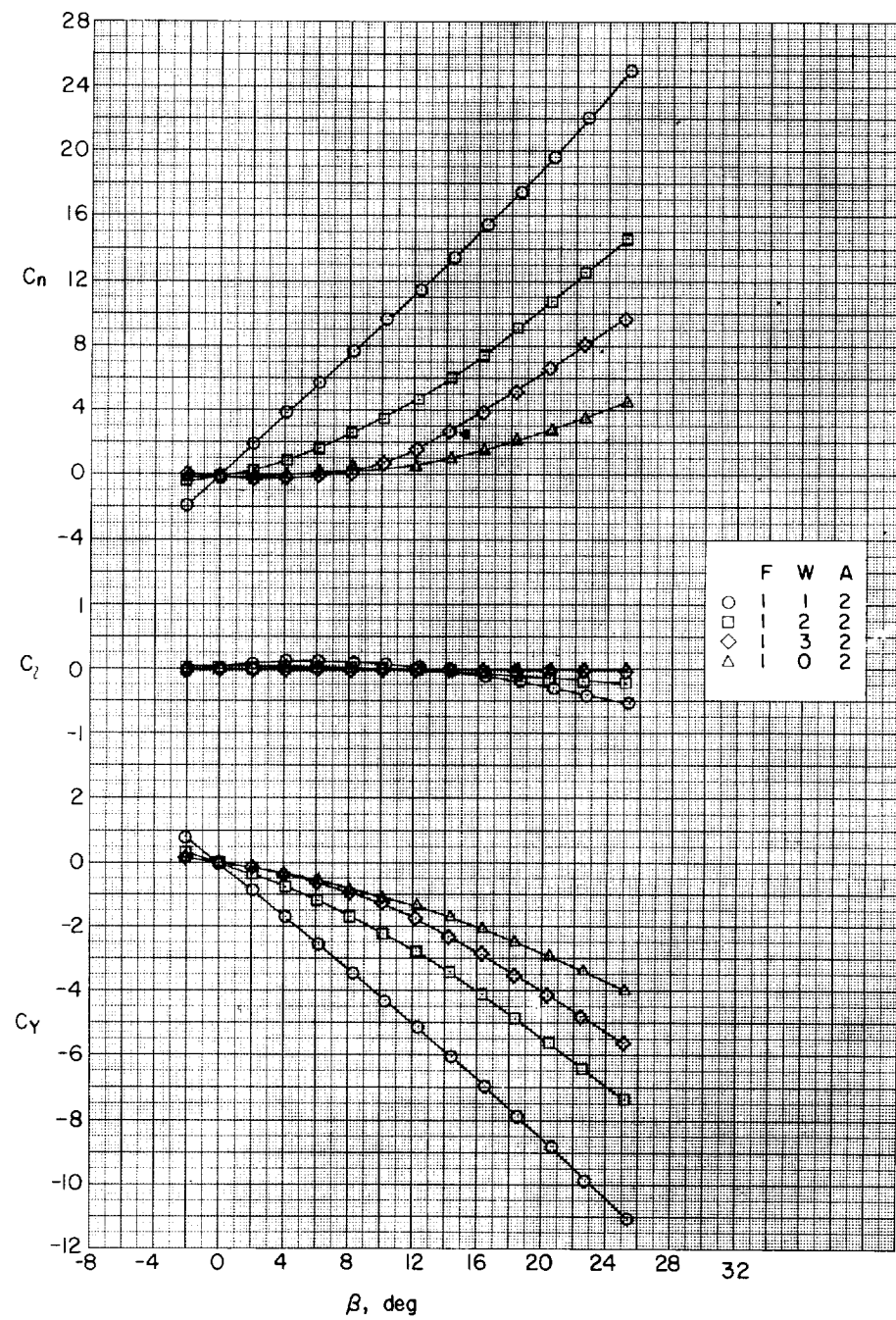
(d) $\alpha \approx 12.3^\circ$.

Figure 9.- Continued.

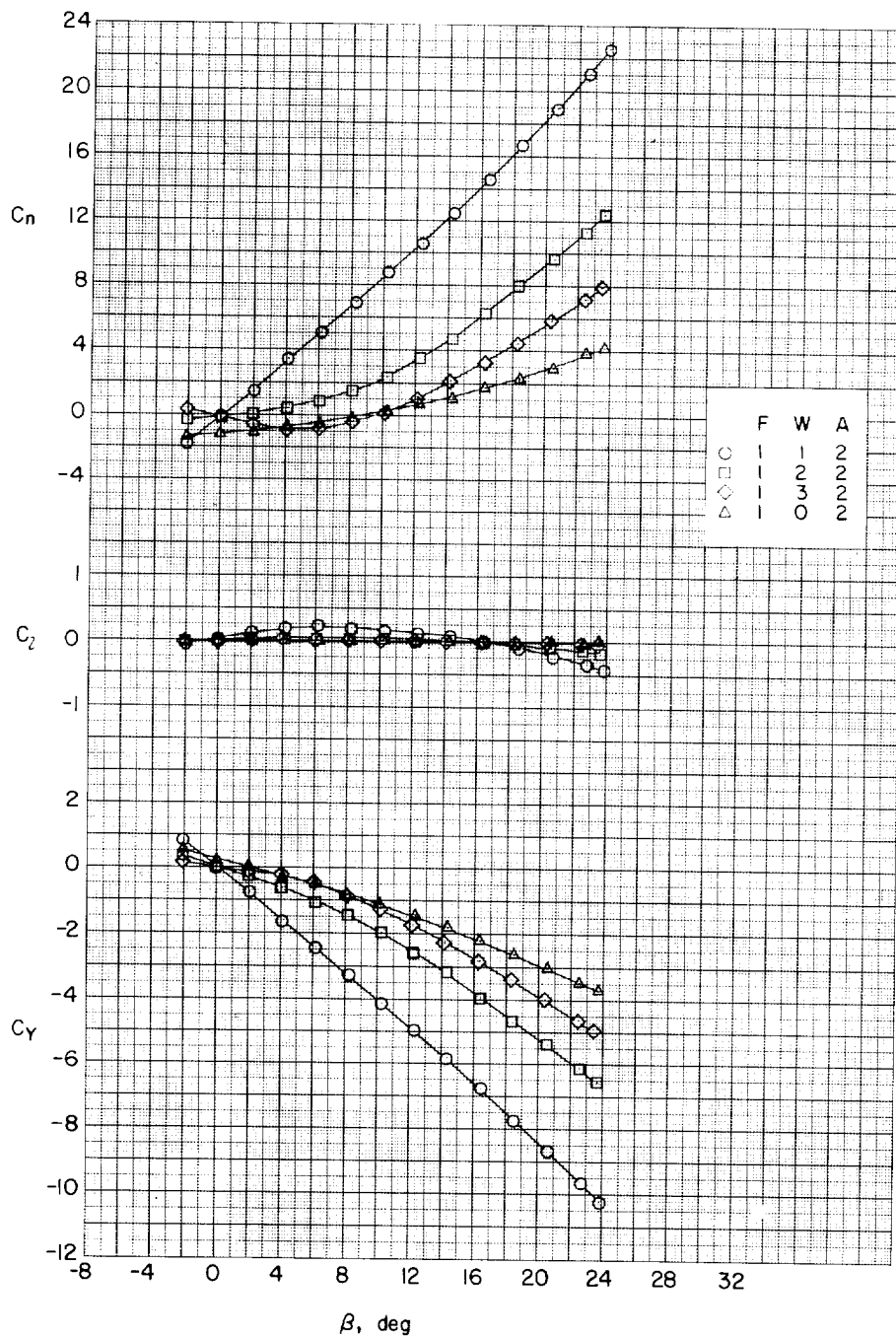
(e) $\alpha \approx 16.4^\circ$.

Figure 9.- Continued.

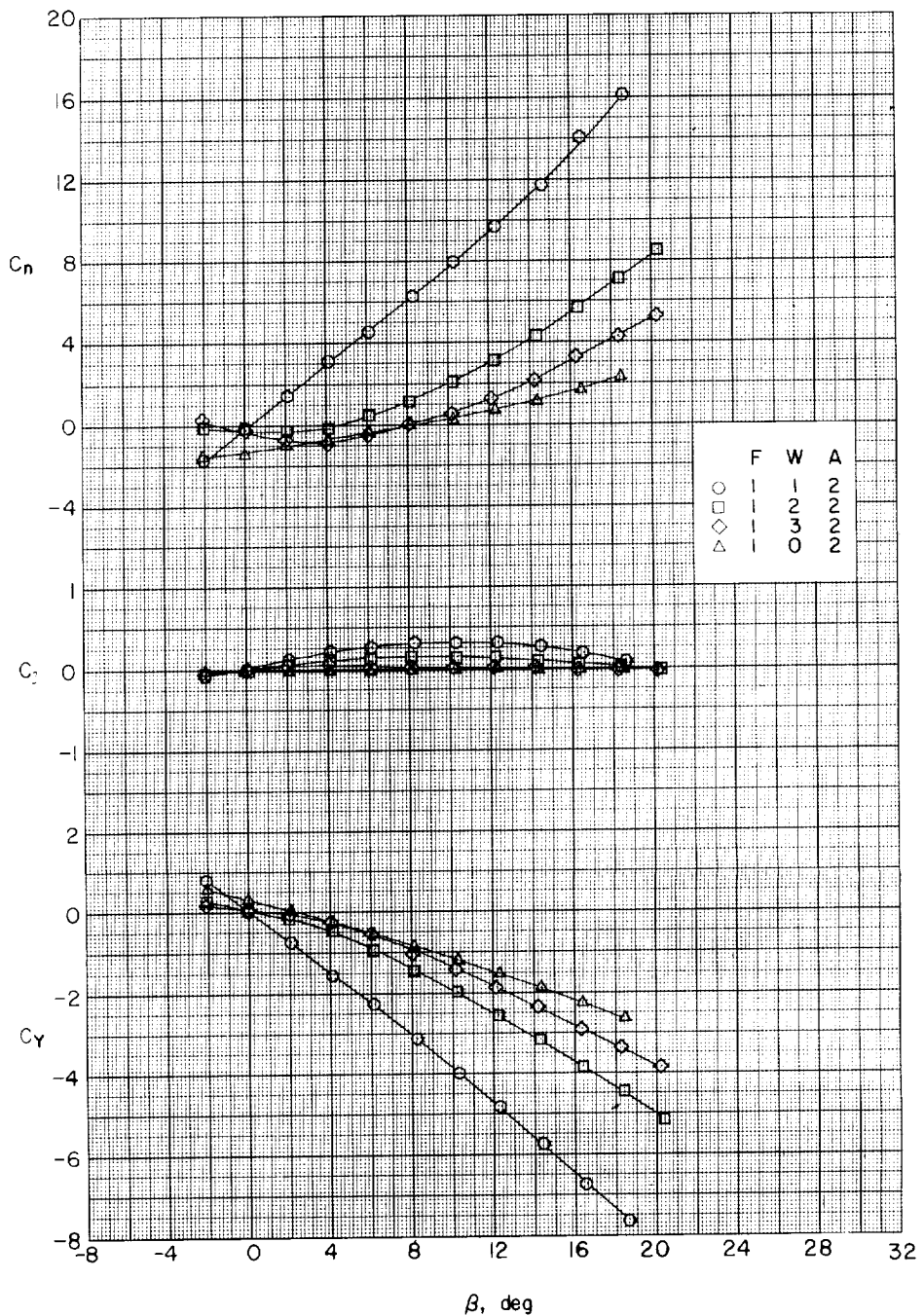
(f) $\alpha \approx 20.5^\circ$.

Figure 9.- Continued.

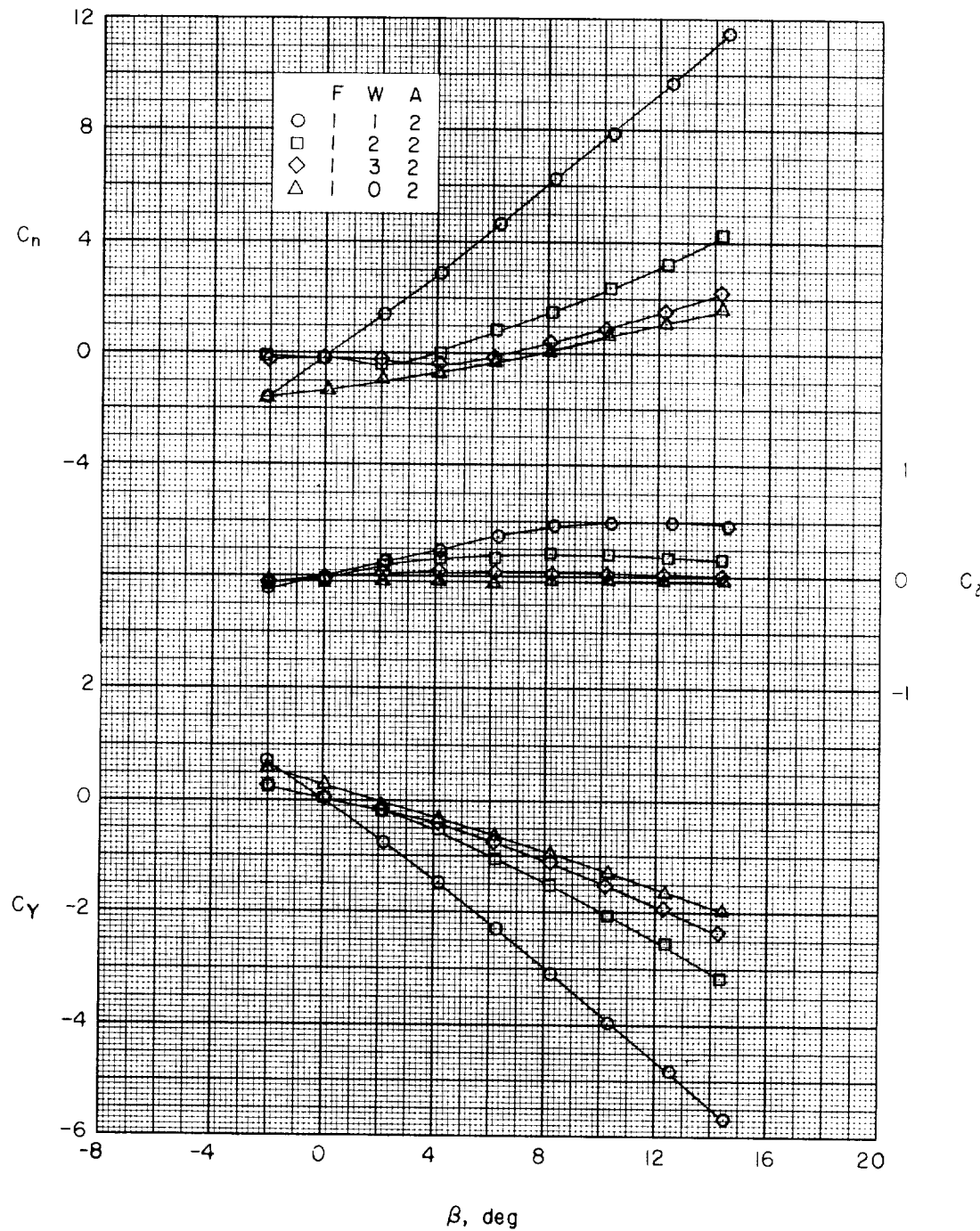
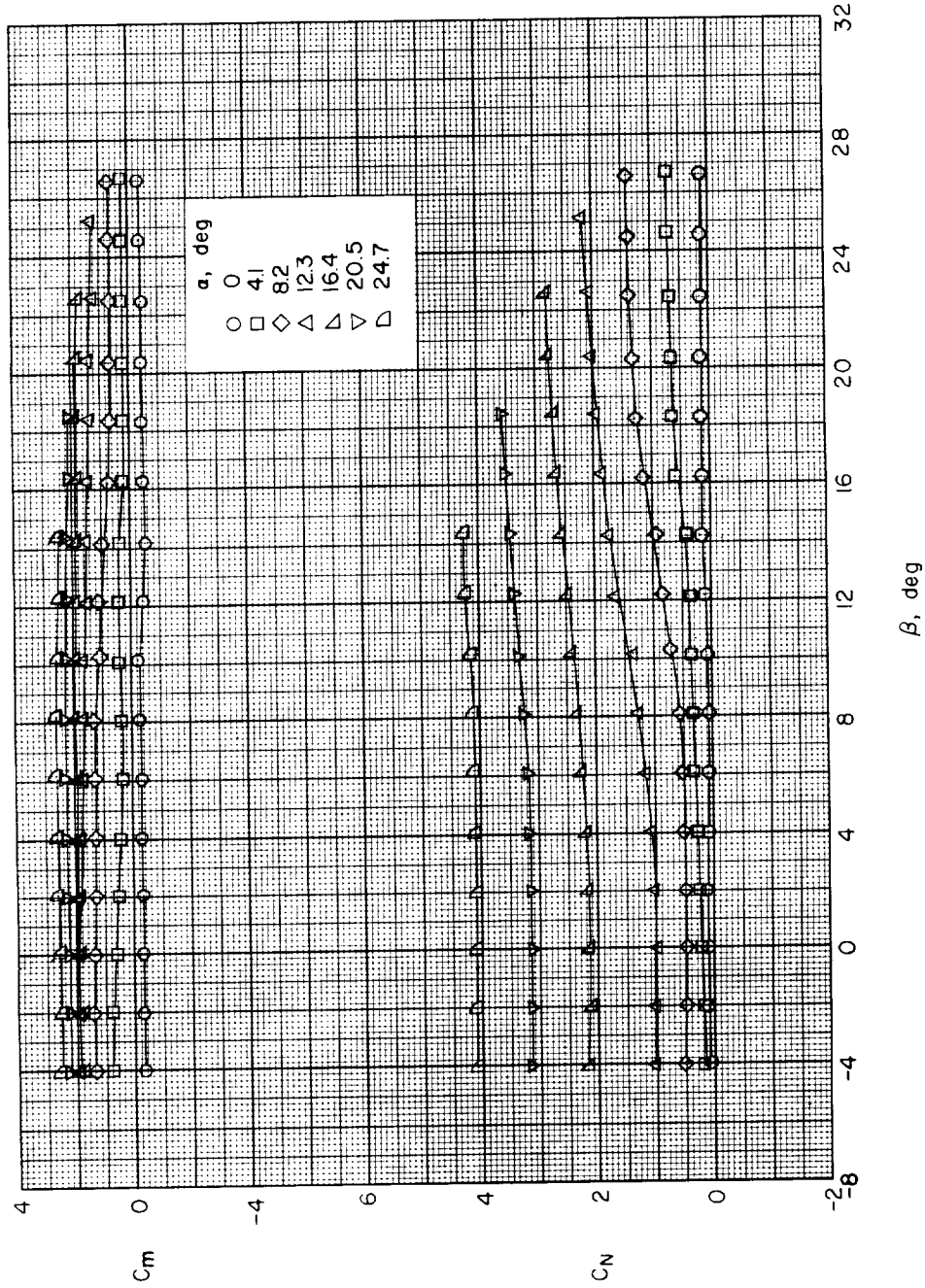
(g) $\alpha \approx 24.7^\circ$.

Figure 9.- Concluded.



(a) Body alone, $F_8 W_0 A_0$.
 Figure 10.- Variation of C_m and C_N with β for various angles of attack. Delta-wing series;
 no afterbody; $l/d = 10$.

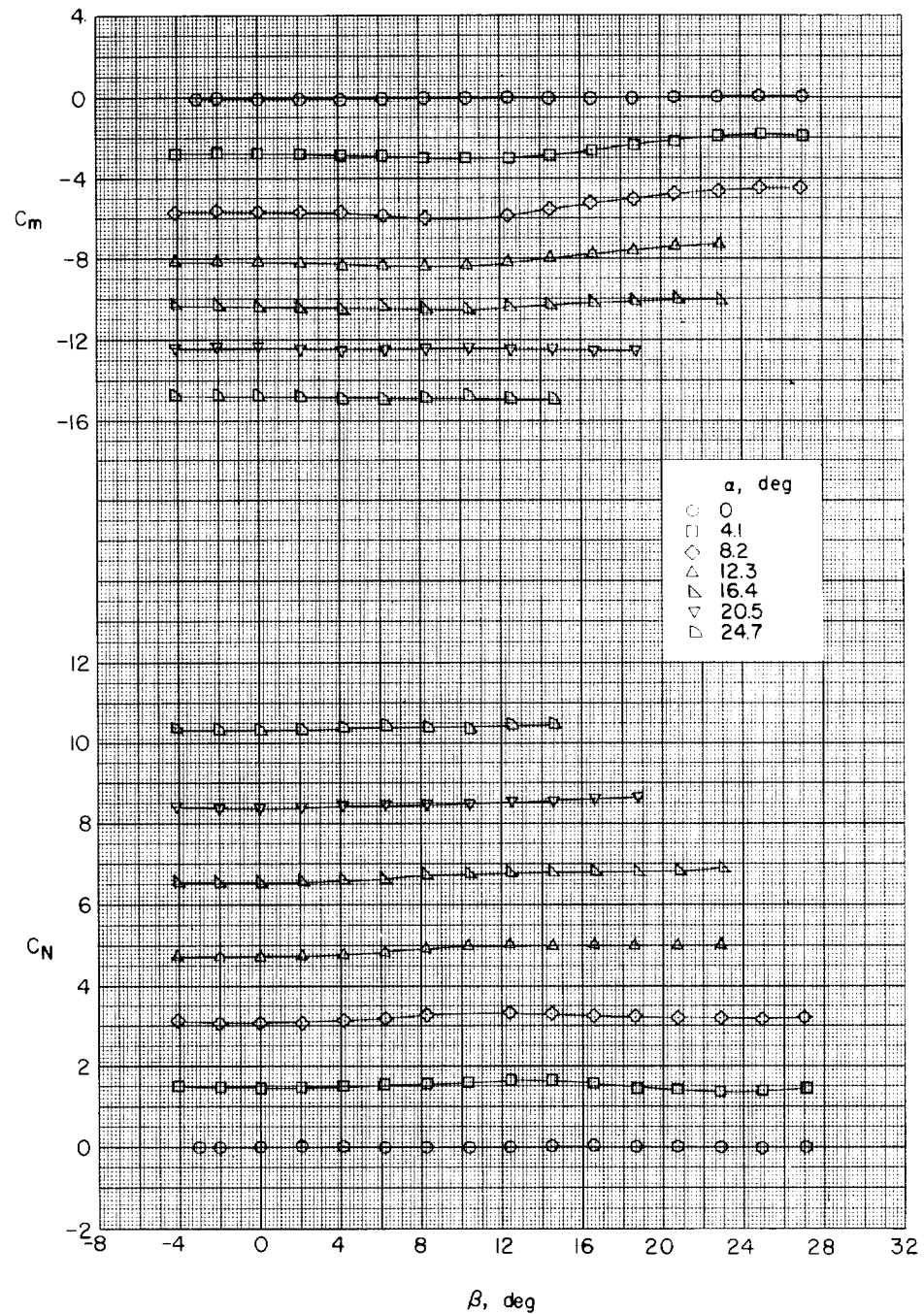
(b) Large delta wing, $F_8W_1A_0$.

Figure 10-- Continued.

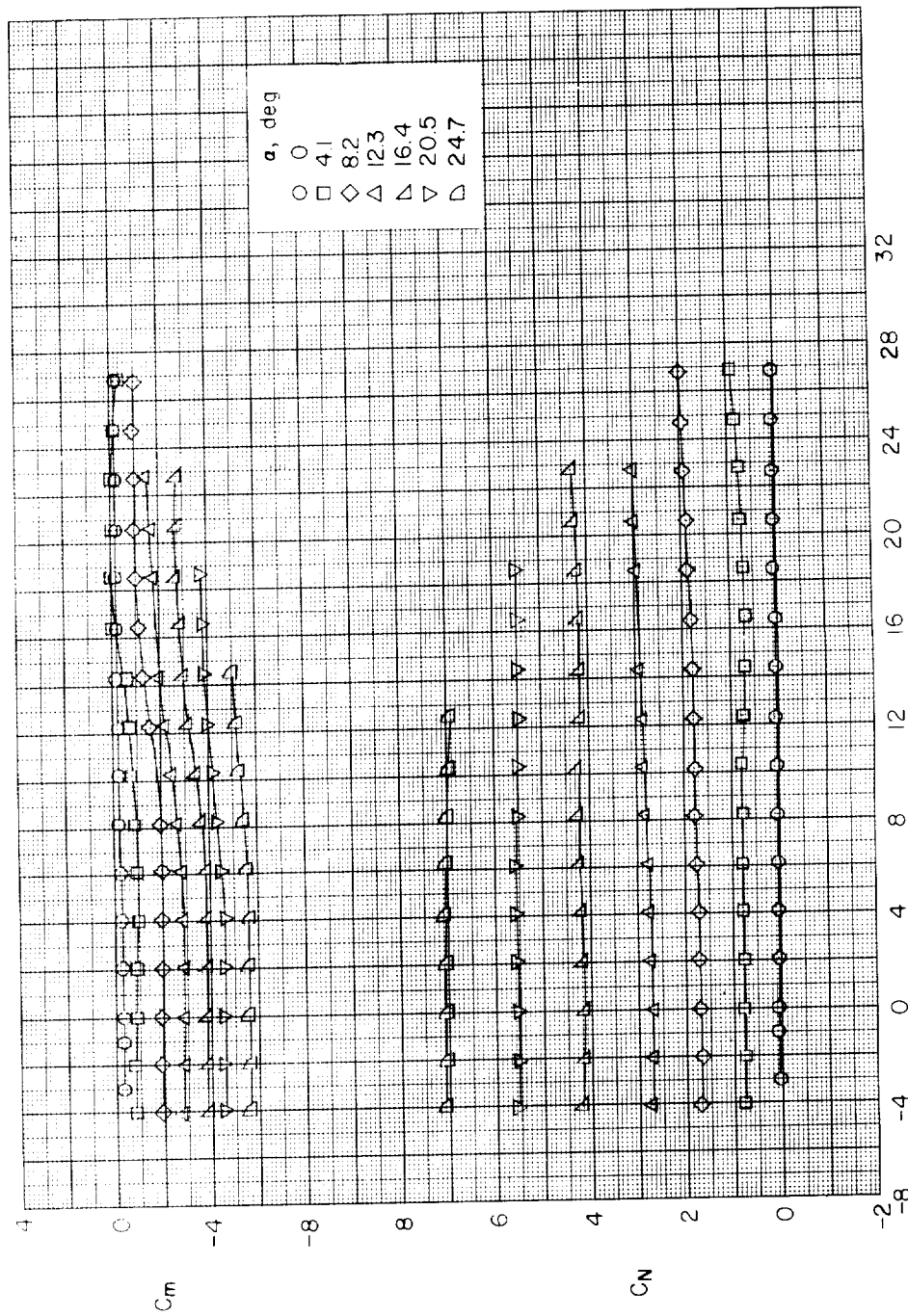
(c) Medium delta wing, $F_8W_2A_0$.

Figure 10.- Continued.

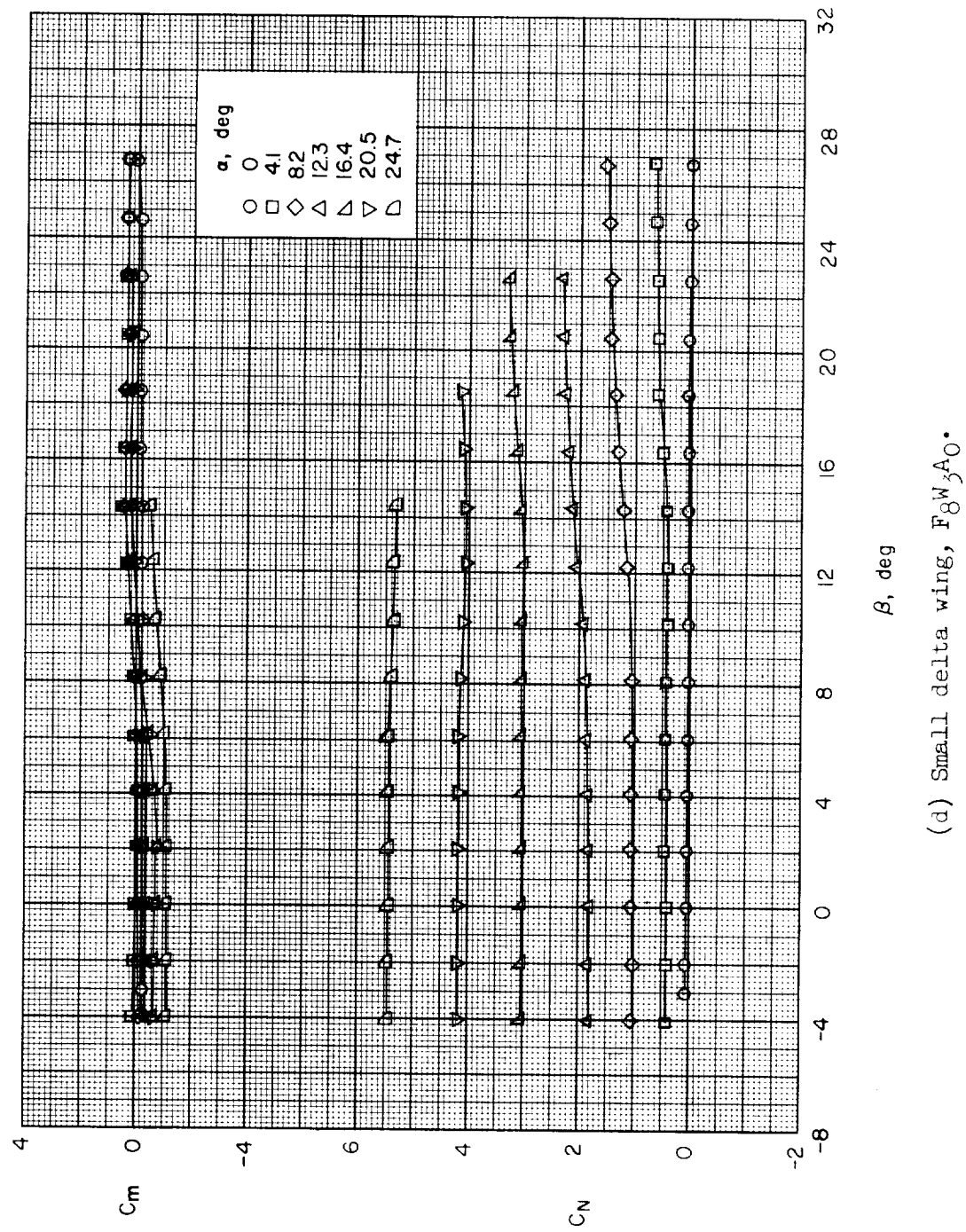
(d) Small delta wing, $F_8 W_{\frac{1}{2}A_0}$.

Figure 10.- Concluded.

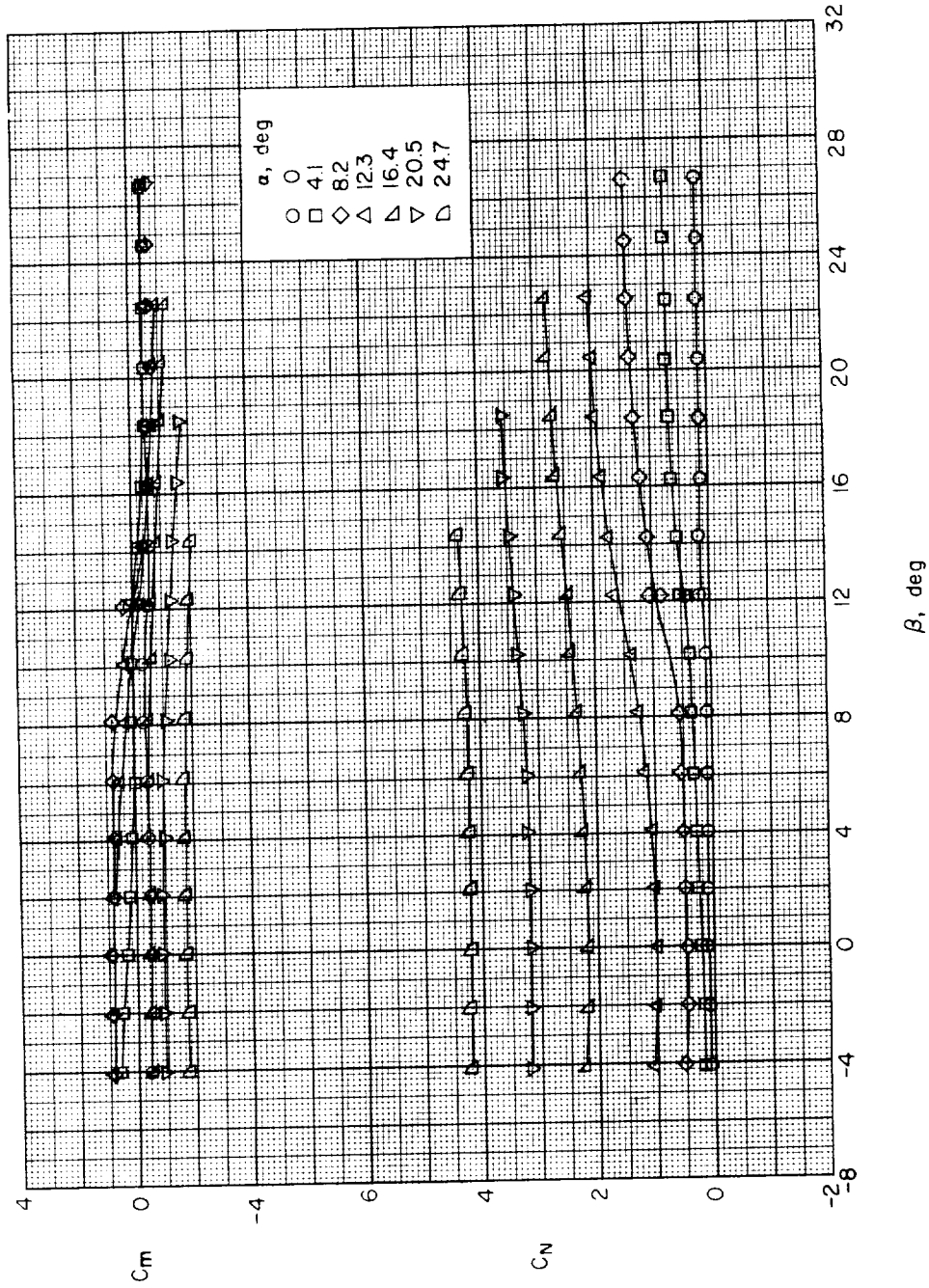
(a) Body alone, F_{7W0A1}.

Figure 11.- Variation of C_m and C_N with β for various angles of attack. Delta-wing series; 1-caliber cylindrical afterbody; $l/d = 10$.

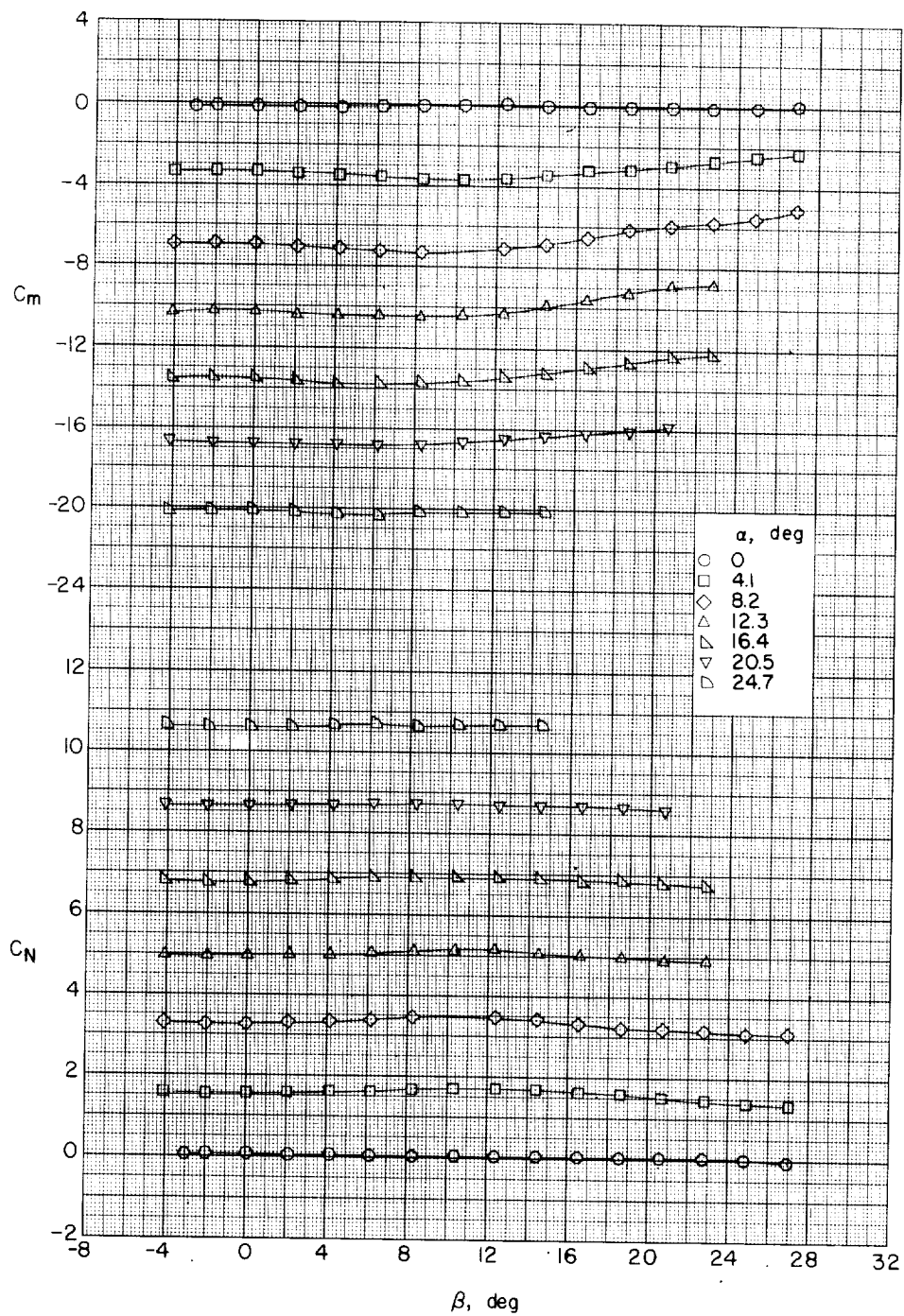
(b) Large delta wing, $F_7W_1A_0$.

Figure 11.- Continued..

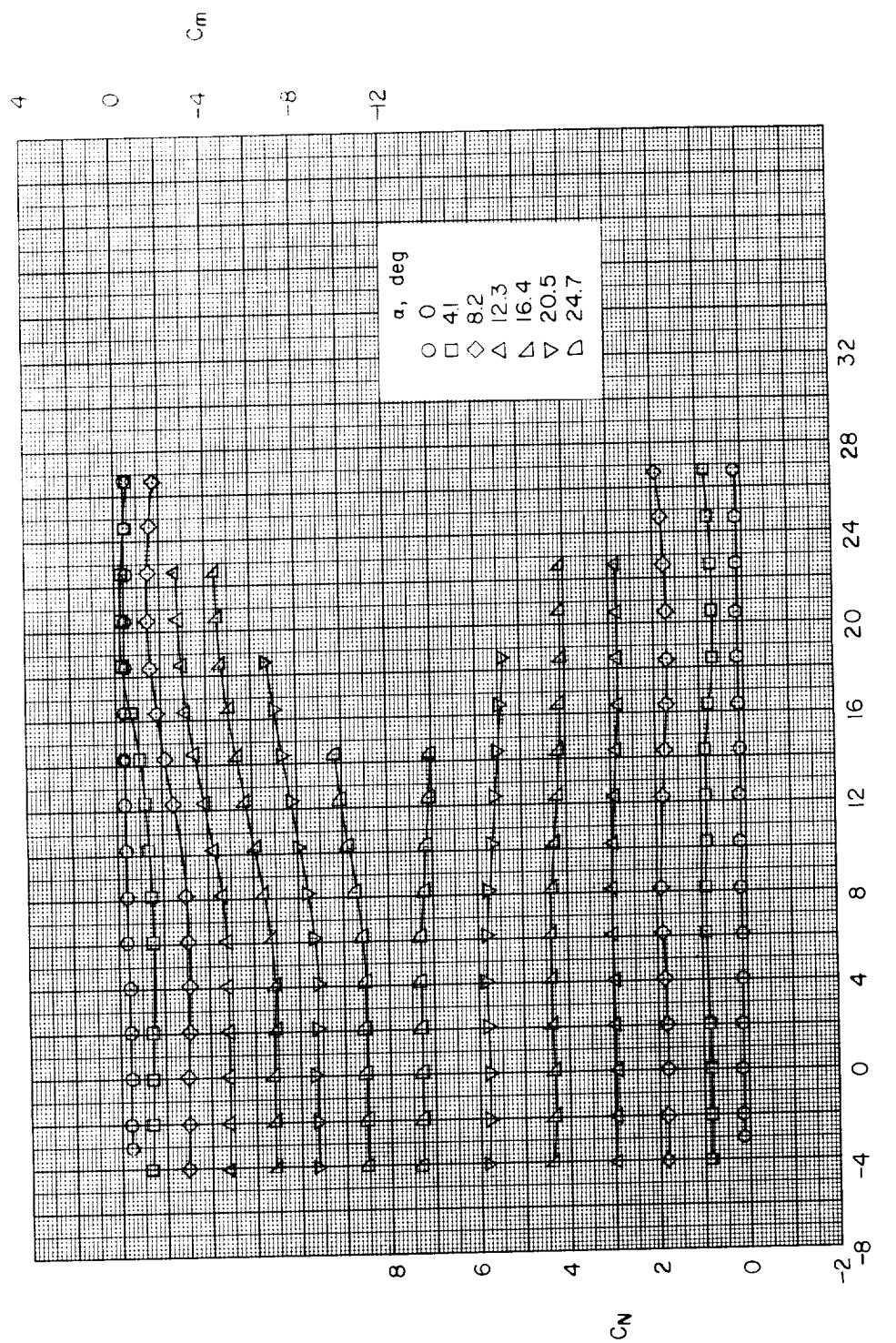
(c) Medium delta wing, $F_7W_2A_1$.

Figure 11.- Continued.

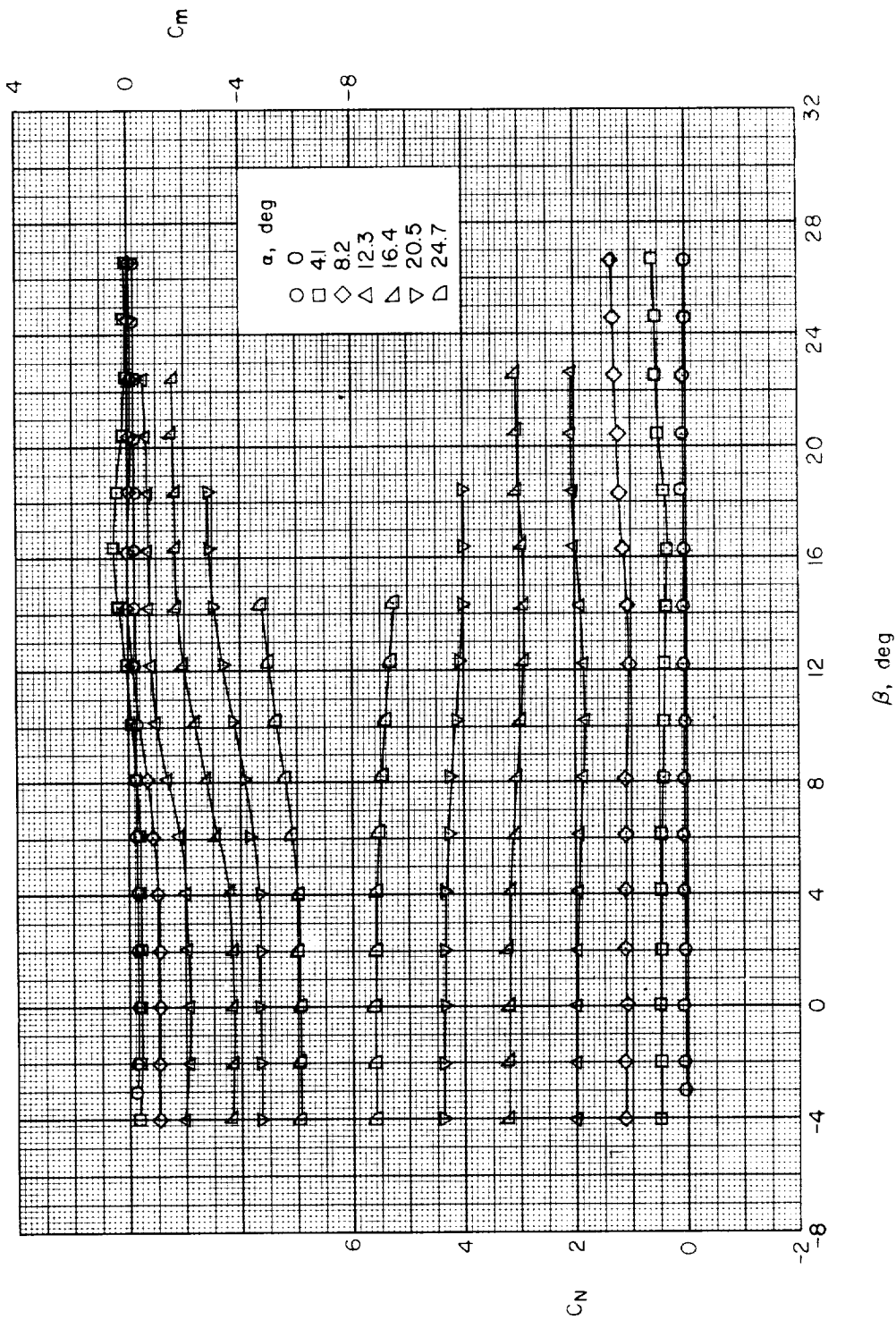
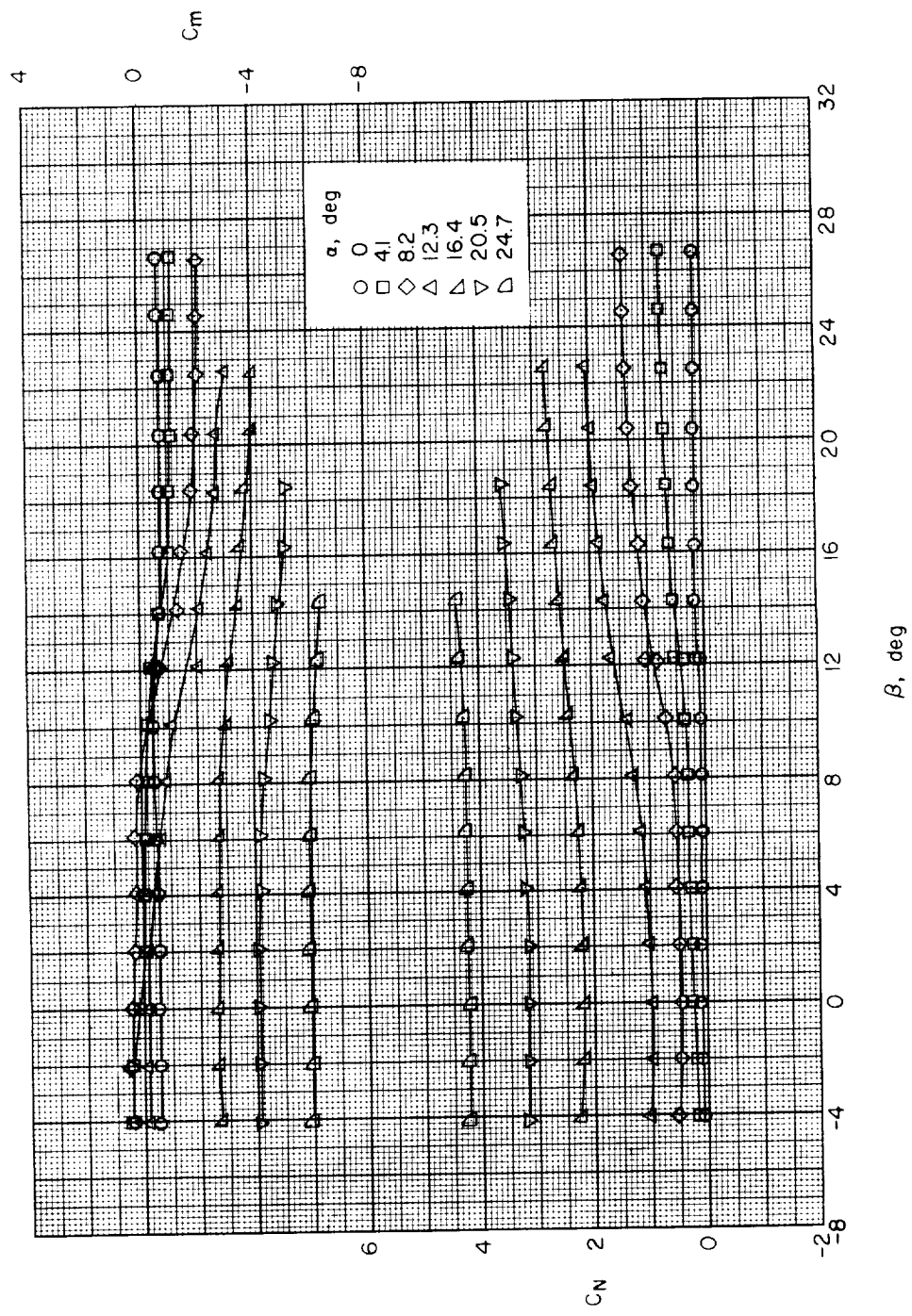
(d) Small delta wing, $F_7^W \delta A_1$.

Figure 11.- Concluded.



(a) Body alone, F1W0A2.

Figure 12.- Variation of C_m and C_N with β for various angles of attack. Delta-wing series;
2-caliber cylindrical afterbody; $l/d = 10$.

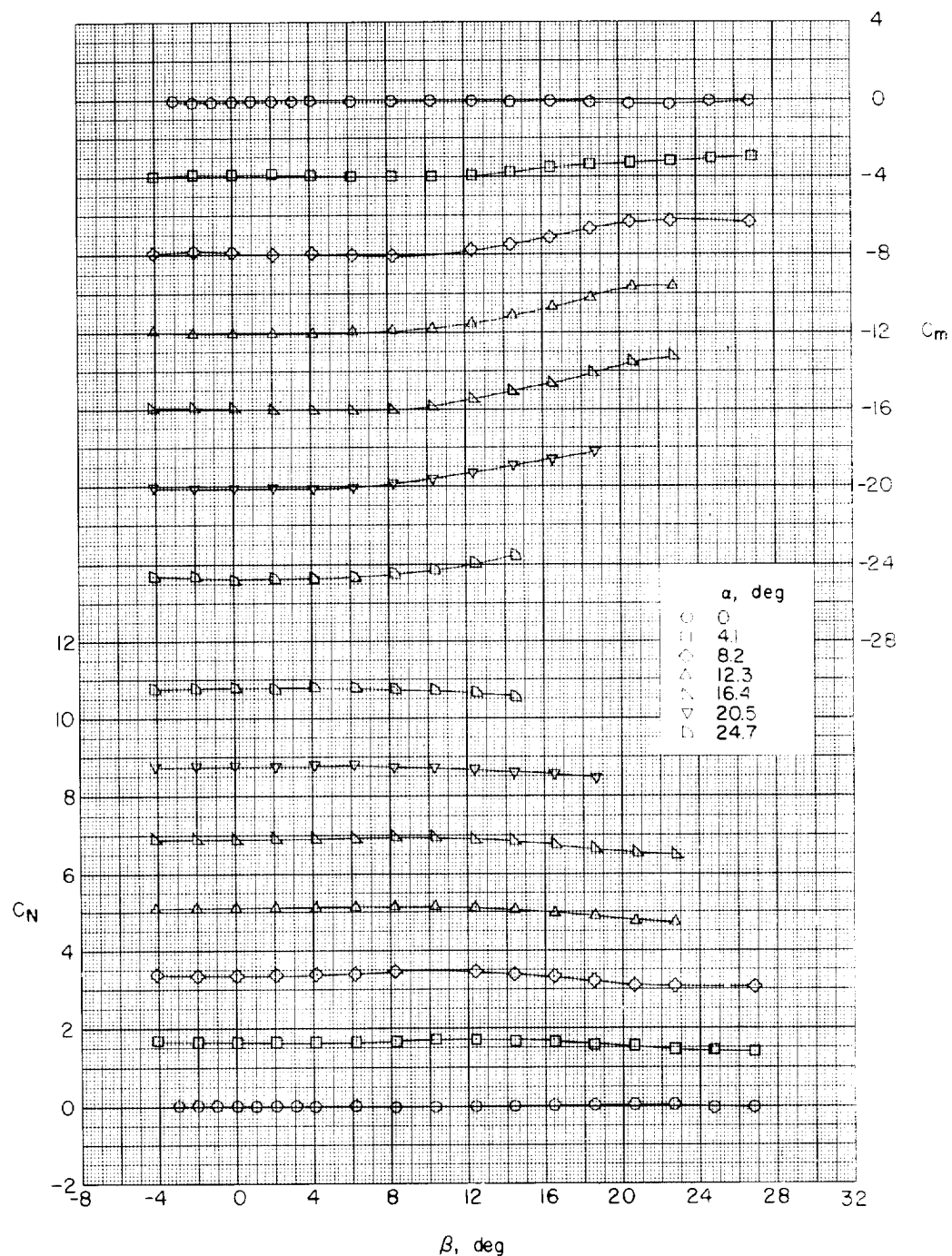
(b) Large delta wing, $F_1 W_1 A_2$.

Figure 12.- Continued.

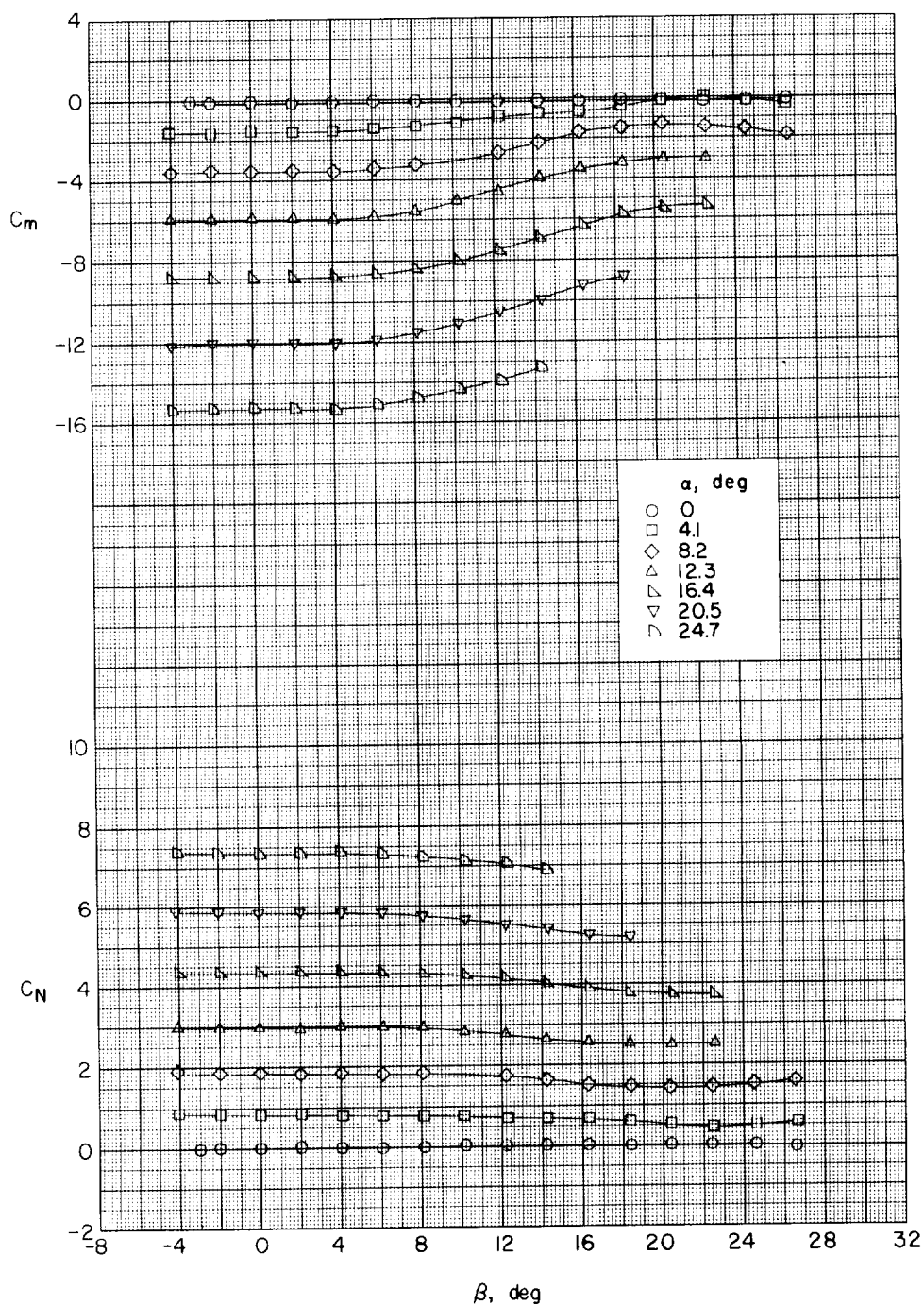
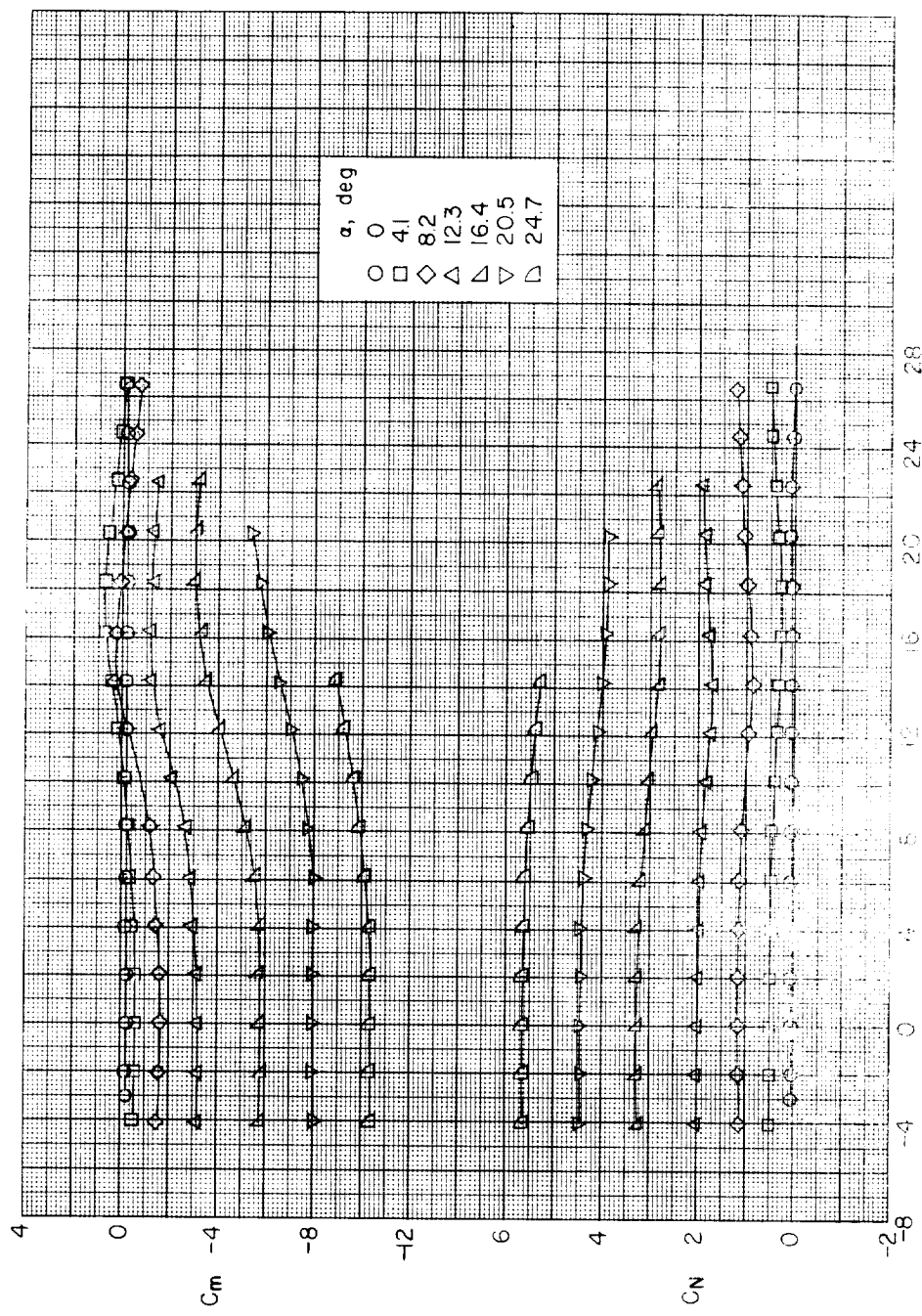
(c) Medium delta wing, $F_1W_2A_2$.

Figure 12.- Continued.



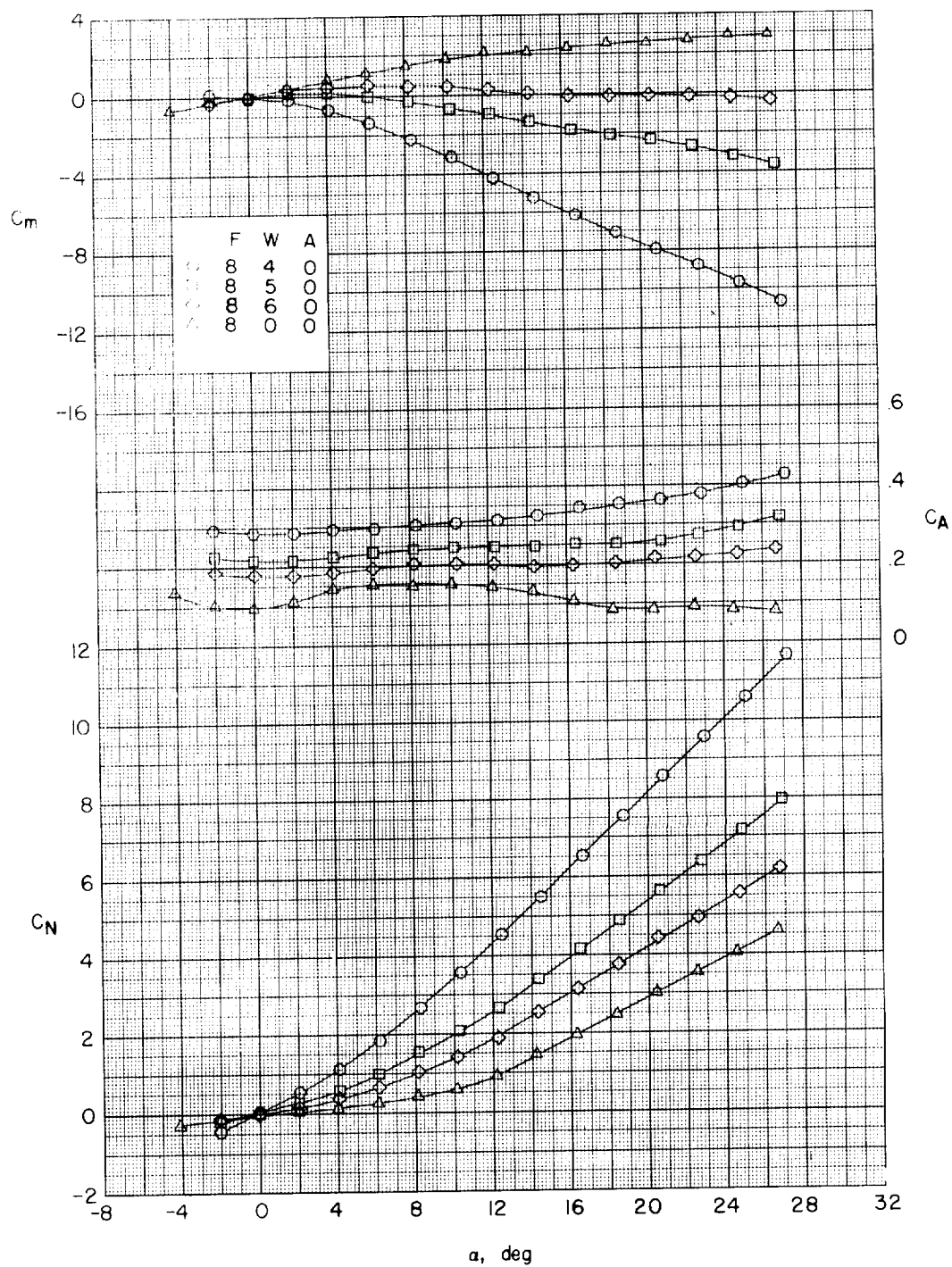


Figure 13.- Effect of rectangular wings on aerodynamic characteristics in pitch. No afterbody; $l/d = 10$.

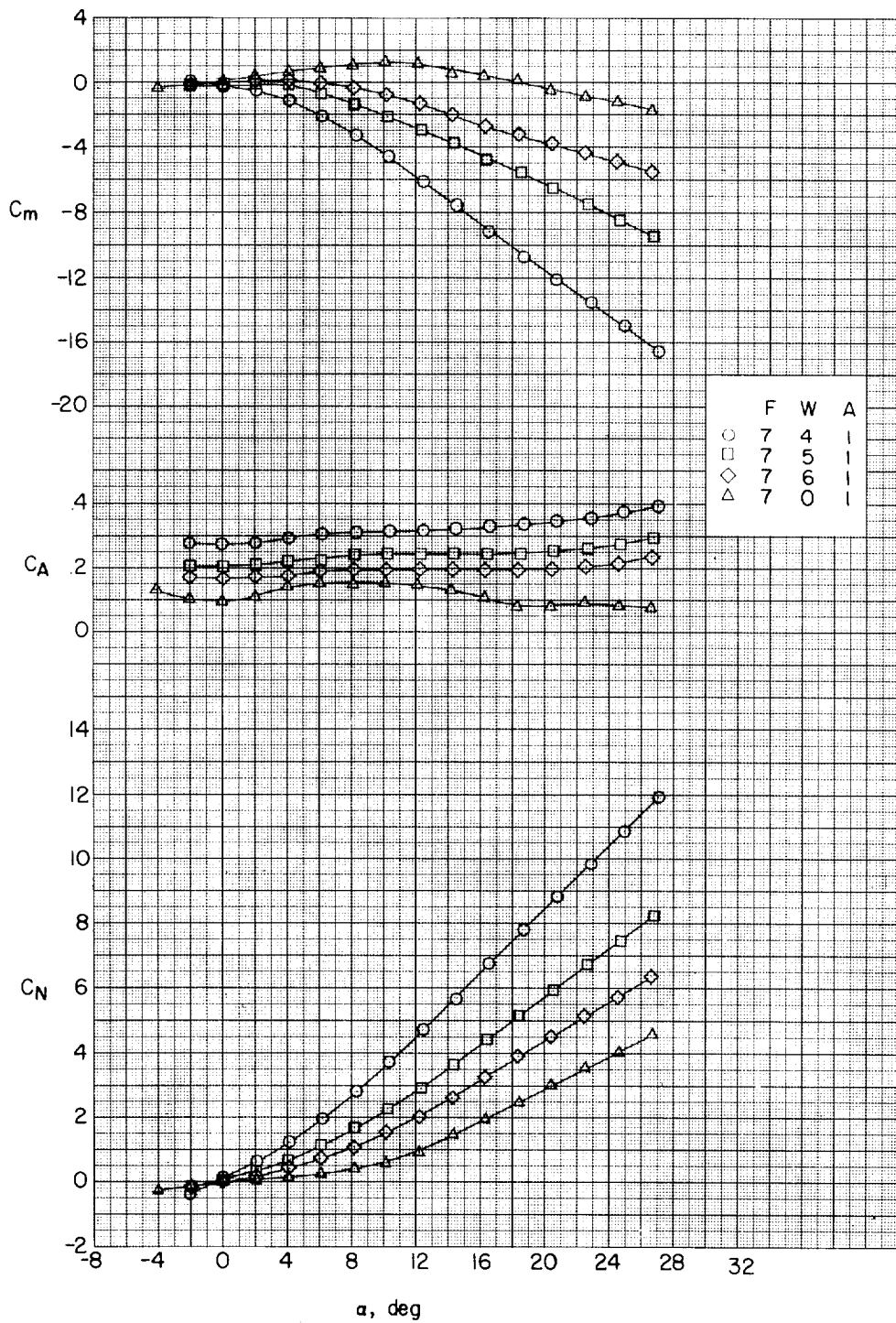


Figure 14.- Effect of rectangular wings on aerodynamic characteristics in pitch. One-caliber cylindrical afterbody; $l/d = 10$.

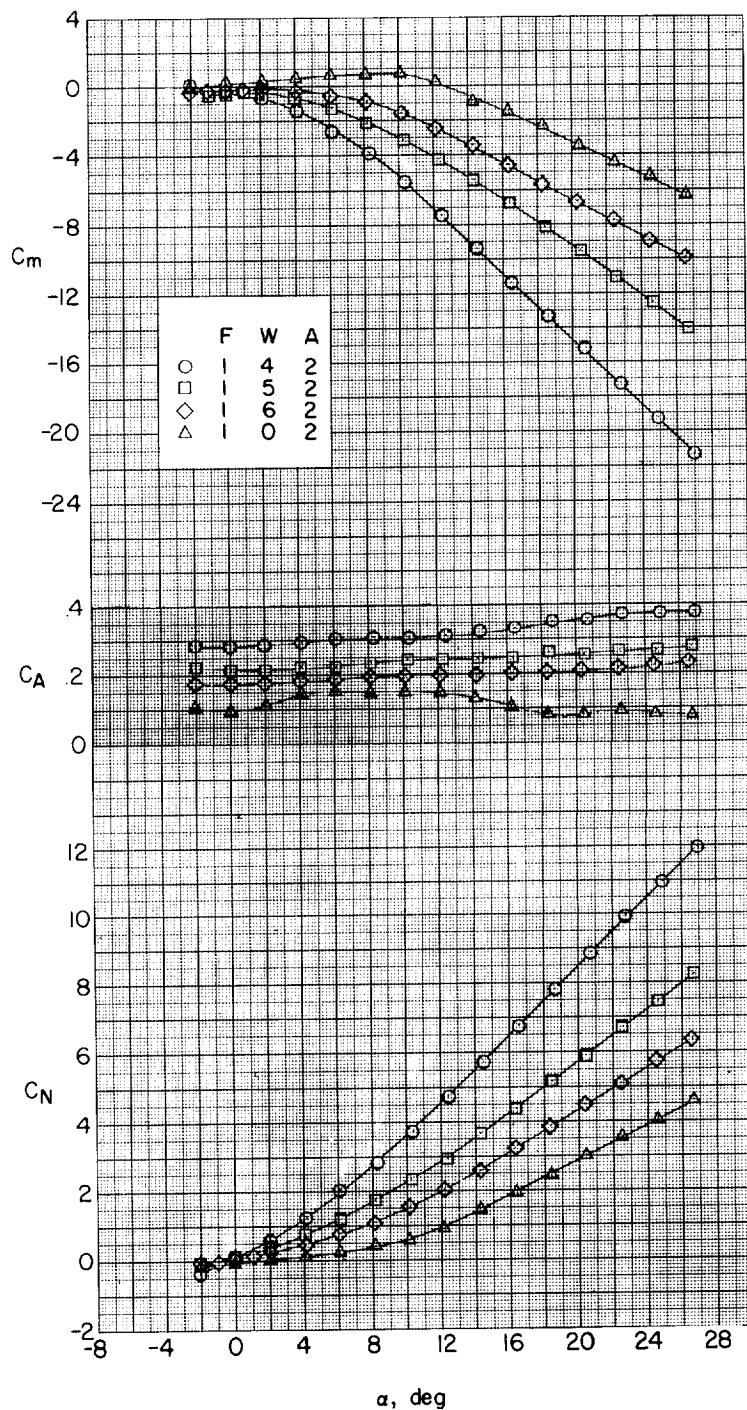


Figure 15.- Effect of rectangular wings on aerodynamic characteristics in pitch. Two-caliber cylindrical afterbody; $l/d = 10$.

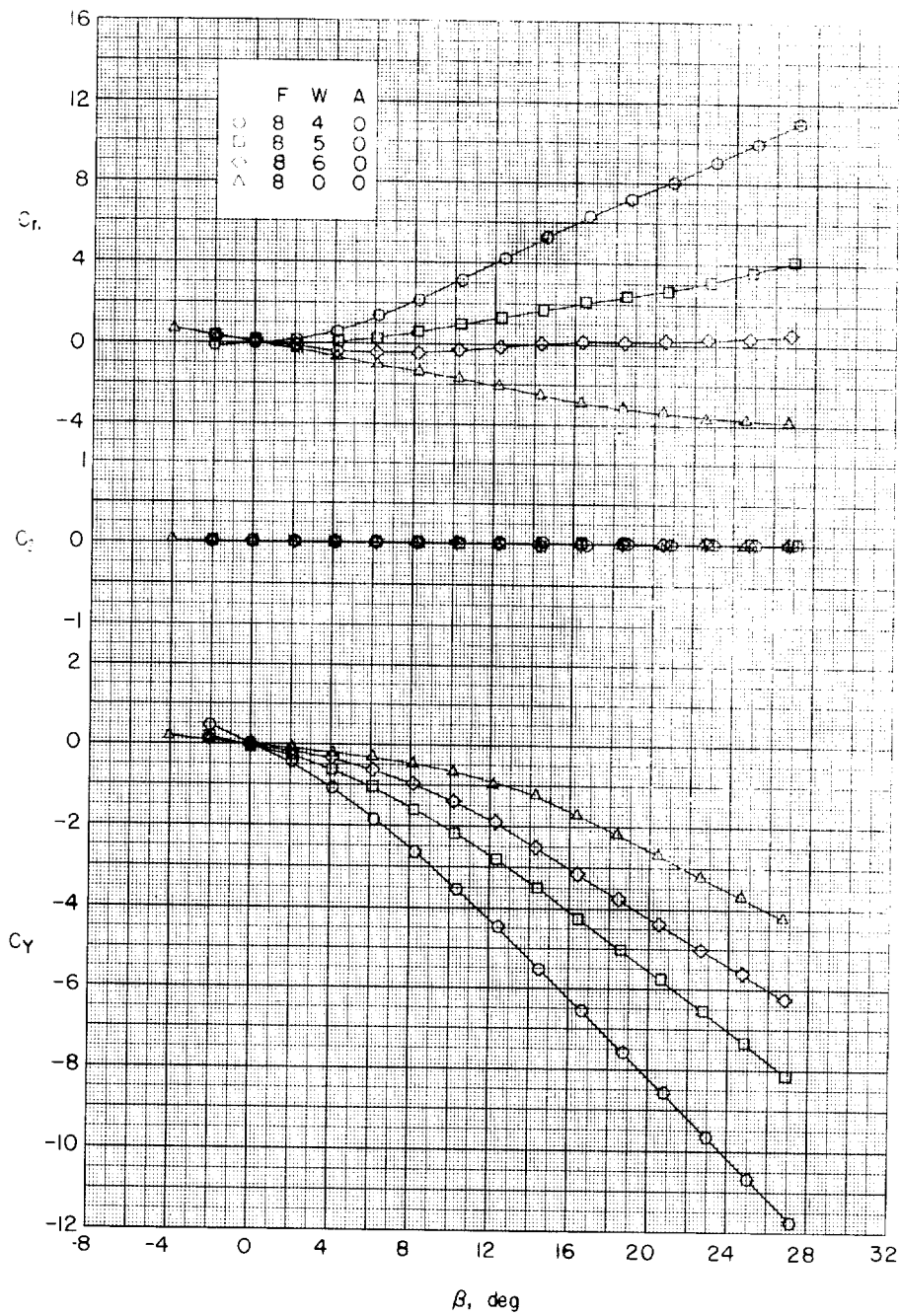
(a) $\alpha \approx 0^\circ$.

Figure 16.- Effect of rectangular wings on aerodynamic characteristics in sideslip. No afterbody; $l/d = 10$.

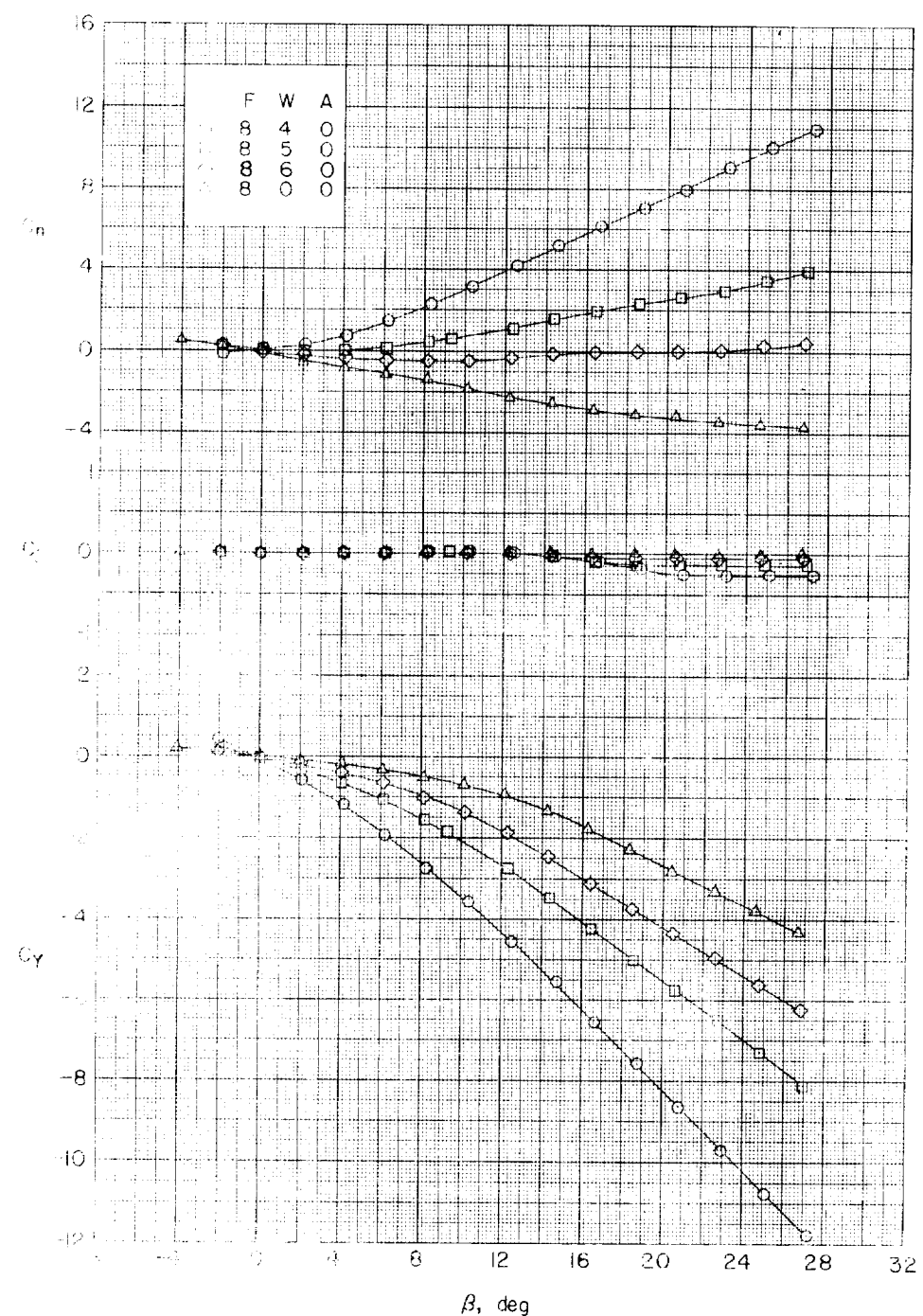
(b) $\alpha \approx 4.1^\circ$.

Figure 16.- Continued.

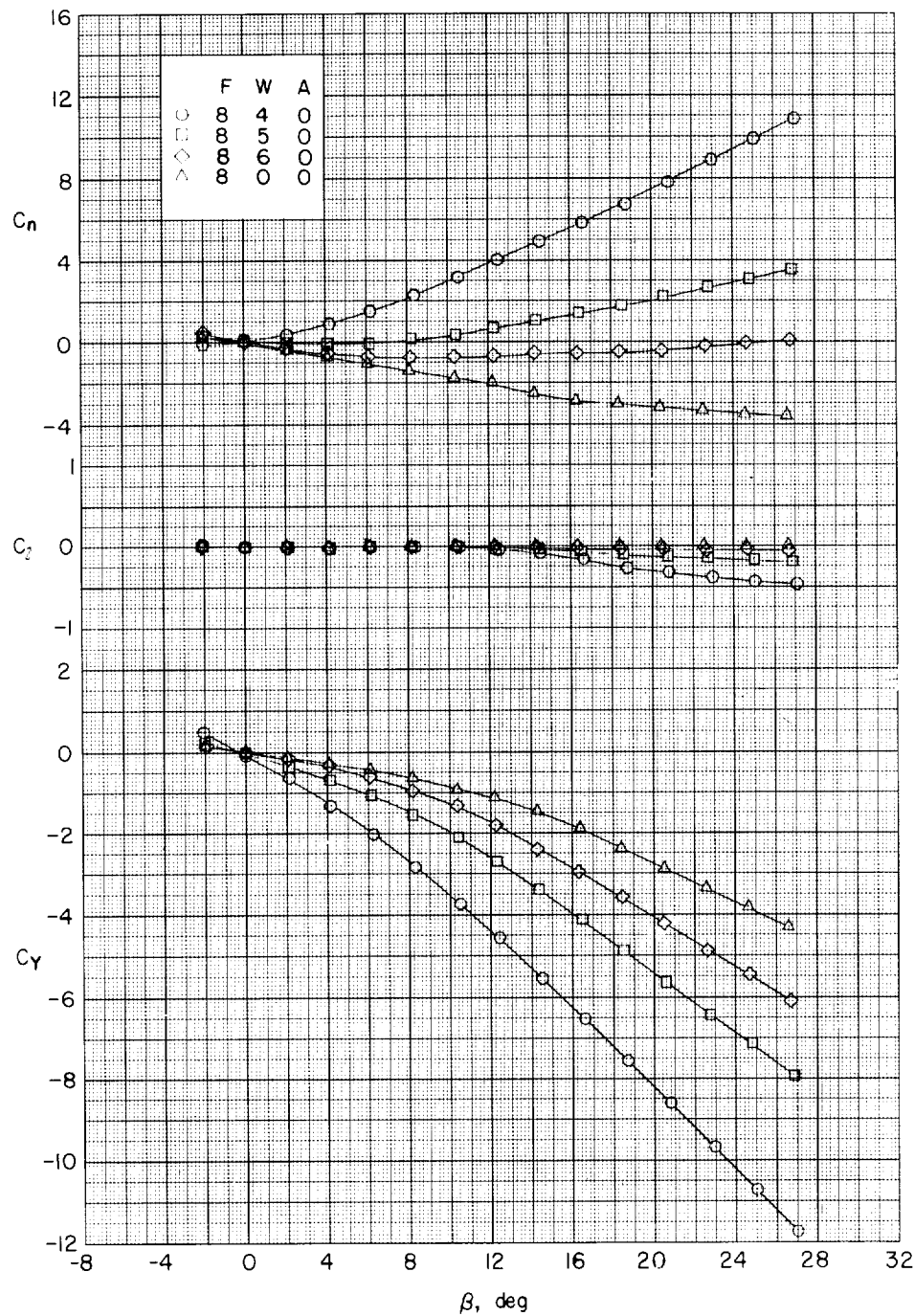
(c) $\alpha \approx 8.2^\circ$.

Figure 16.- Continued.

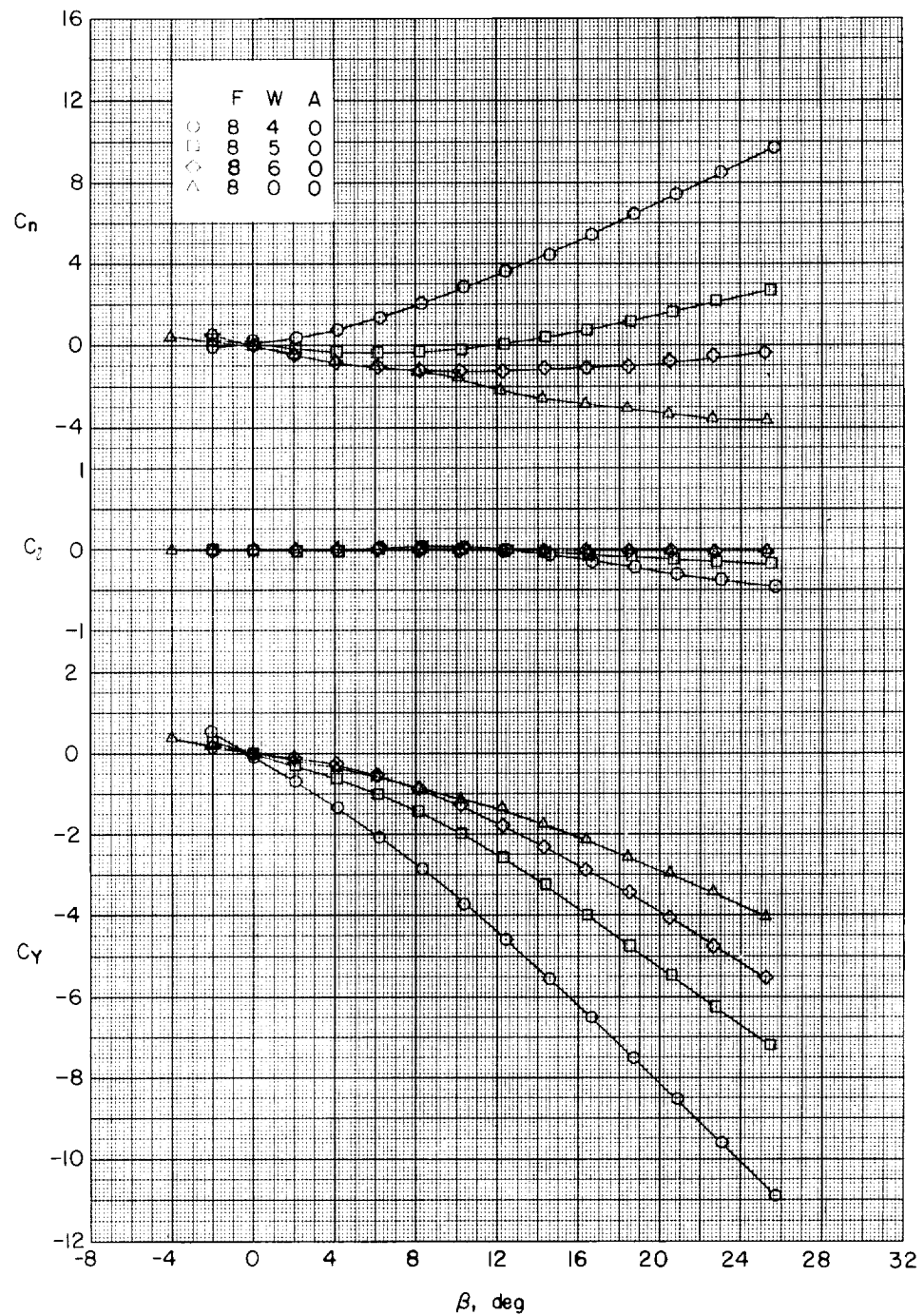
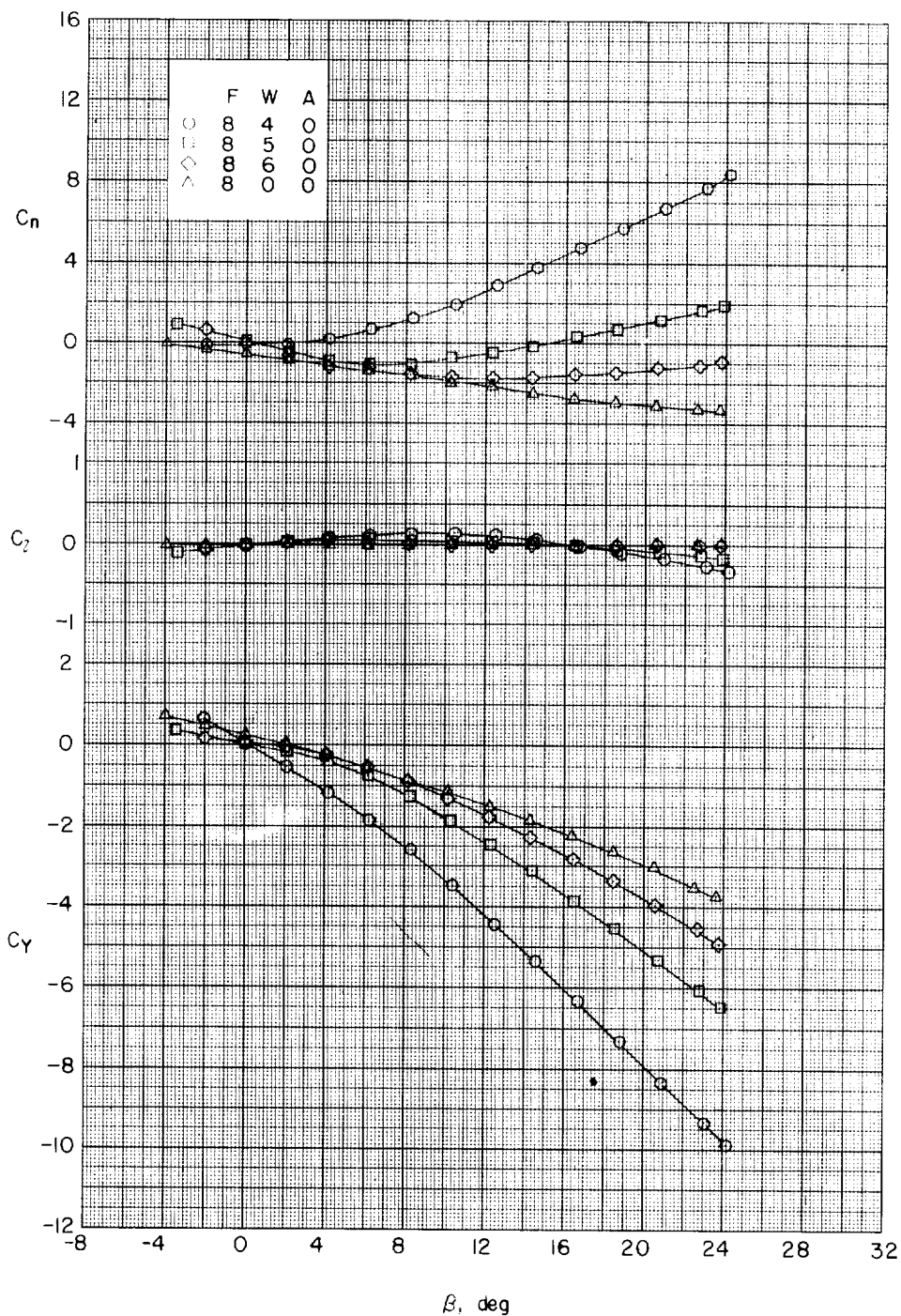
(d) $\alpha \approx 12.3^\circ$.

Figure 16.- Continued.



(e) $\alpha \approx 16.4^\circ$.

Figure 16.- Continued.

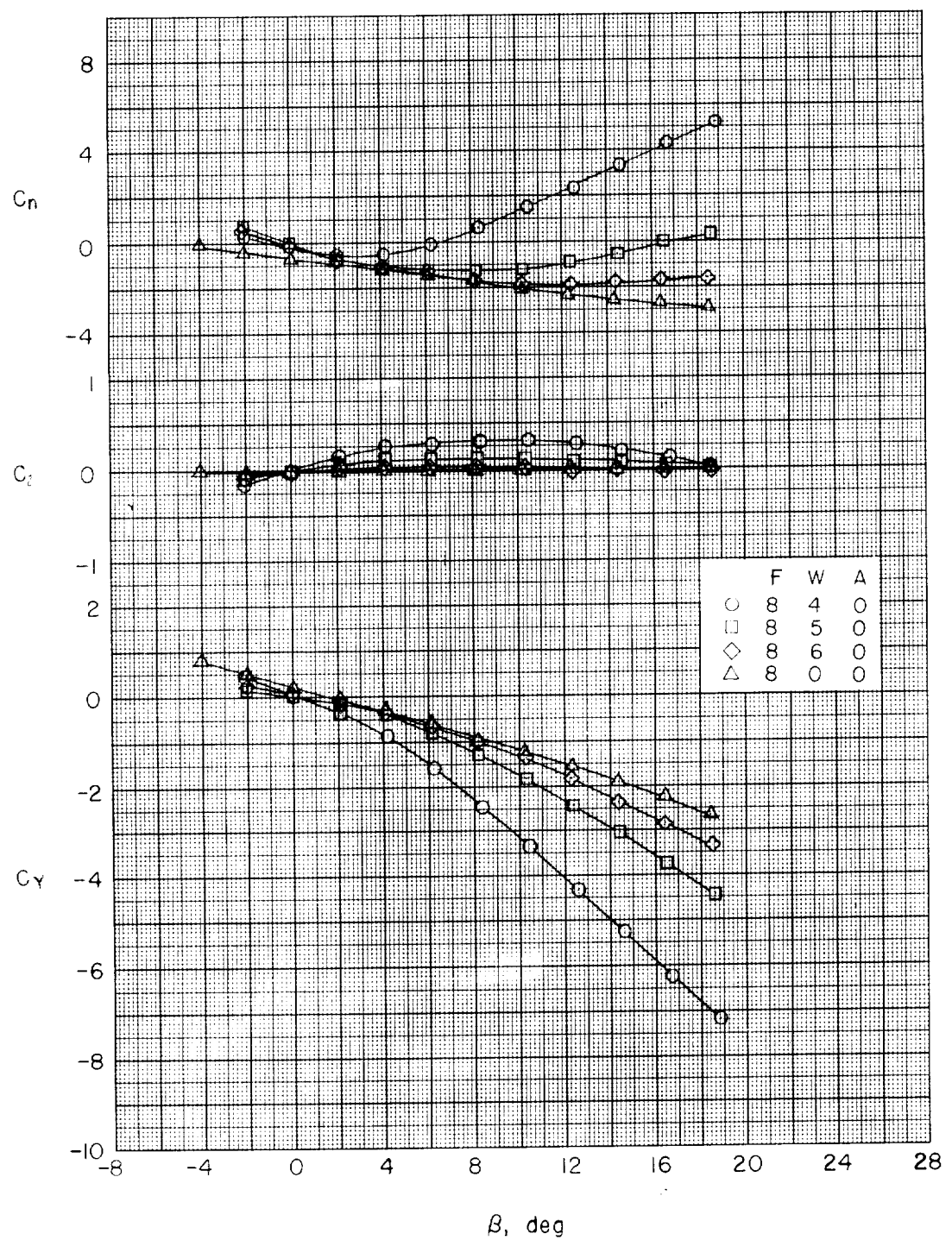
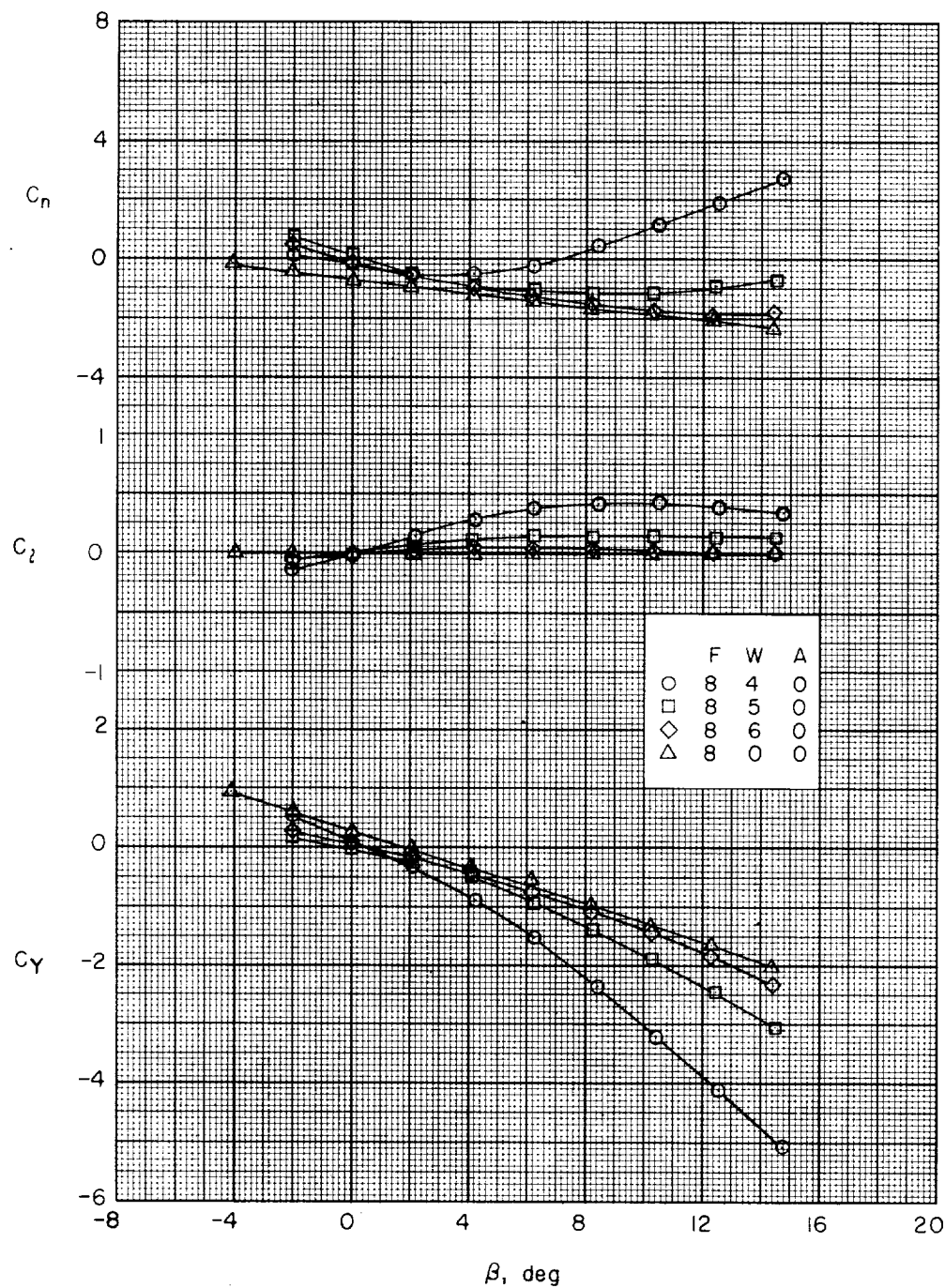
(f) $\alpha \approx 20.5^\circ$.

Figure 16.- Continued.



(g) $\alpha \approx 24.7^\circ$.

Figure 16.- Concluded.

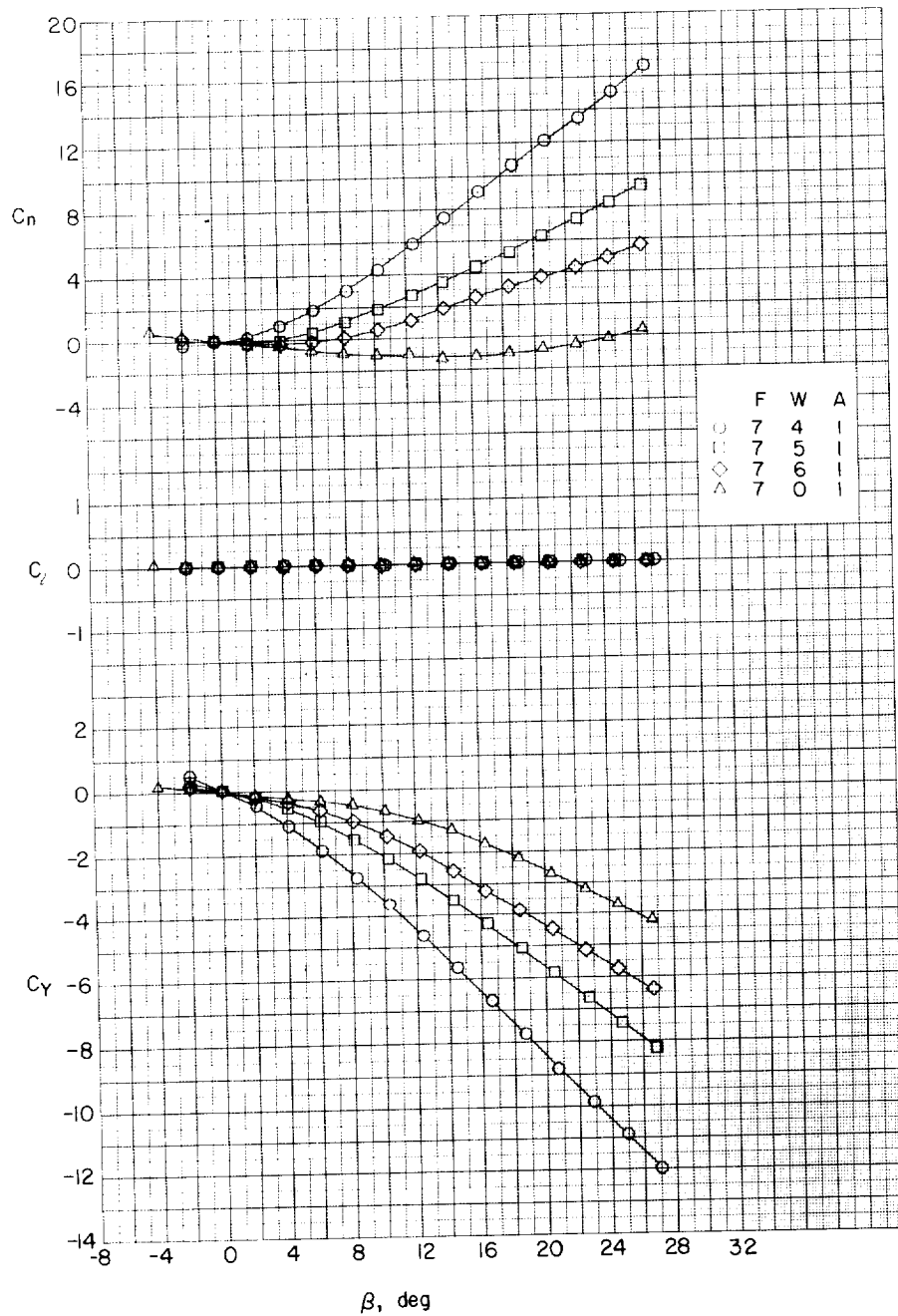
(a) $\alpha \approx 0^\circ$.

Figure 17.- Effects of rectangular wings on aerodynamic characteristics in sideslip. One-caliber cylindrical afterbody; $l/d = 10$.

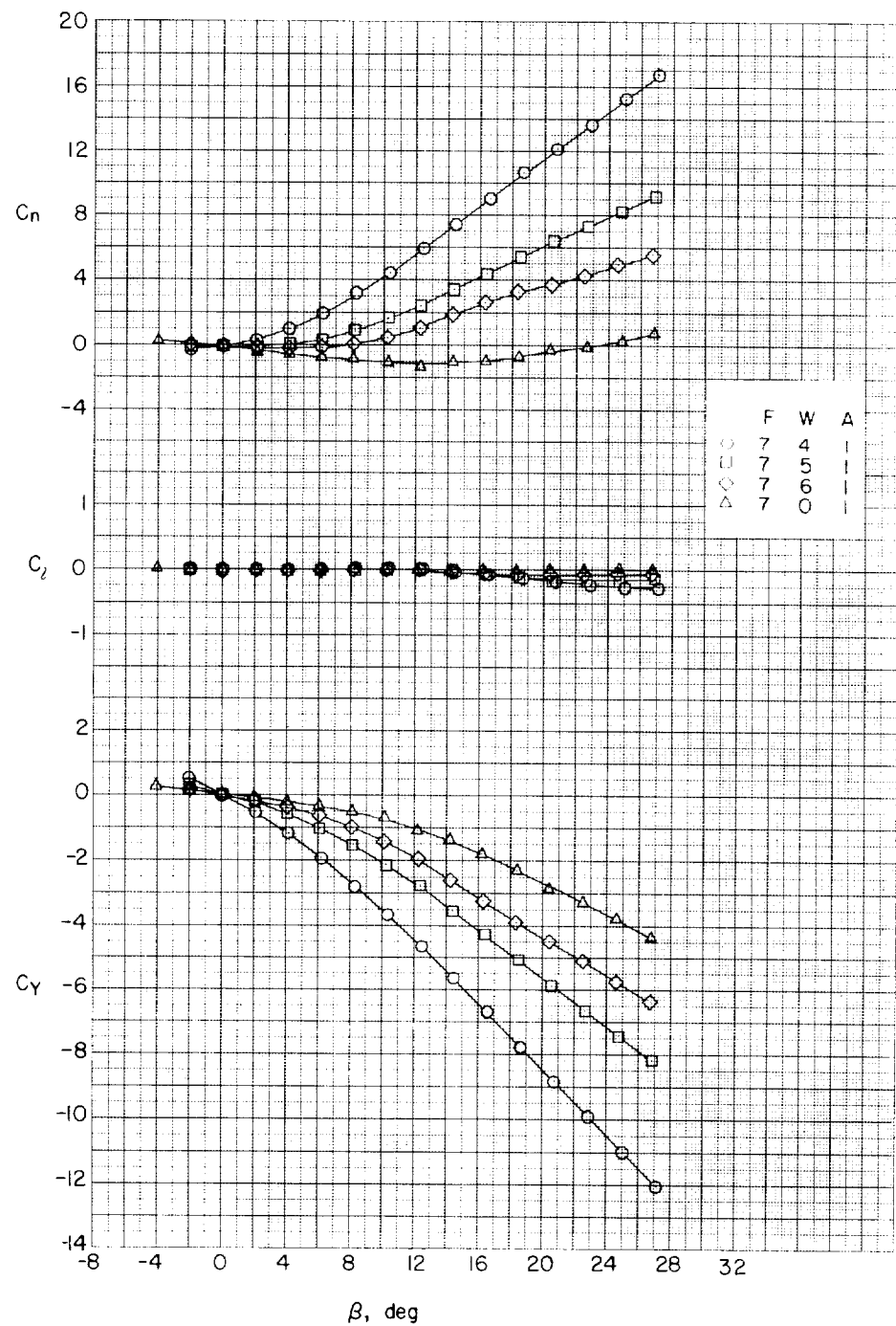
(b) $\alpha \approx 4.1^\circ$.

Figure 17.- Continued.

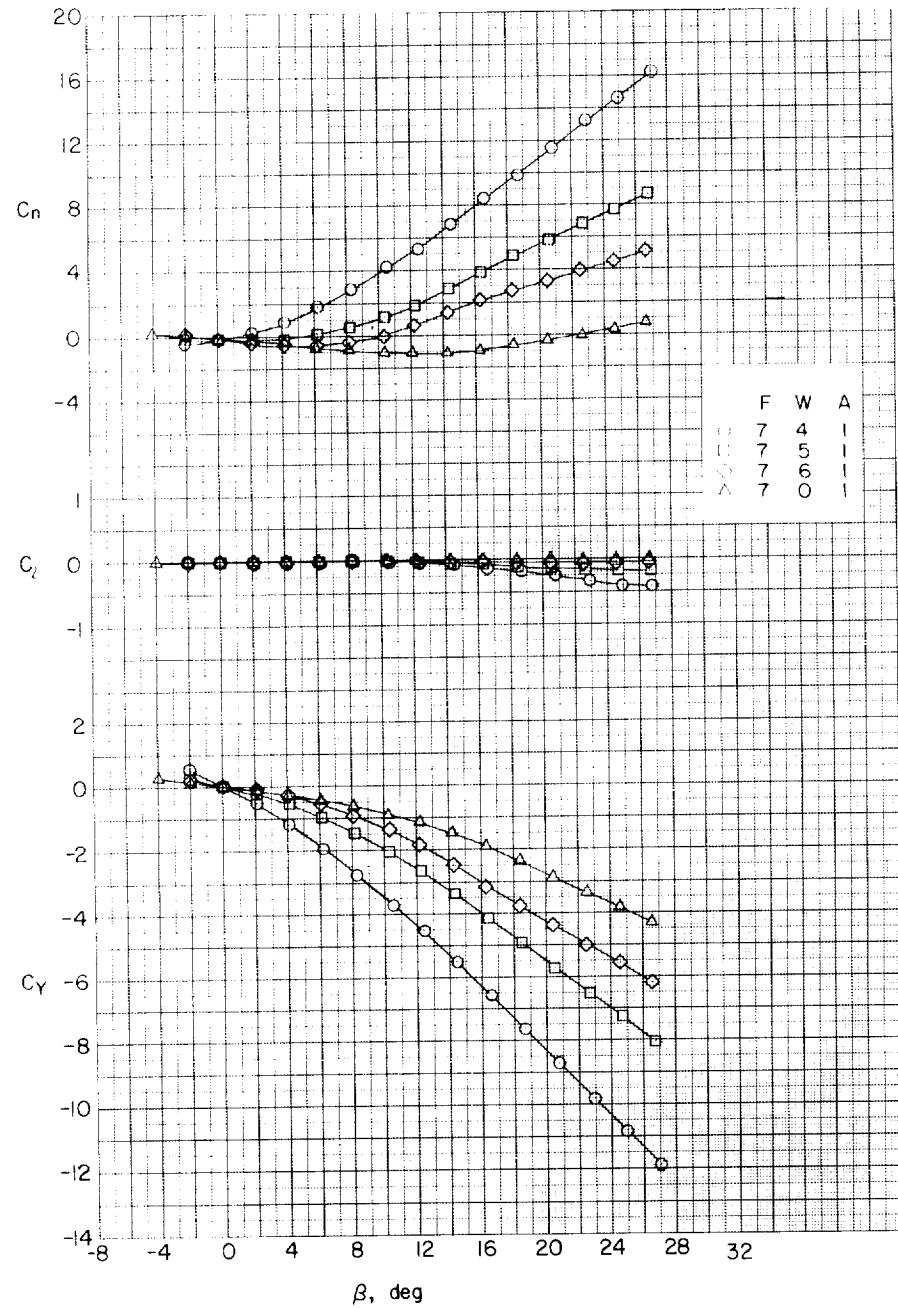
(c) $\alpha \approx 8.2^\circ$.

Figure 17.- Continued.

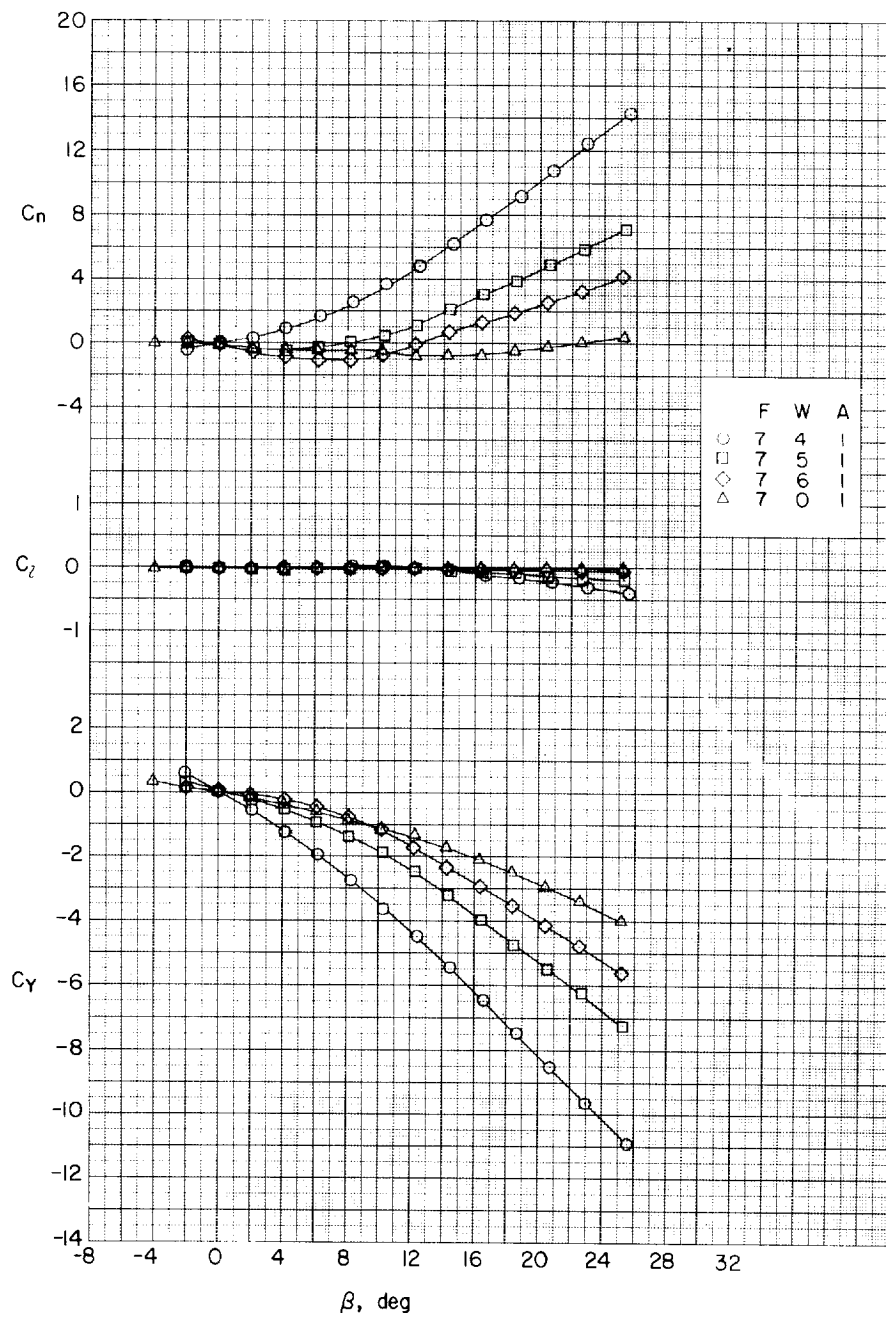
(a) $\alpha \approx 12.3^\circ$.

Figure 17.- Continued.

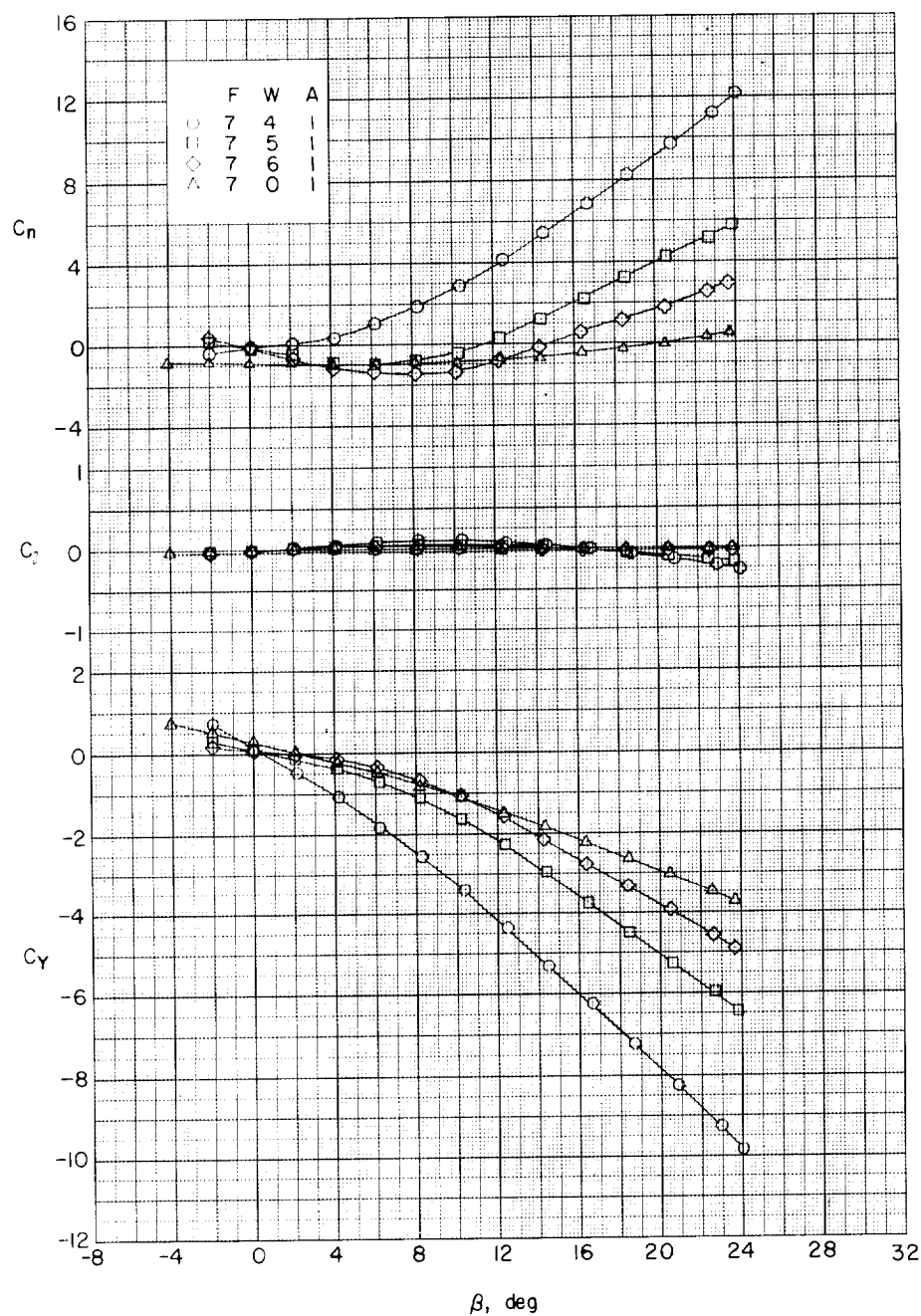
(e) $\alpha \approx 16.4^\circ$.

Figure 17.- Continued.

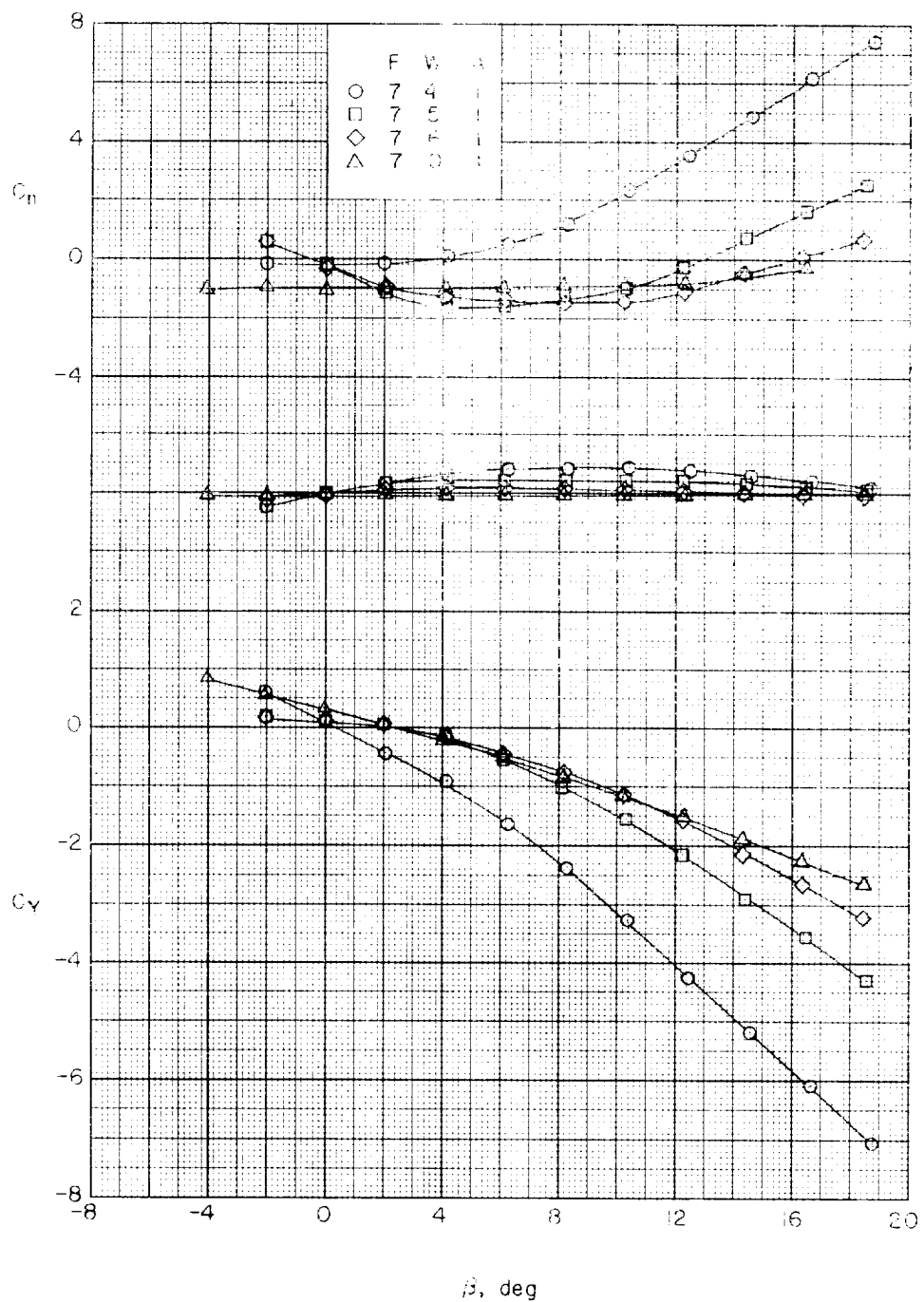
(f) $\alpha \approx 20.5^\circ$.

Figure 17.- Continued.

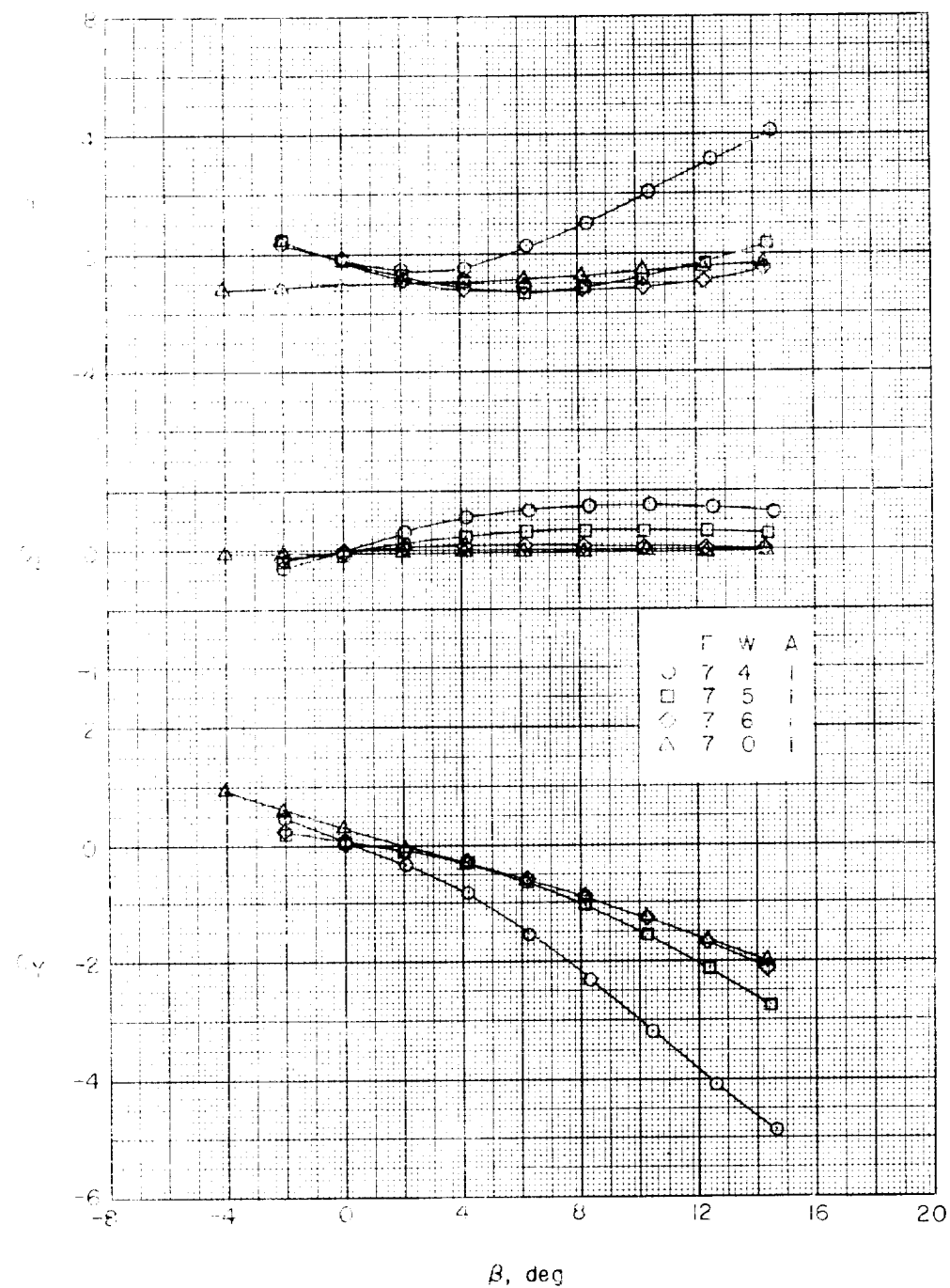
(g) $\alpha \approx 24.7^\circ$.

Figure 17.- Concluded.

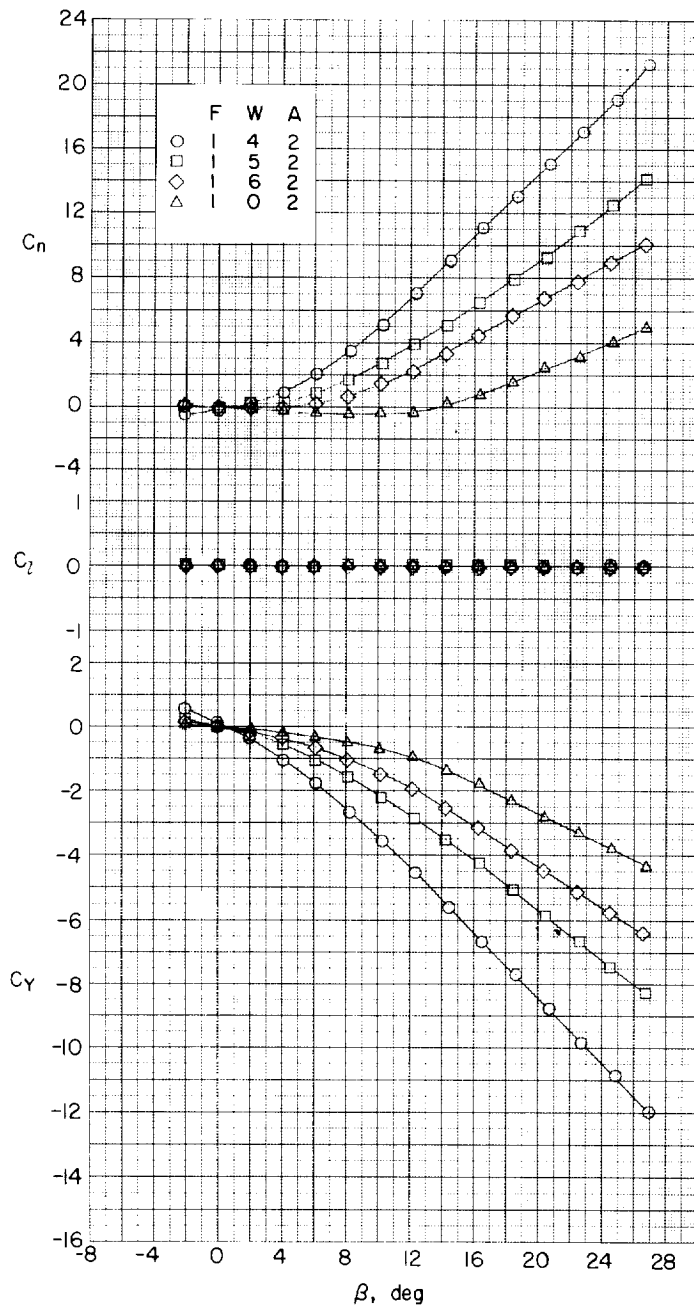
(a) $\alpha \approx 0^\circ$.

Figure 18.- Effect of rectangular wings on aerodynamic characteristics in sideslip. Two-caliber cylindrical afterbody; $l/d = 10$.

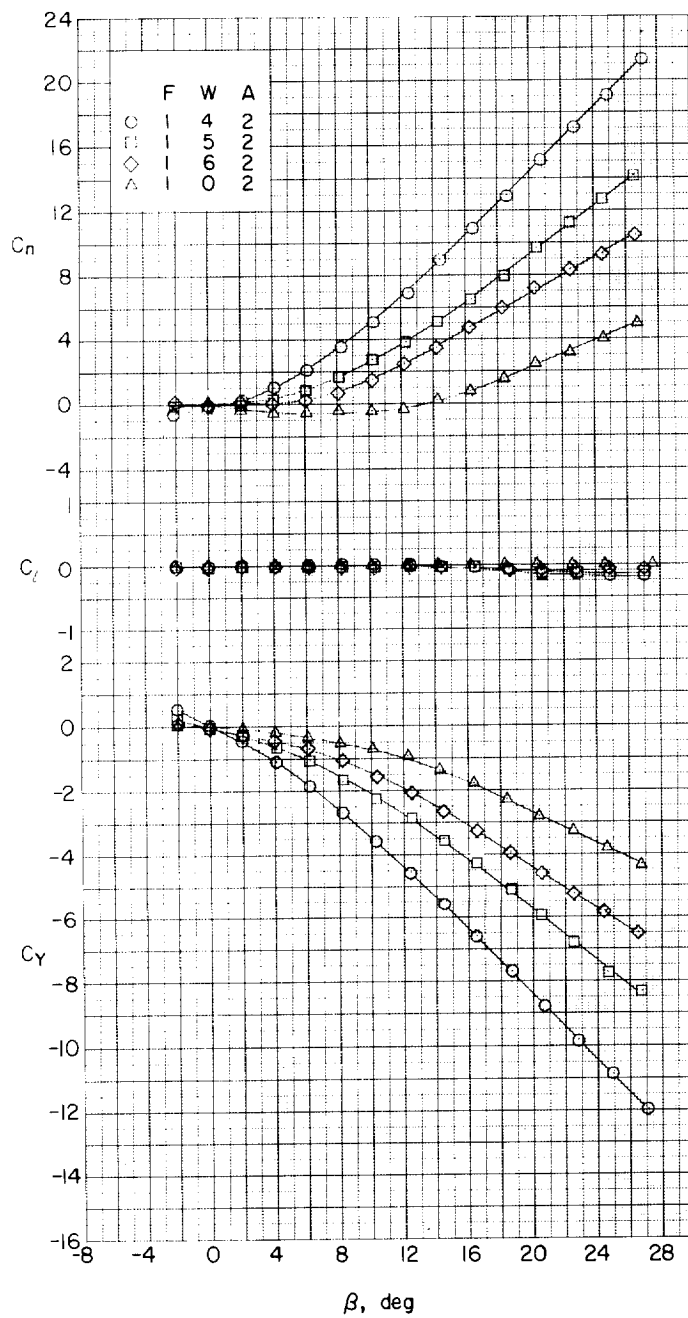
(b) $\alpha \approx 4.1^\circ$.

Figure 18.- Continued.

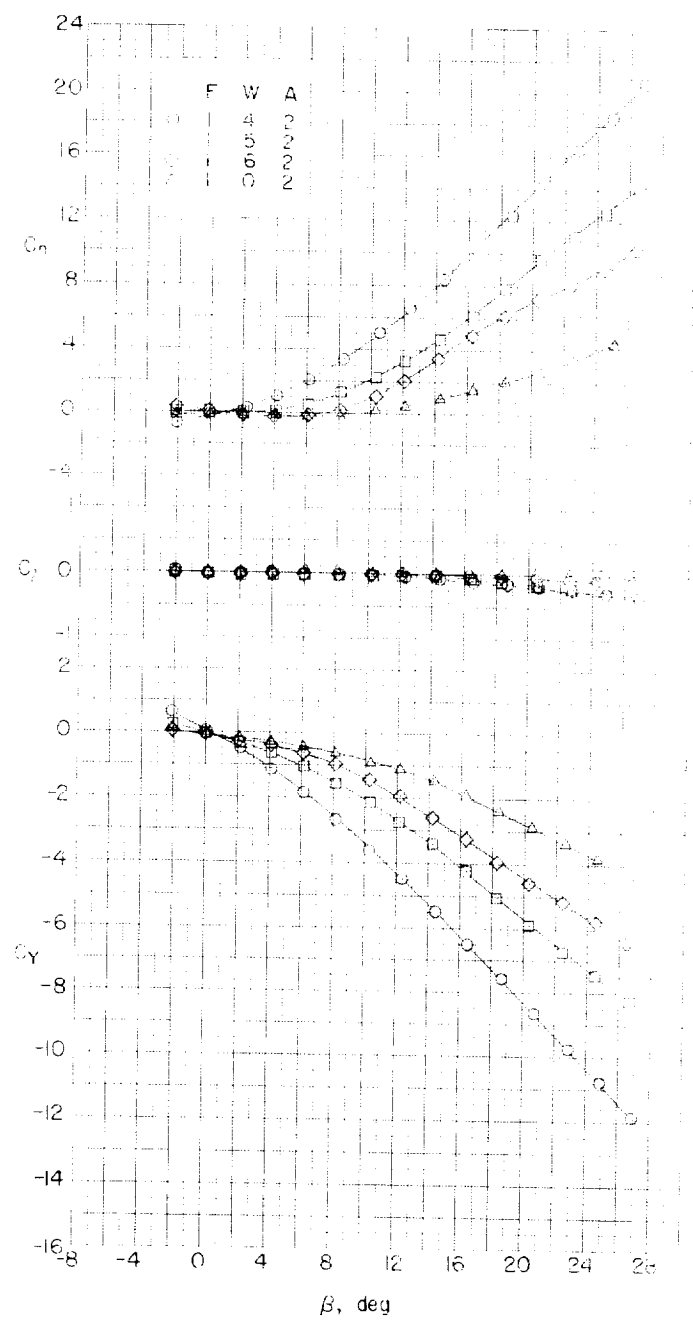
(c) $\alpha \approx 8.2^\circ$.

Figure 18.- Continued.

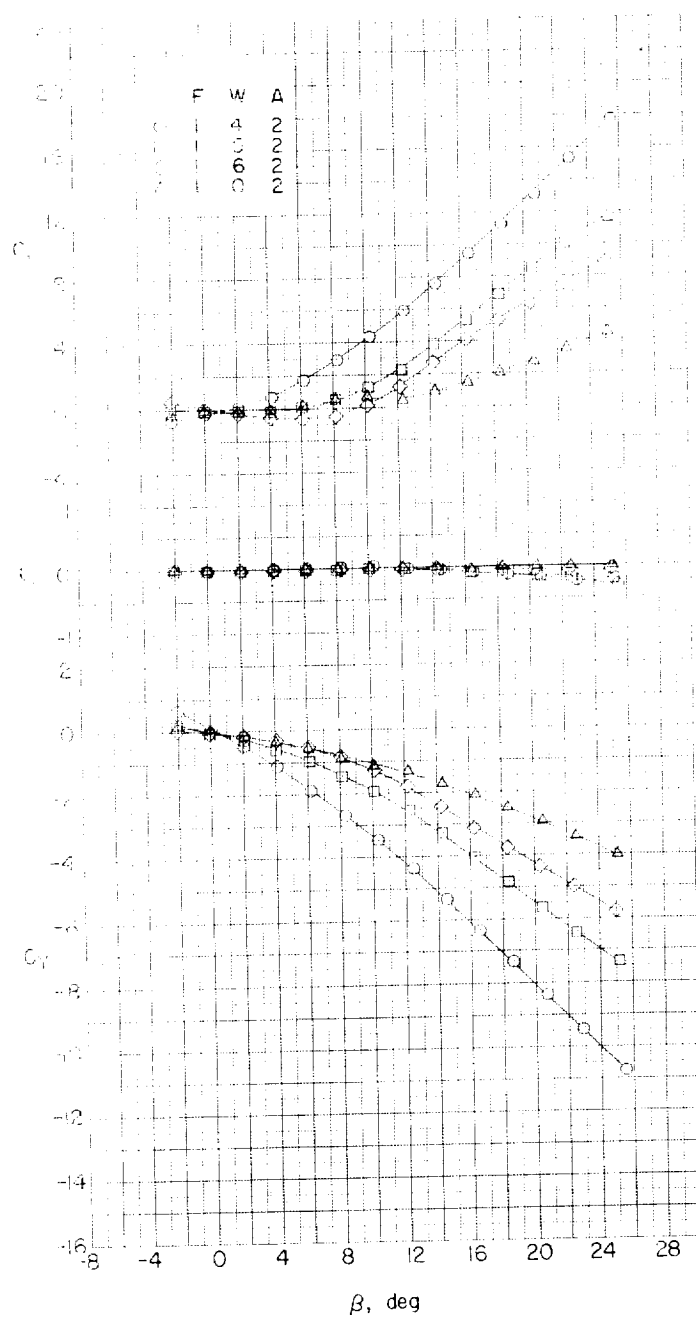
(d) $\alpha \approx 12.5^\circ$.

Figure 18.- Continued.

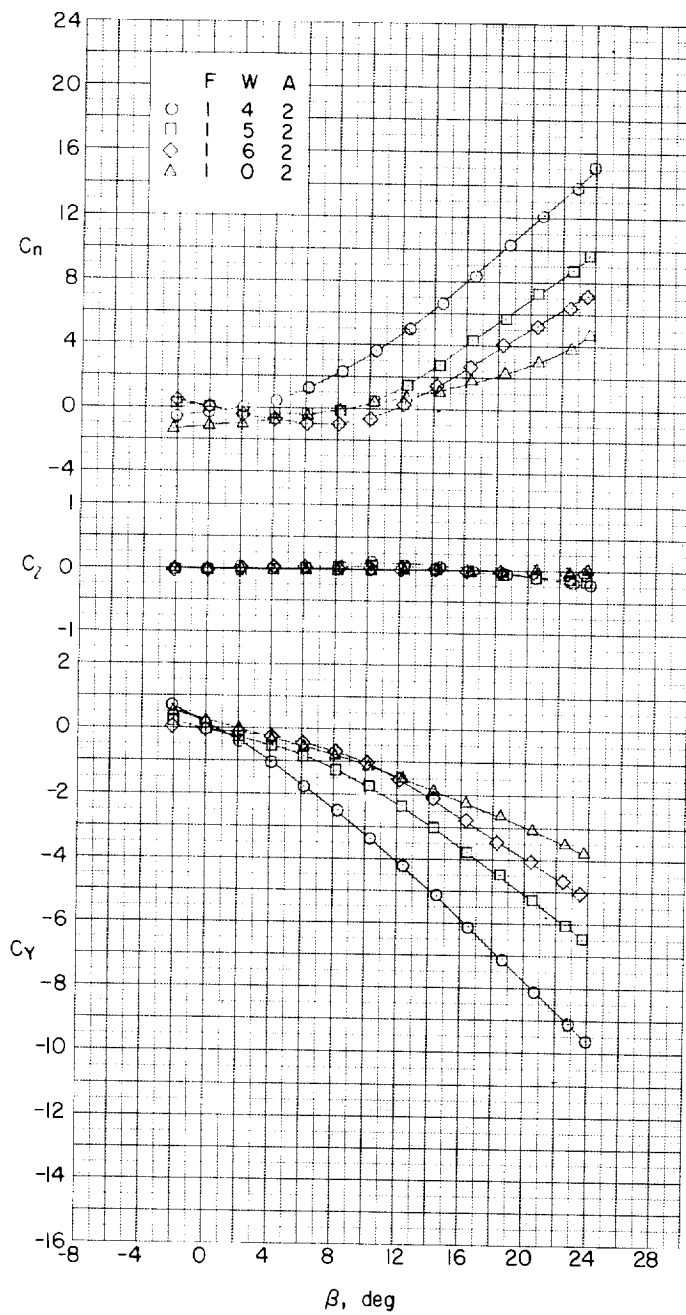
(e) $\alpha \approx 16.4^\circ$.

Figure 18.- Continued.

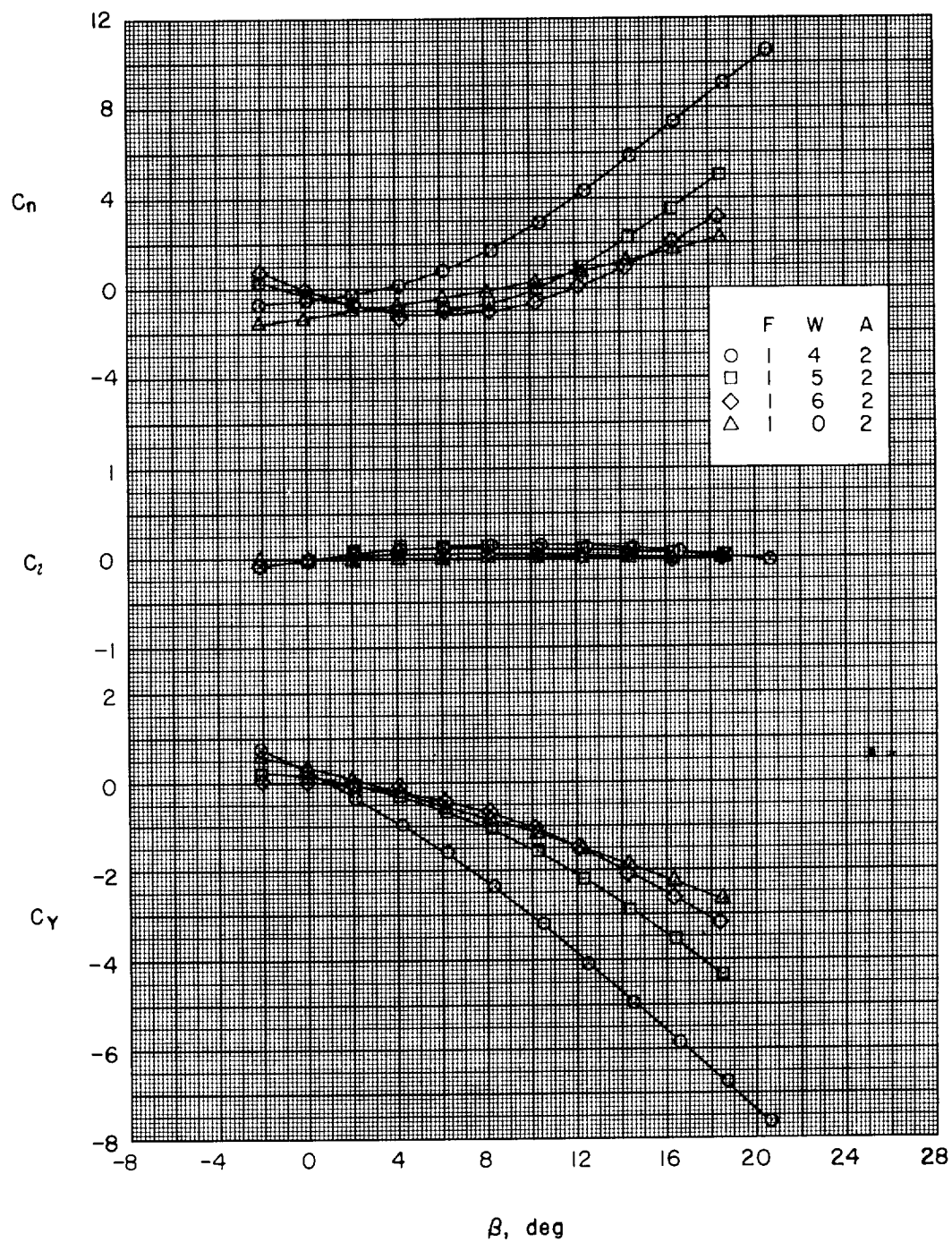
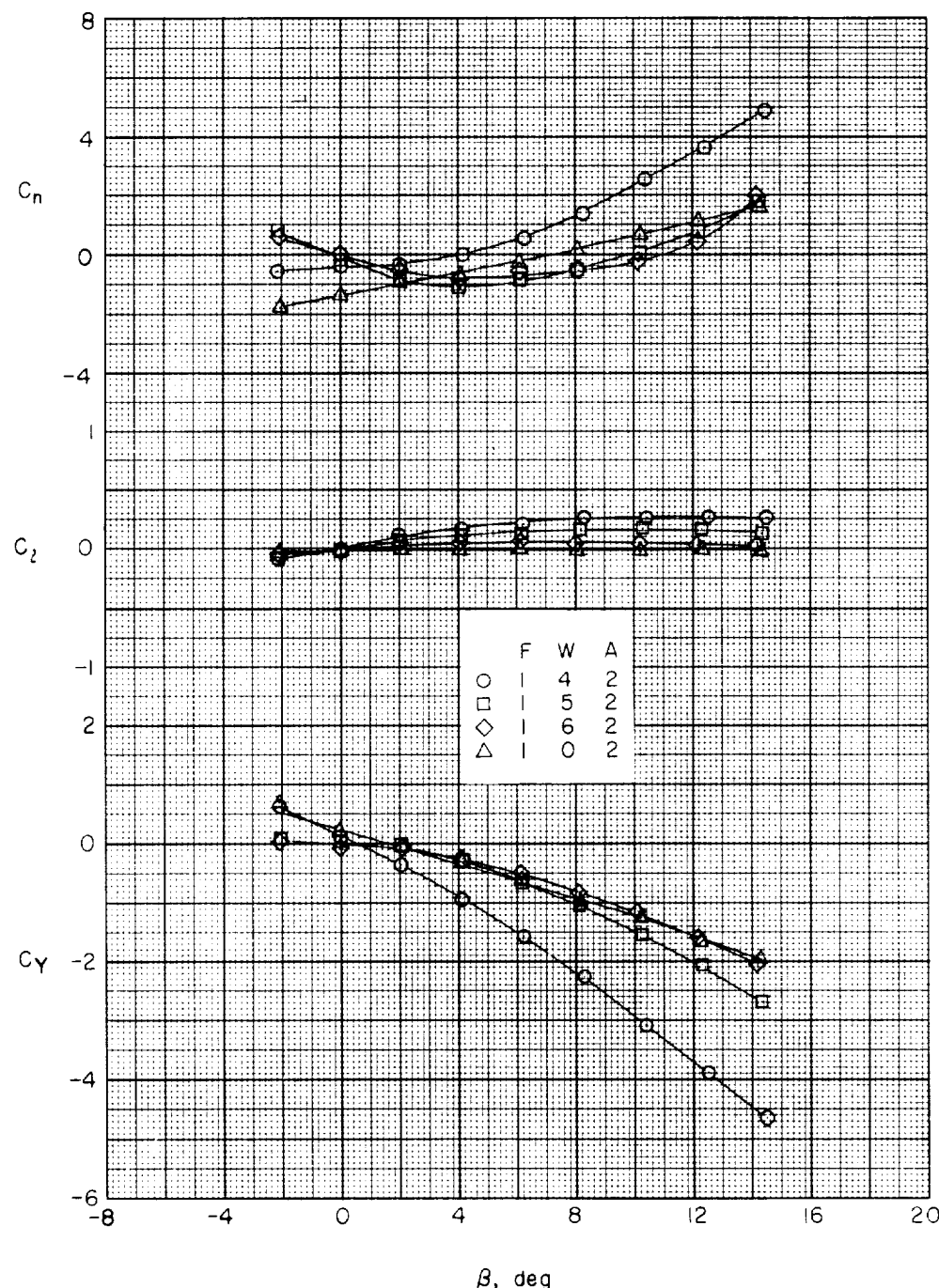
(f) $\alpha \approx 20.5^\circ$.

Figure 18-- Continued.



(g) $\alpha \approx 24.7^\circ$.

Figure 18.- Concluded.

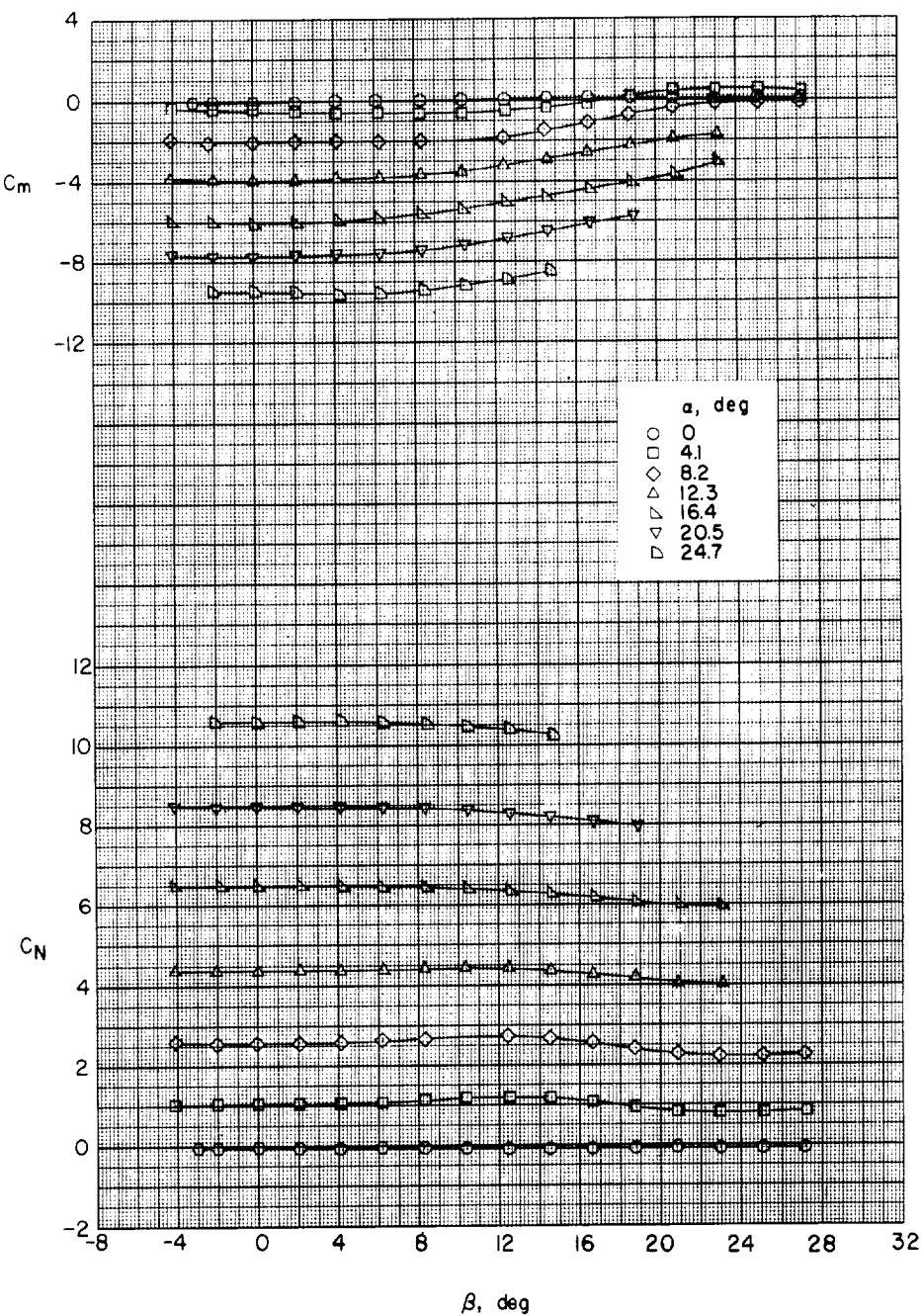
(a) Large rectangular wing, $F_8W_4A_0$.

Figure 19.- Variation of C_m and C_N with β for various angles of attack. Rectangular wings; no afterbody; $l/d = 10$.

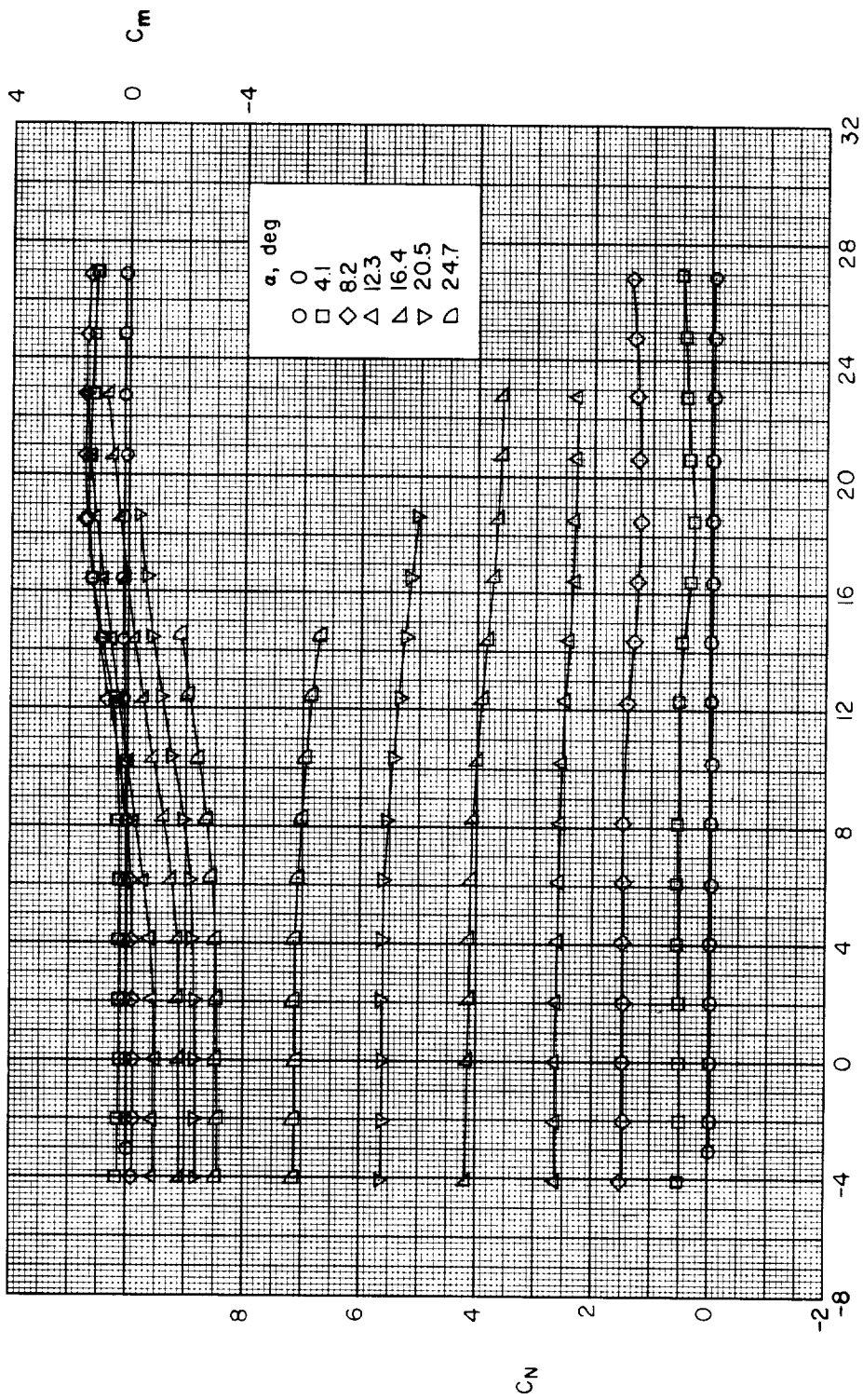
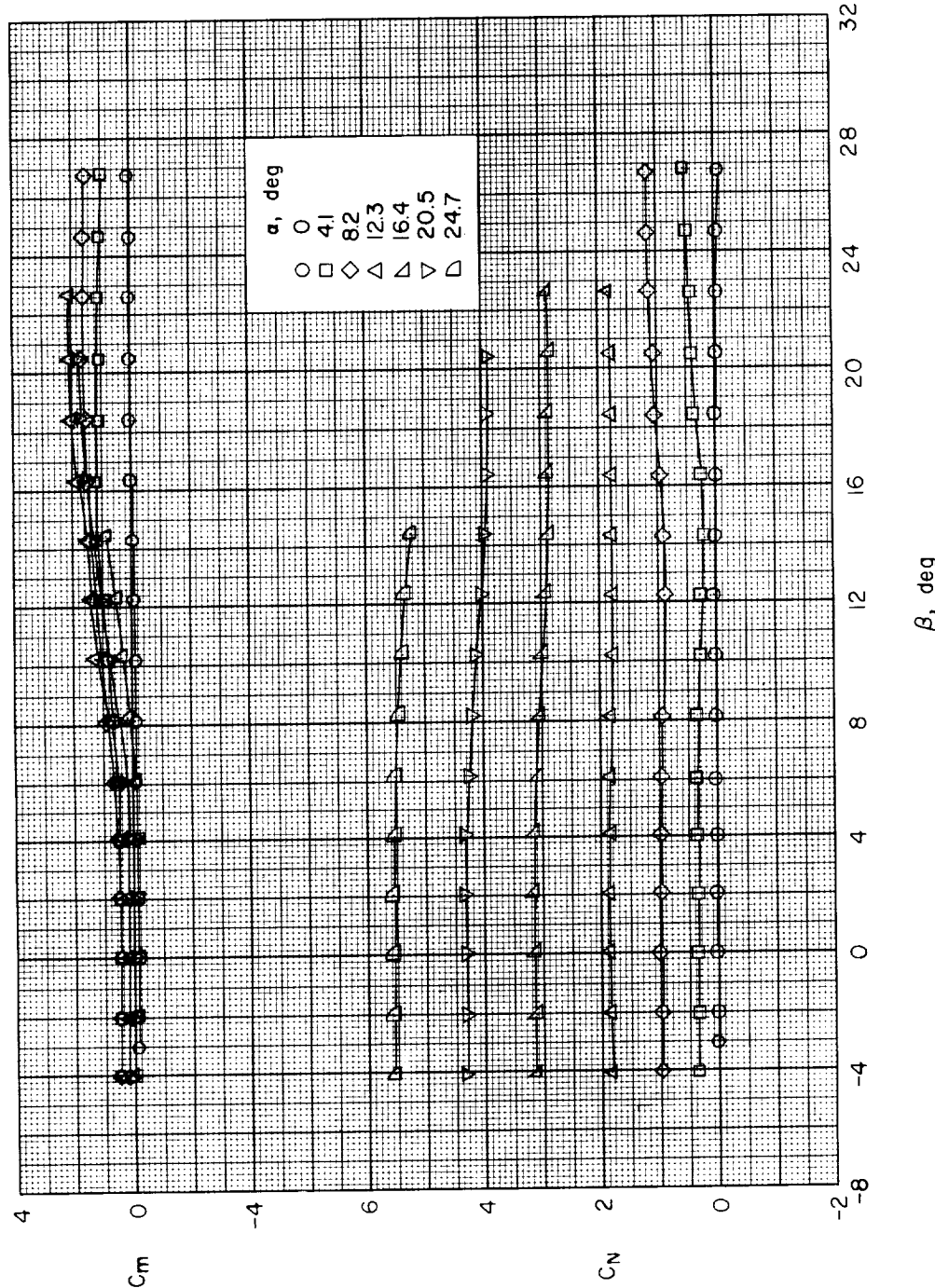
(b) Medium rectangular wing, F_{8W₅A₀}.

Figure 19.- Continued.



(c) Small rectangular wing, F8W6A0.

Figure 19.- Concluded.

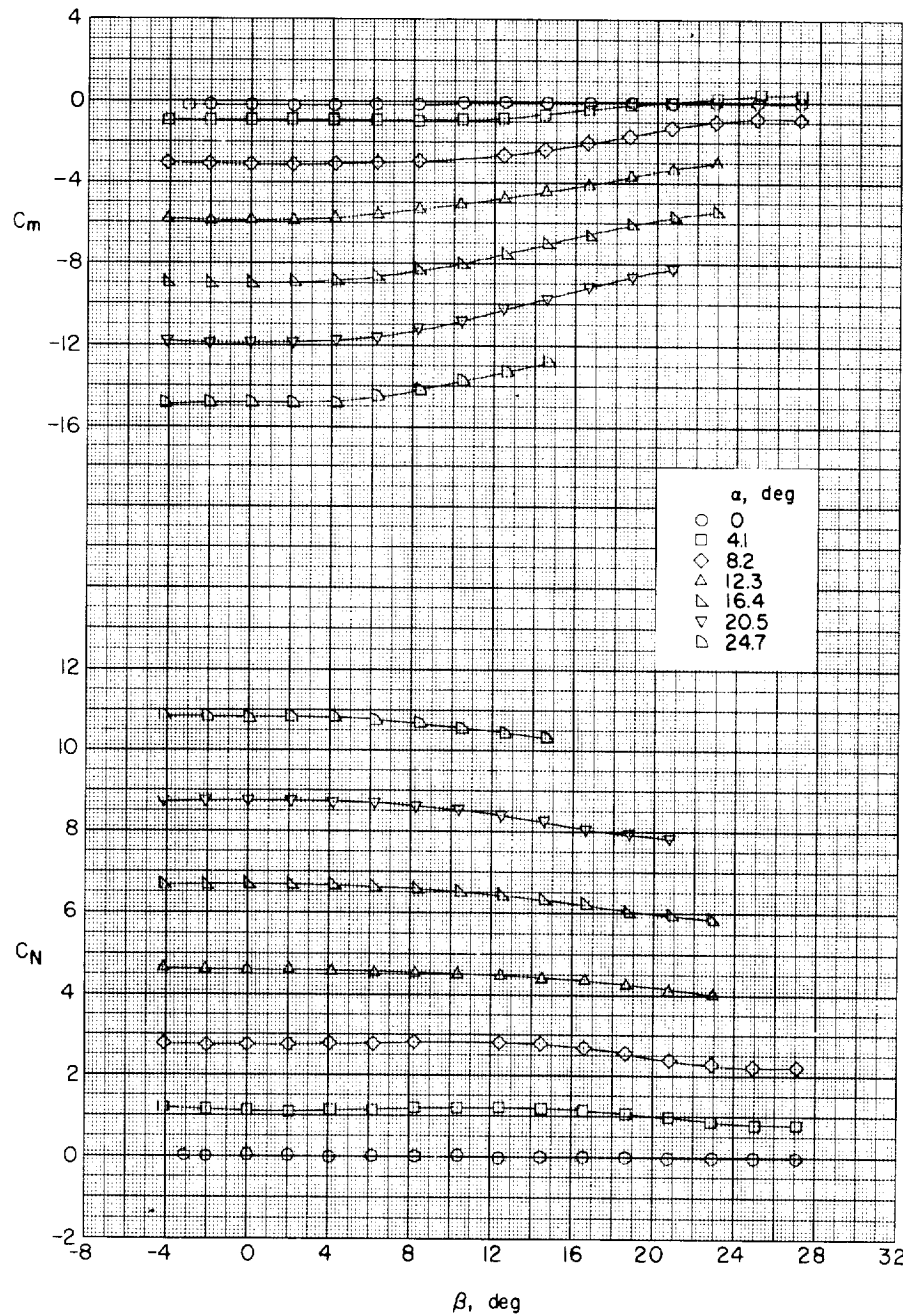
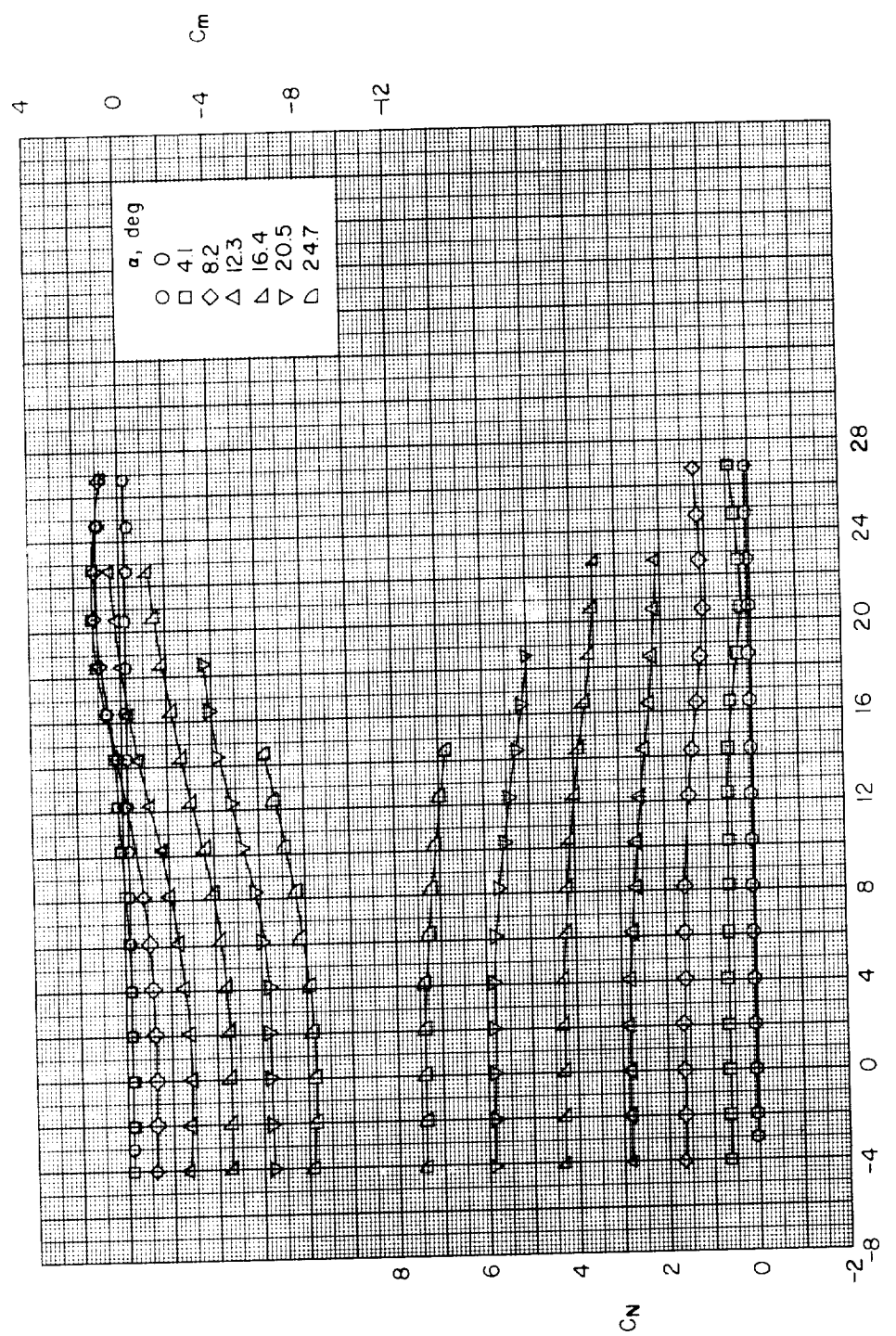
(a) Large rectangular wing, F₇W₄A₁.

Figure 20.- Variation of C_m and C_N with β for various angles of attack. Rectangular wings; 1-caliber cylindrical afterbody; $l/d = 10$.



(b) Medium rectangular wing, F7W5Al.

Figure 20.- Continued.

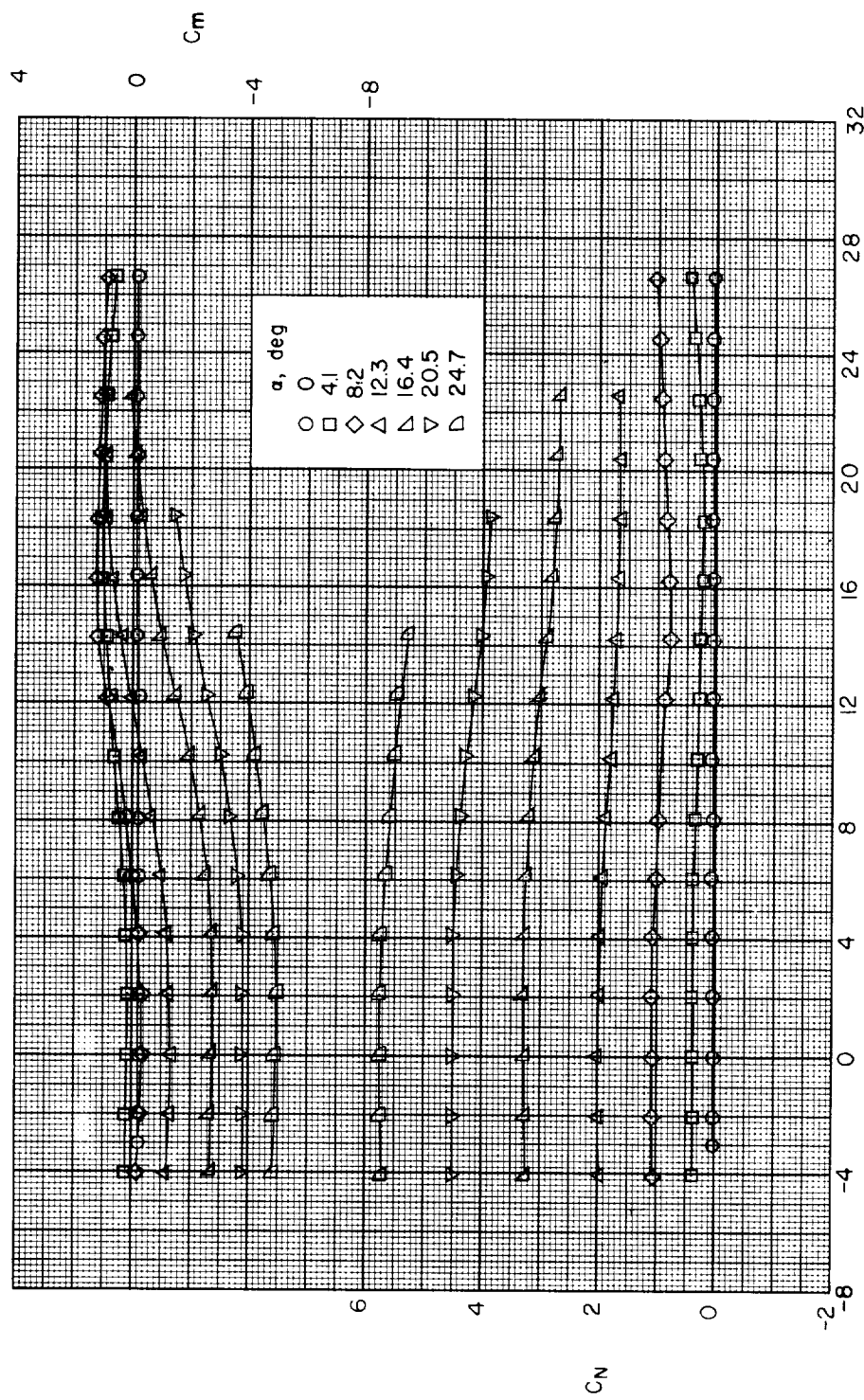
(c) Small rectangular wings, F_{7W6A1}.

Figure 20.- Concluded.

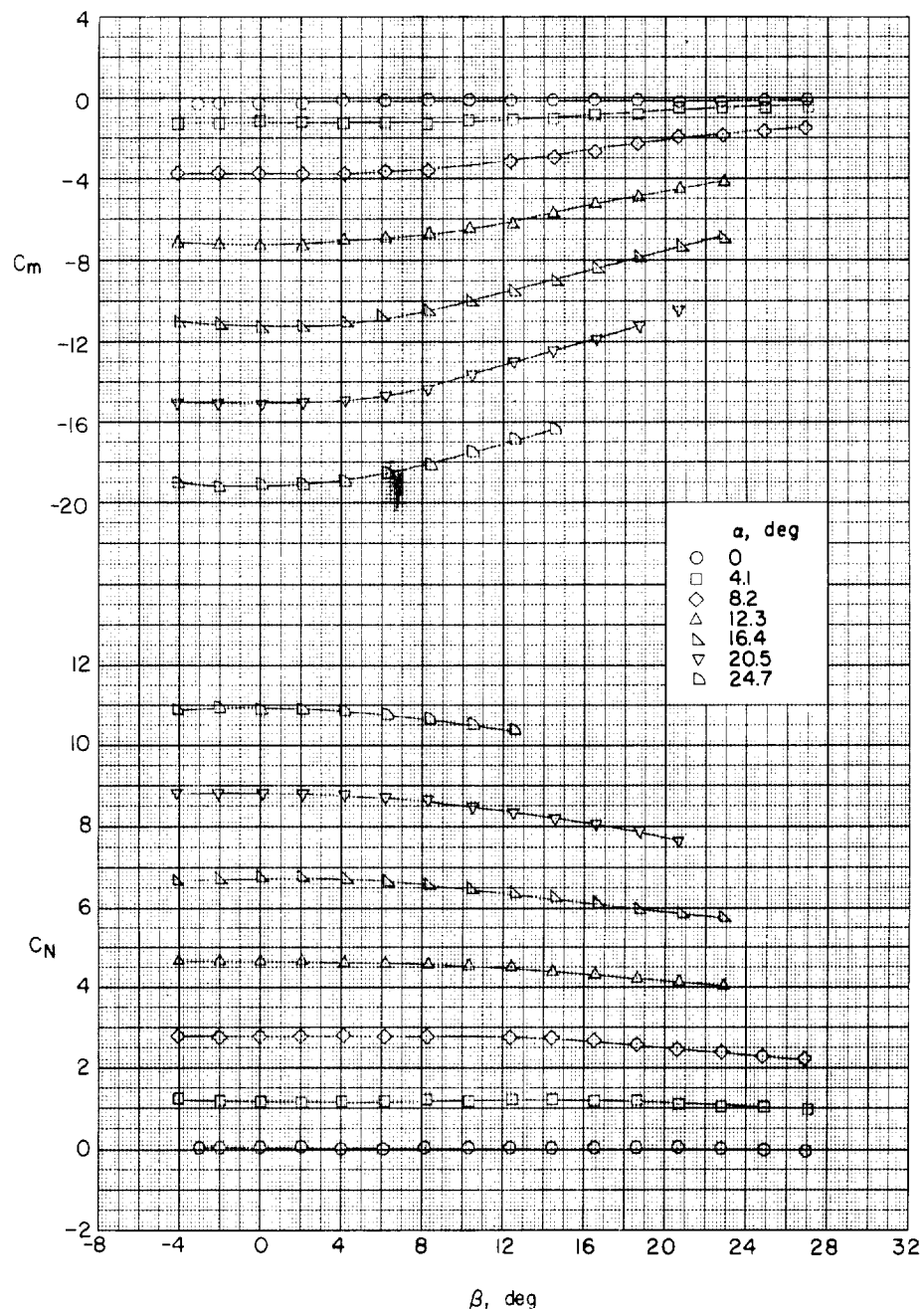
(a) Large rectangular wing, $F_1W_4A_2$.

Figure 21.- Variation of C_m and C_N with β for various angles of attack. Rectangular wings; 2-caliber cylindrical afterbody; $l/d = 10$.

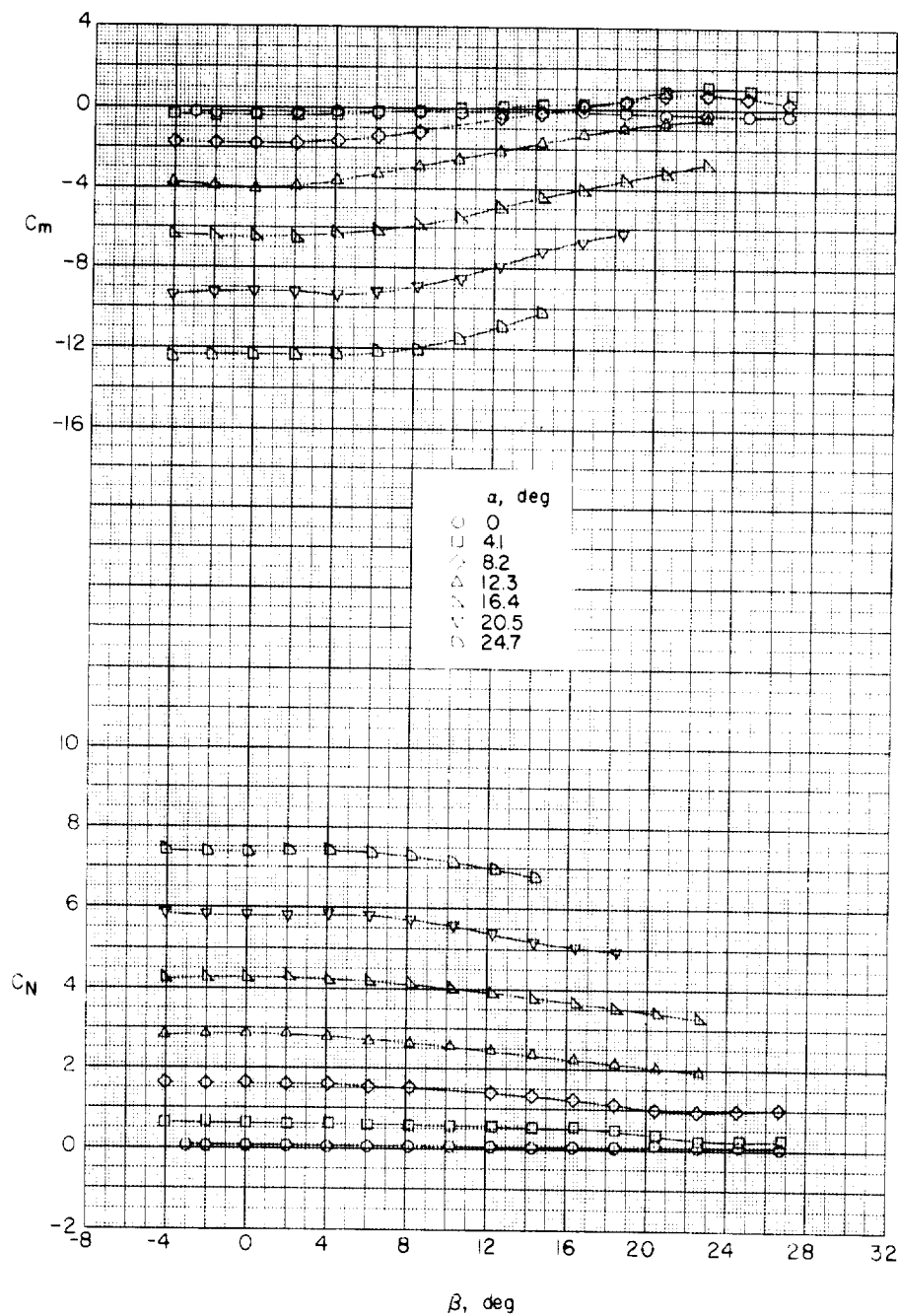
(b) Medium rectangular wing, F₁W6A₂.

Figure 21.- Continued.

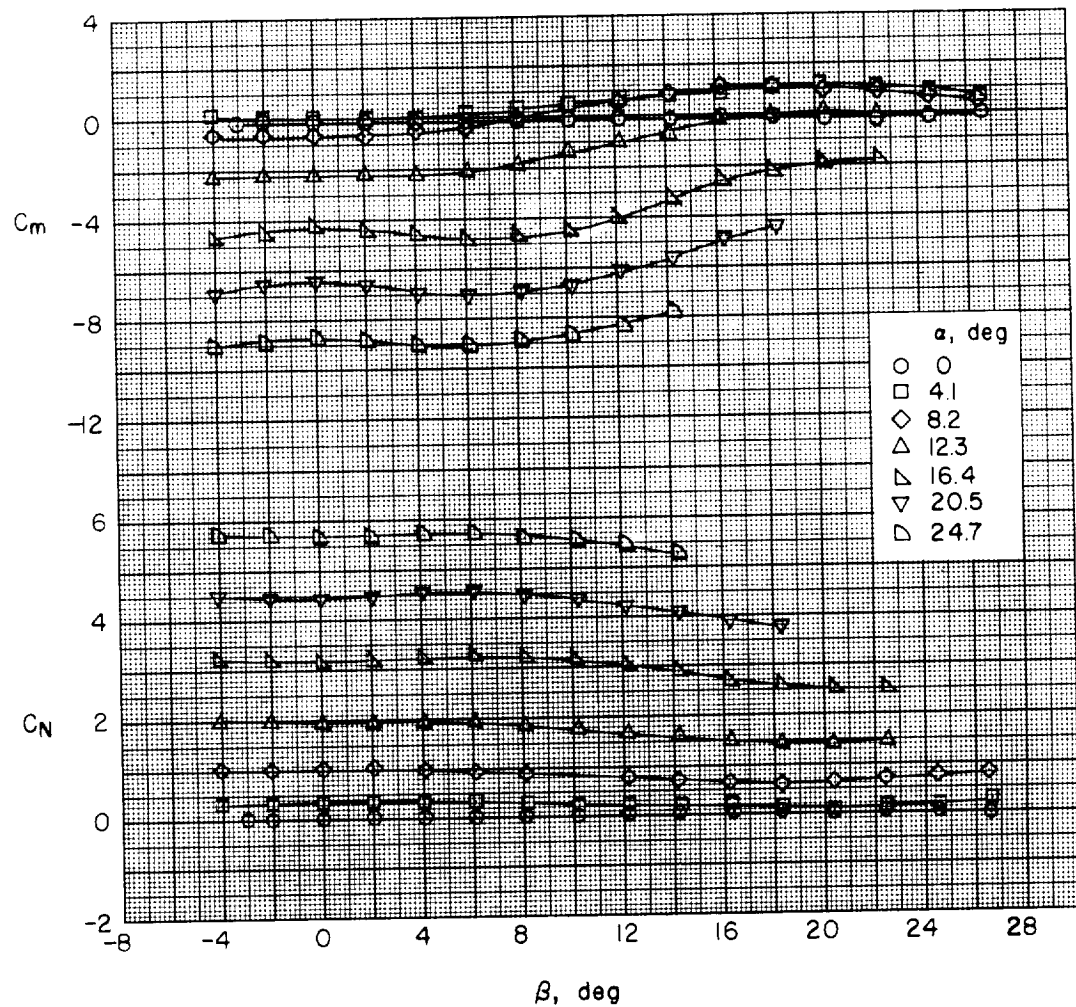
(c) Small rectangular wing, F₁W₆A₂.

Figure 21.- Concluded.

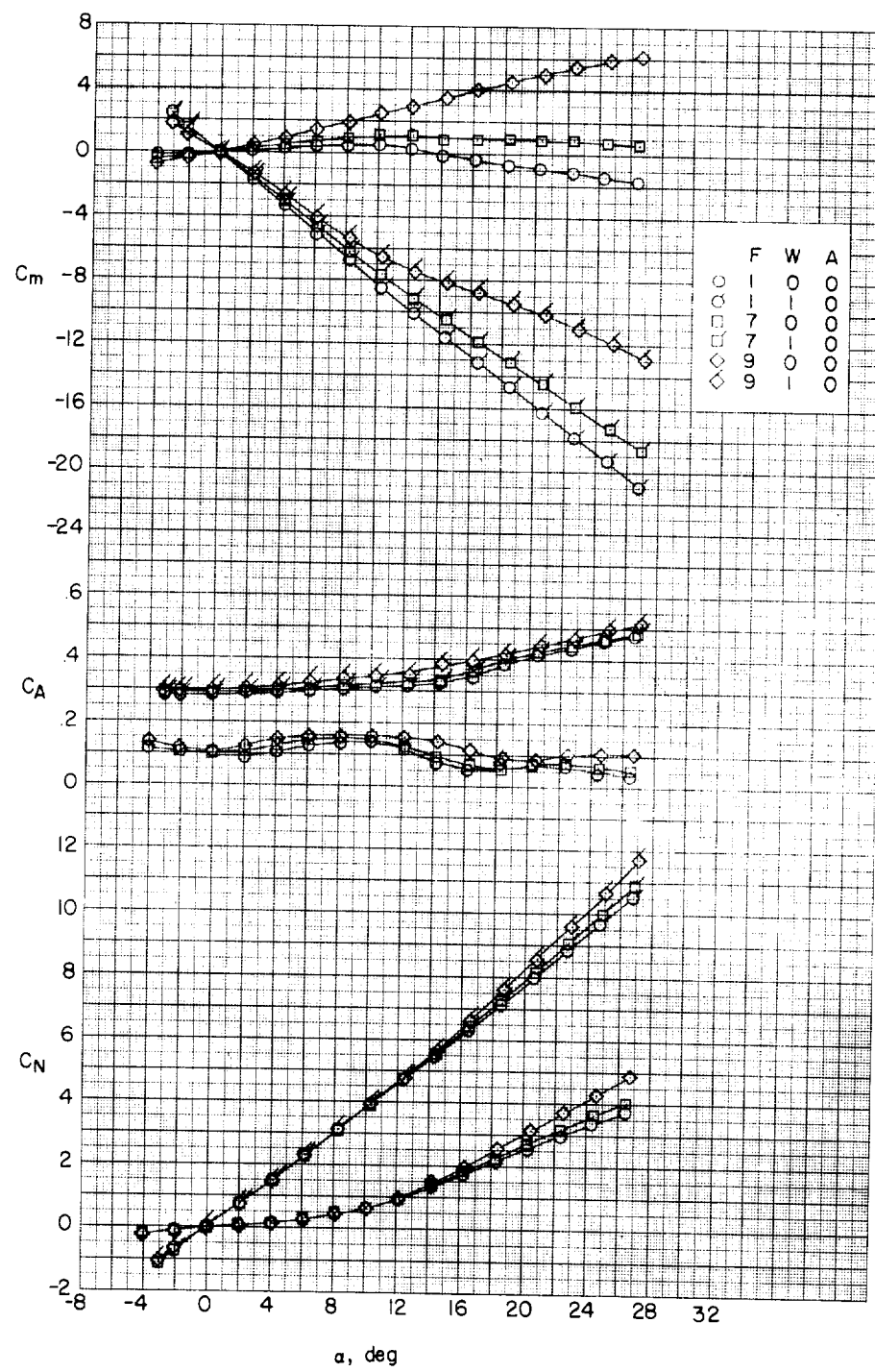


Figure 22.- Effect of forebody length on aerodynamic characteristics in pitch. Large delta wing; no afterbody.

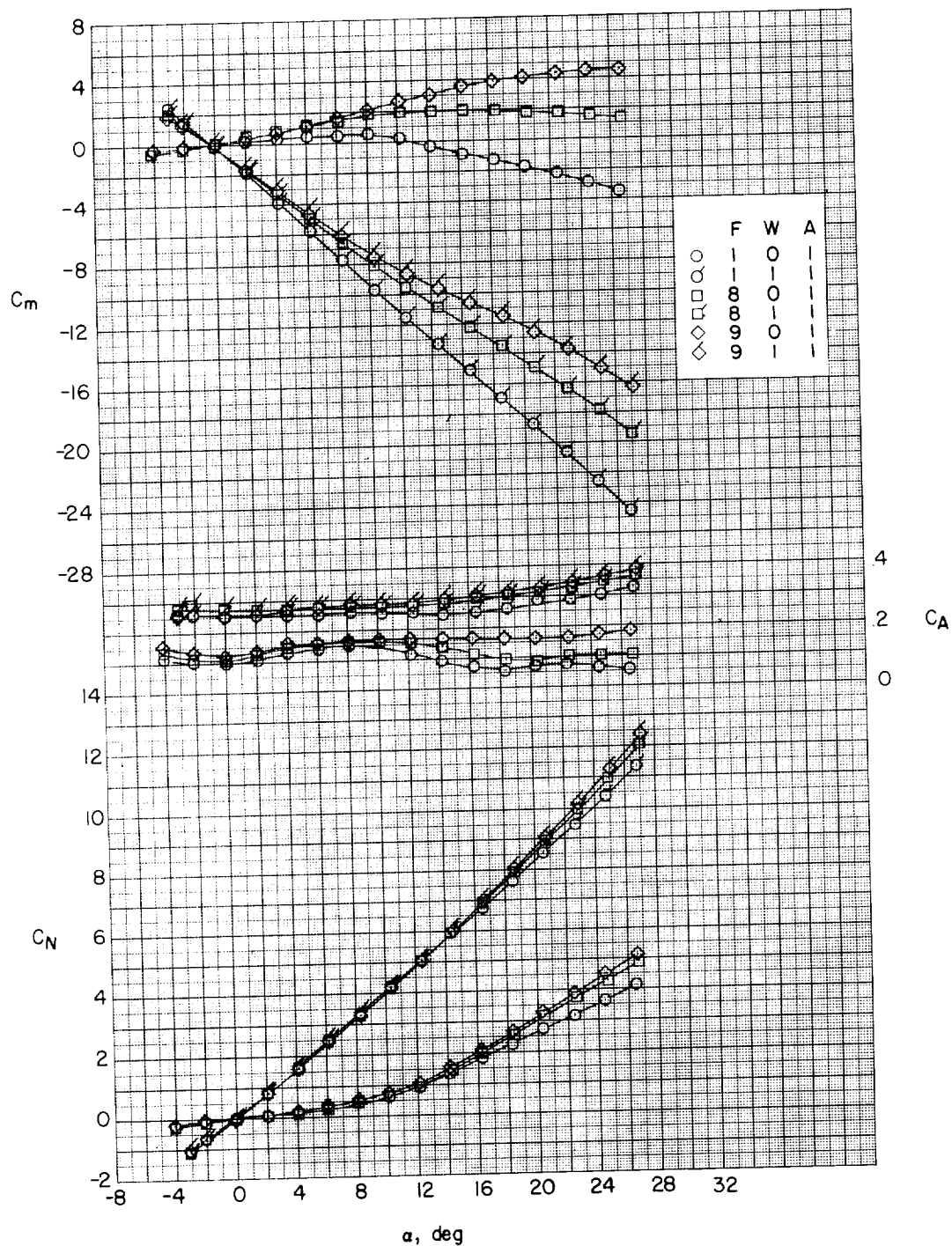


Figure 23.- Effects of forebody length on aerodynamic characteristics in pitch. Large delta wings; 1-caliber cylindrical afterbody.

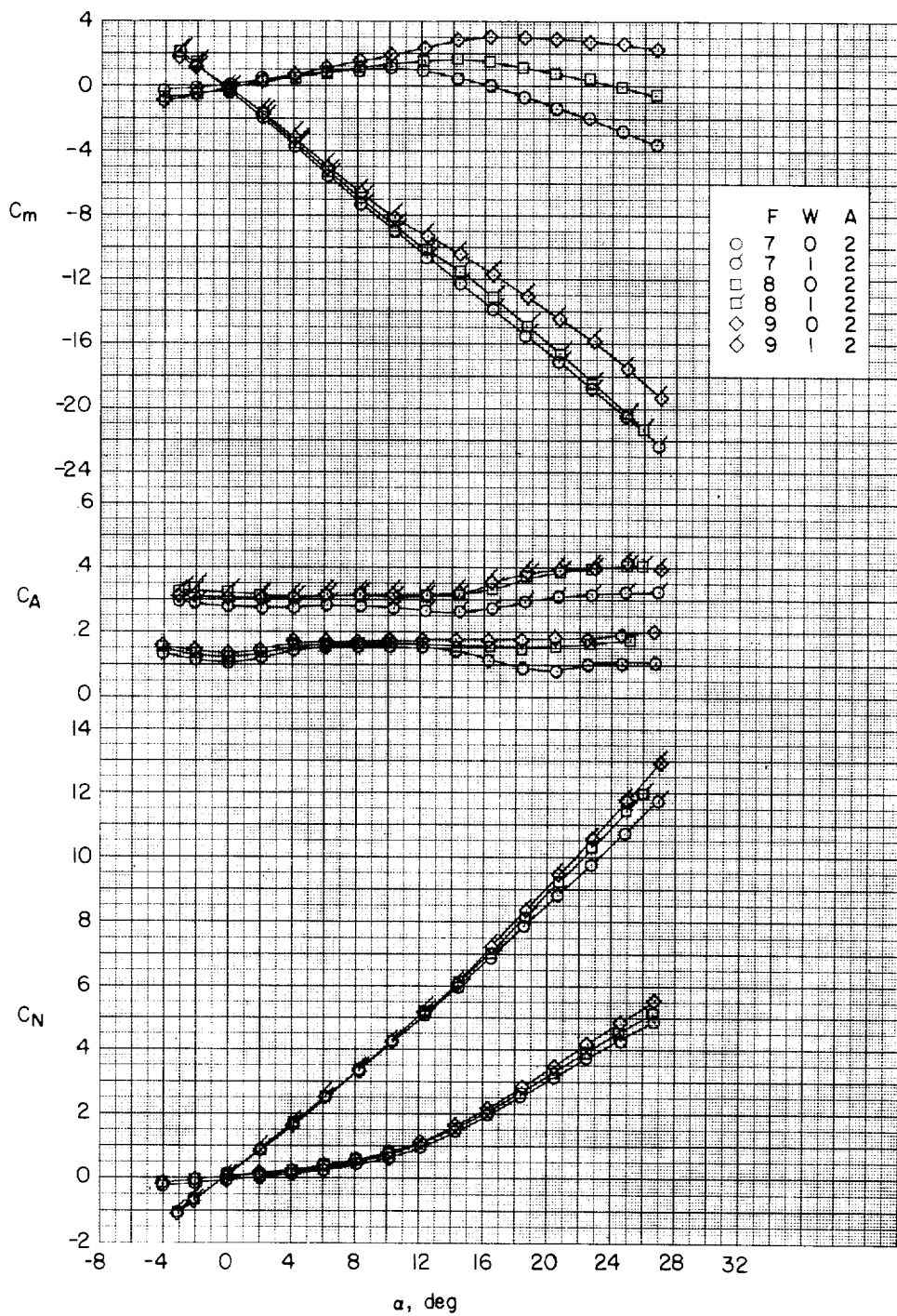


Figure 24.- Effects of forebody length on aerodynamic characteristics in pitch. Large delta wings; 2-caliber cylindrical afterbody.

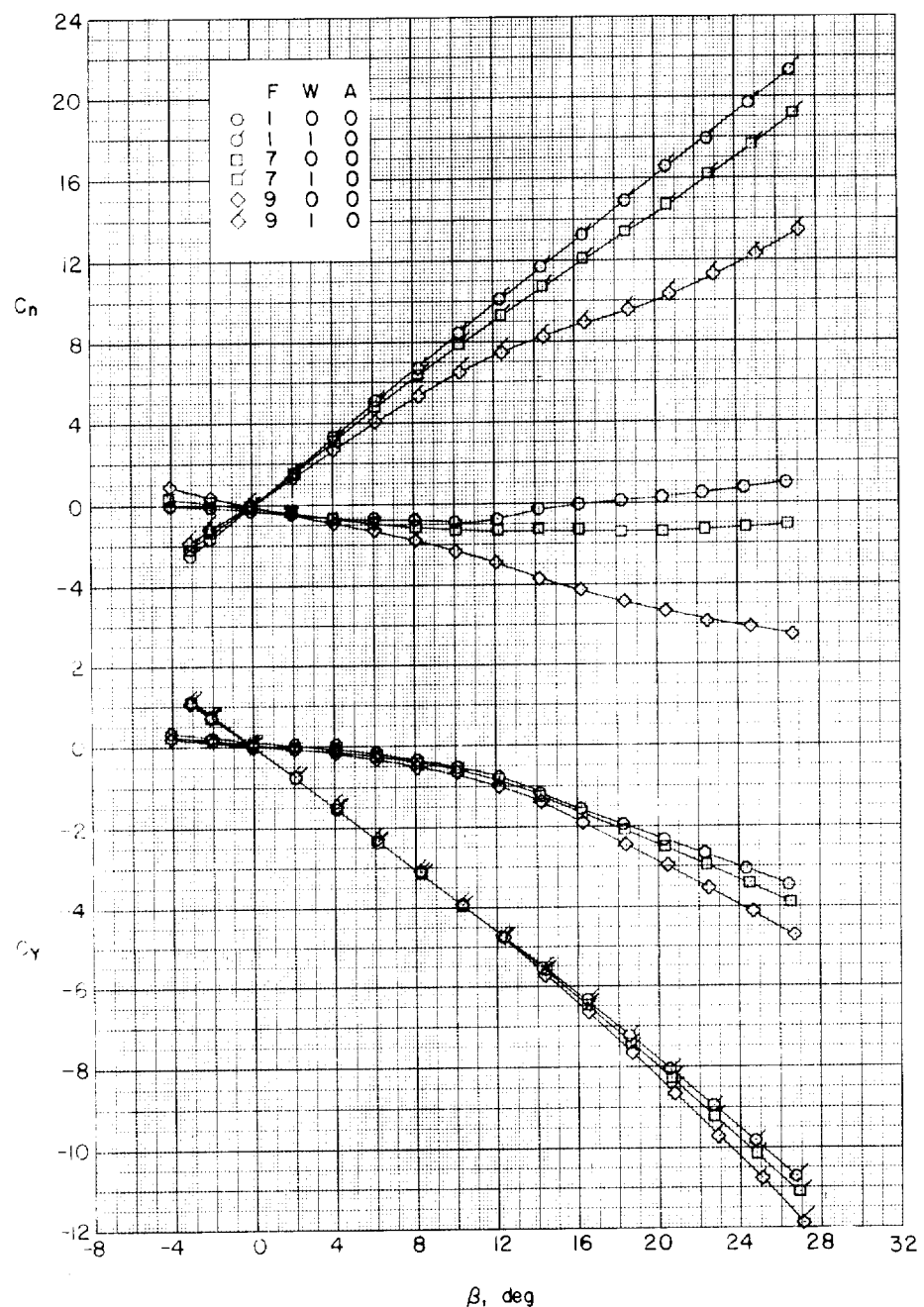
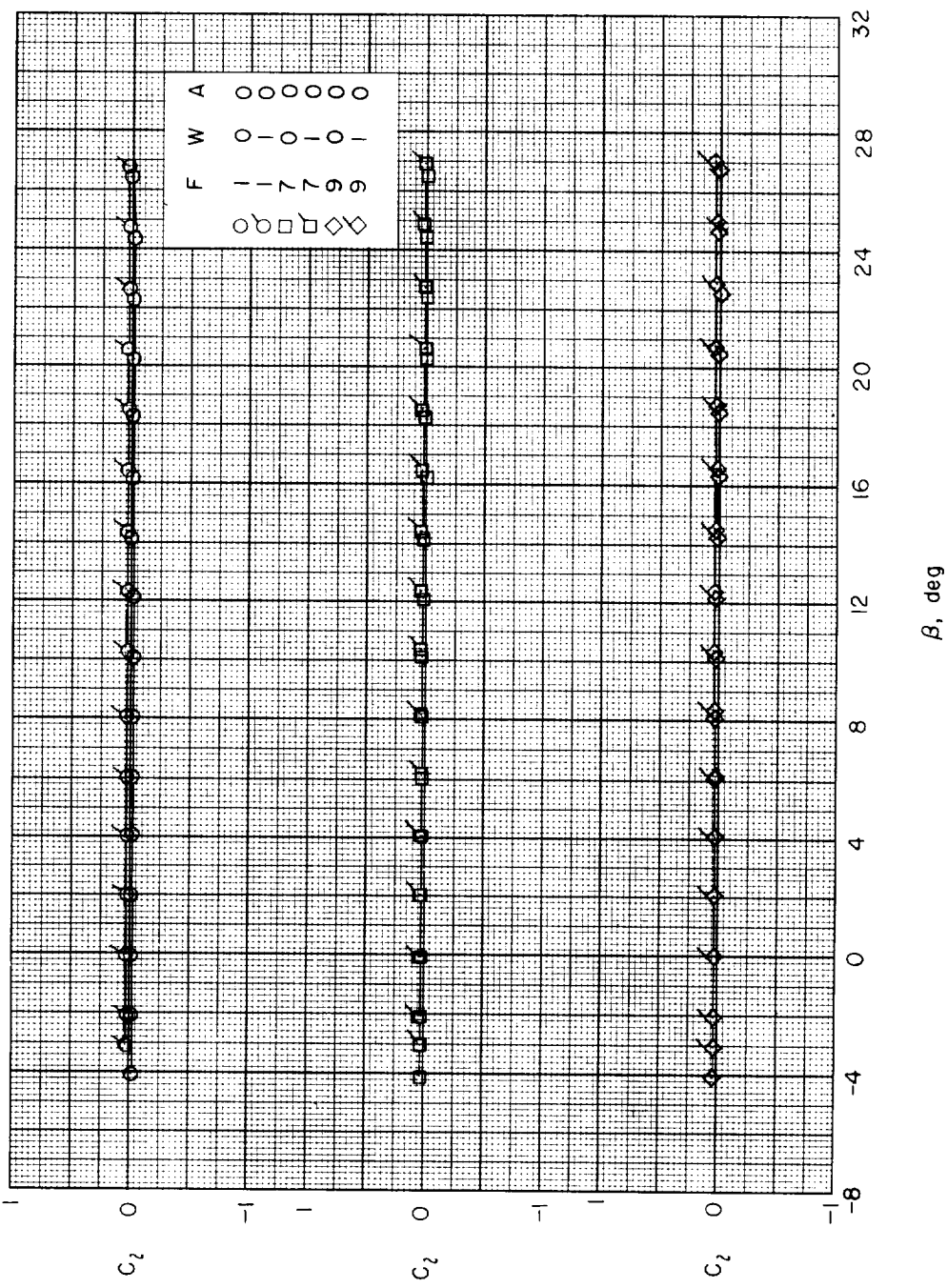
(a) $\alpha \approx 0^\circ$.

Figure 25.- Effect of forebody length on aerodynamic characteristics in sideslip. Large delta wings; no afterbody.



(a) Concluded.

Figure 25.- Continued.

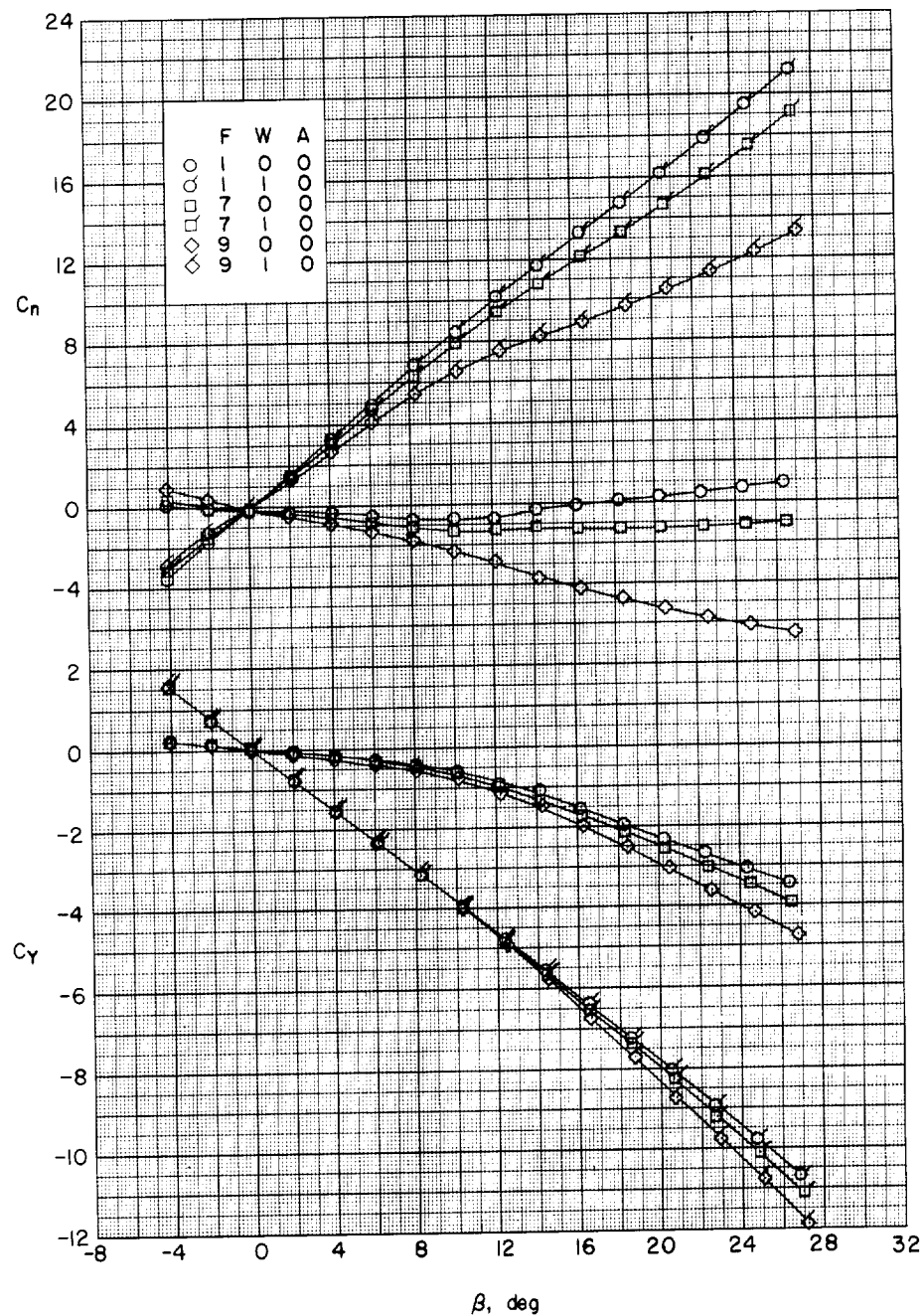
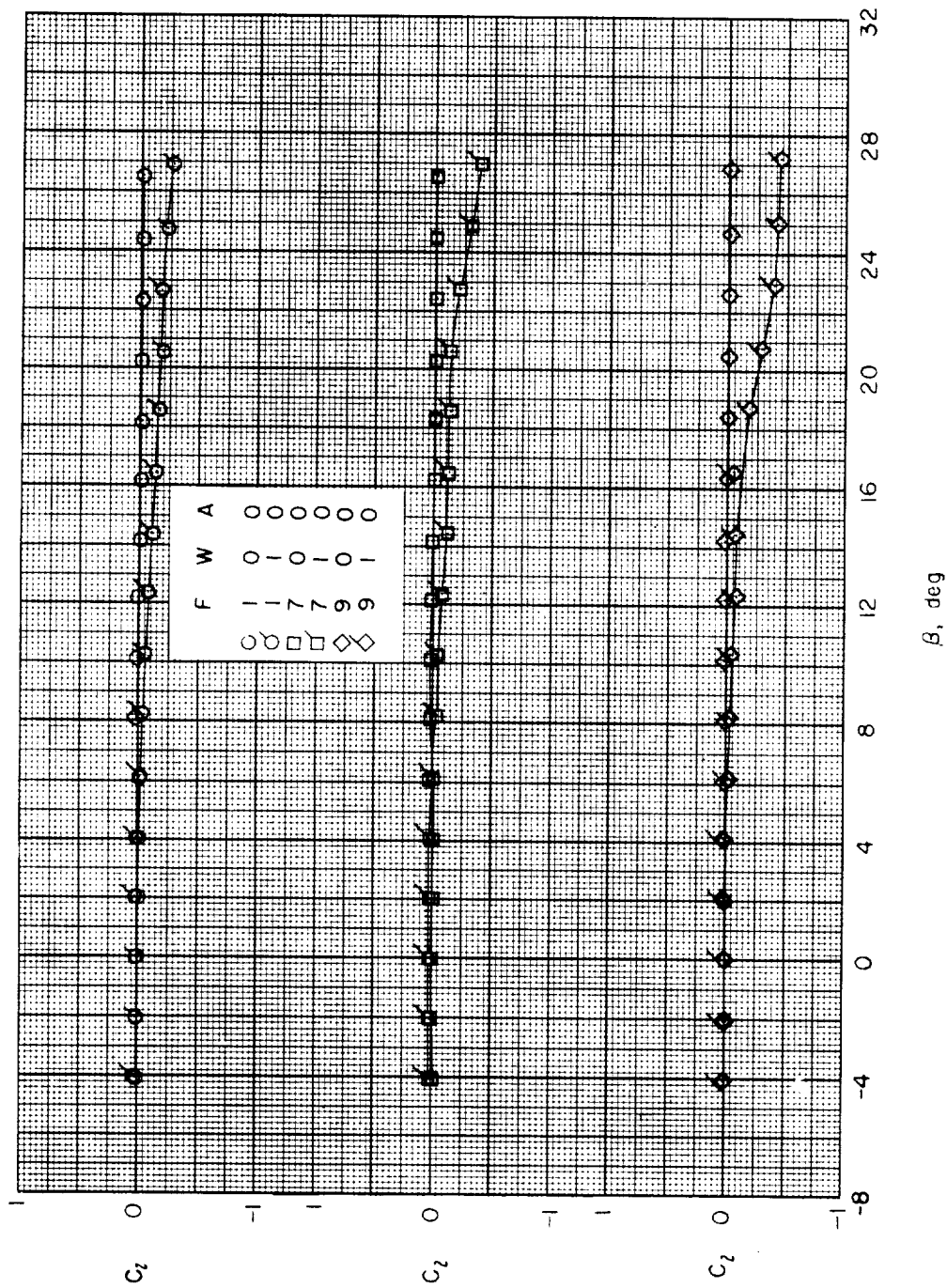
(b) $\alpha \approx 4.1^\circ$.

Figure 25.-- Continued.



(v) Concluded.

Figure 25.—Continued.

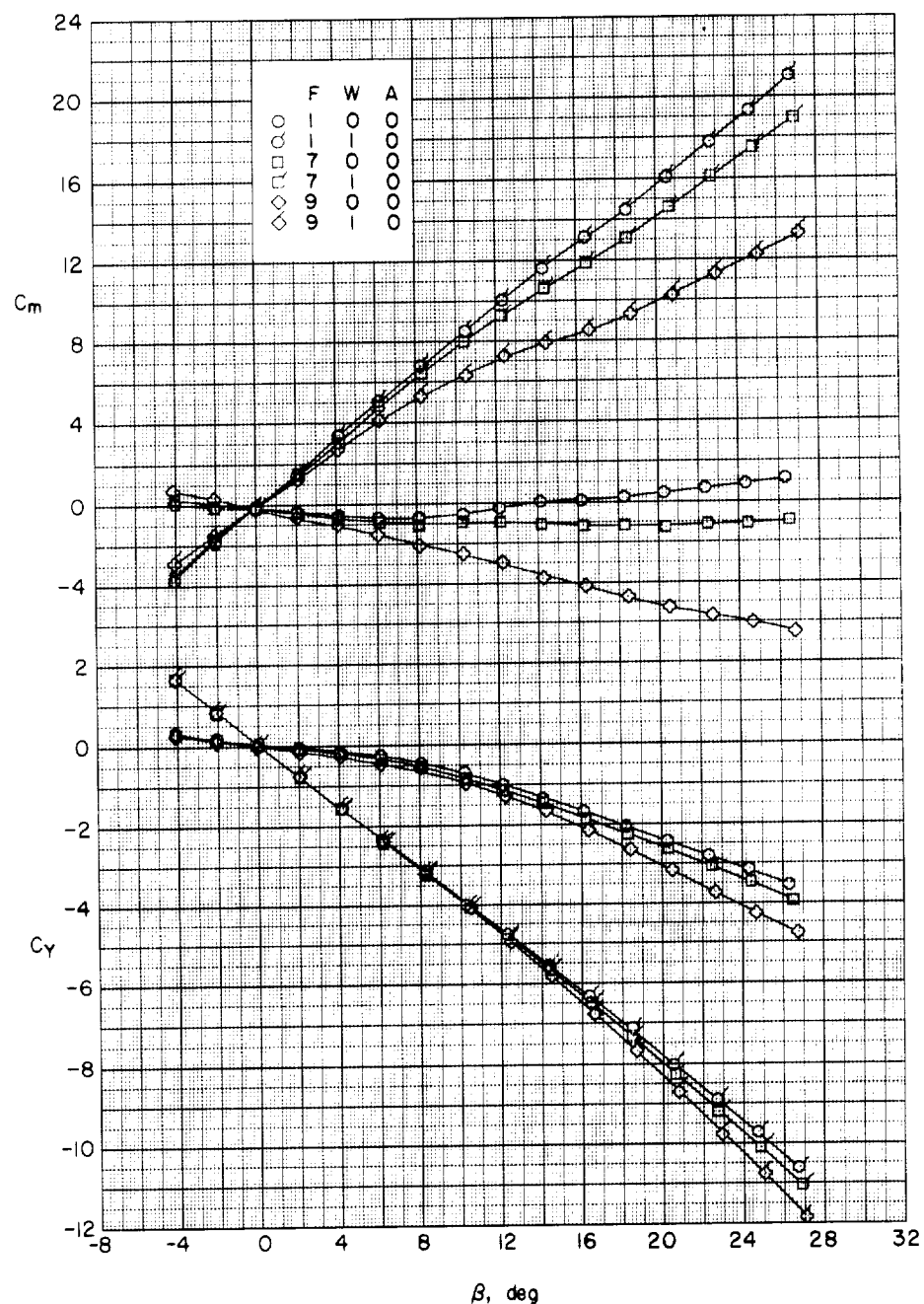
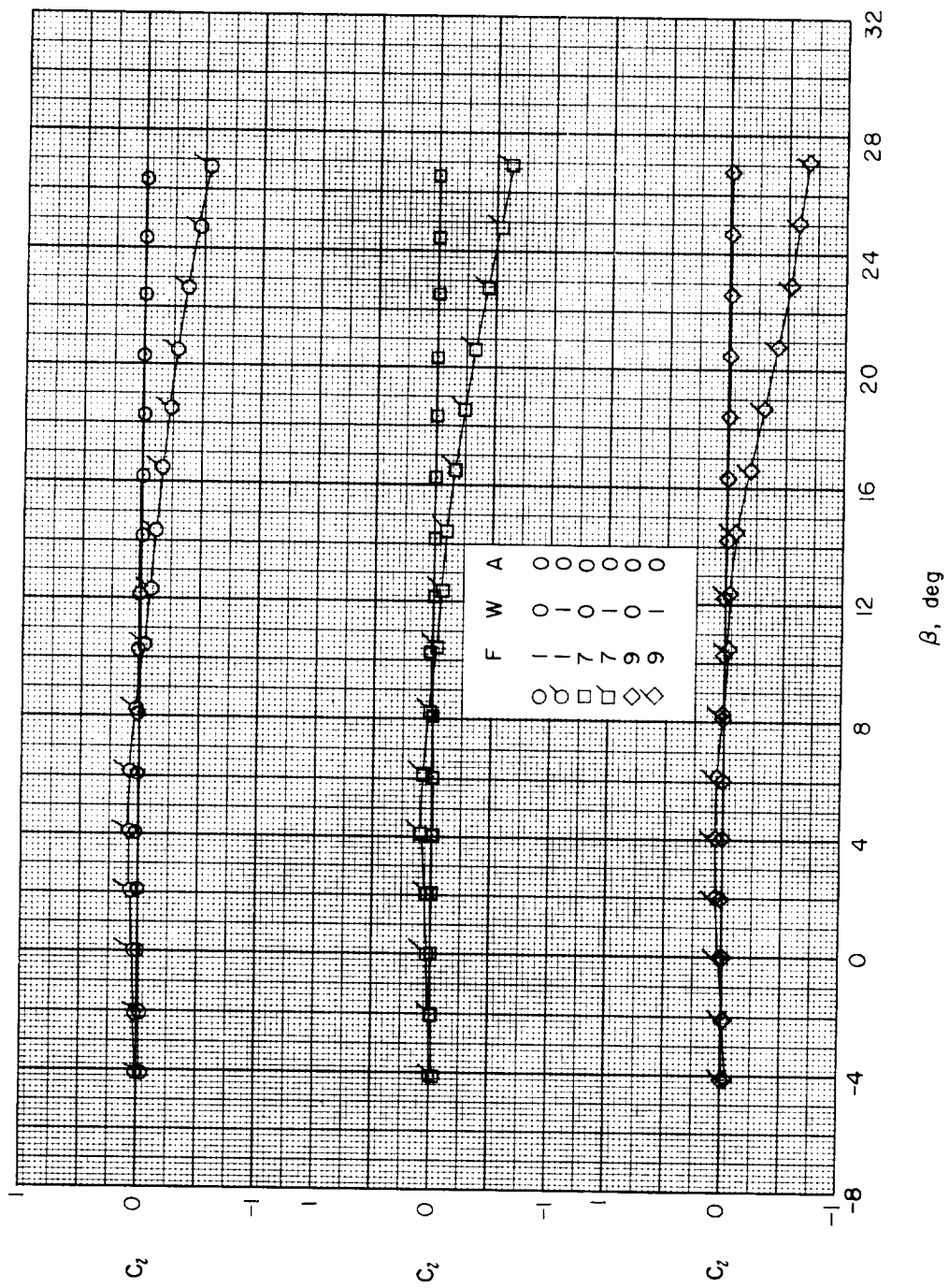
(c) $\alpha \approx 8.2^\circ$.

Figure 25.- Continued.



(c) Concluded.

Figure 25.- Continued.

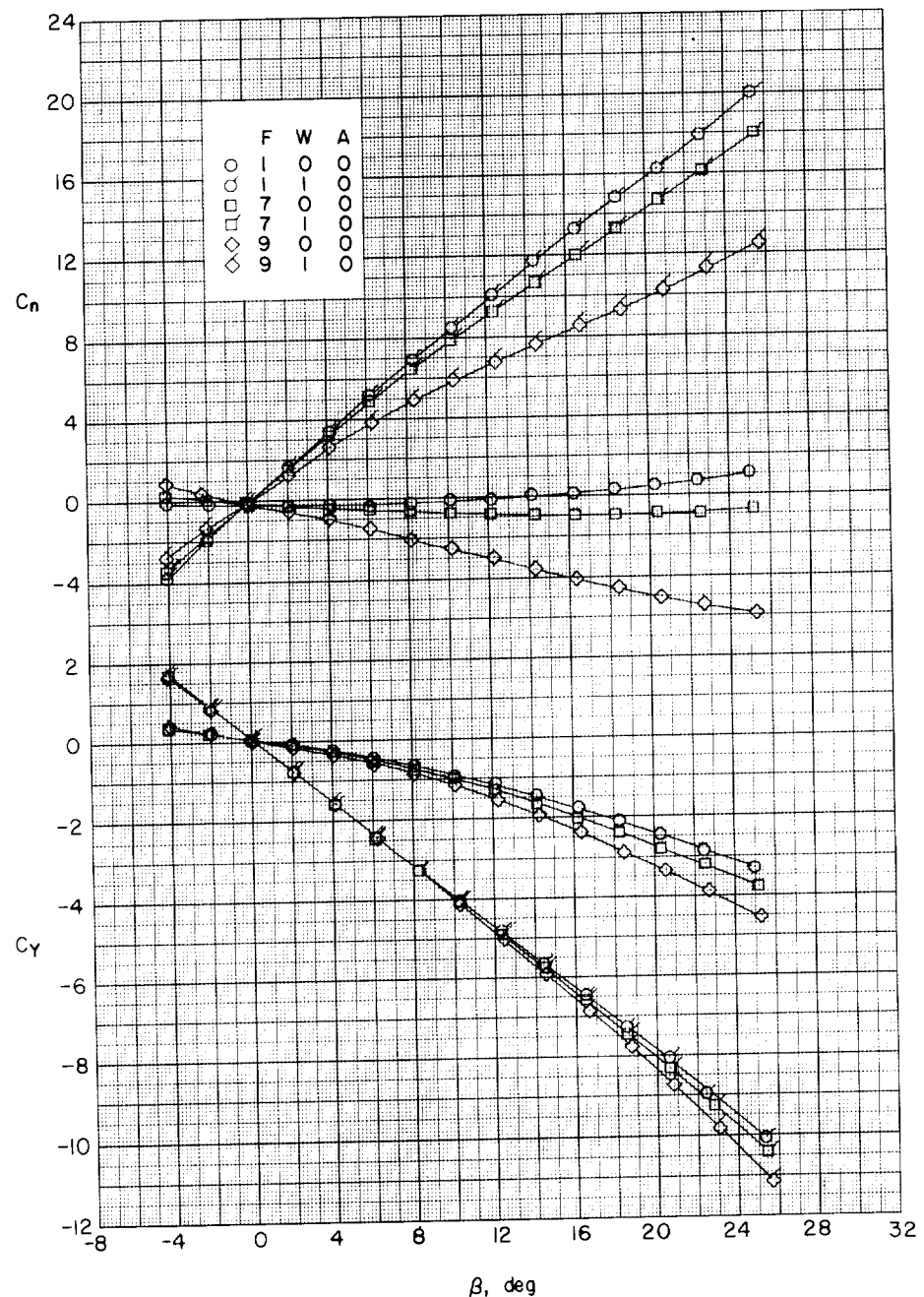
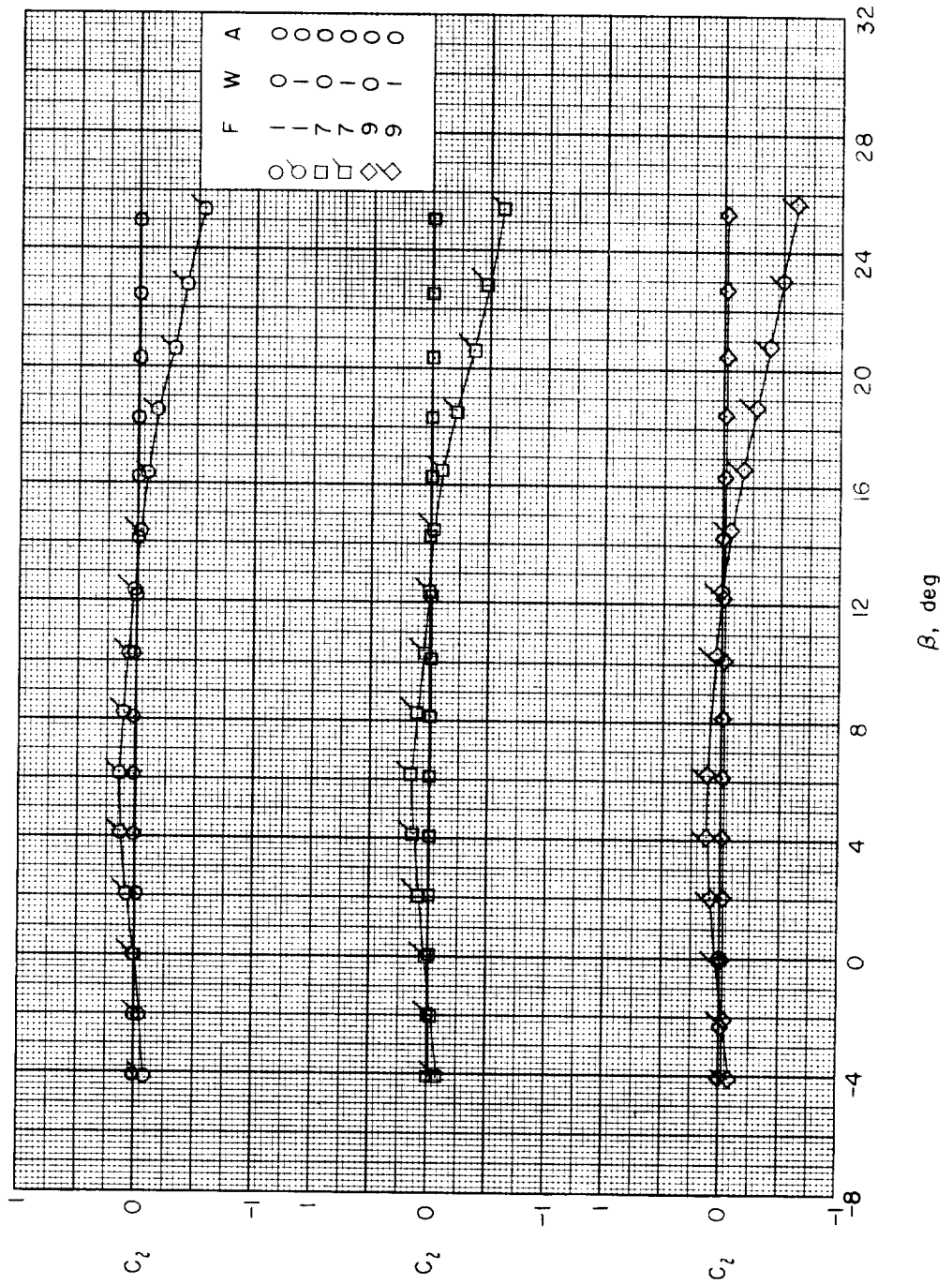
(d) $\alpha \approx 12.3^\circ$.

Figure 25.- Continued.



(d) Concluded.

Figure 25.- Continued.

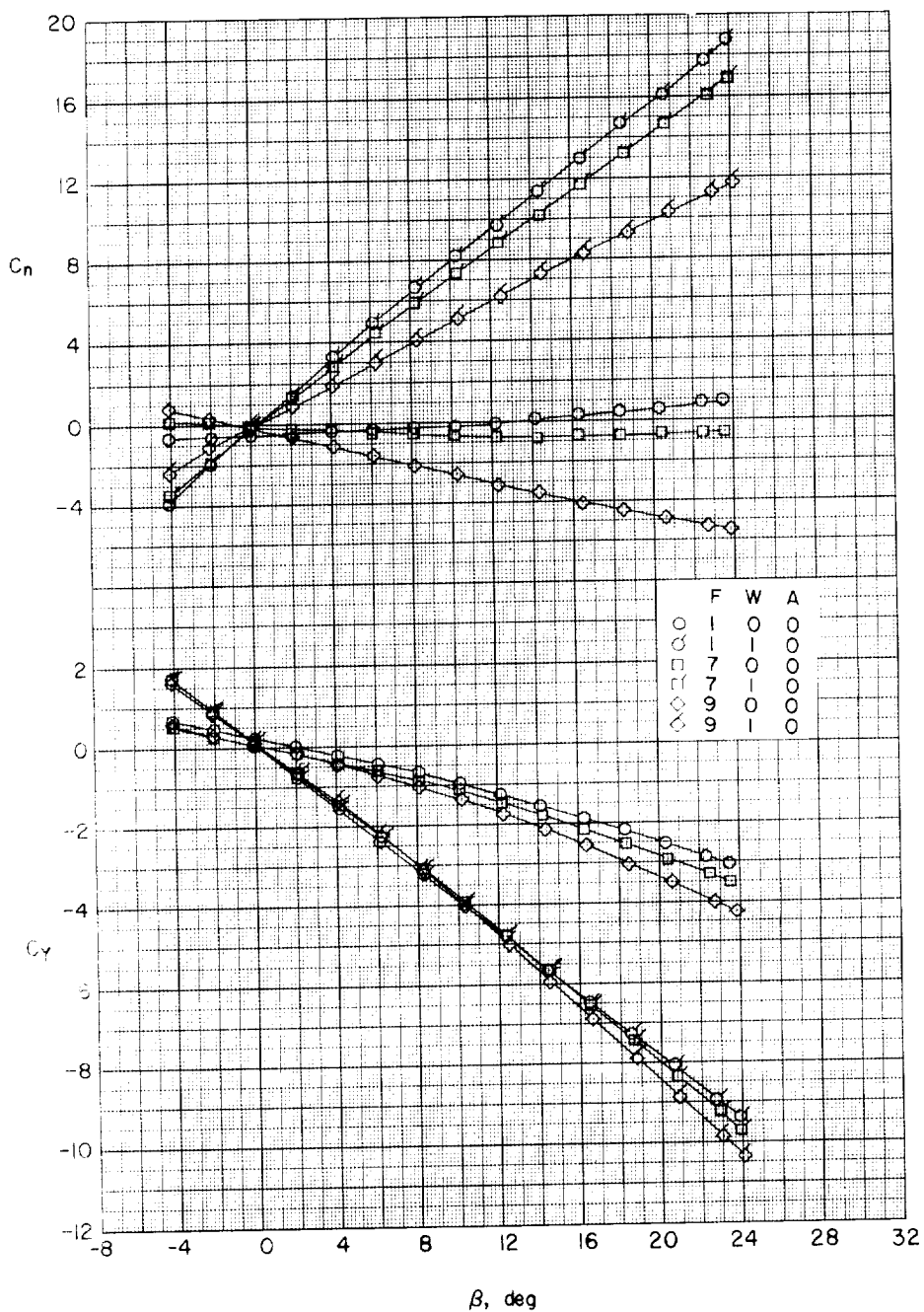
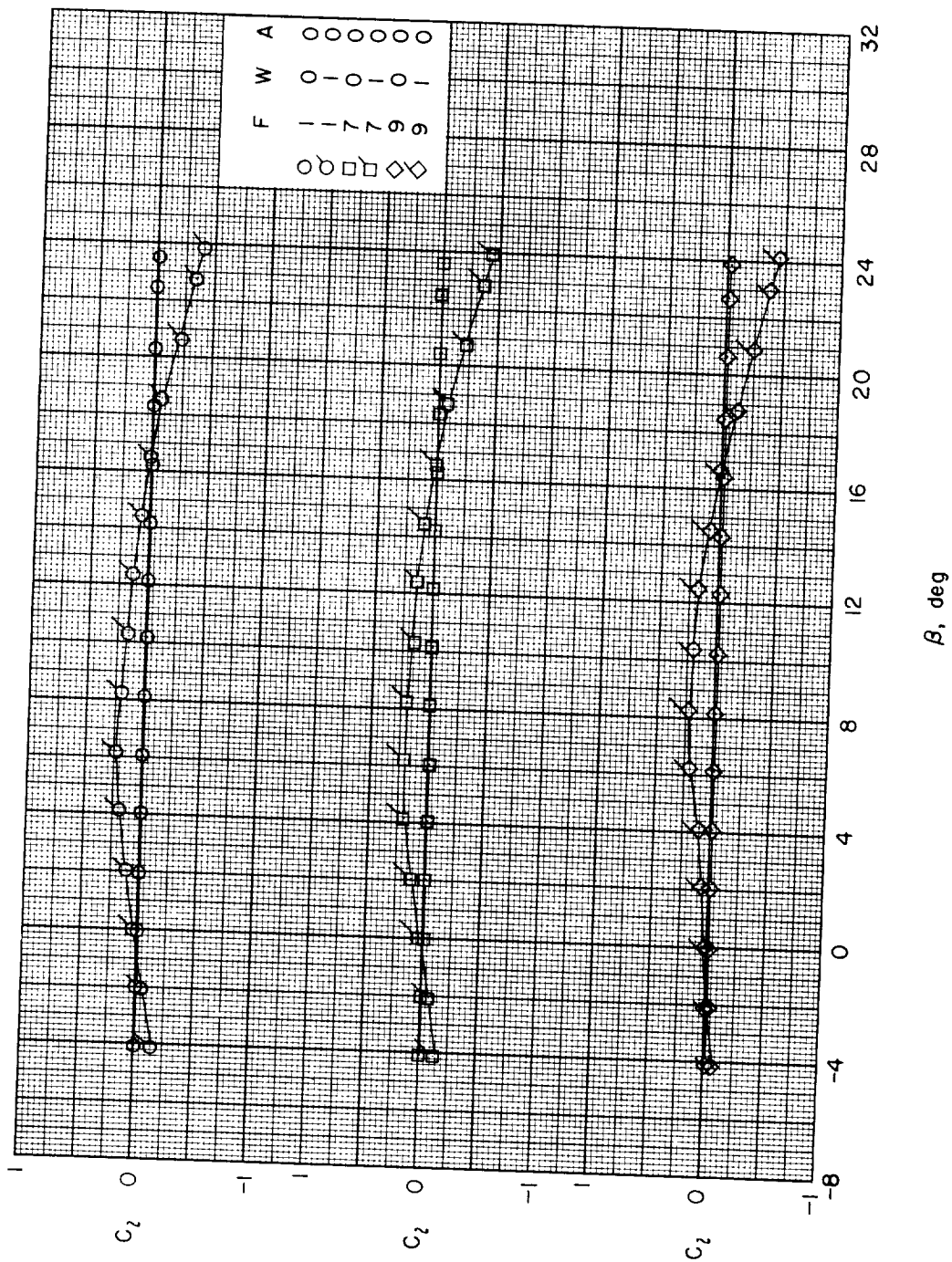
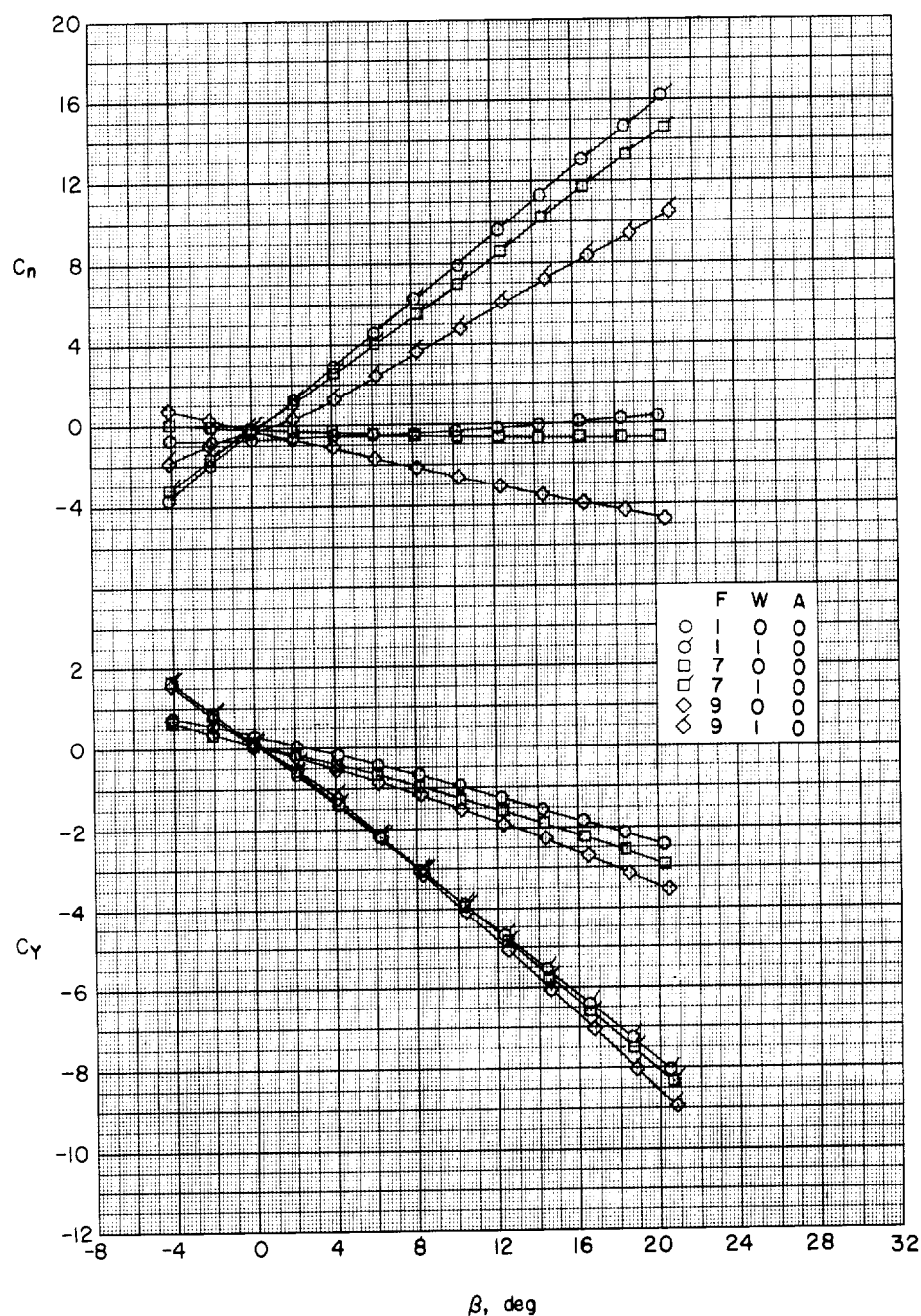
(e) $\alpha \approx 16.4^\circ$.

Figure 25.- Continued.



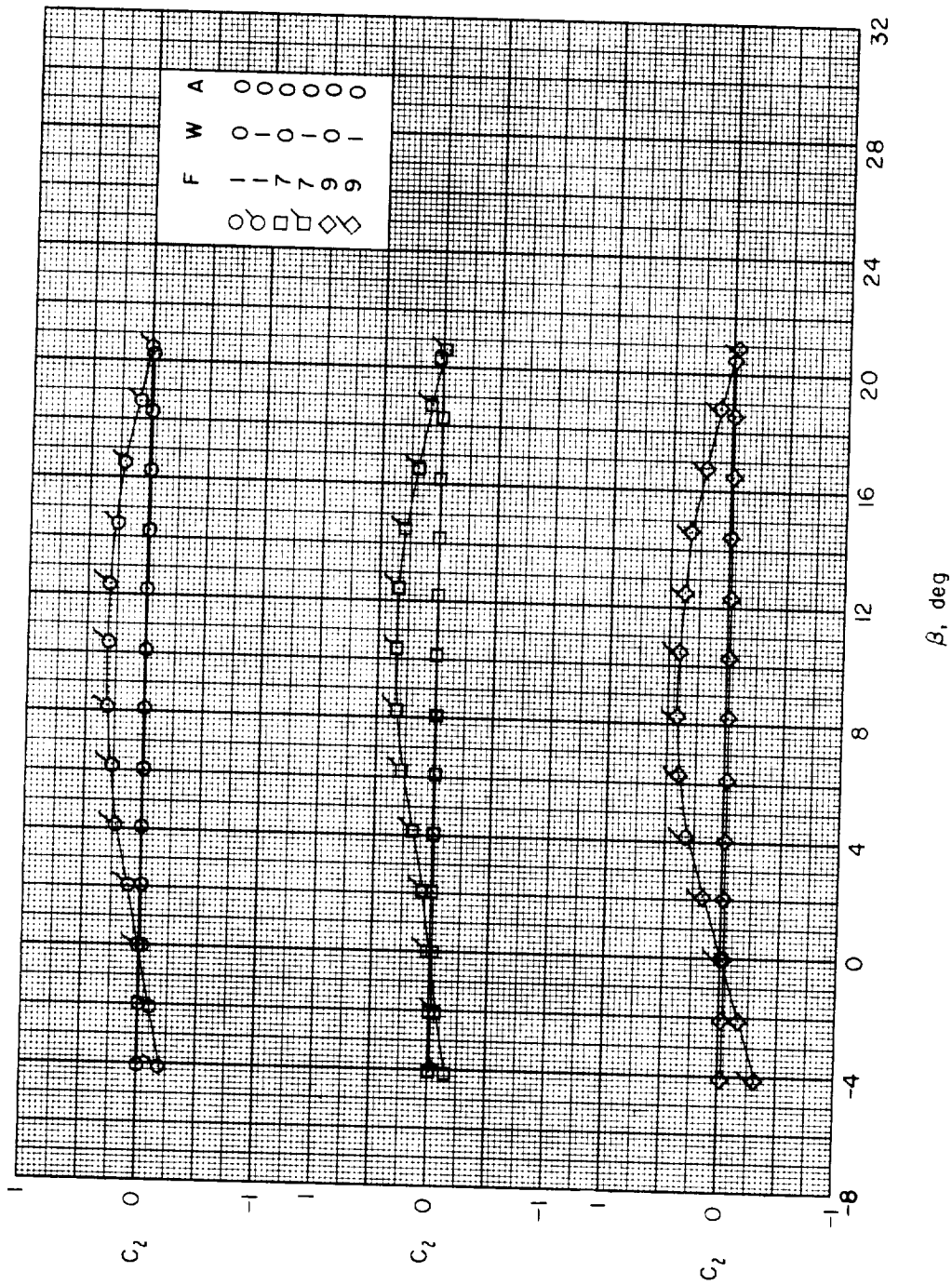
(e) Concluded.

Figure 25.- Continued.



(f) $\alpha \approx 20.5^\circ$.

Figure 25.- Continued.



(F) Concluded.

Figure 25.- Continued.

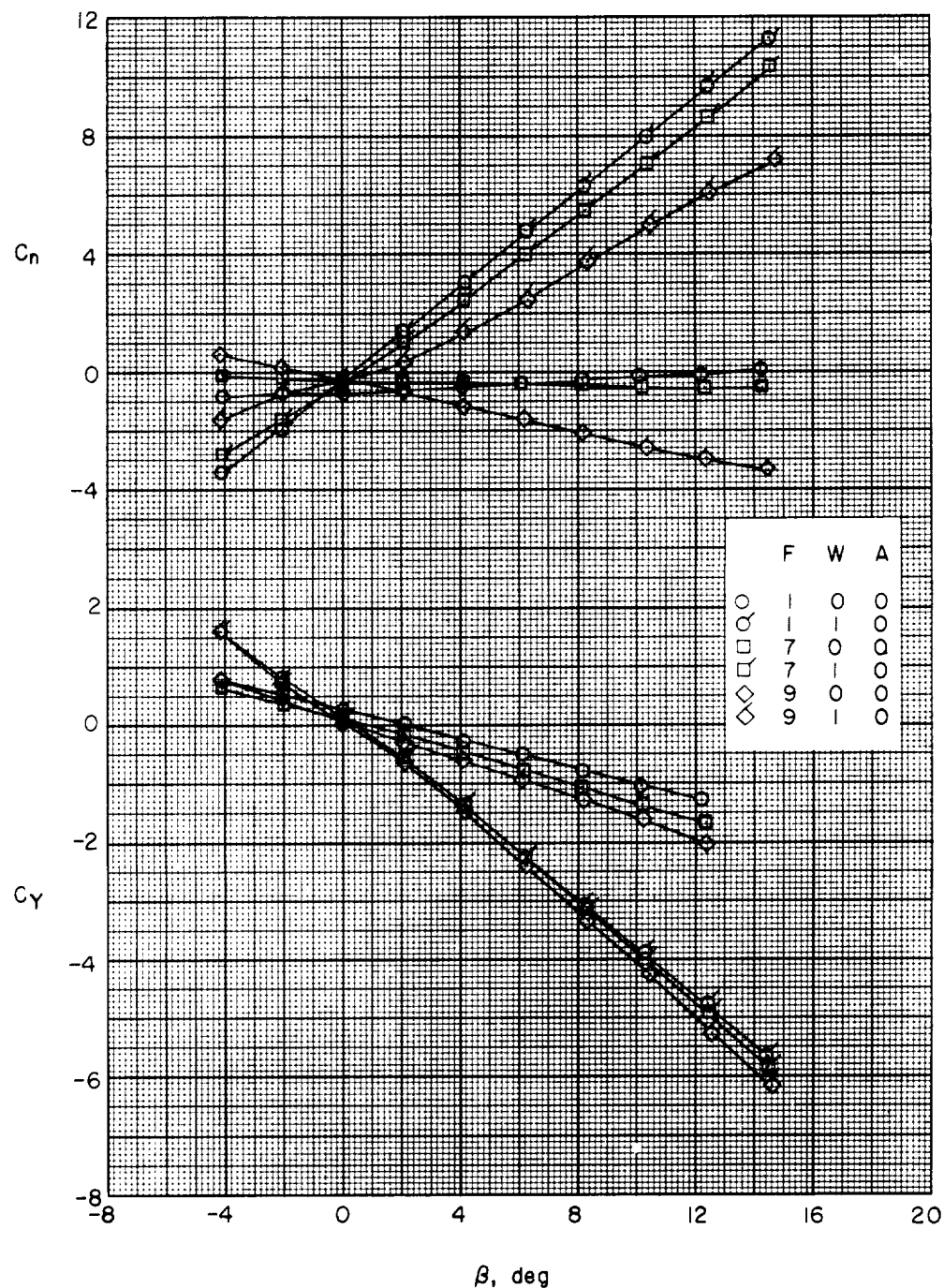
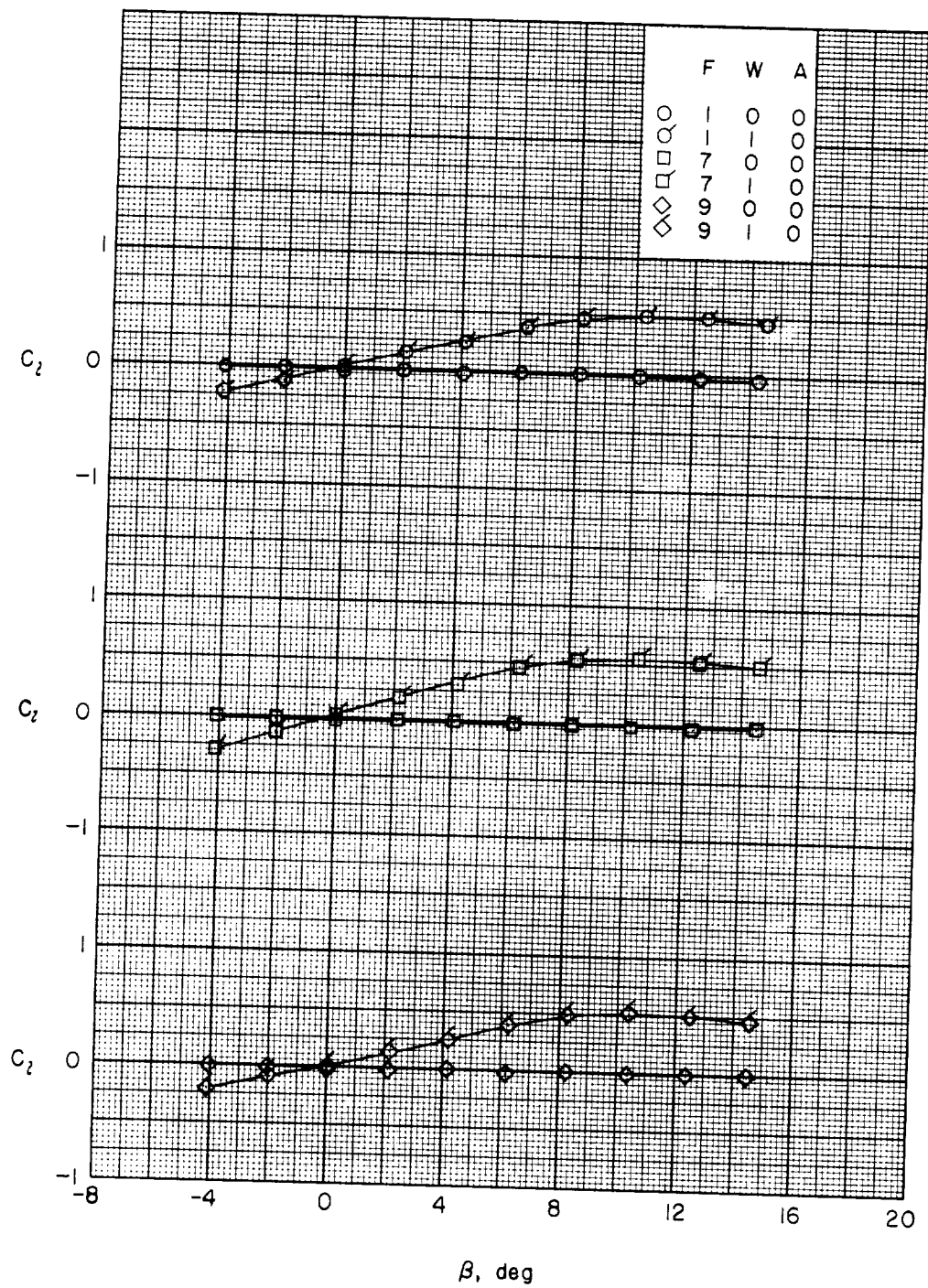
(g) $\alpha \approx 24.7^\circ$.

Figure 25.- Continued.



(g) Concluded.

Figure 25.- Concluded.

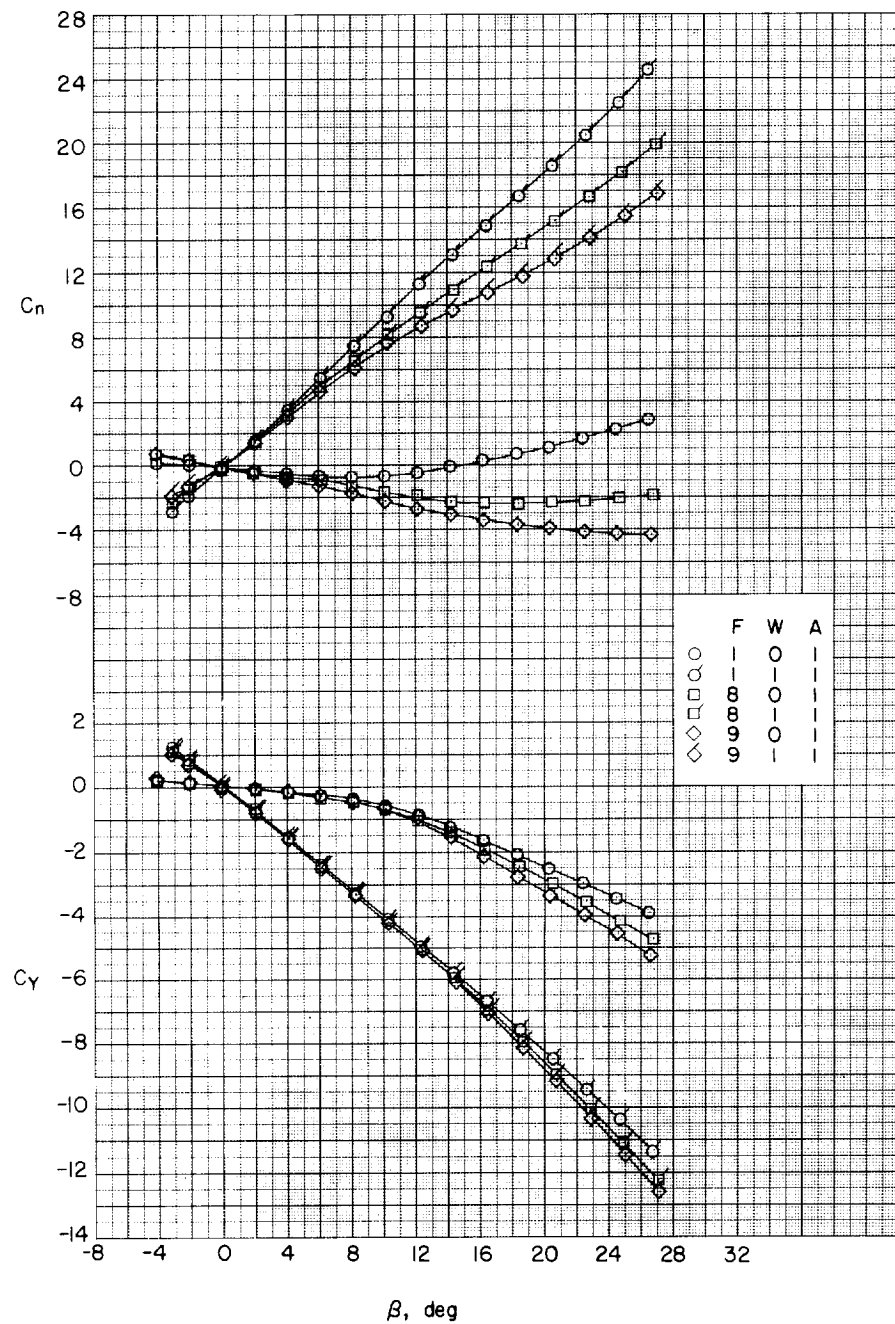
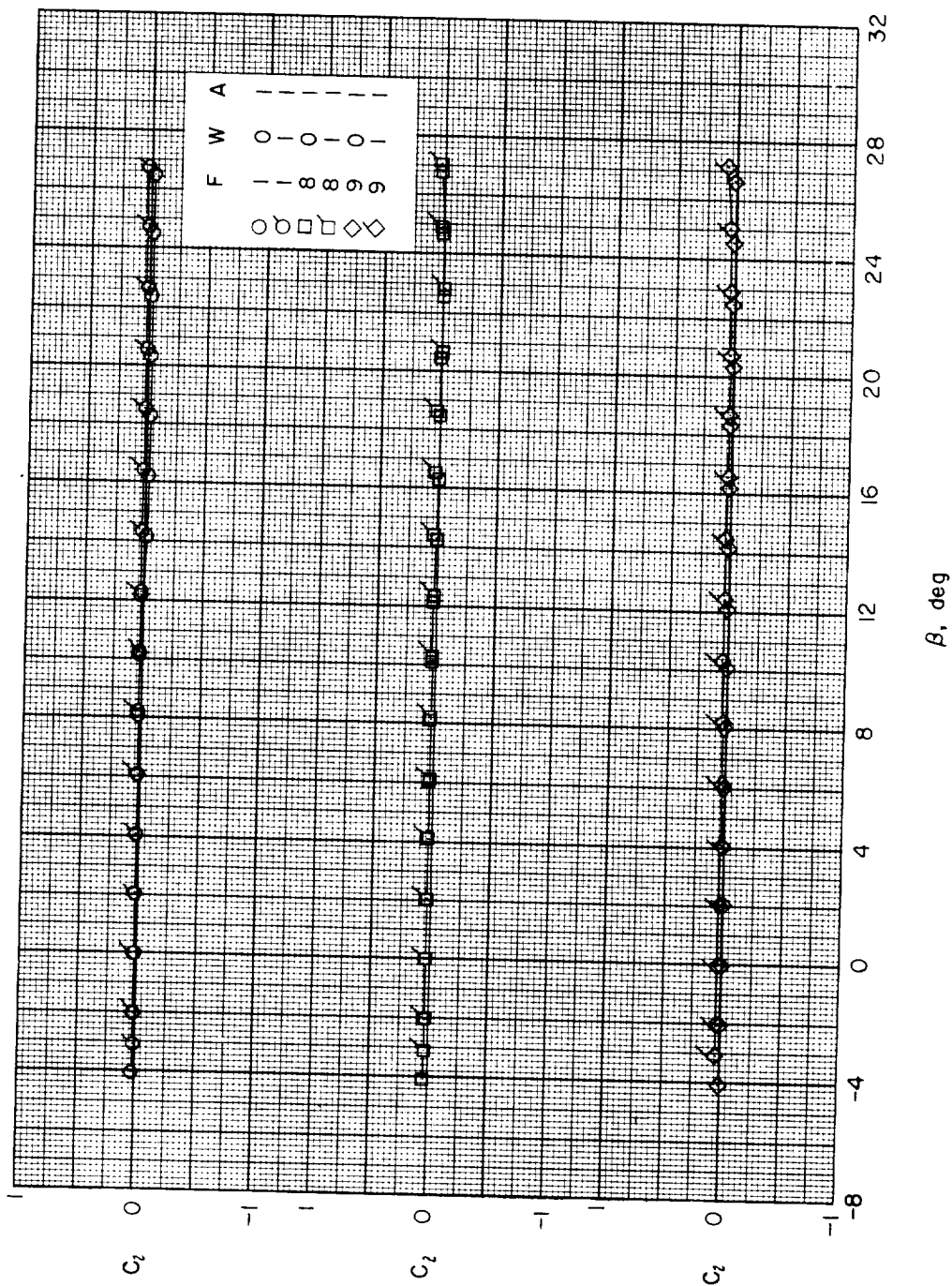
(a) $\alpha \approx 0^\circ$.

Figure 26.- Effect of forebody length on aerodynamic characteristics in sideslip. Large delta wings; 1-caliber cylindrical afterbody.



(a) Concluded.

Figure 26.- Continued.

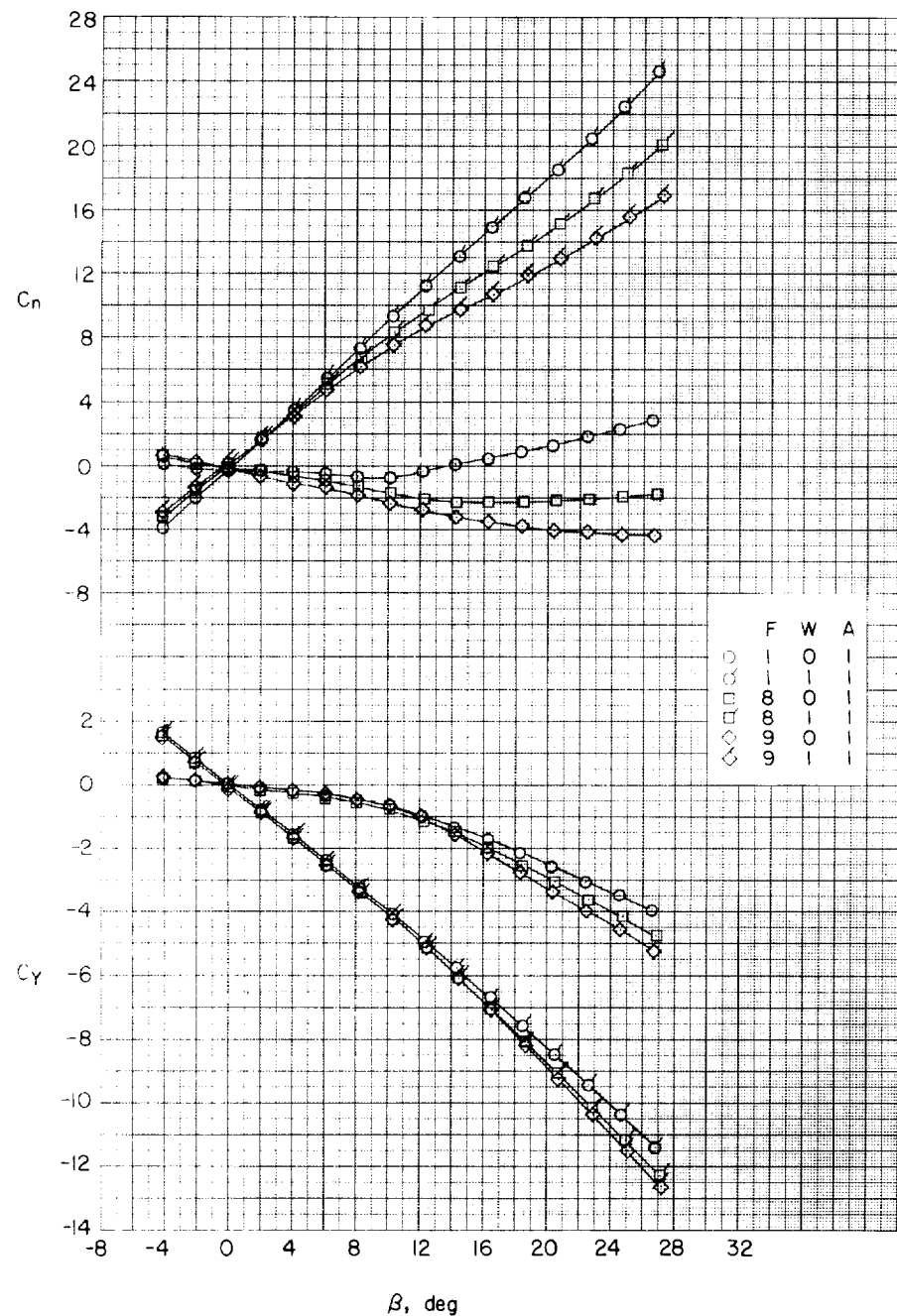
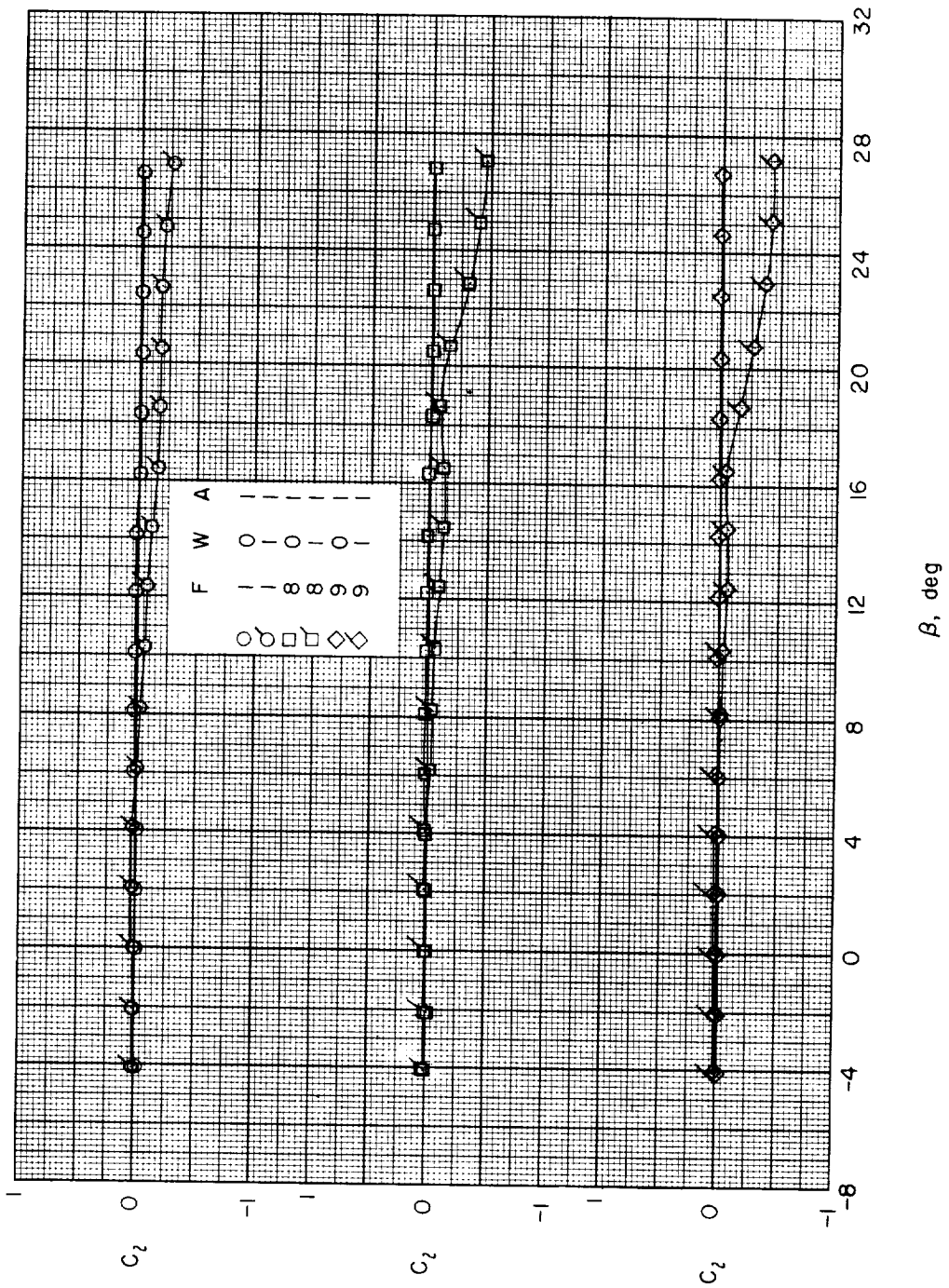
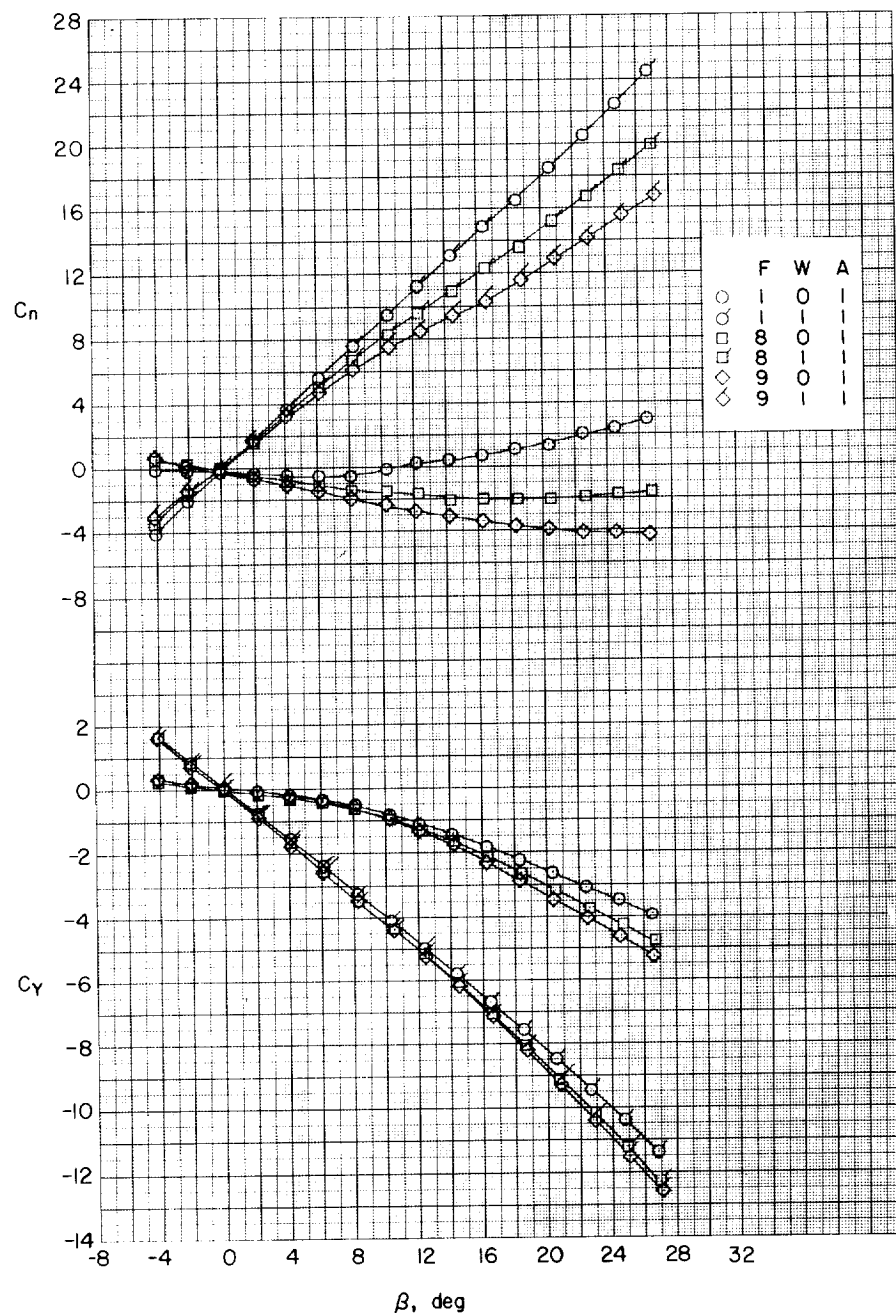
(b) $\alpha \approx 4.1^\circ$.

Figure 26.- Continued.



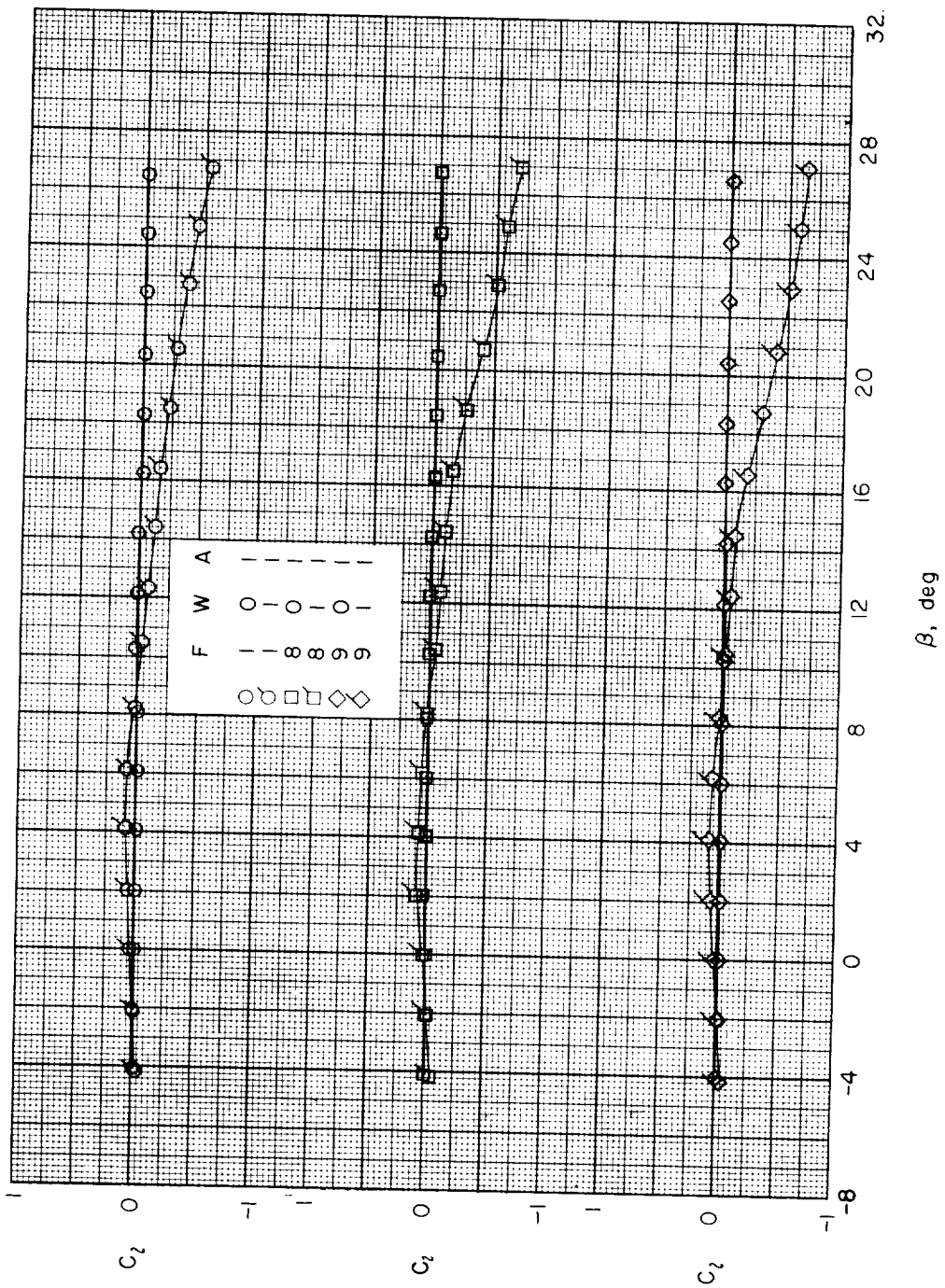
(b) Concluded.

Figure 26.- Continued.



(c) $\alpha \approx 8.2^\circ$.

Figure 26.- Continued.



(c) Concluded.

Figure 26.- Continued.

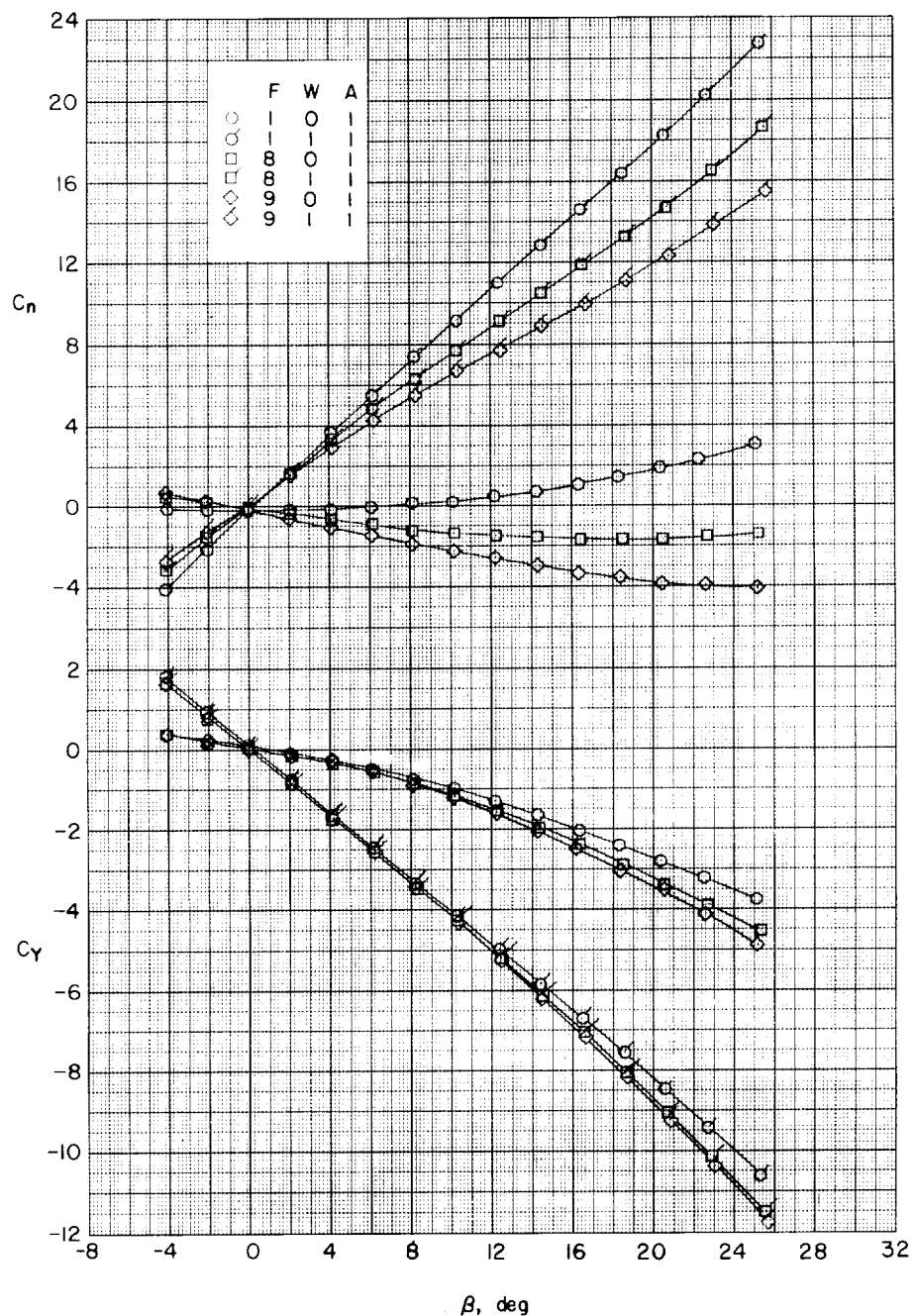
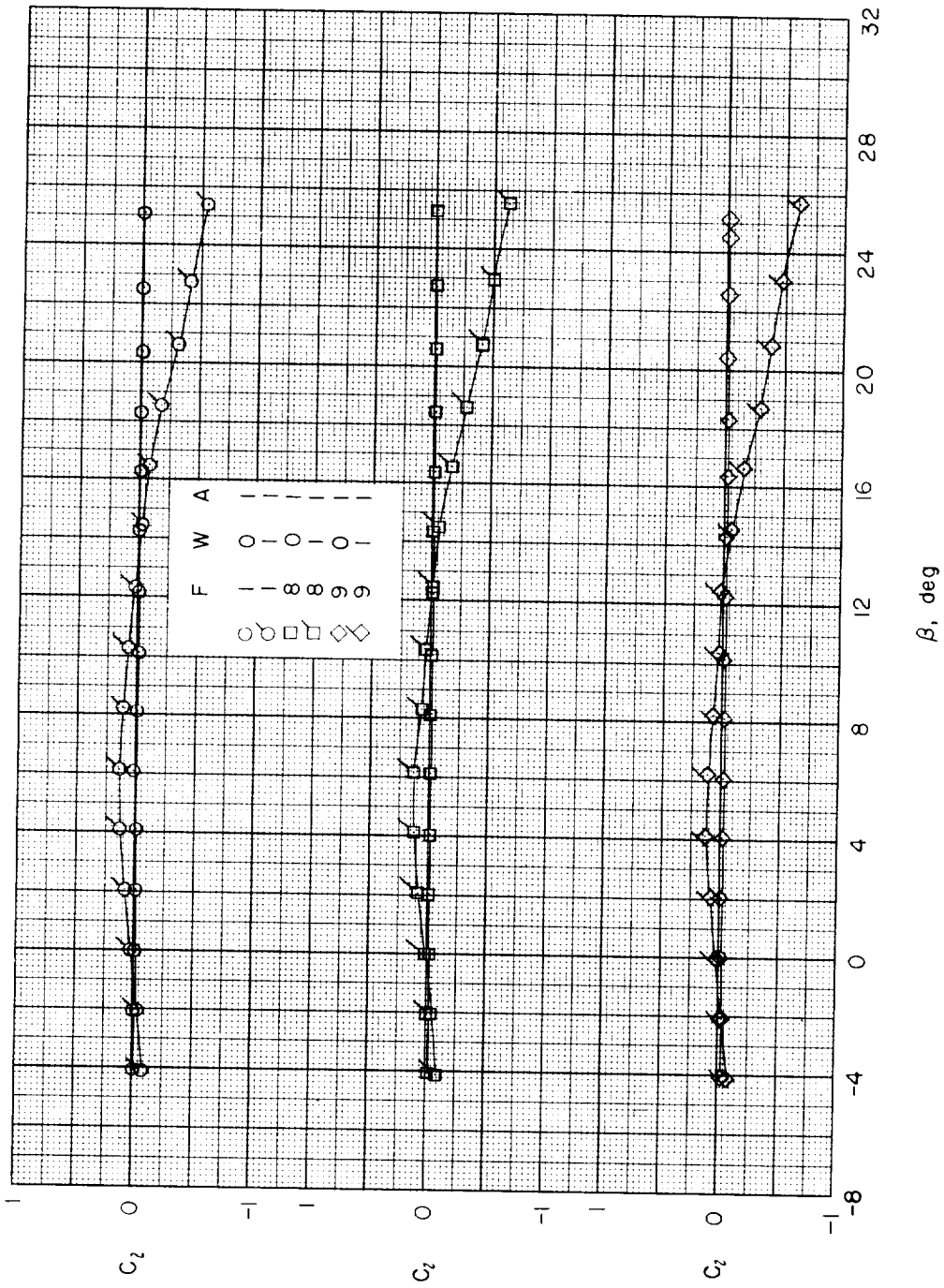
(d) $\alpha \approx 12.3^\circ$.

Figure 26.- Continued.



(d) Concluded.

Figure 26.- Continued.

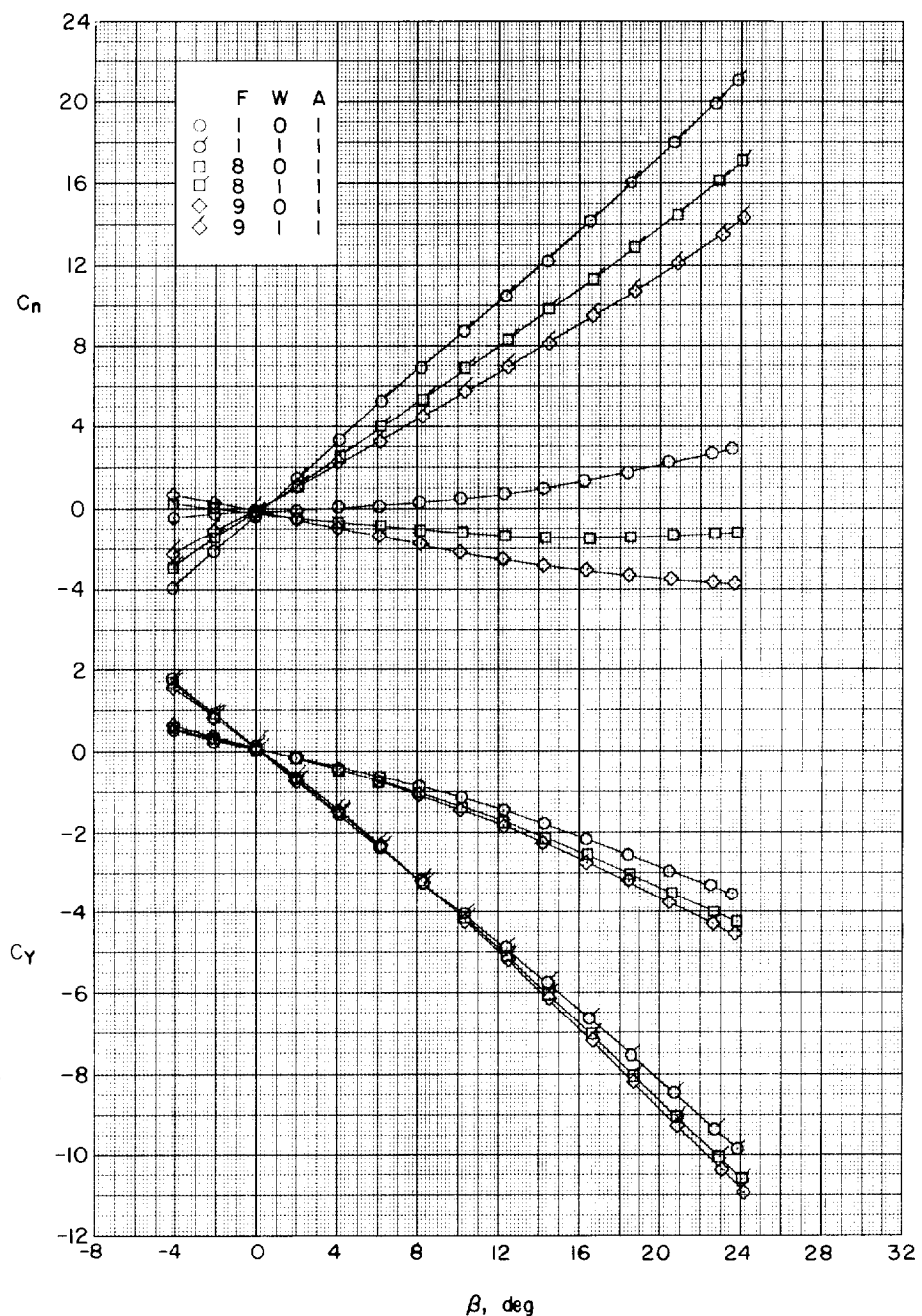
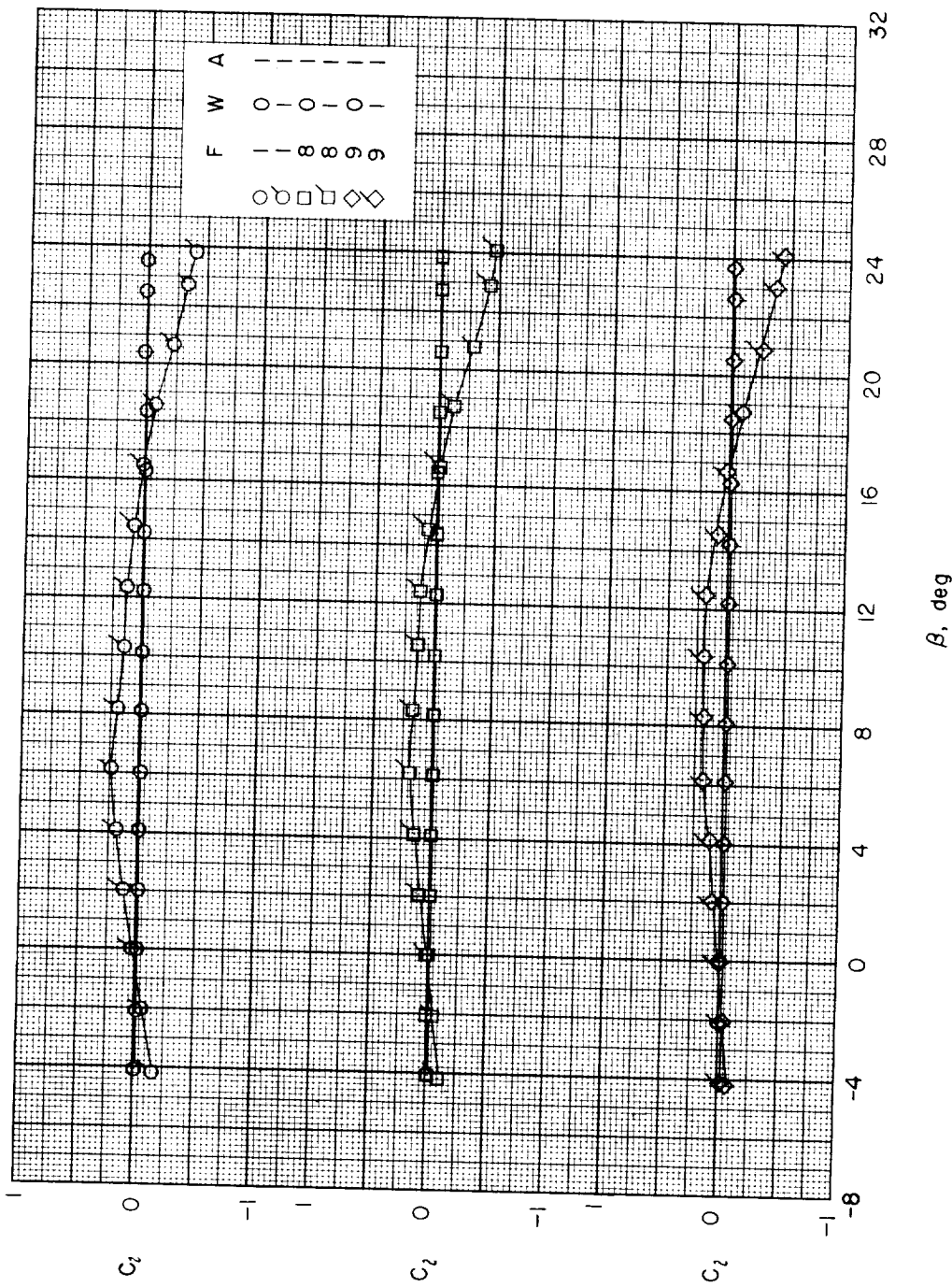
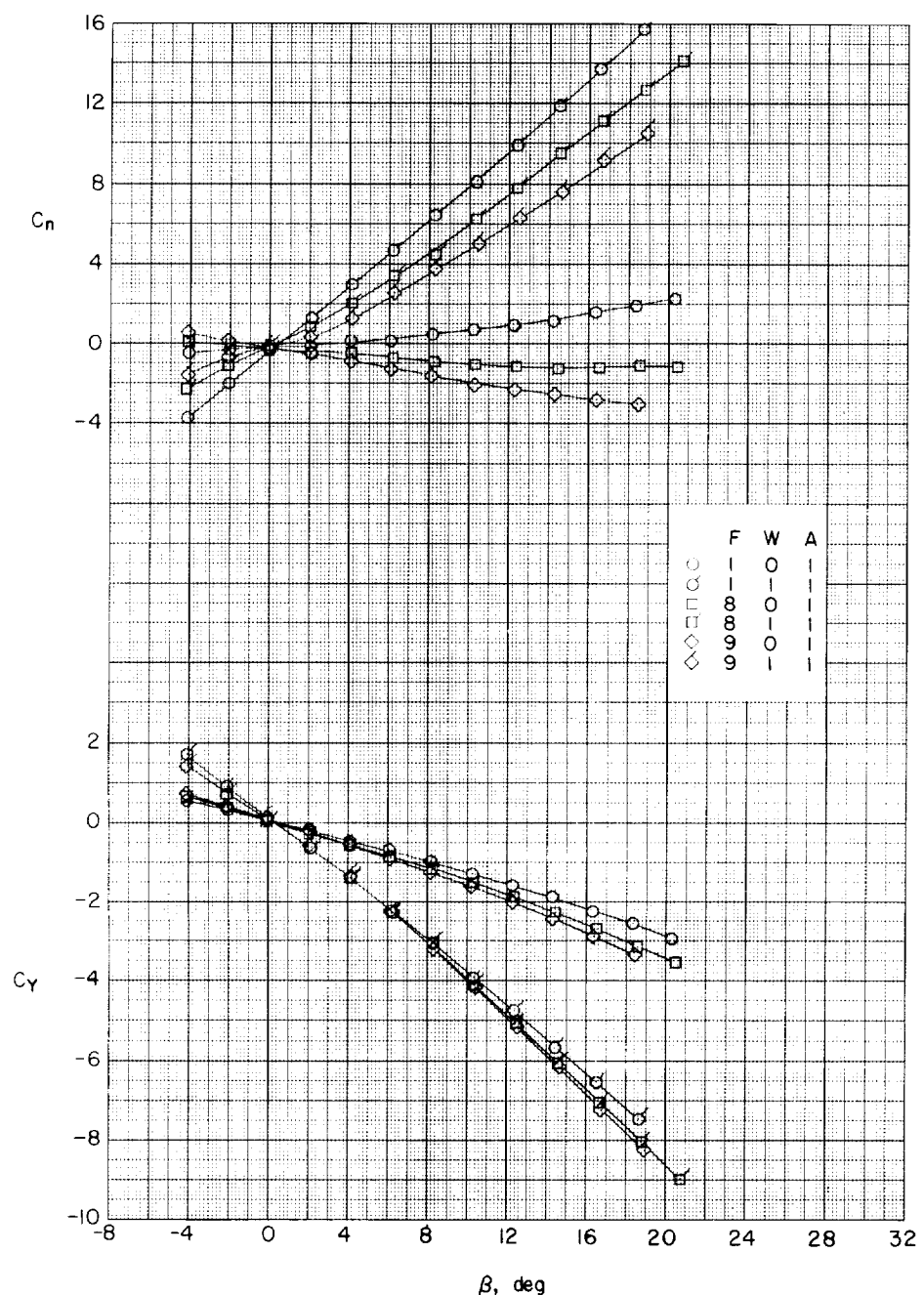
(e) $\alpha \approx 16.4^\circ$.

Figure 26.- Continued.



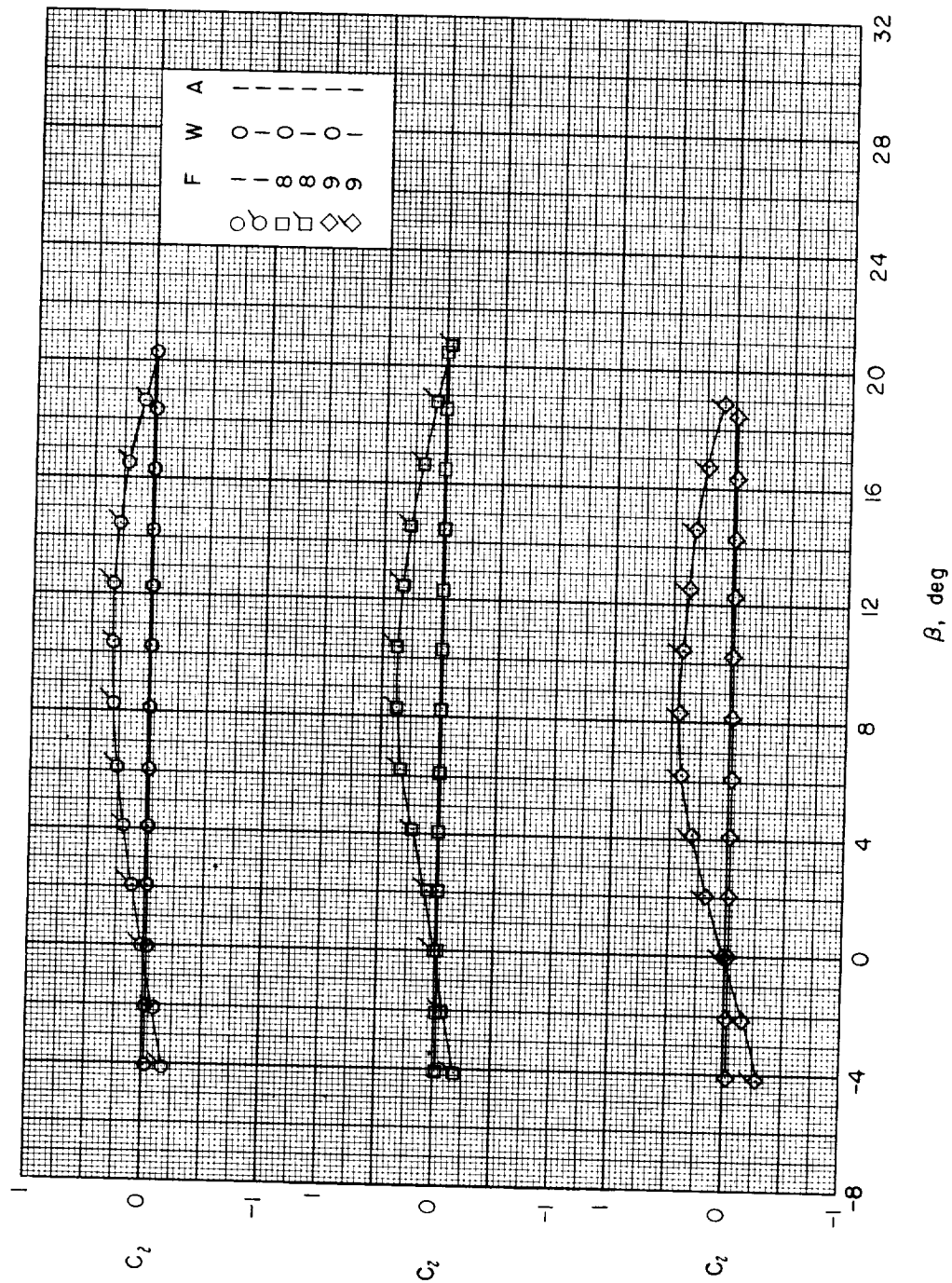
(e) Concluded.

Figure 26.- Continued.



(f) $\alpha \approx 20.5^\circ$.

Figure 26.- Continued.



(f) Concluded.

Figure 26.- Continued.

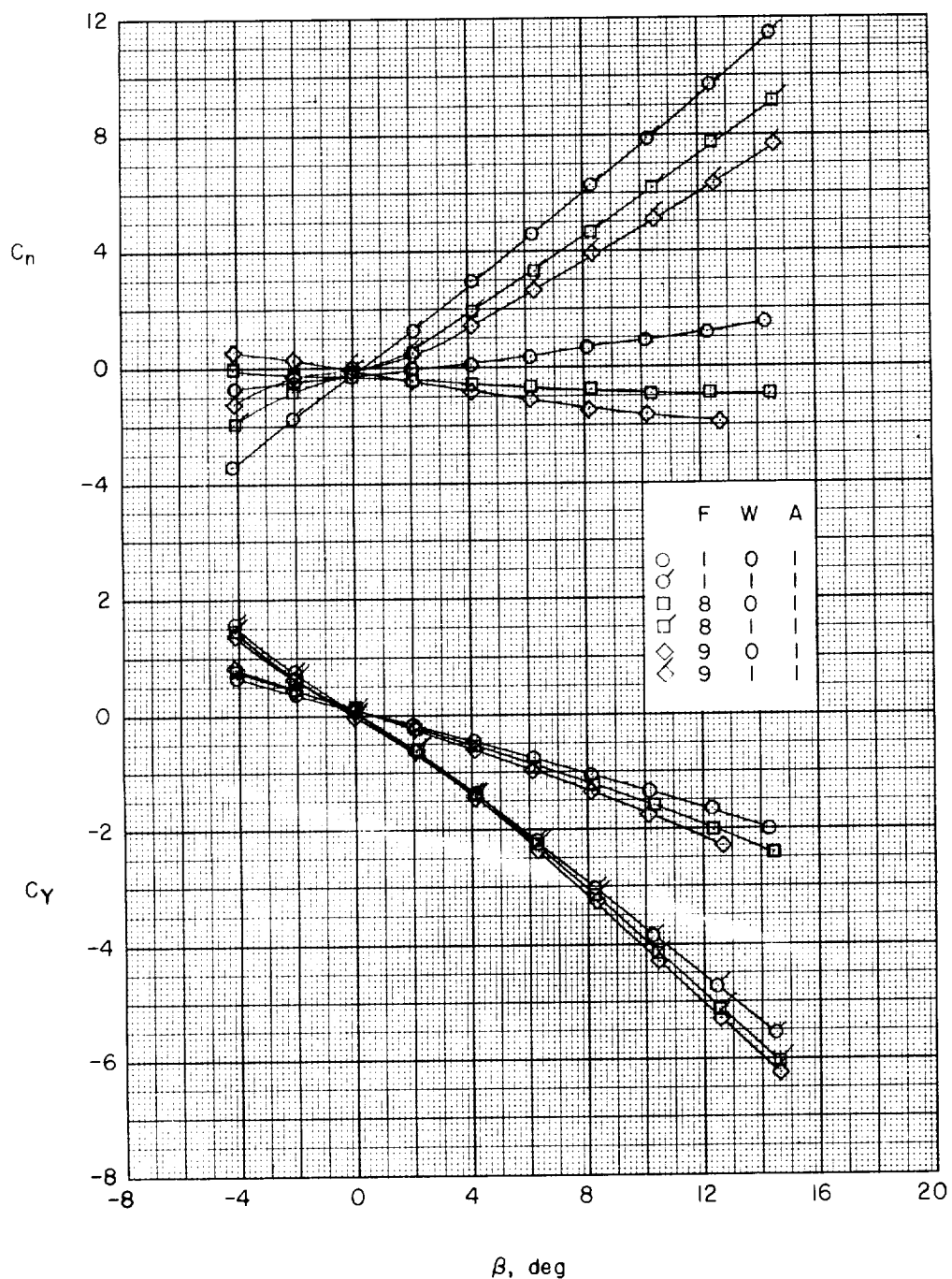
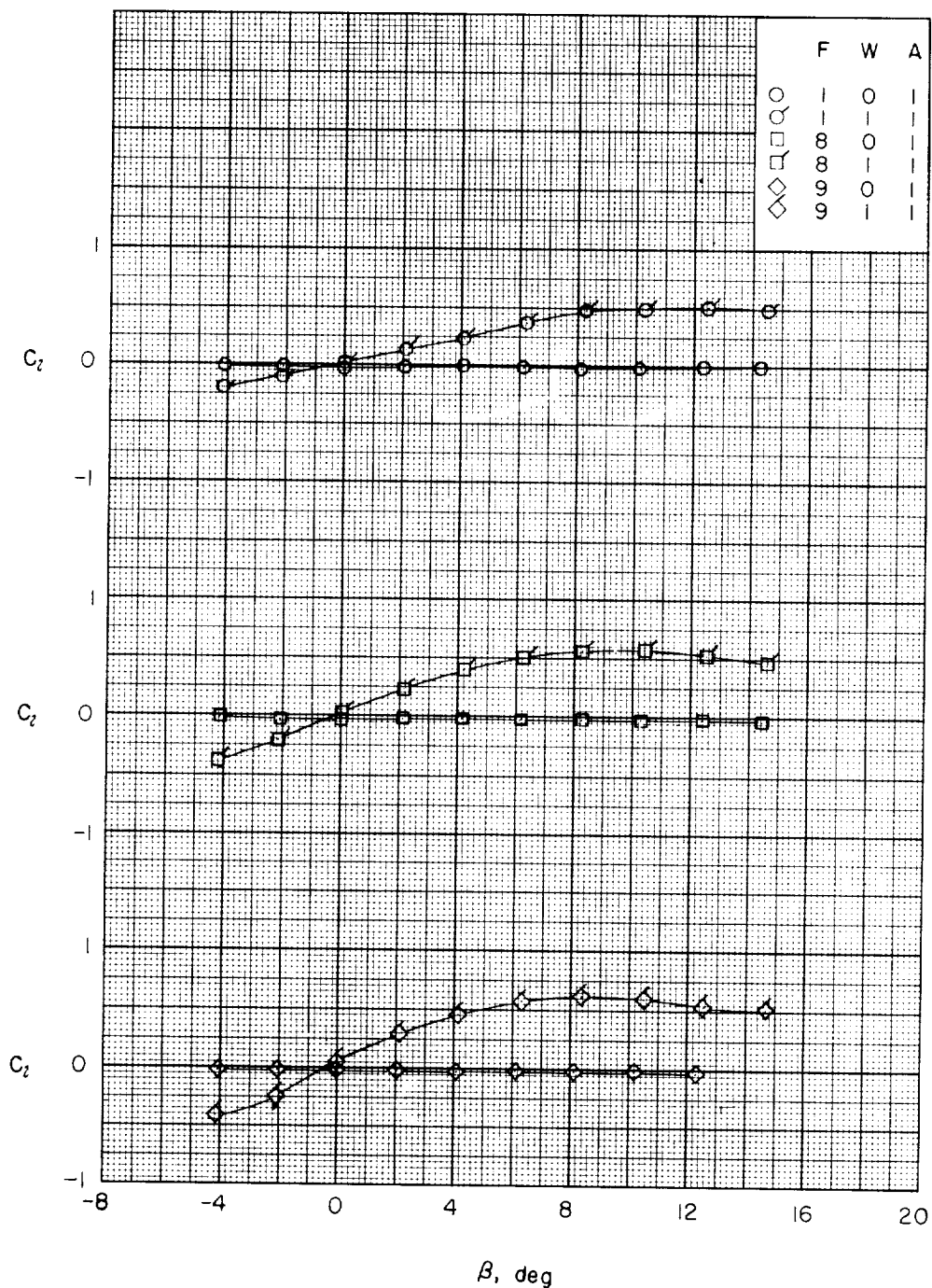
(g) $\alpha \approx 24.7^\circ$.

Figure 26.- Continued.



(g) Concluded.

Figure 26.- Concluded.

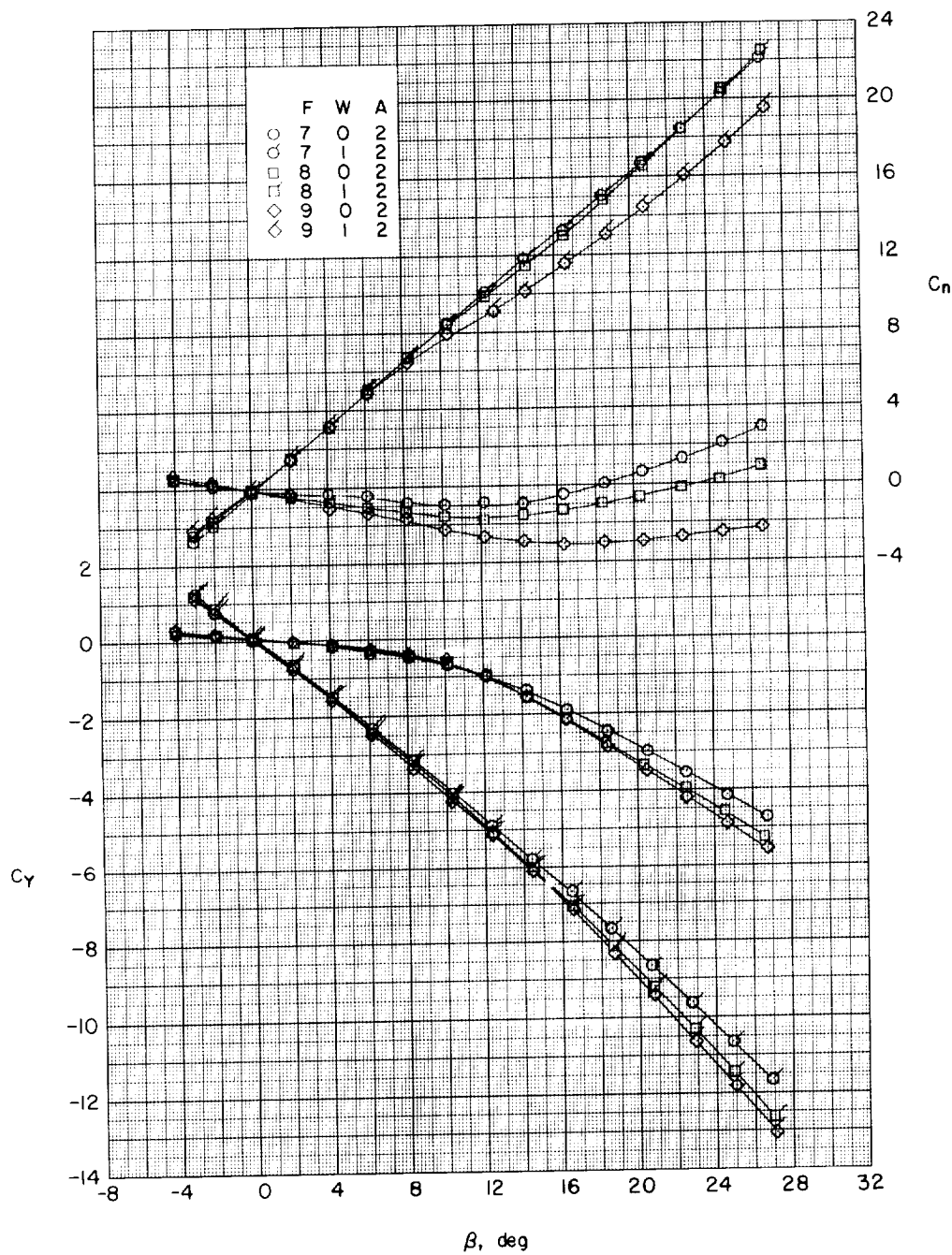
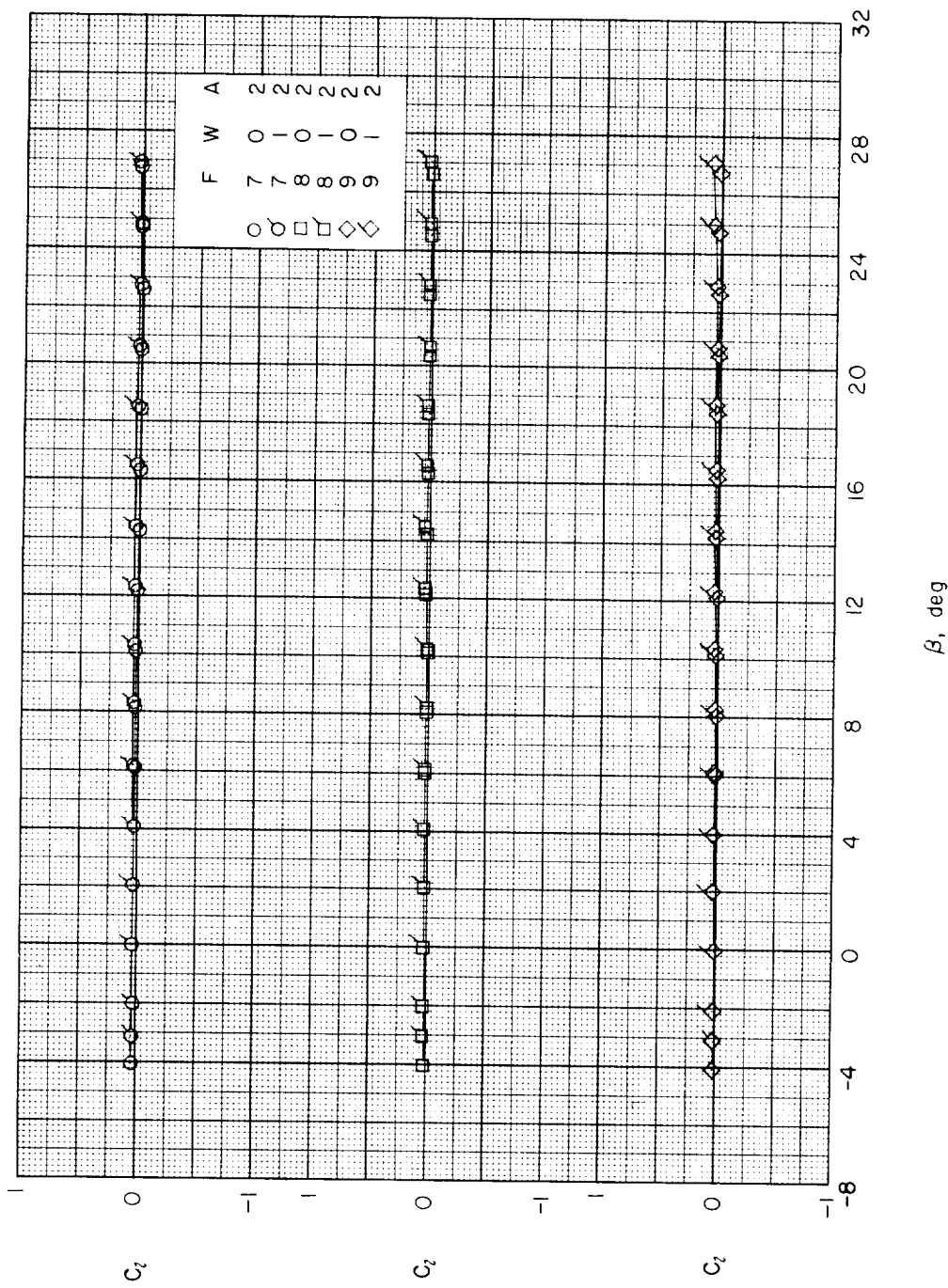
(a) $\alpha \approx 0^\circ$.

Figure 27.- Effects of forebody length on aerodynamic characteristics in sideslip. Large delta wings; 2-caliber cylindrical afterbody.



(a) Concluded.

Figure 27.- Continued.

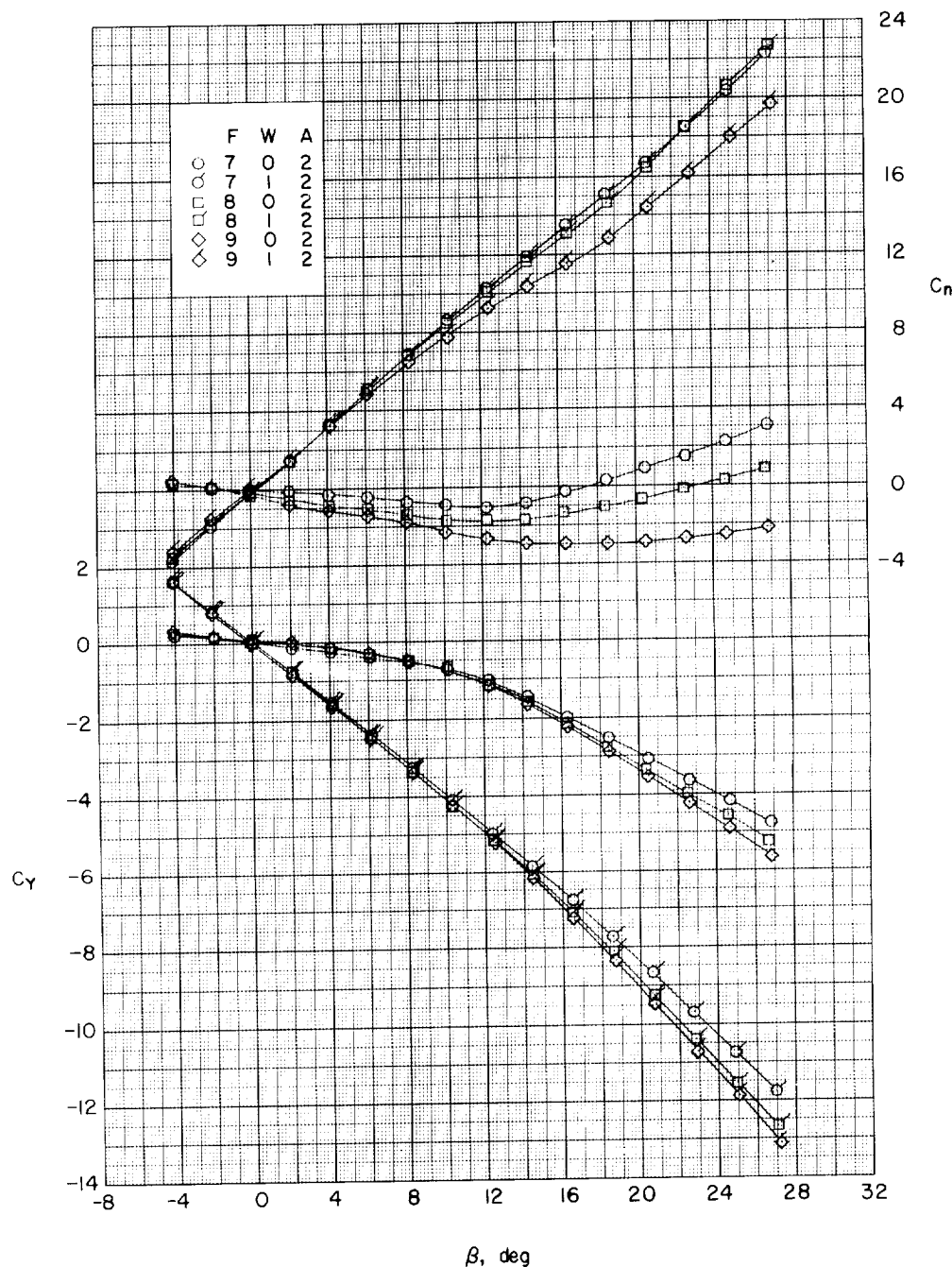
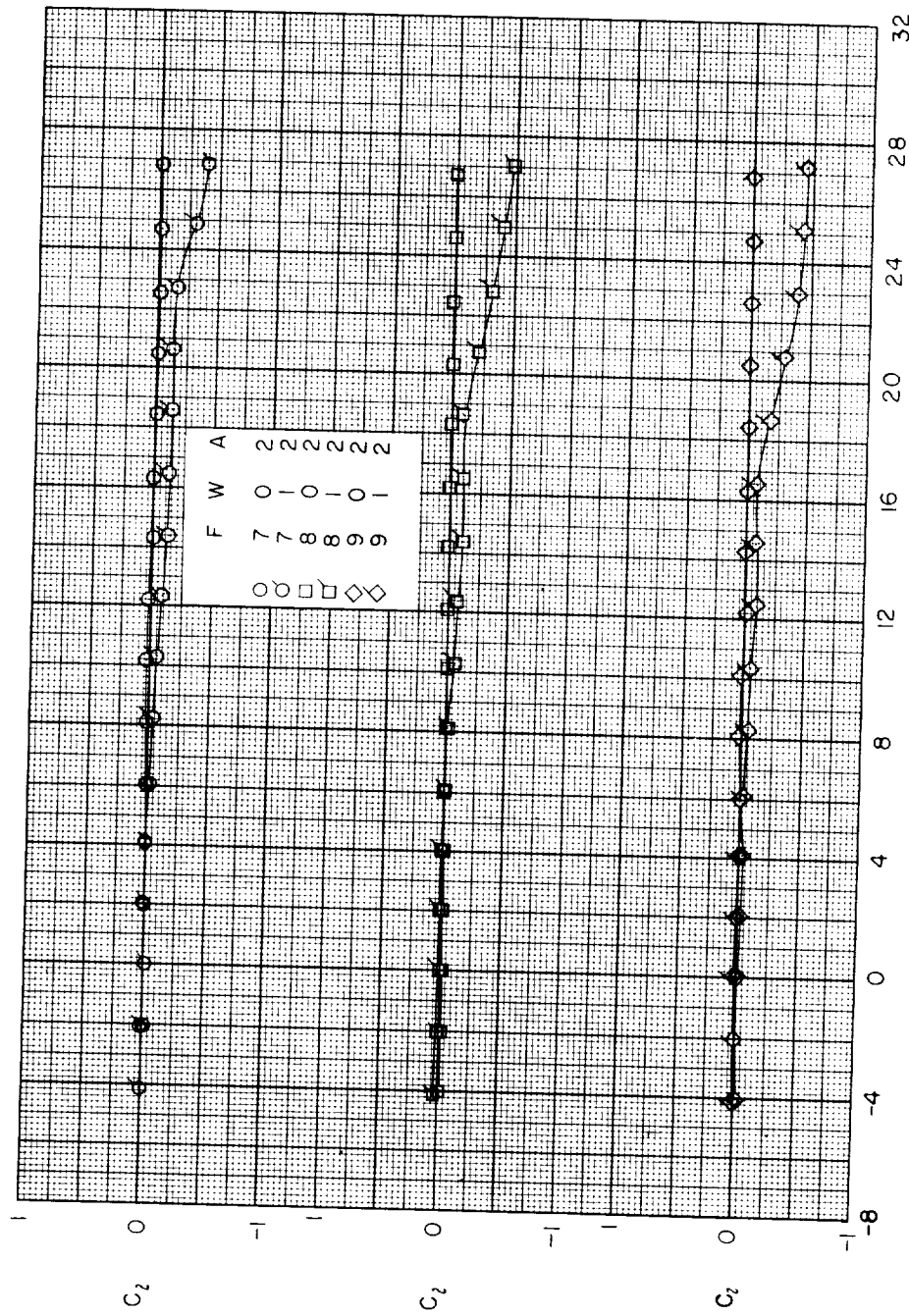
(b) $\alpha \approx 4.1^\circ$.

Figure 27.- Continued.



(b) Concluded.

Figure 27.- Continued.

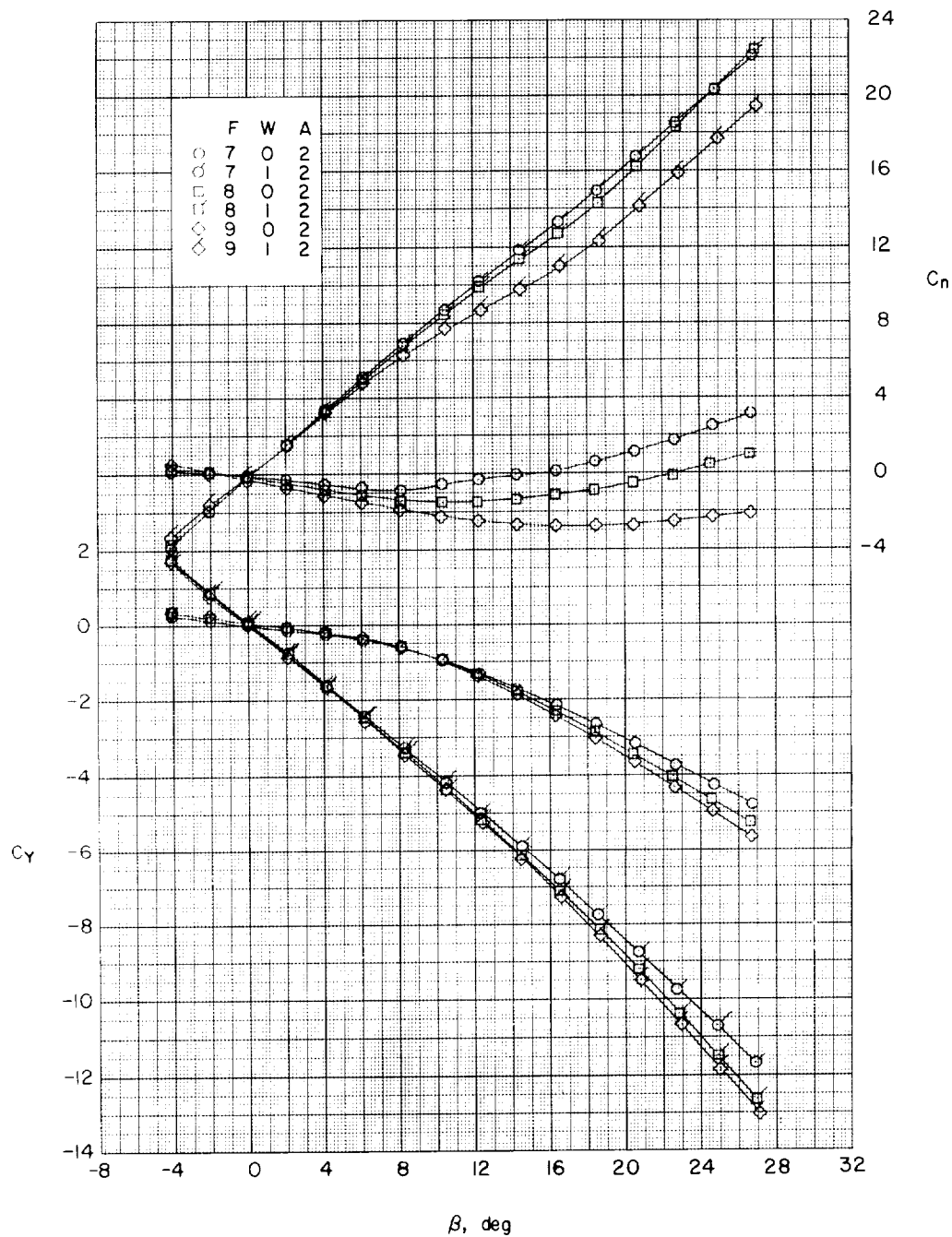
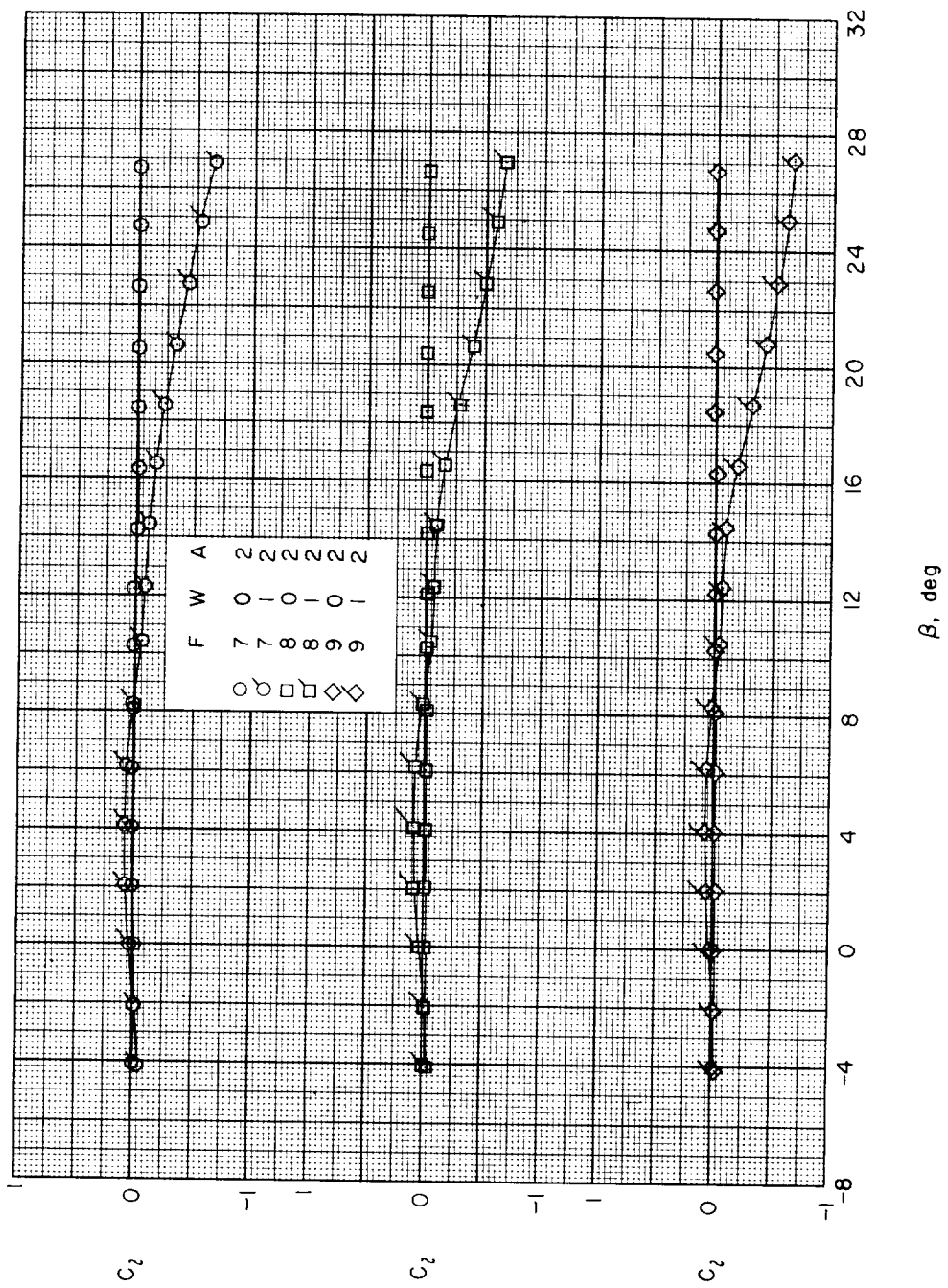
(c) $\alpha \approx 8.2^\circ$.

Figure 27.- Continued.



(c) Concluded.

Figure 27.- Continued.

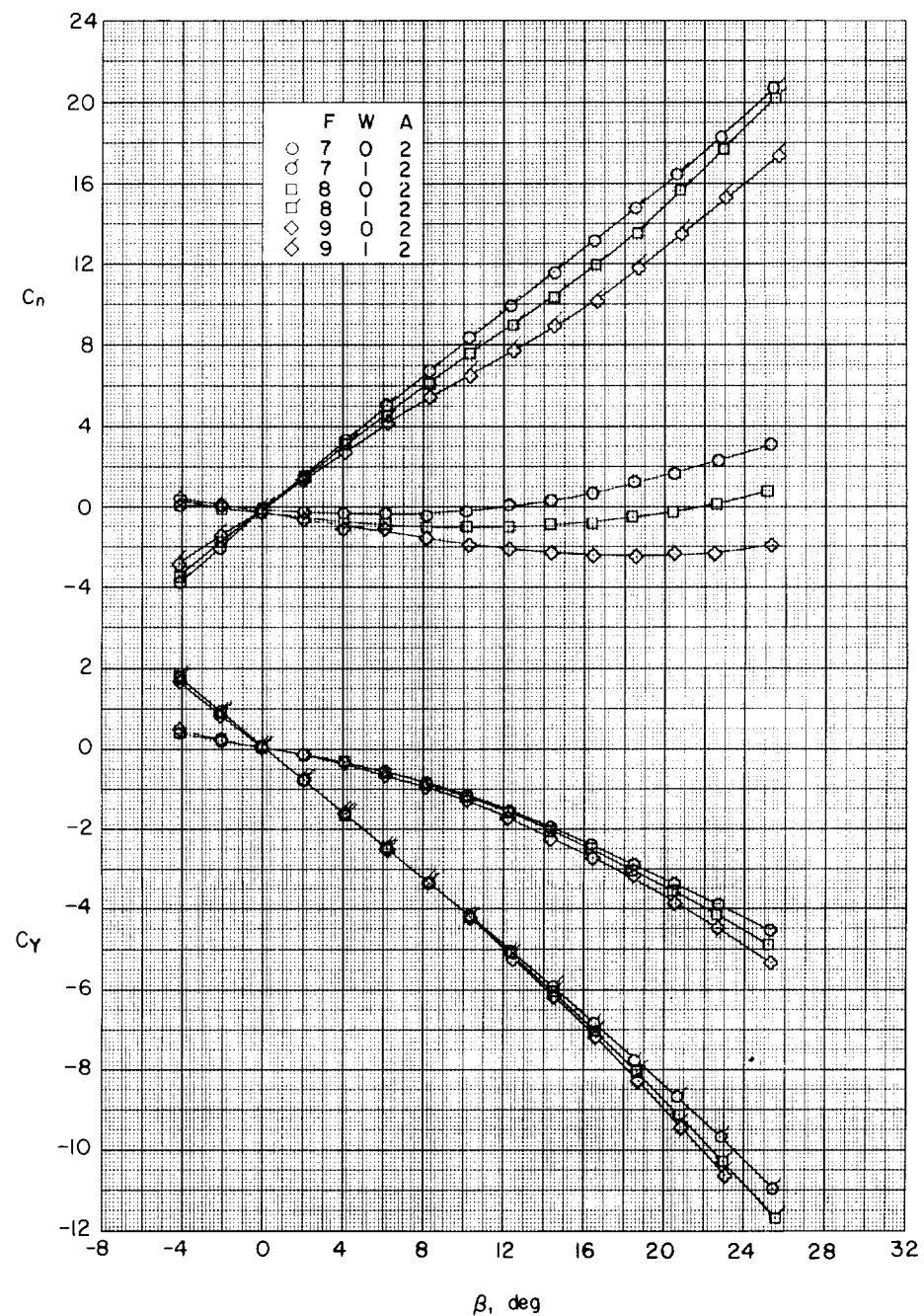
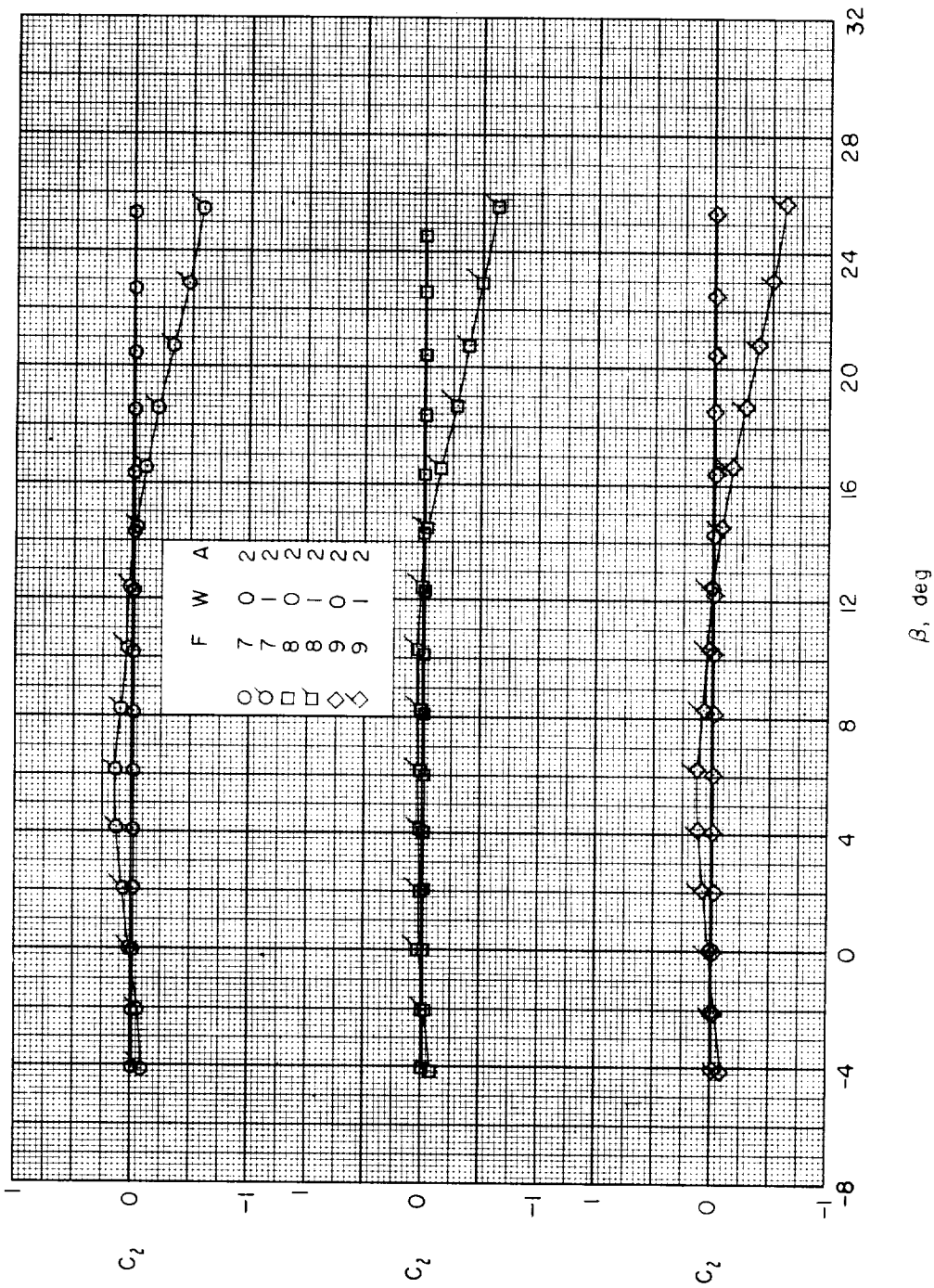
(d) $\alpha \approx 12.3^\circ$.

Figure 27.- Continued.



(d) Concluded.

Figure 27.- Continued.

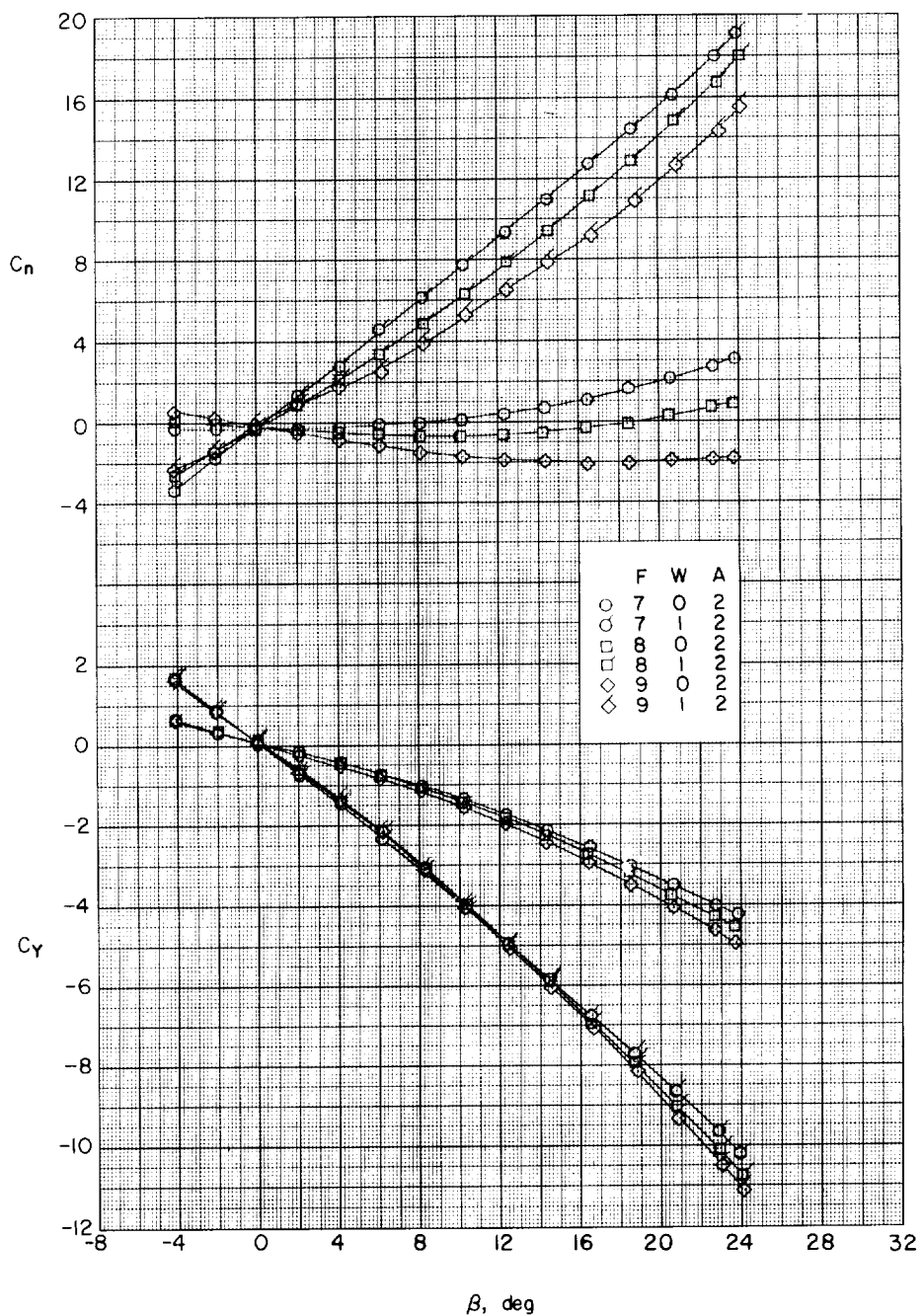
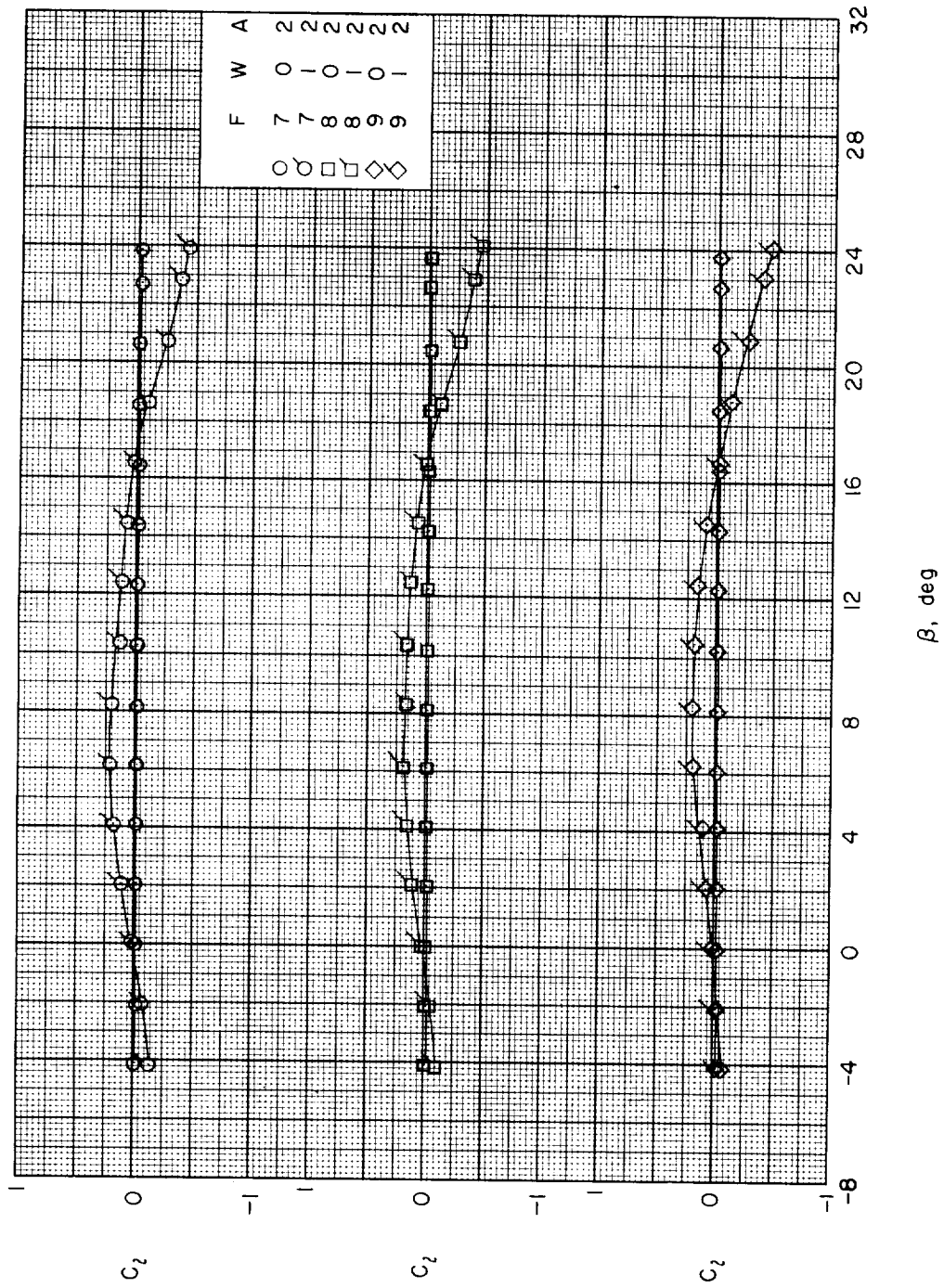
(e) $\alpha \approx 16.4^\circ$.

Figure 27.- Continued.



(e) Concluded.

Figure 27.- Continued.

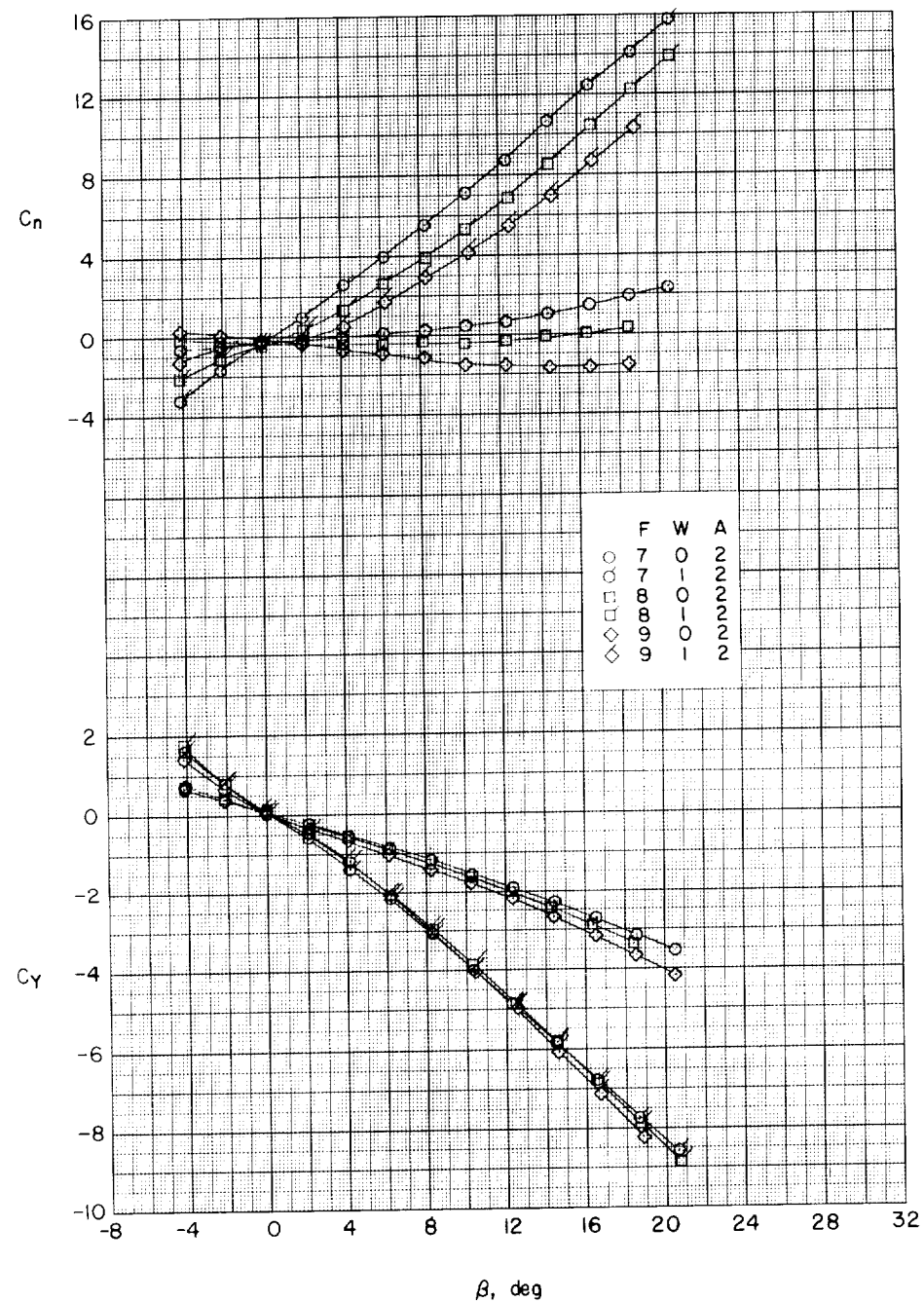
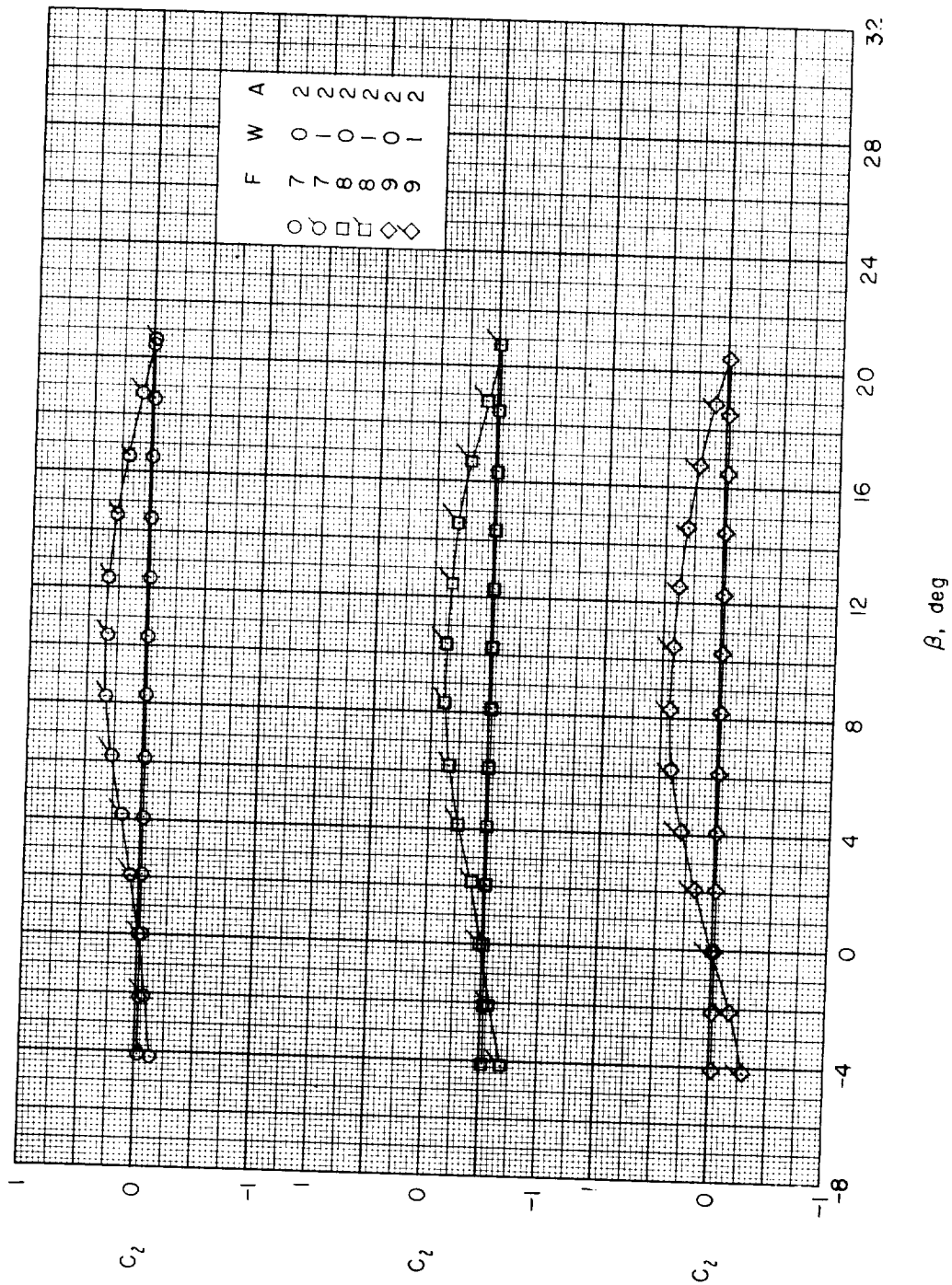
(f) $\alpha \approx 20.5^\circ$.

Figure 27.- Continued.



(f) Concluded.

Figure 27.- Continued.

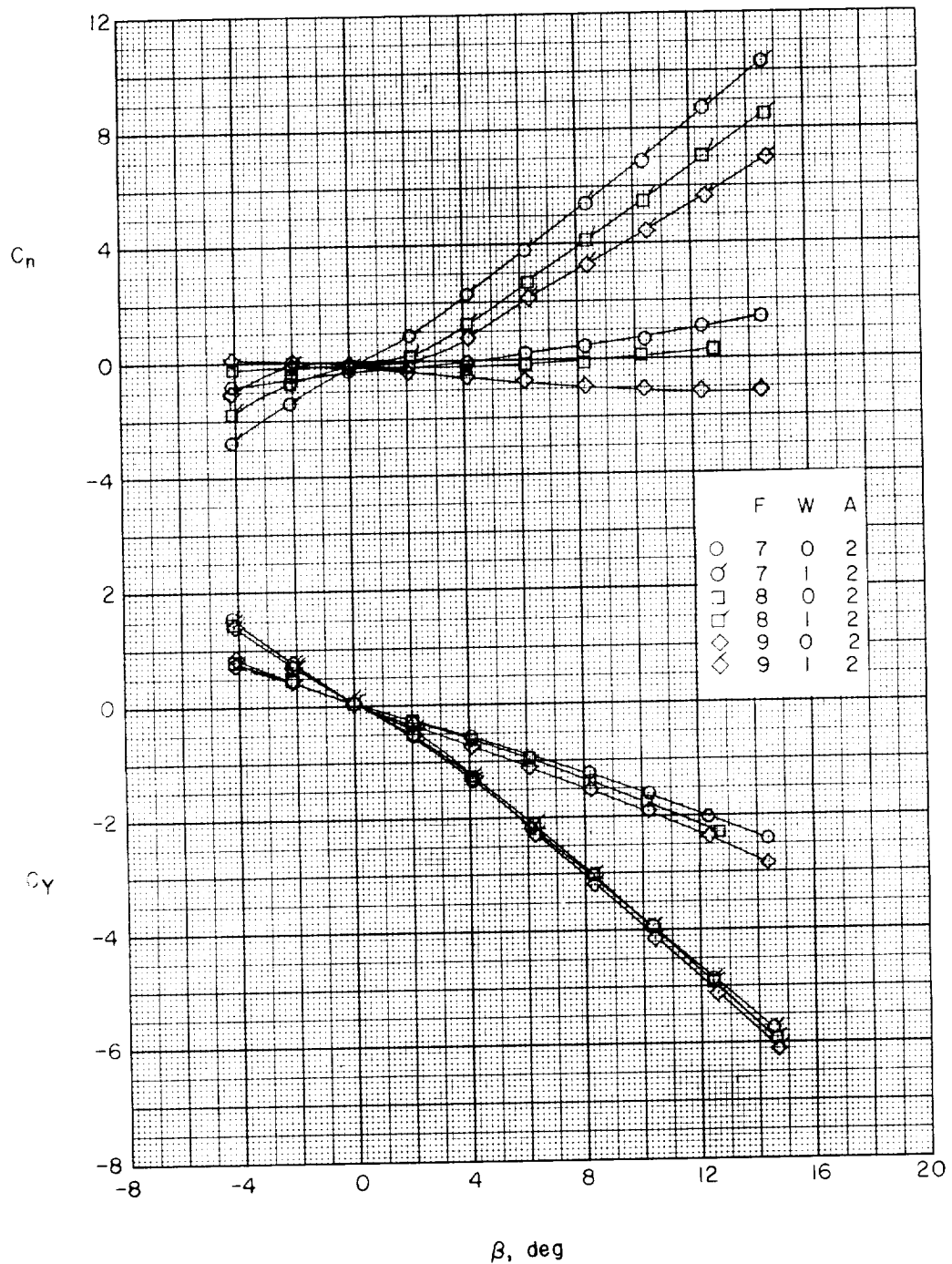
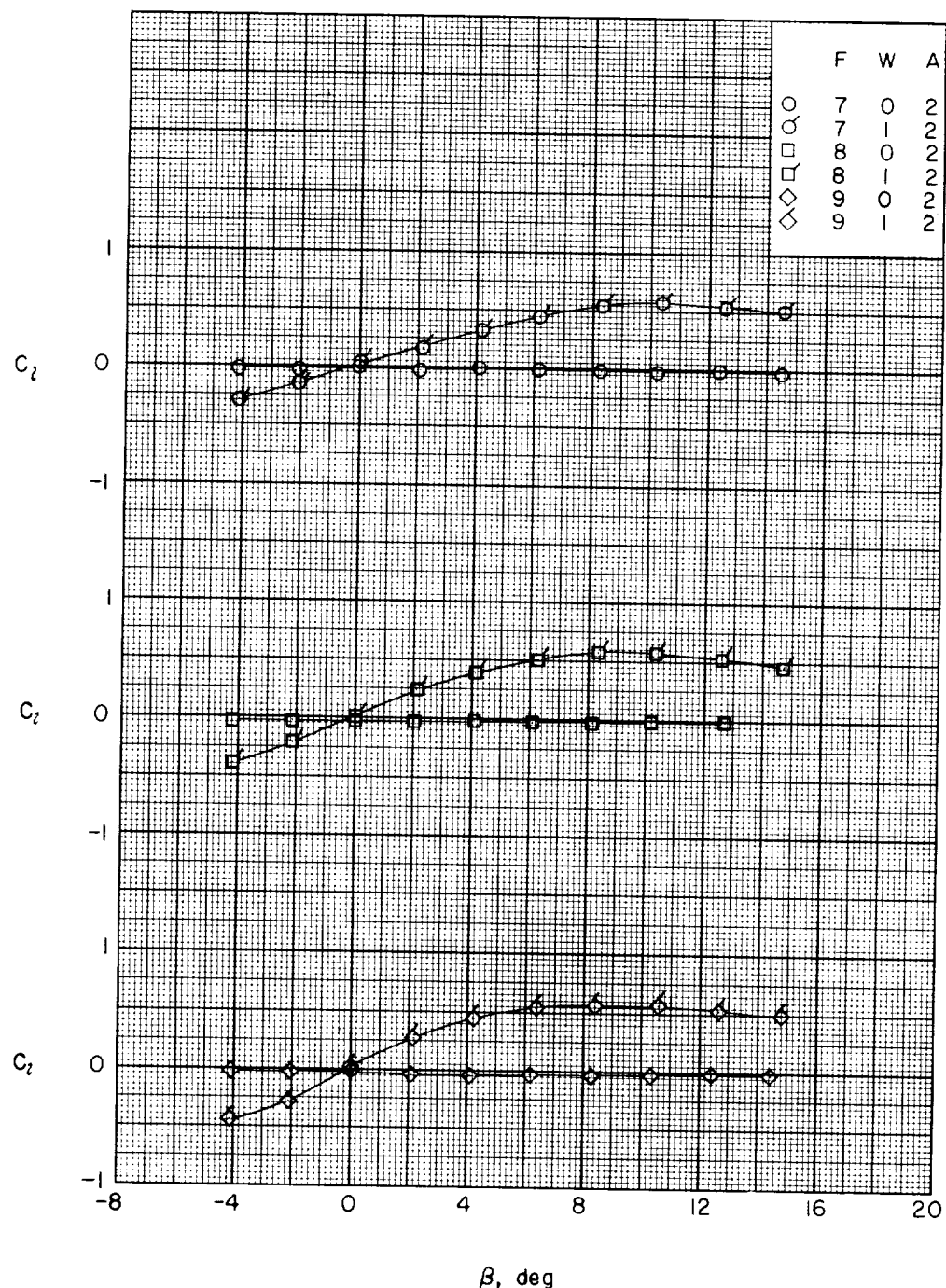
(g) $\alpha \approx 24.7^\circ$.

Figure 27--Continued.



(g) Concluded.

Figure 27.-- Concluded.

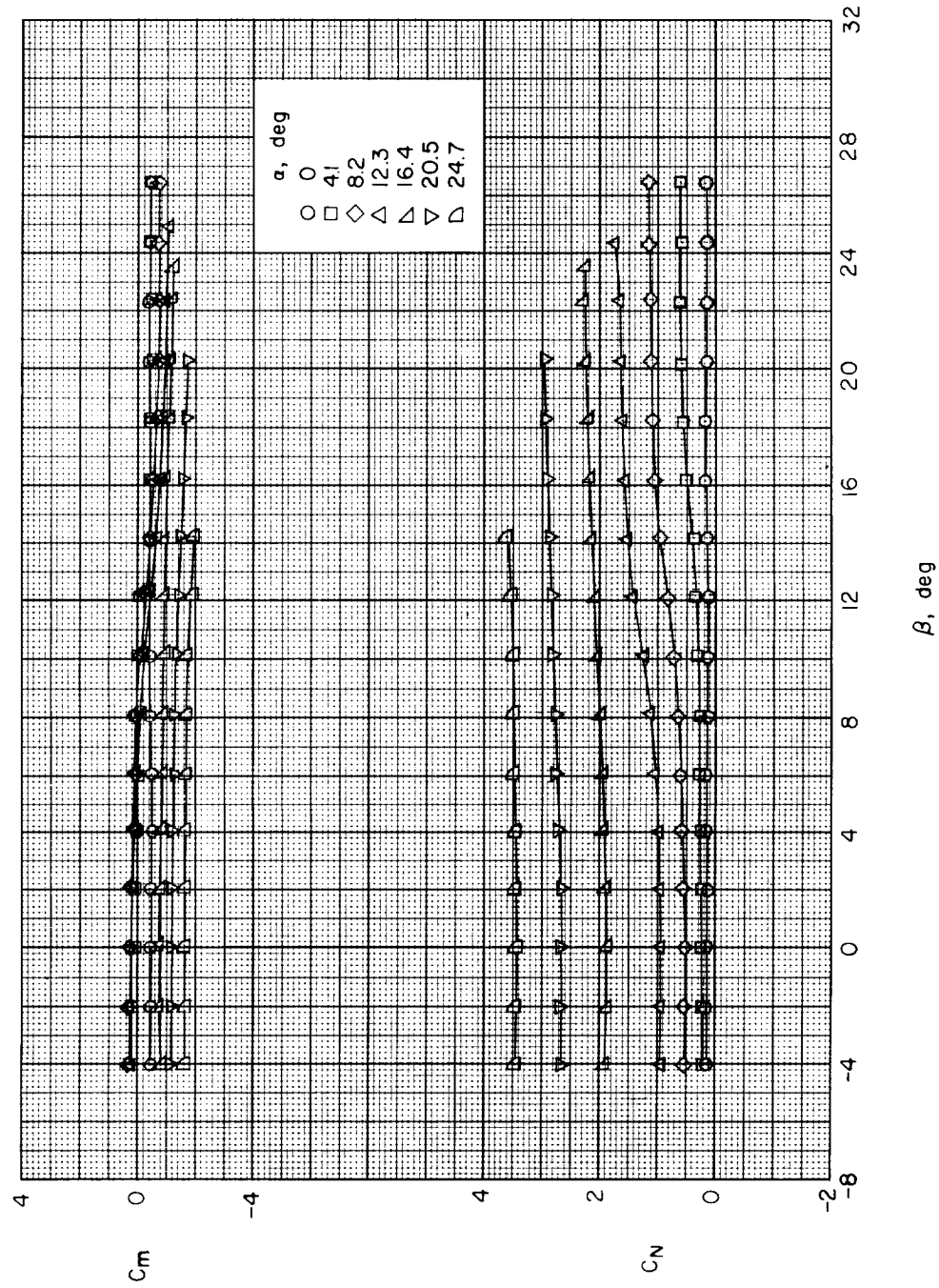
(a) Body alone, $F_1 W_0 A_0$.

Figure 28.- Variation of C_m and C_N with β for various angles of attack. Various forebody lengths; large delta wings; no afterbody.

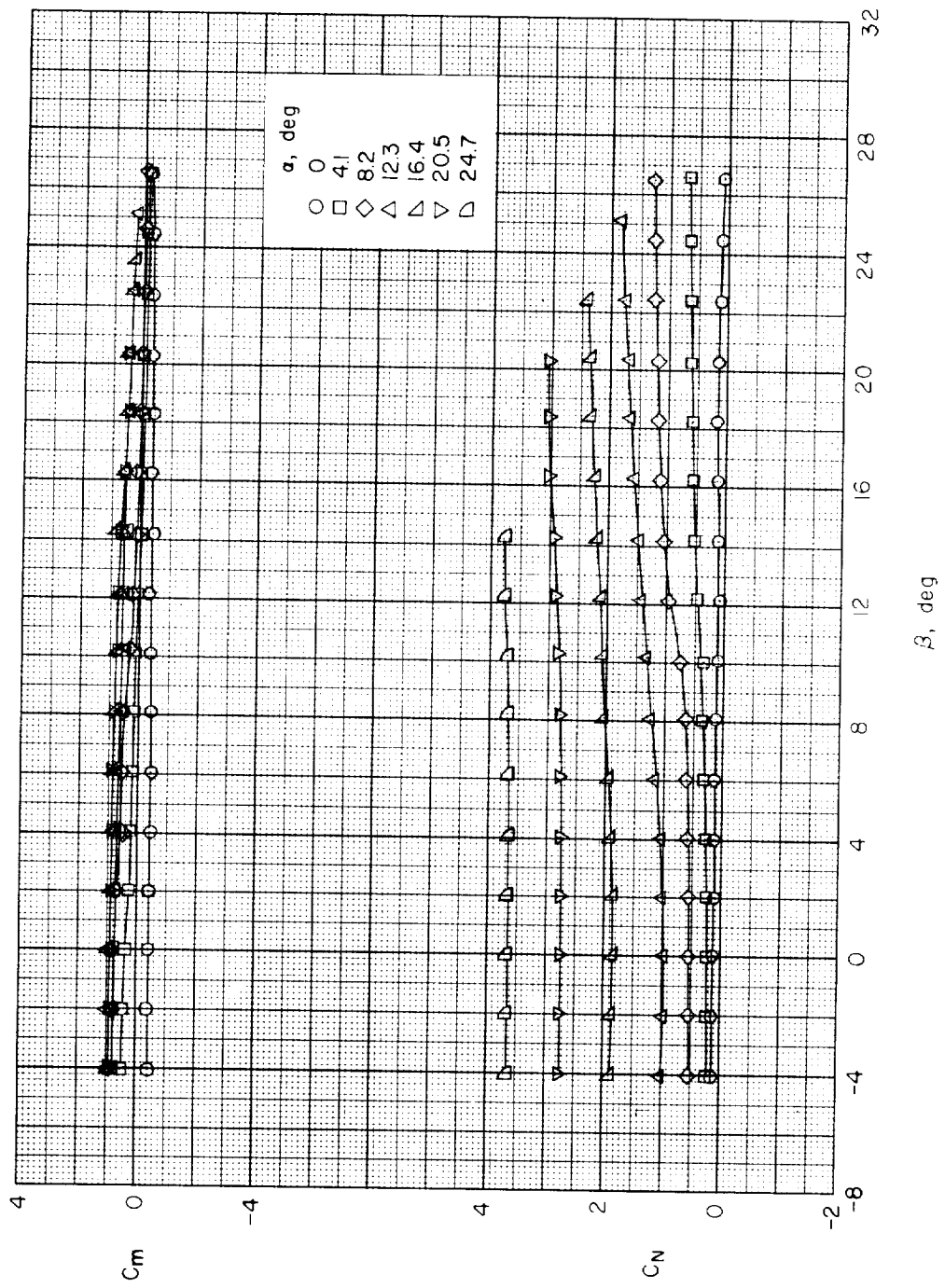
(b) Body alone, $F_7 W G A_0$.

Figure 28.- Continued.

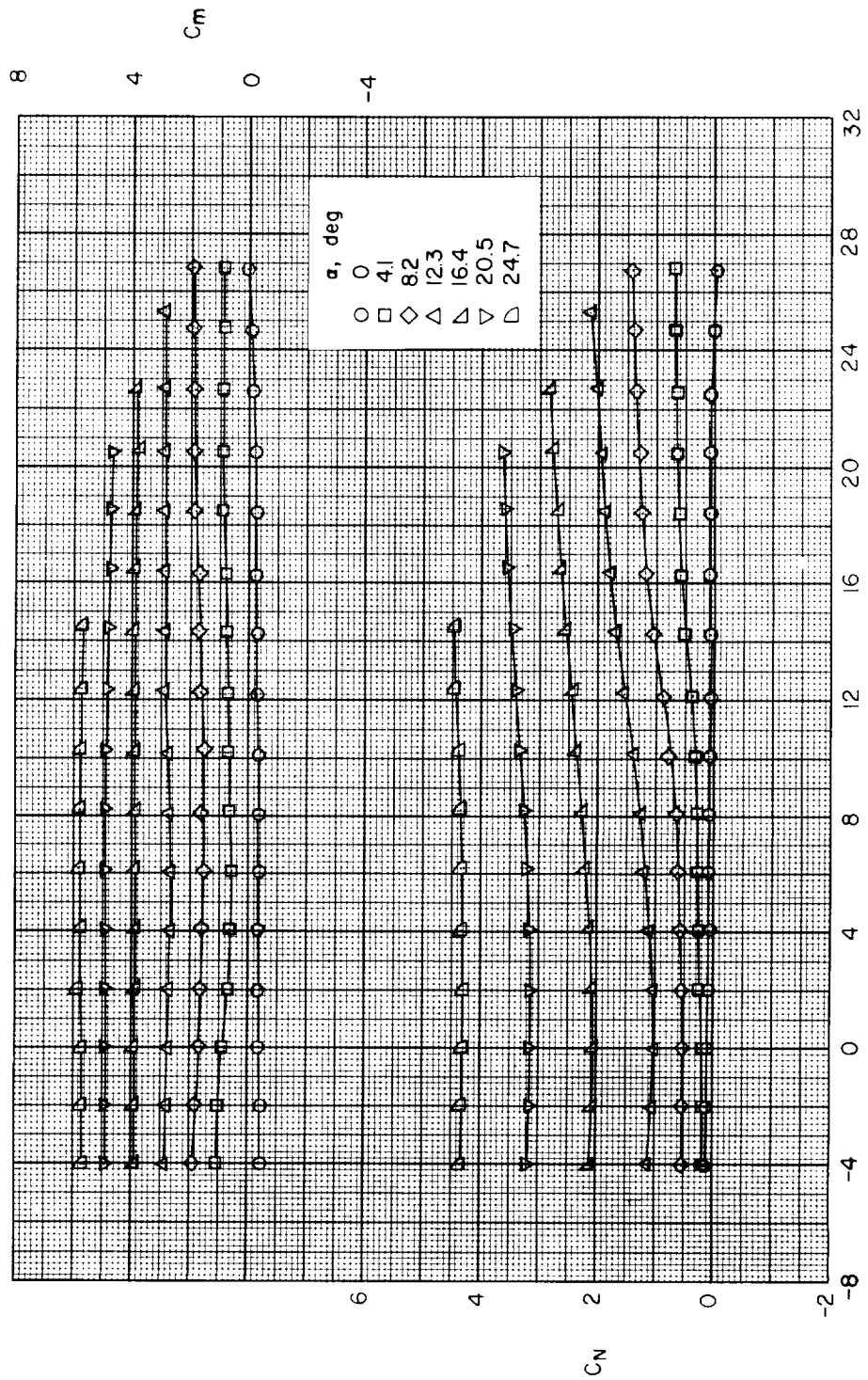
(c) Body alone, $F_g W_0 A_0$.

Figure 28.- Continued.

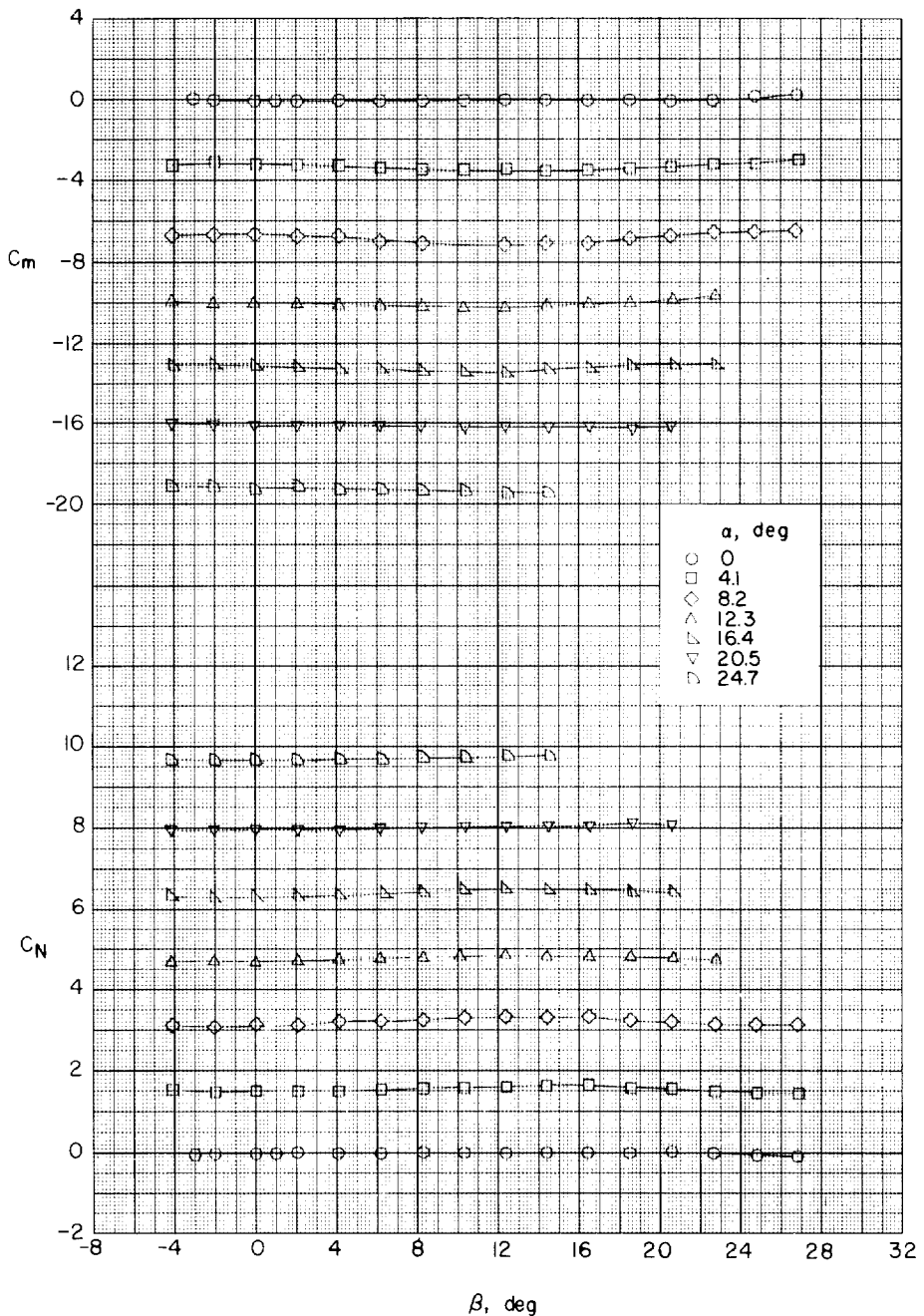
(d) Large delta wing, $F_1W_1A_0$.

Figure 28.- Continued.

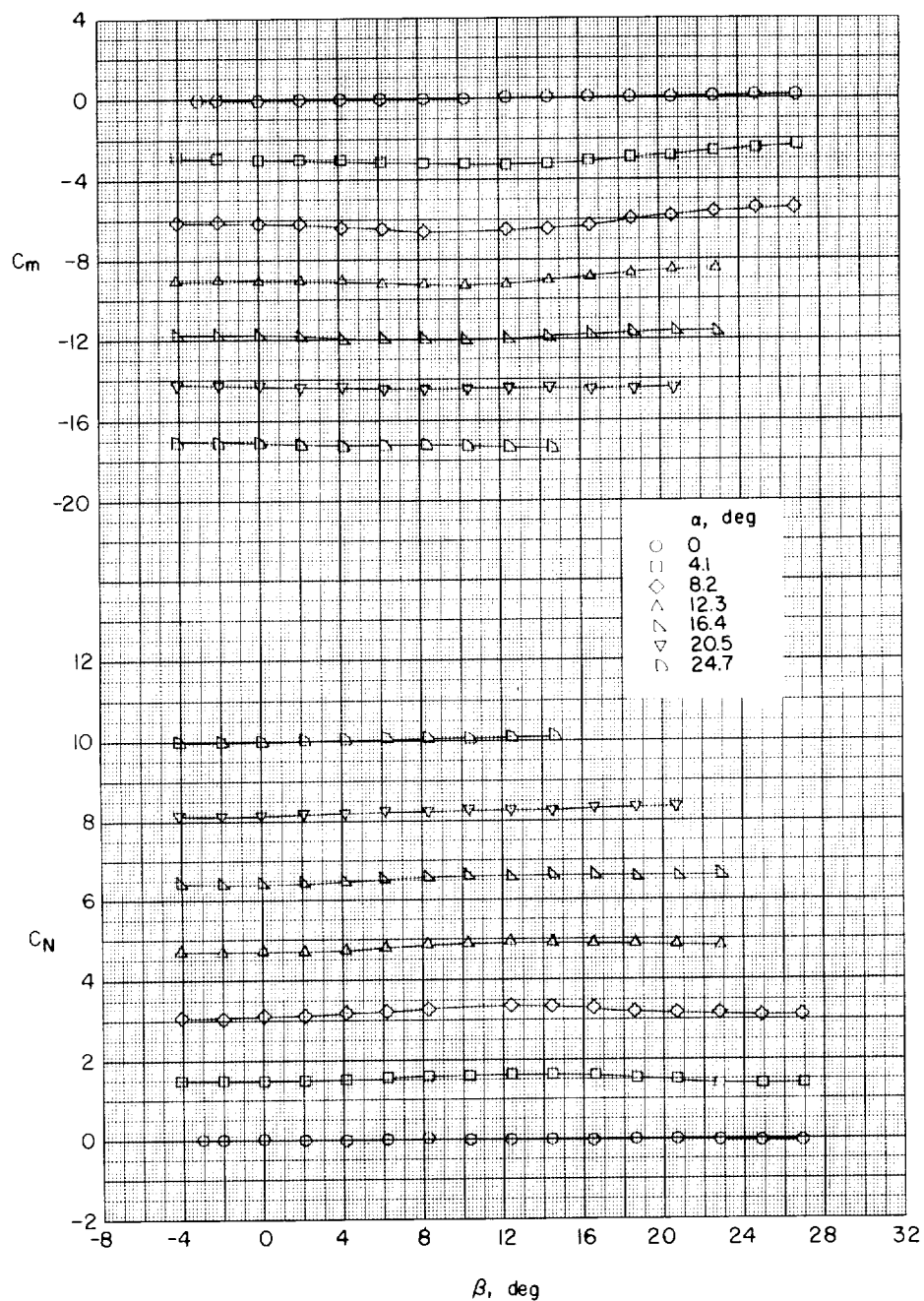
(e) Large delta wing, $F_7^W A_0$.

Figure 28.- Continued.

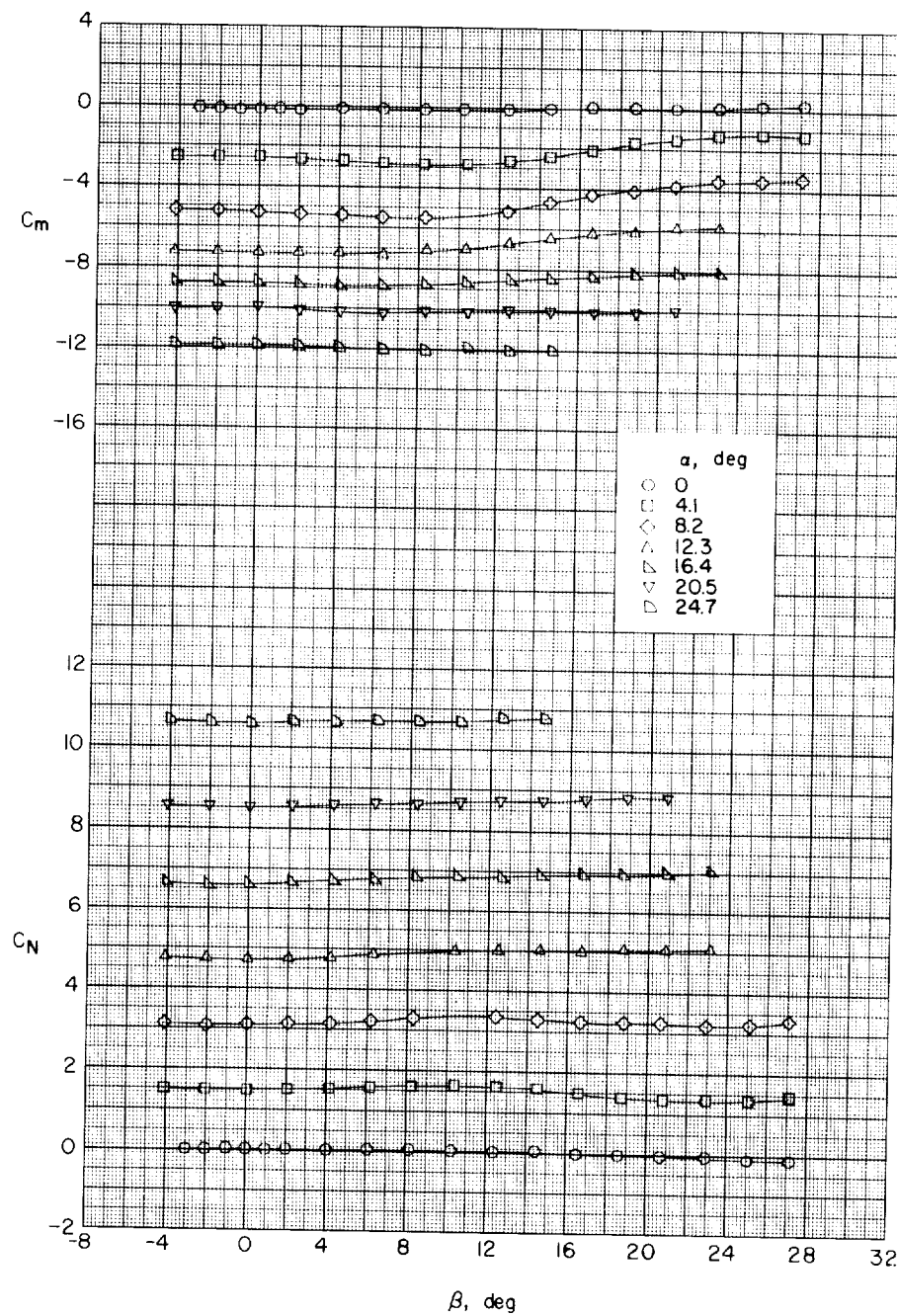
(f) Large delta wing, F_{9W1A0} .

Figure 28.- Concluded.

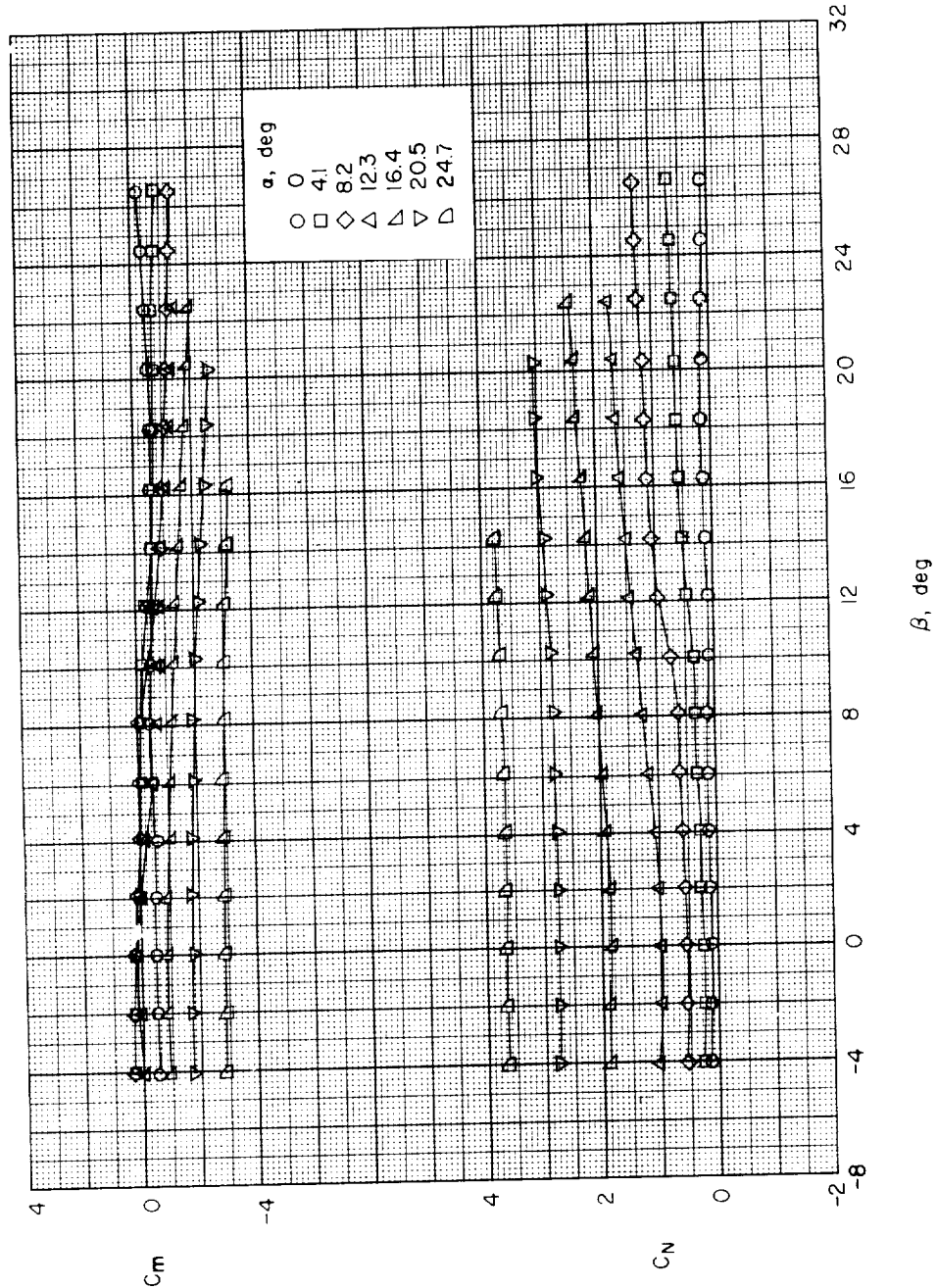
(a) Body alone, $F_{LW_0A_1}$.

Figure 29.- Variation of C_m and C_N with β for various angles of attack. Various forebody lengths; large delta wings; 1-caliber cylindrical afterbody.

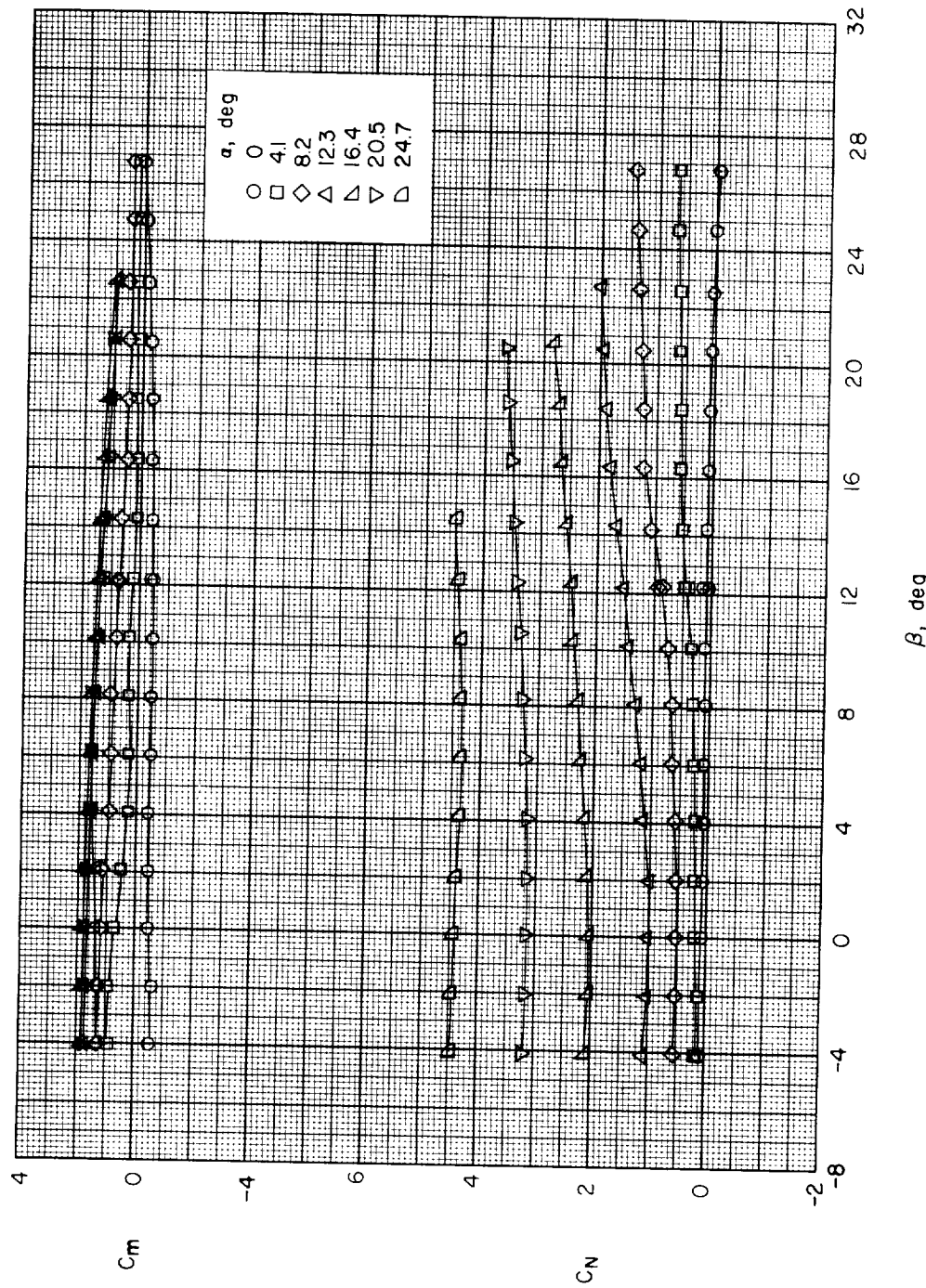
(b) Body alone, $F_8 W_{0A_1}$.

Figure 29.- Continued.

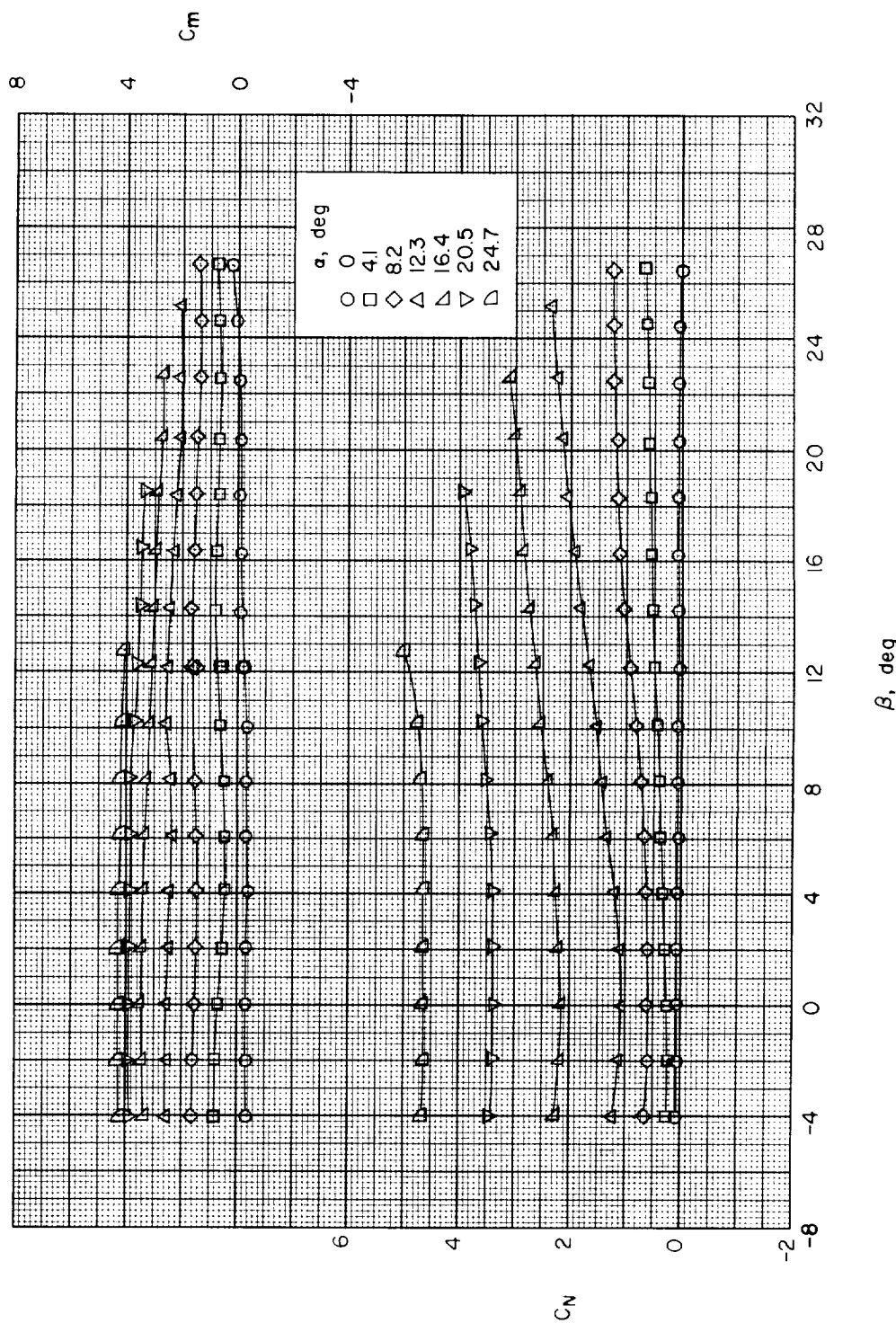
(c) Body alone, $F_9 W_{0A1}$.

Figure 29.- Continued.

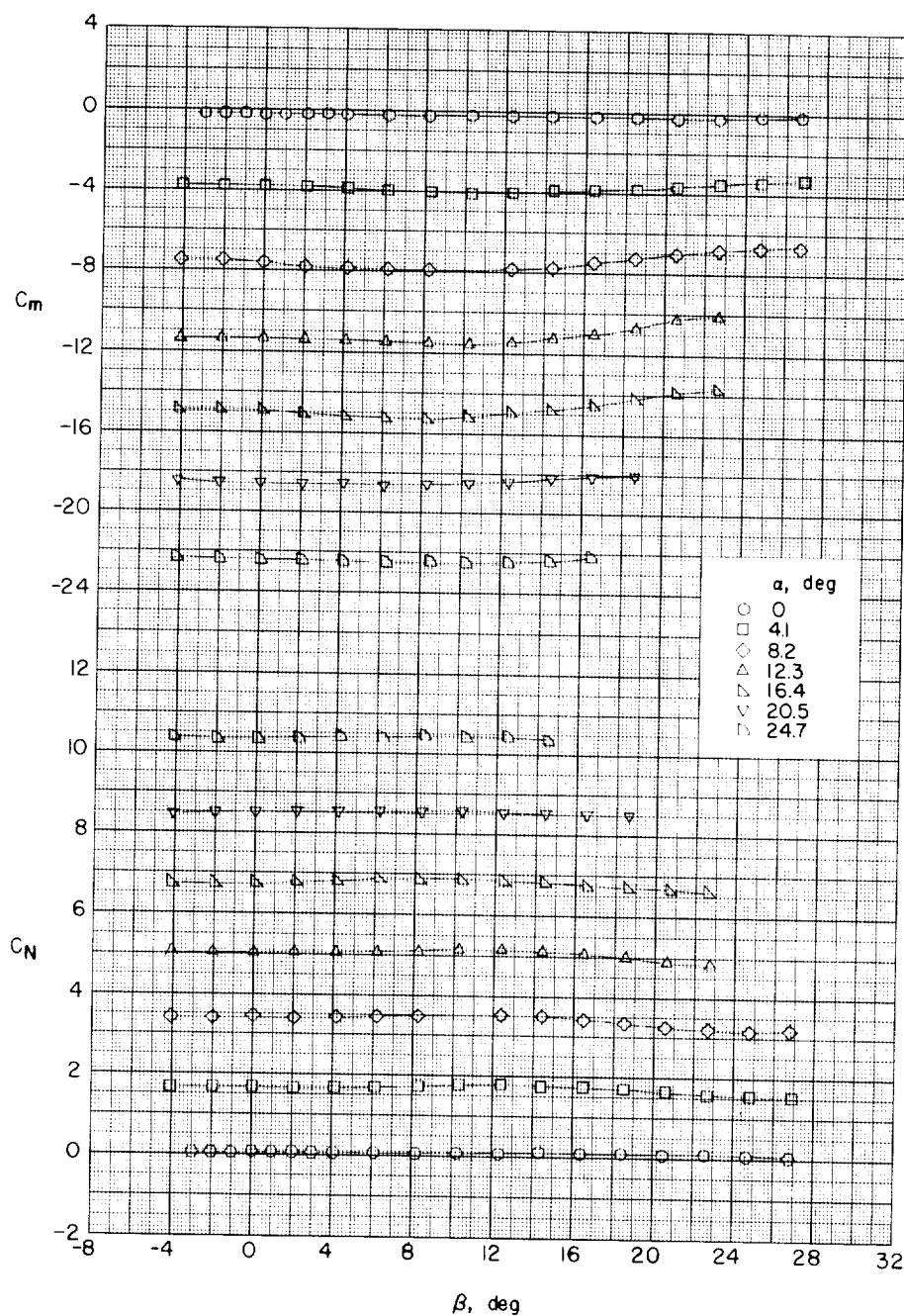
(d) Large delta wing, $F_1 W_1 A_1$.

Figure 29.- Continued.

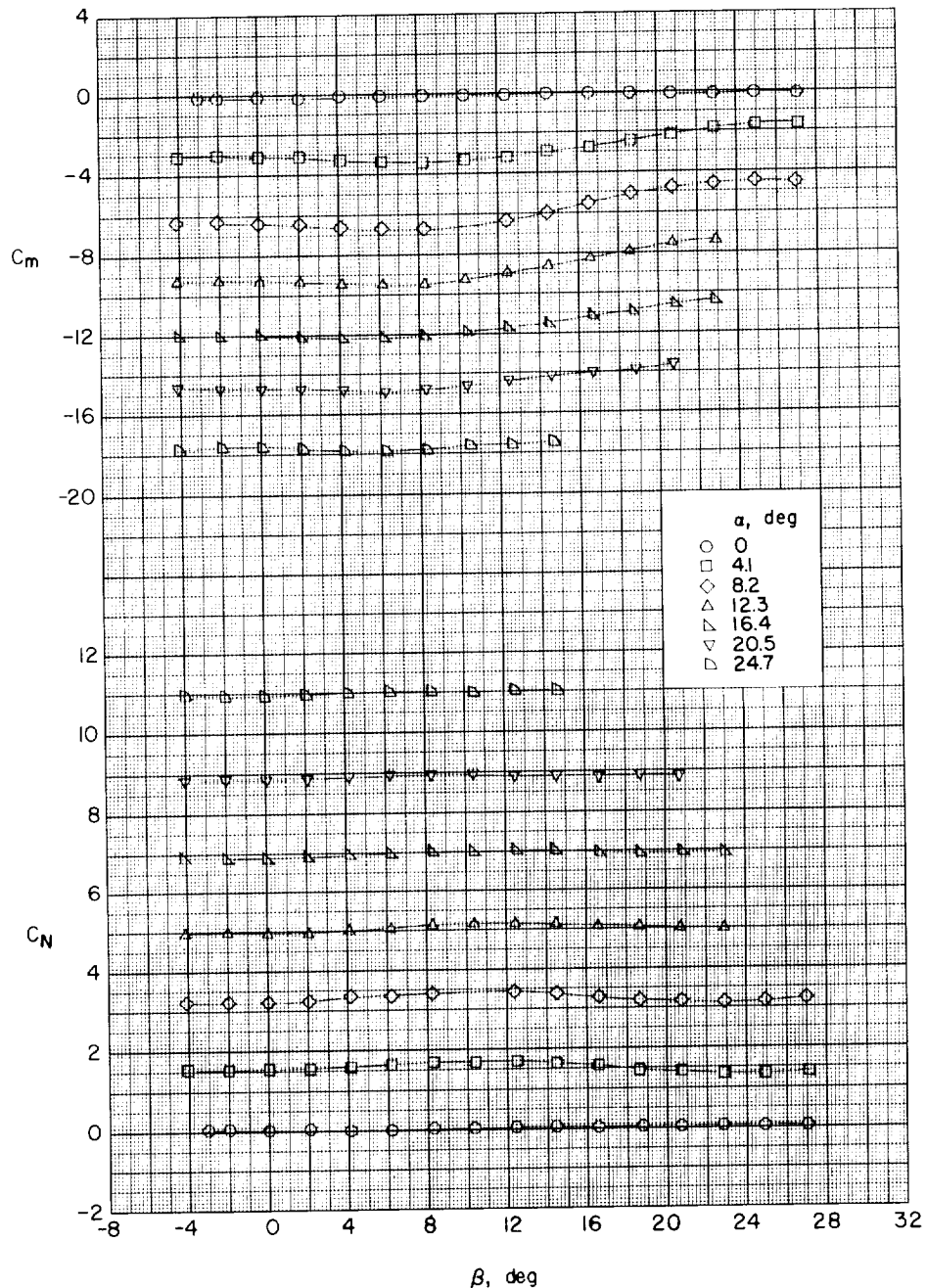
(e) Large delta wing, F₈W₁A₁.

Figure 29.- Continued.

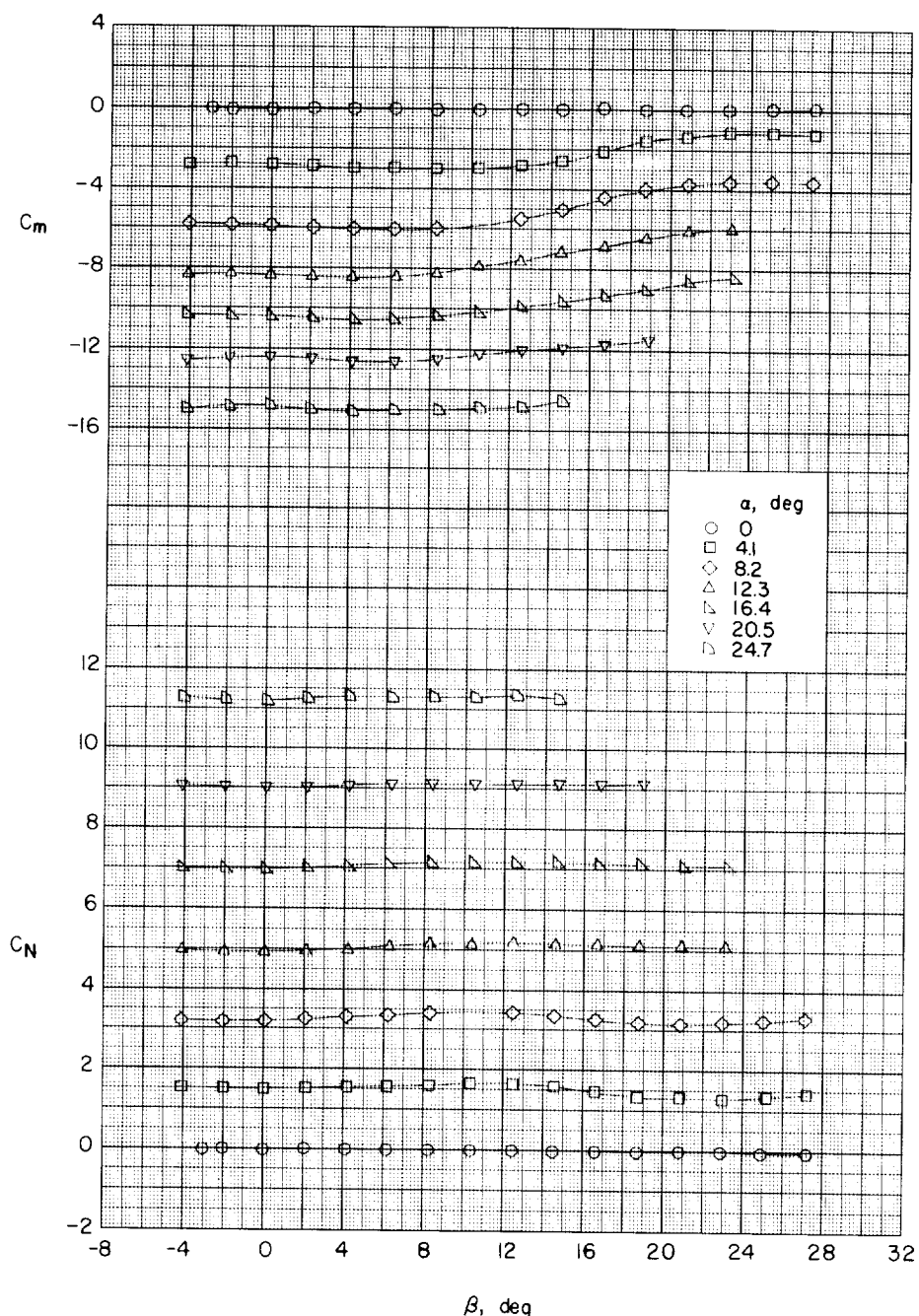
(f) Large delta wing, $F_{9W_1A_1}$.

Figure 29.- Concluded.

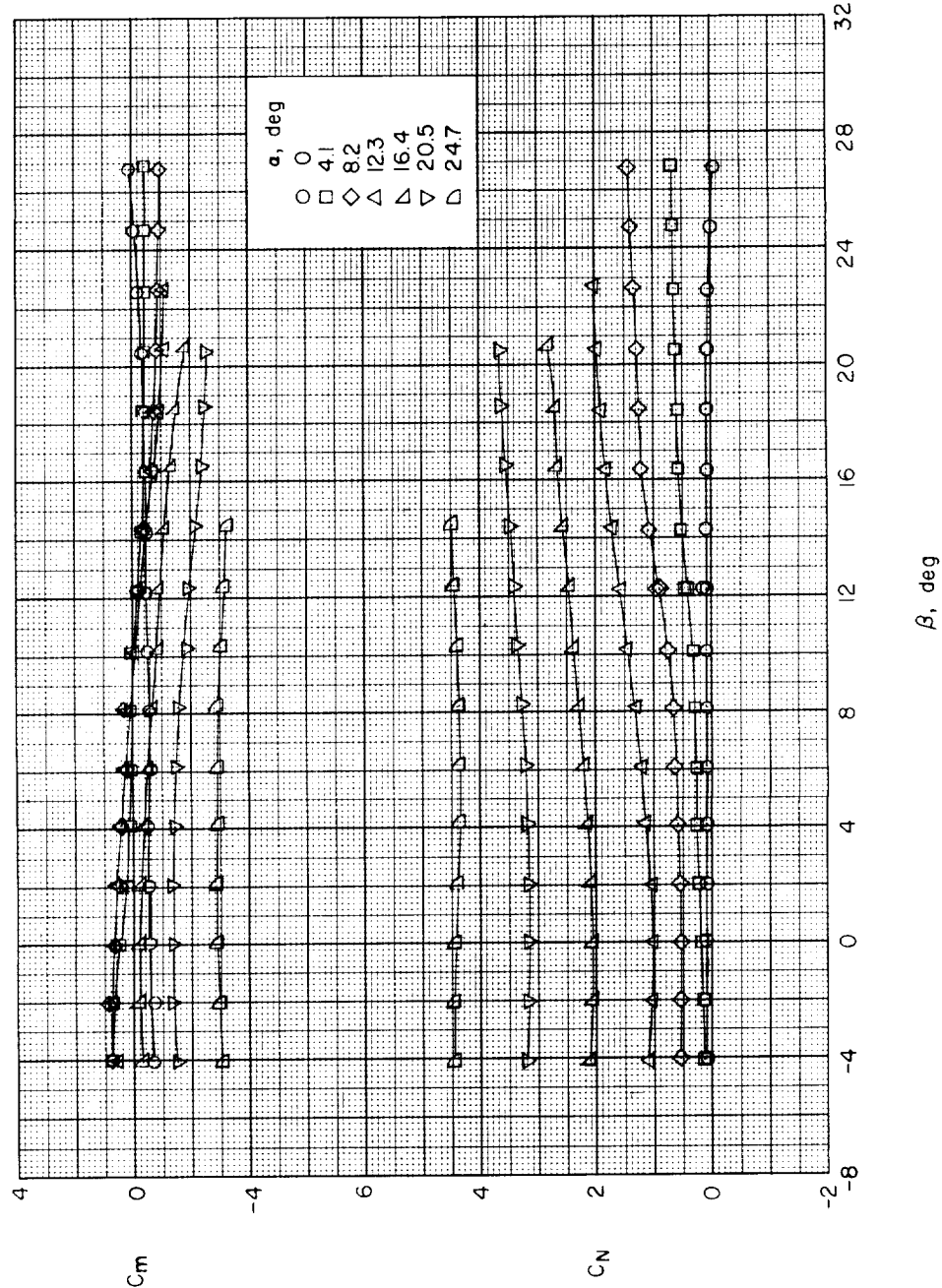
(a) Body alone, $F_7W_0A_2$.

Figure 30.- Variation of C_m and C_N with β for various angles of attack. Various forebody lengths; large delta wings; 2-caliber cylindrical afterbody.

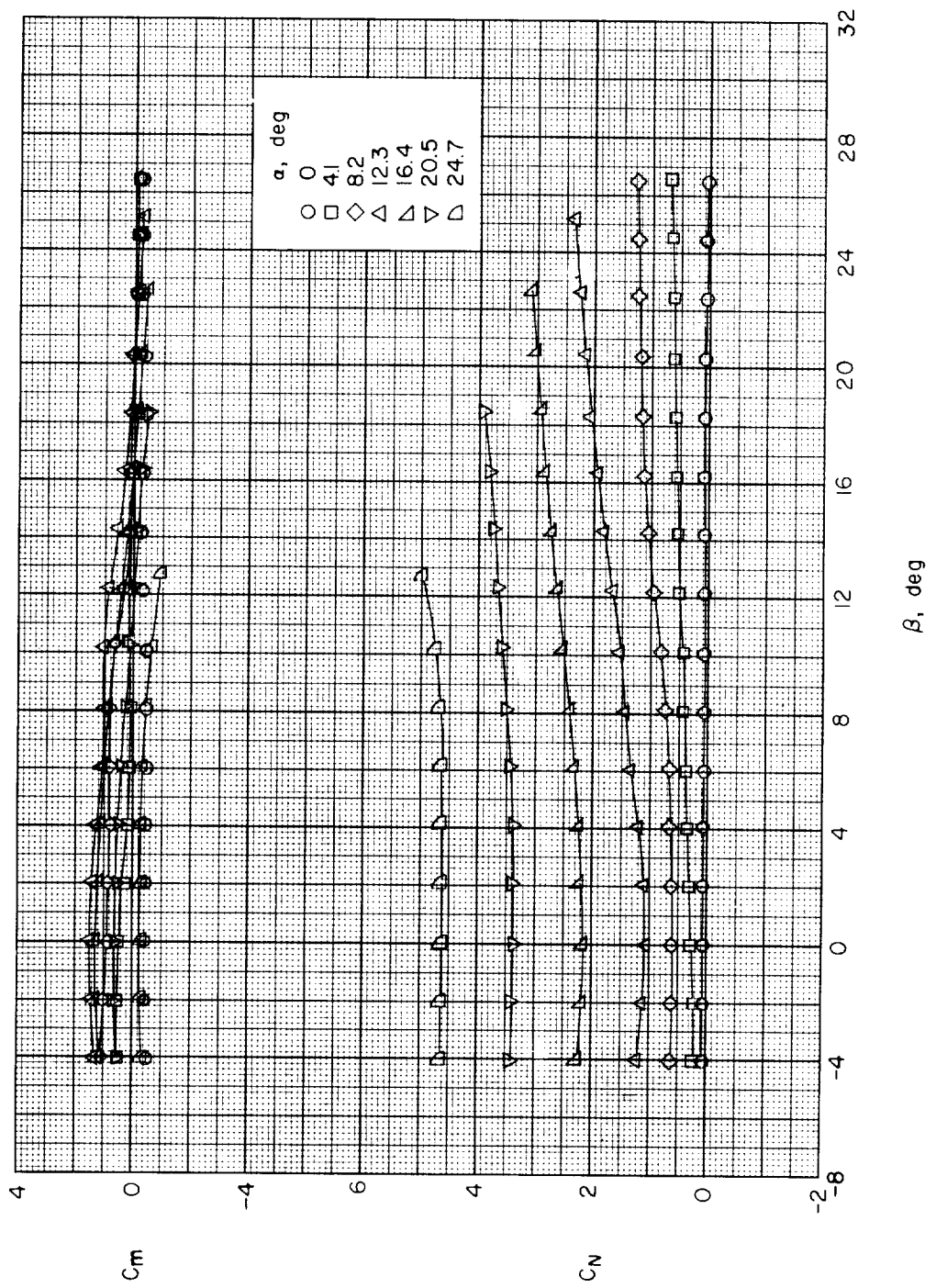
(b) Body alone, $F_8W_0A_2$.

Figure 30.- Continued.

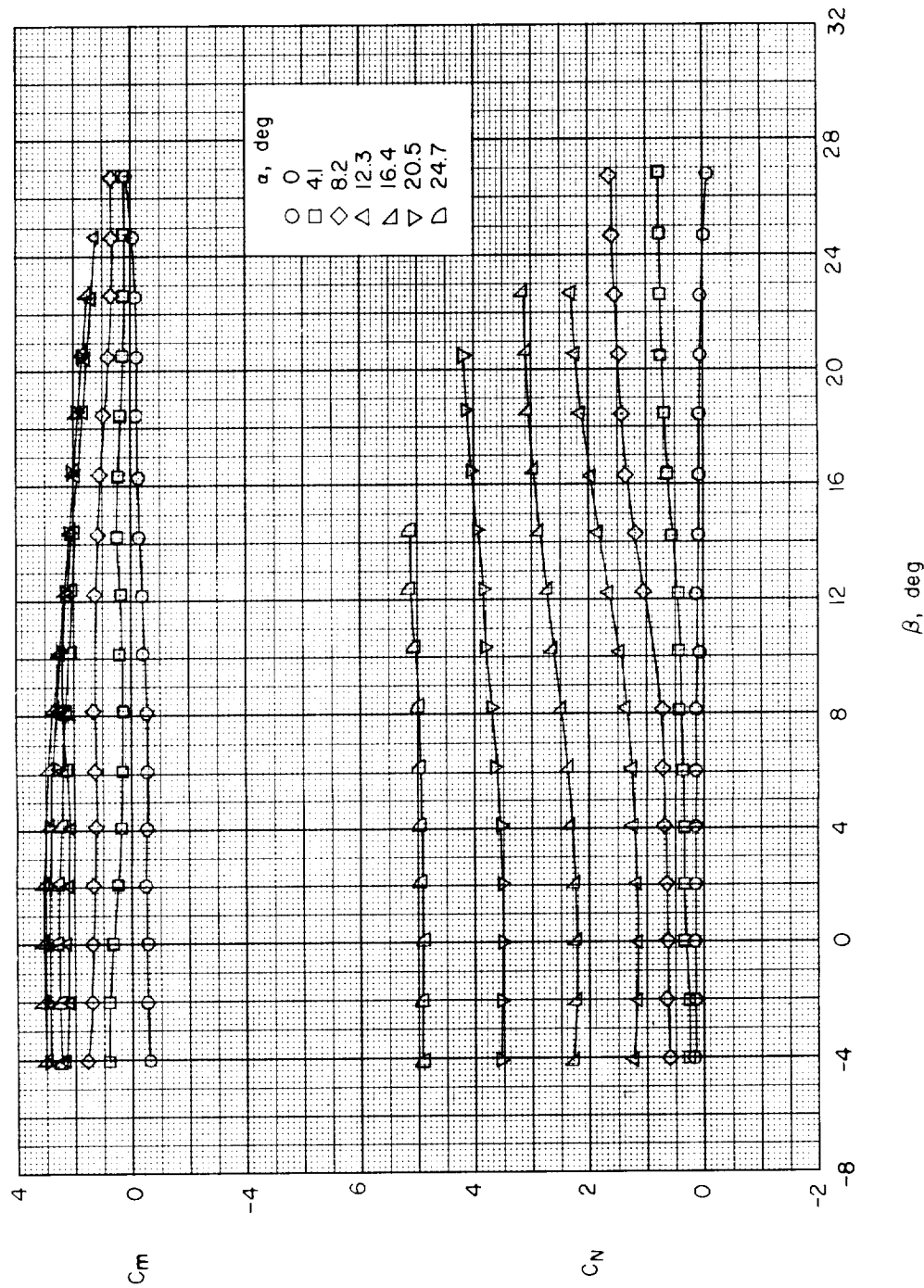
(c) Body alone, $F_9W_1A_2$.

Figure 30.- Continued.

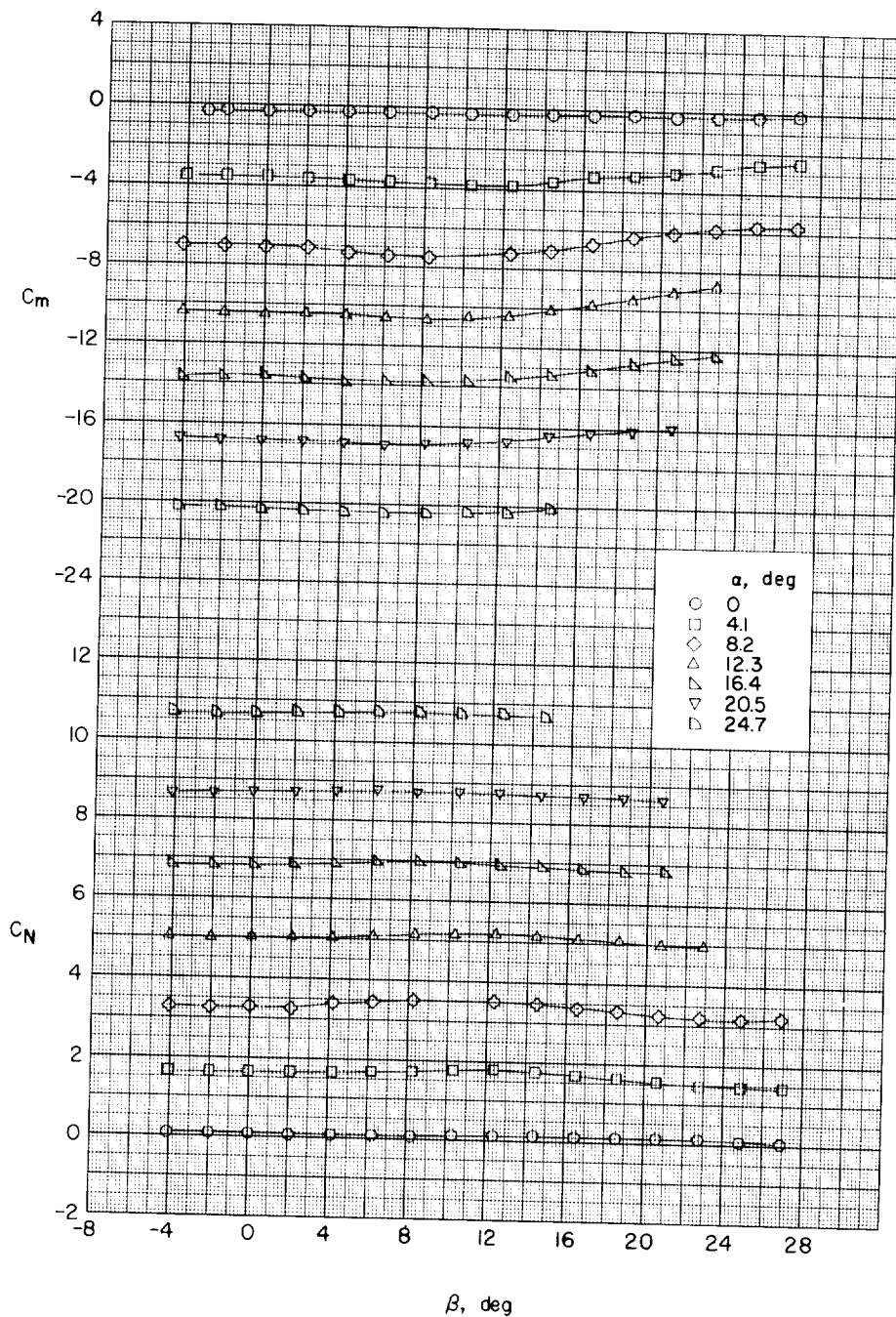
(d) Large delta wing, F₇W₁A₂.

Figure 30.- Continued.

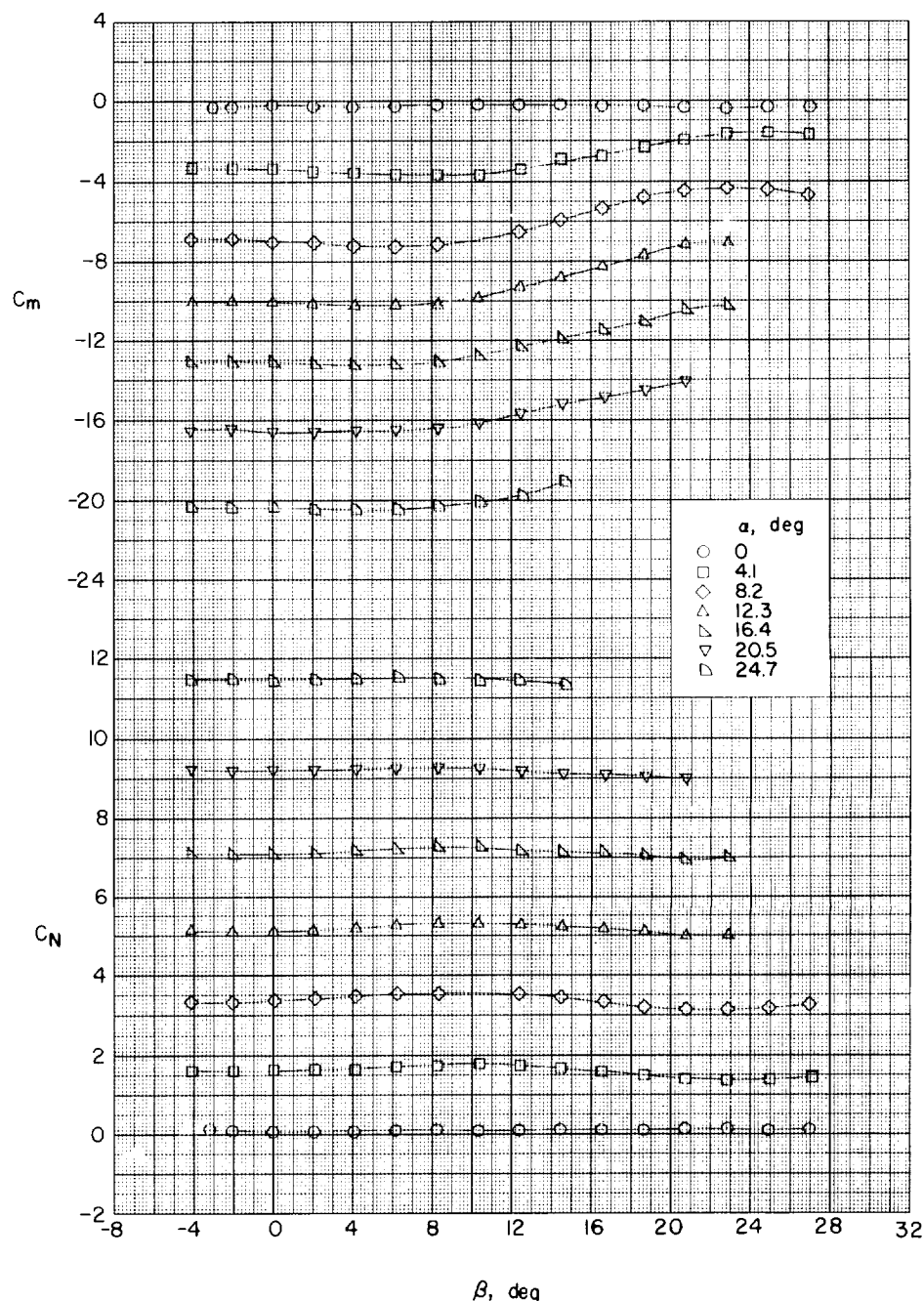
(e) Large delta wing, $F_8W_1A_2$.

Figure 30.- Continued.

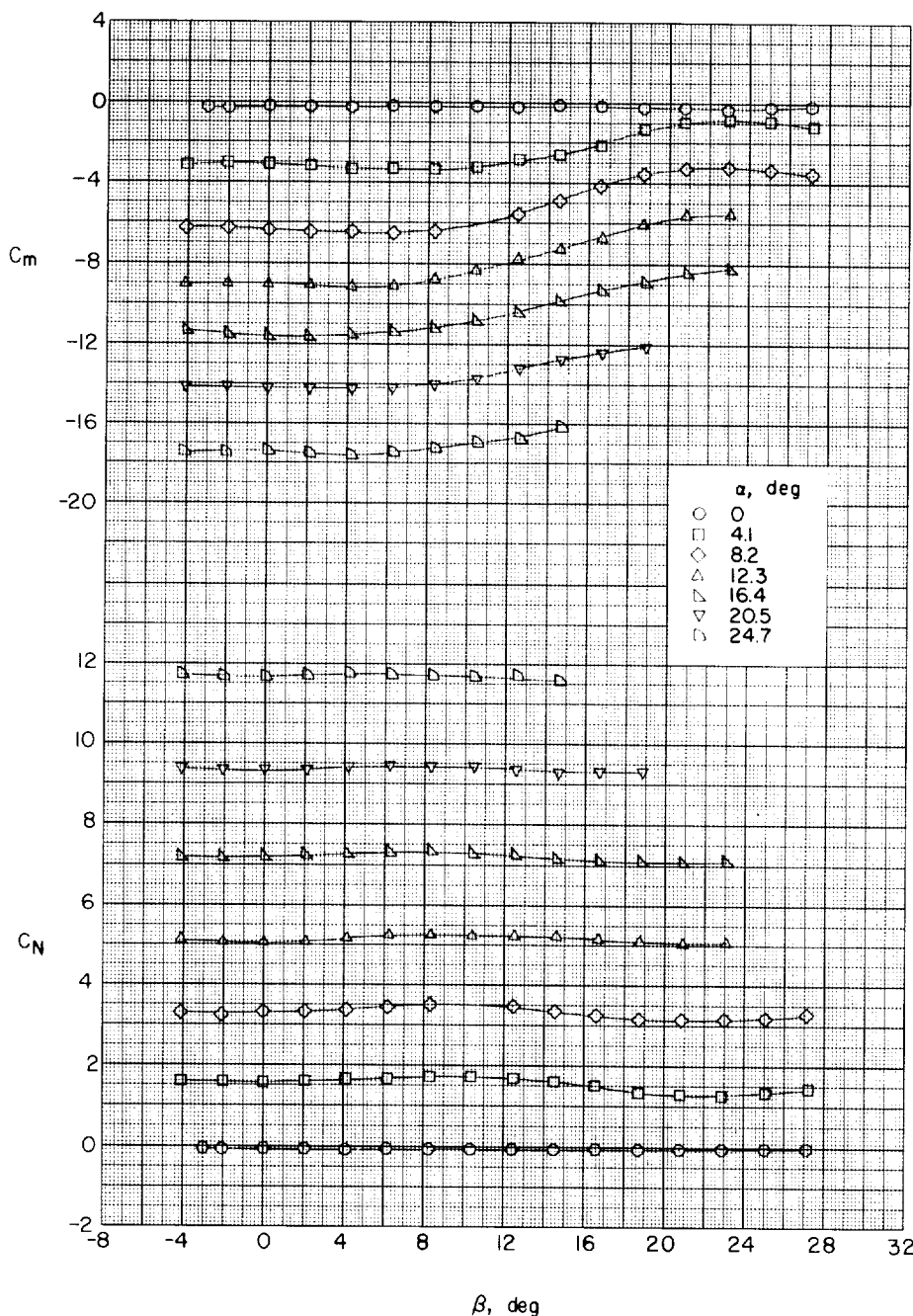
(f) Large delta wing, $F_9W_1A_2$.

Figure 30.- Concluded.

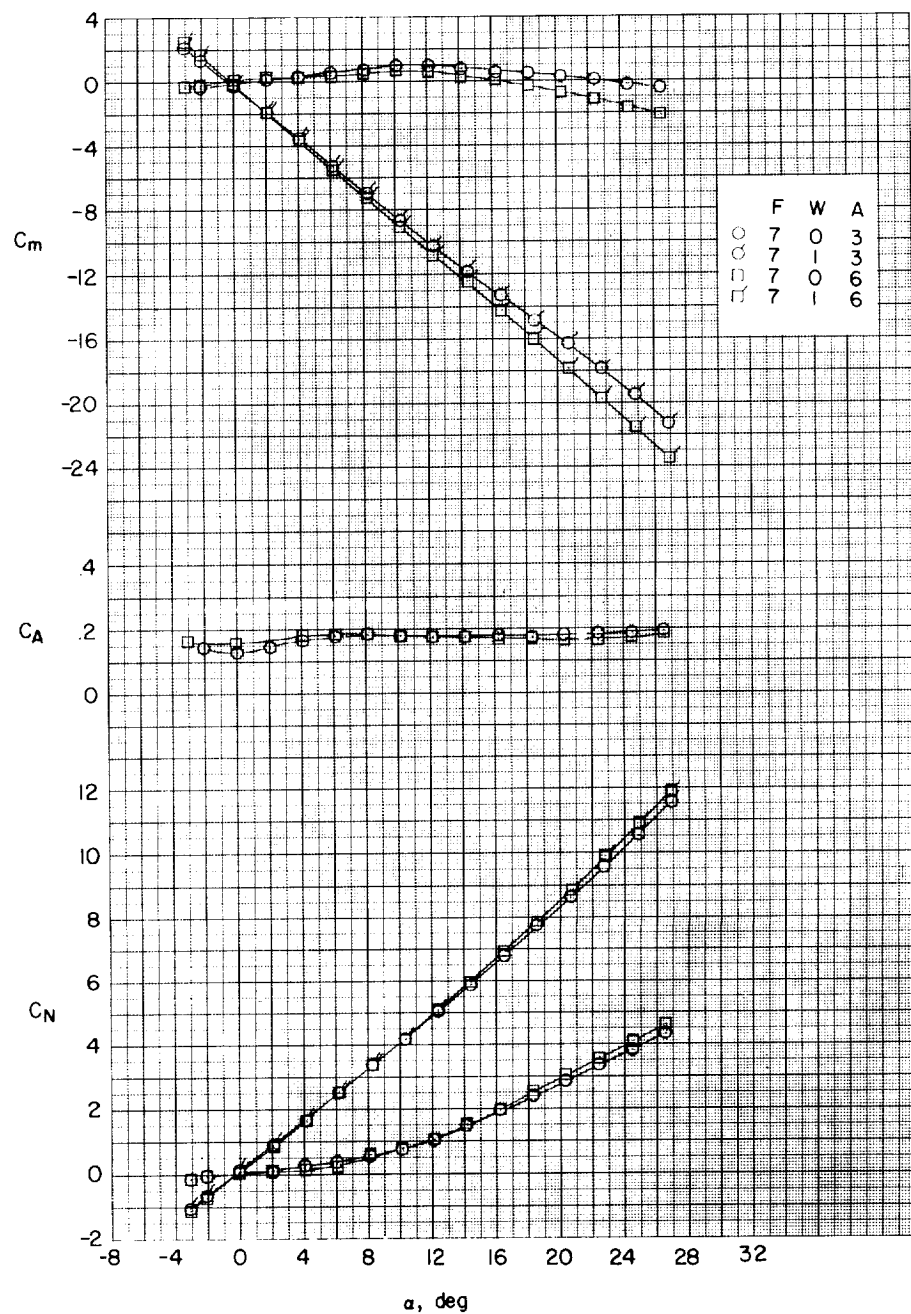


Figure 31.- Effects of 1-caliber boattail (A_3) and 1-caliber flare (A_6) afterbodies on aerodynamic characteristics in pitch. Large delta wings; $l/d = 10$.

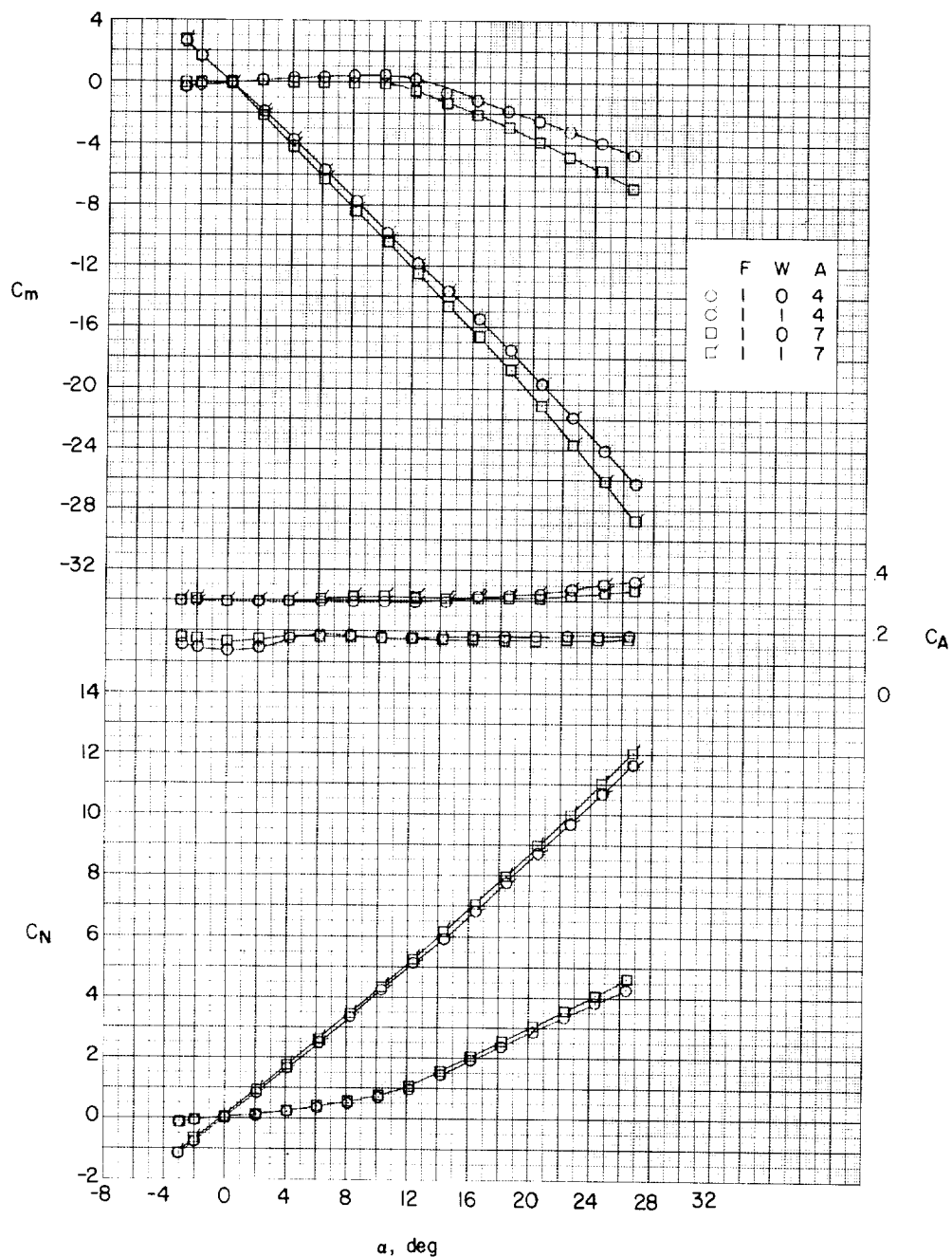


Figure 32.- Effects of 2-caliber cylinder-boattail (A_4) and 2-caliber cylinder-flare (A_7) afterbodies on aerodynamic characteristics in pitch. Large delta wings; $l/d = 10$.

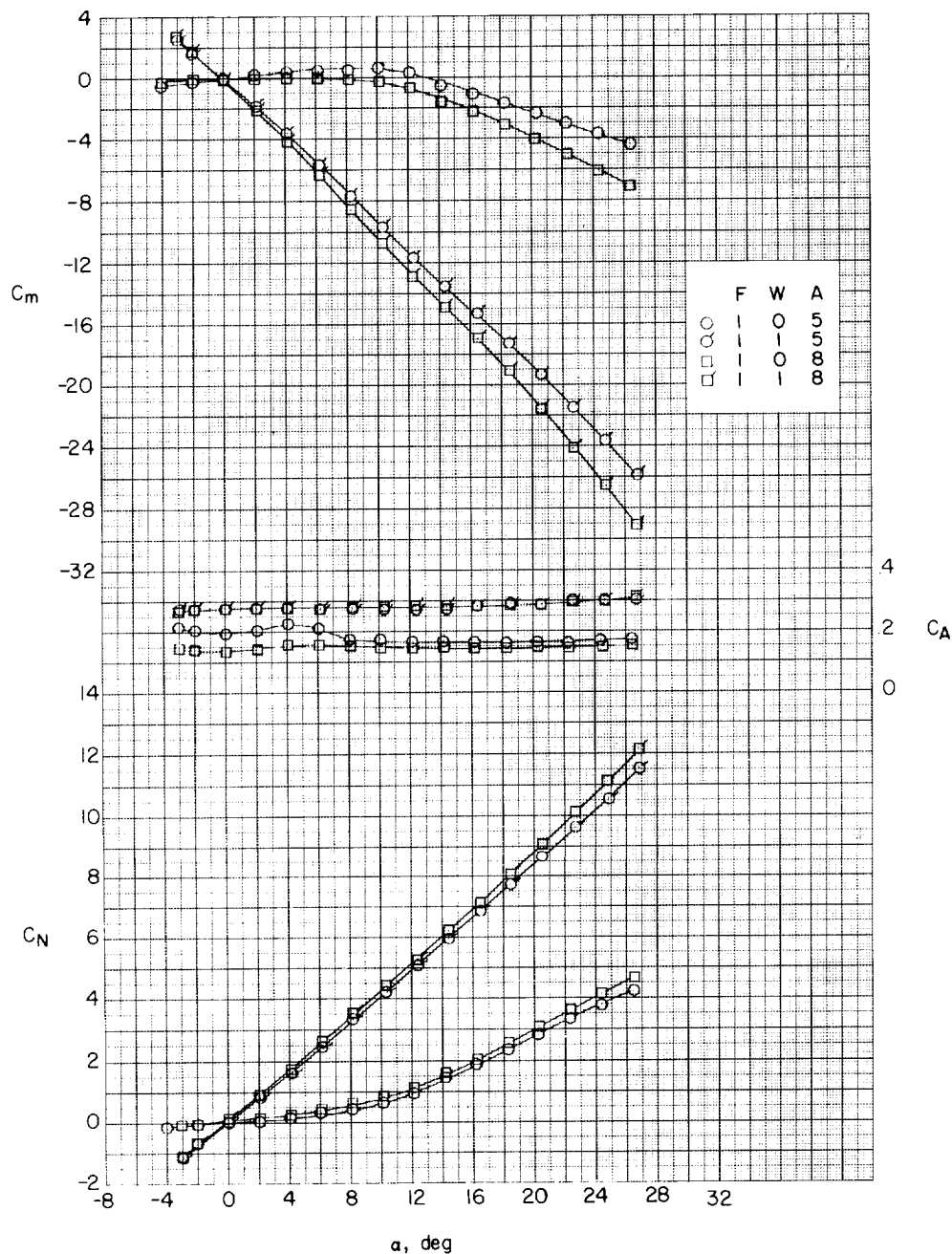


Figure 33.- Effects of 2-diameter boattail (A_5) and 2-caliber flare (A_8) afterbodies on aerodynamic characteristics in pitch. Large delta wings; $l/d = 10$.

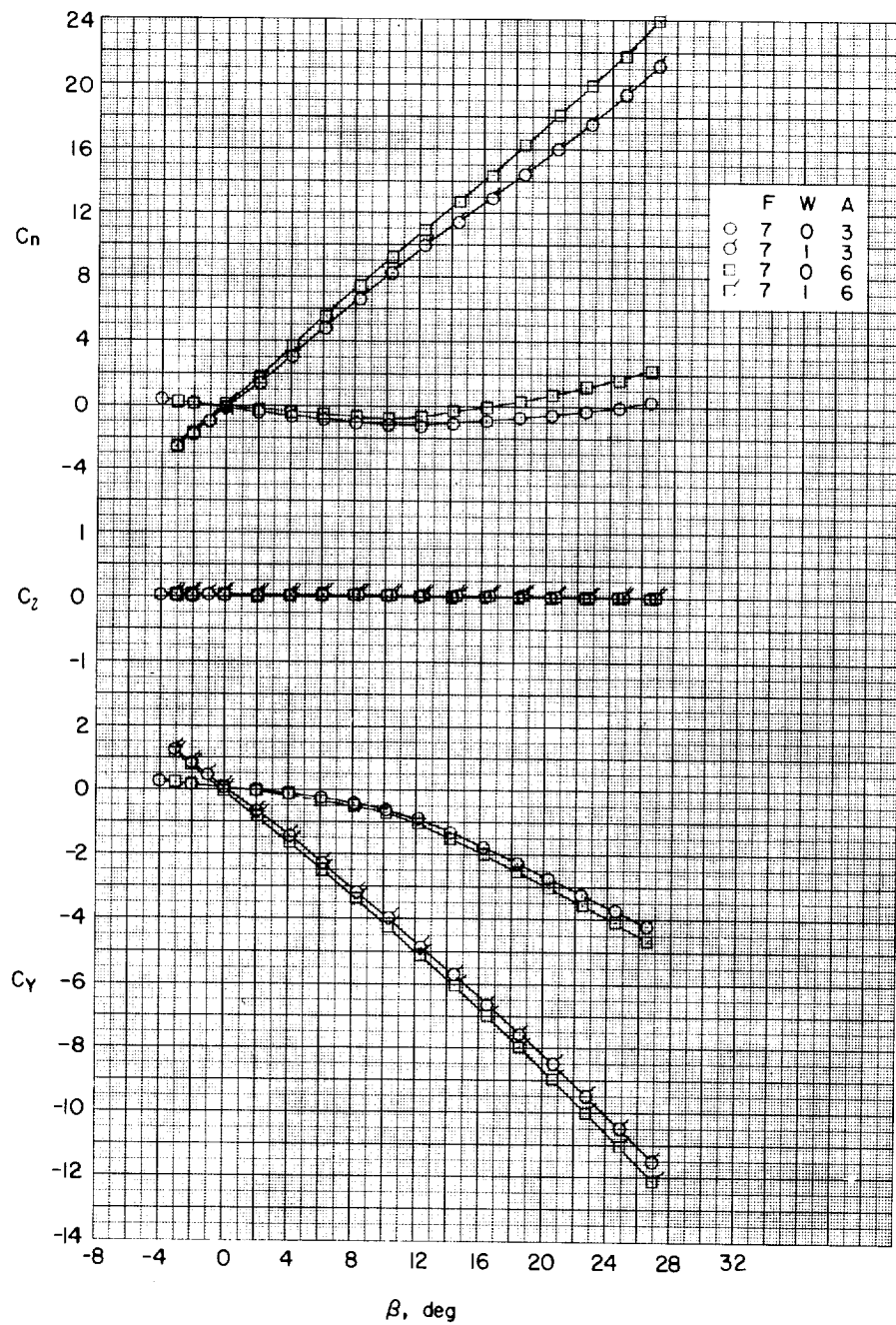
(a) $\alpha \approx 0^\circ$.

Figure 34.- Effects of 1-caliber boattail (A_3) and 1-caliber flare (A_6) afterbodies on aerodynamic characteristics in sideslip. Large delta wings; $l/d = 10$.

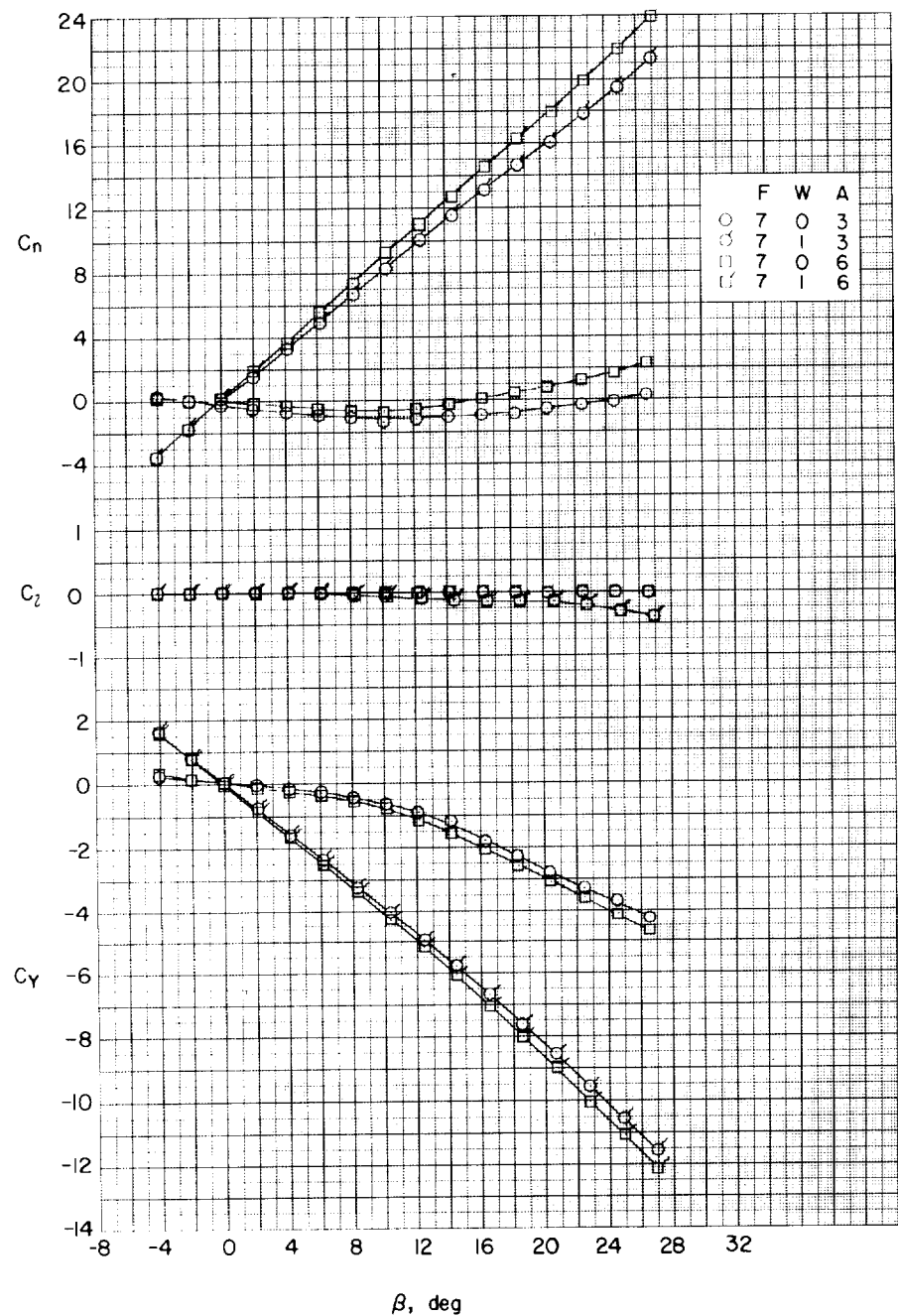
(b) $\alpha \approx 4.1^\circ$.

Figure 34.- Continued.

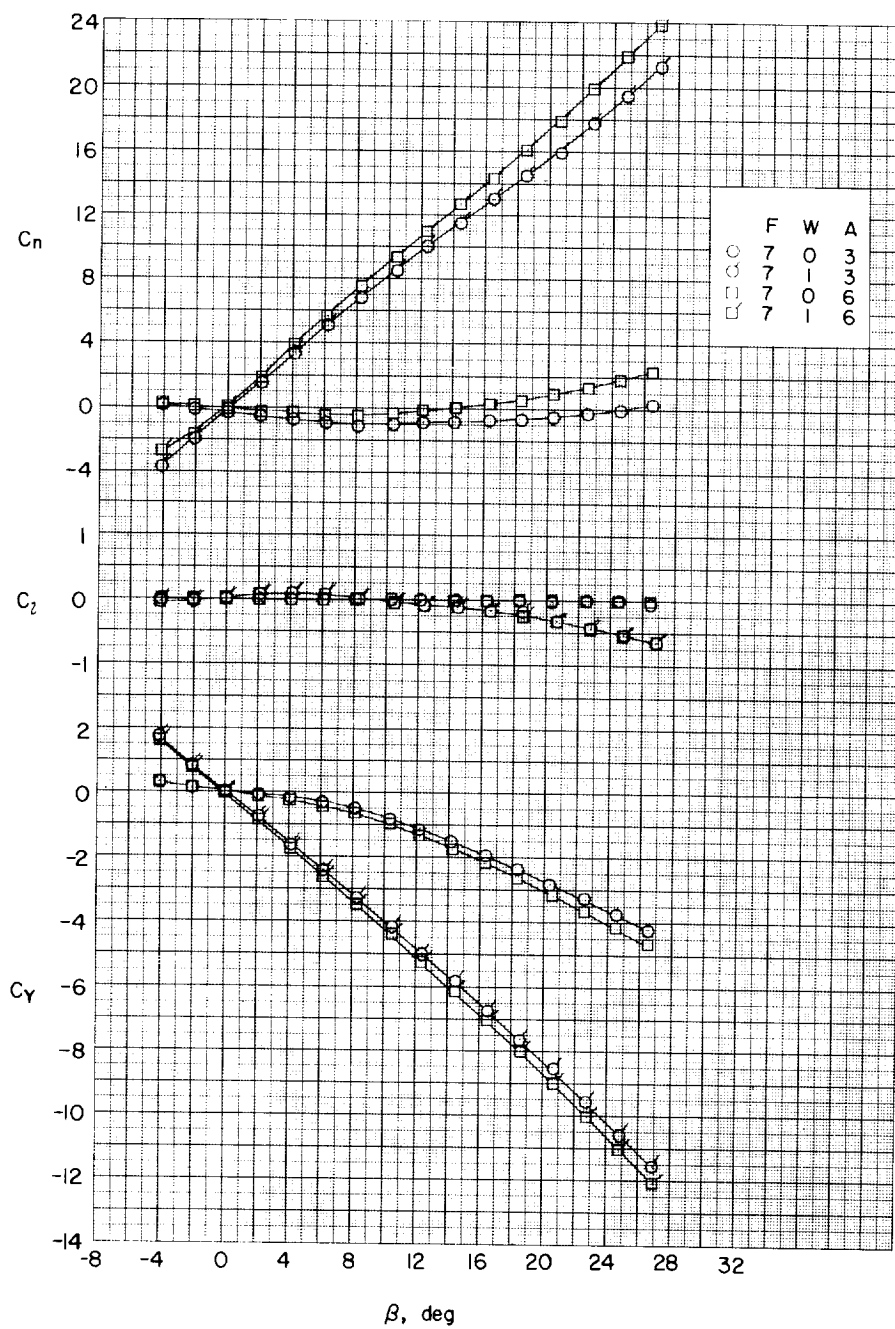
(c) $\alpha \approx 8.2^\circ$.

Figure 34.- Continued.

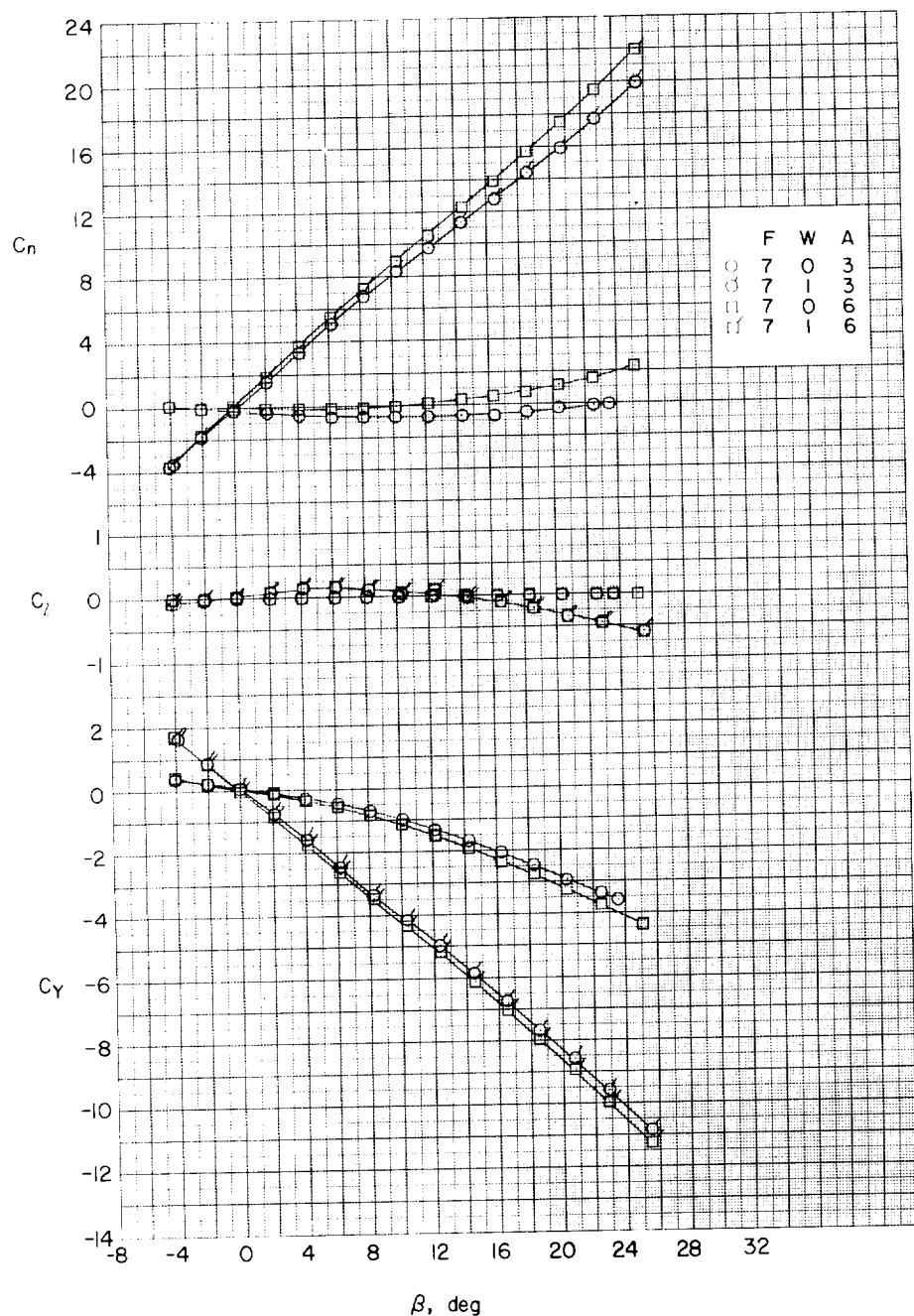
(d) $\alpha \approx 12.3^\circ$.

Figure 34.- Continued.

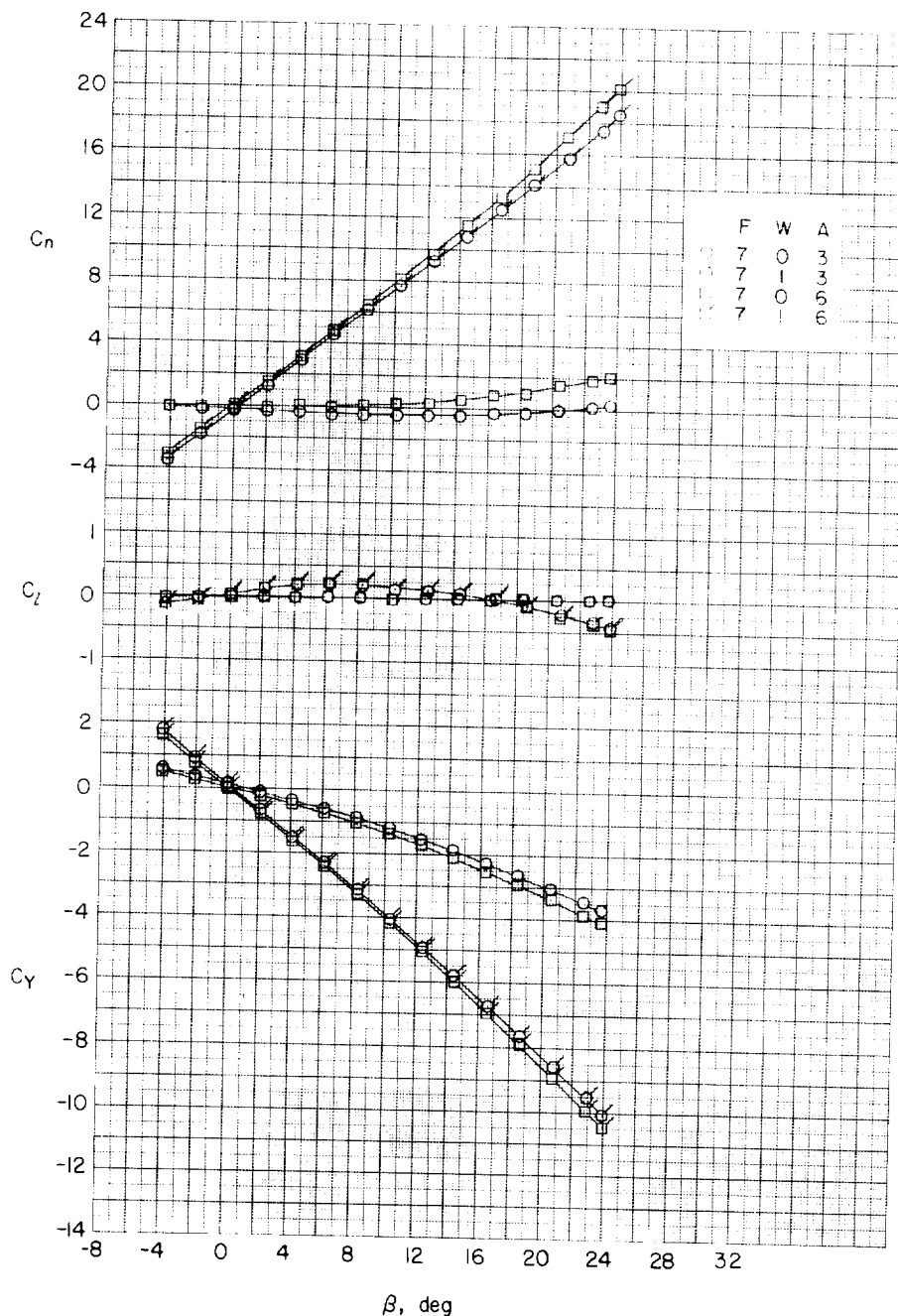
(e) $\alpha \approx 16.4^\circ$.

Figure 34--Continued.

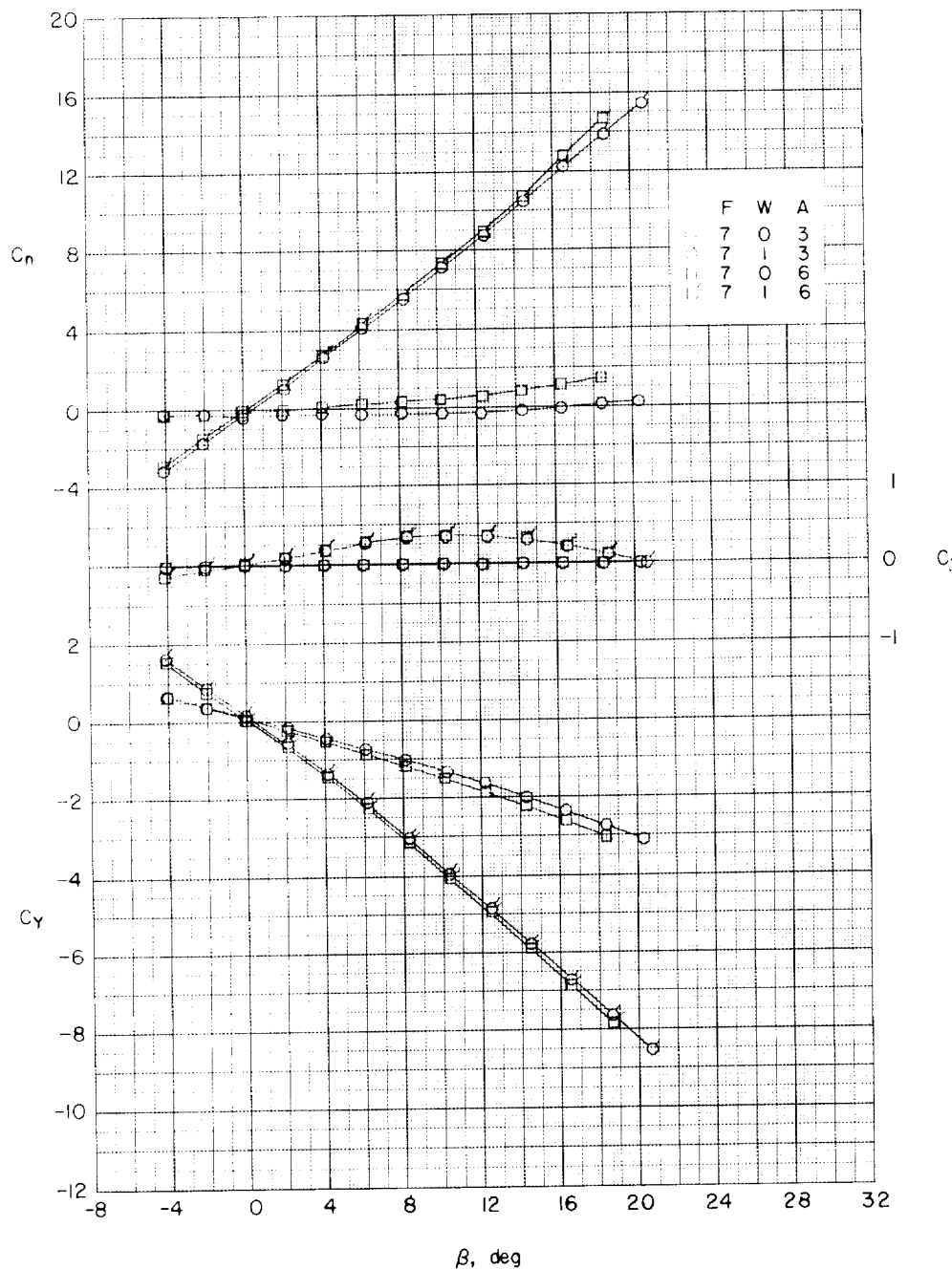
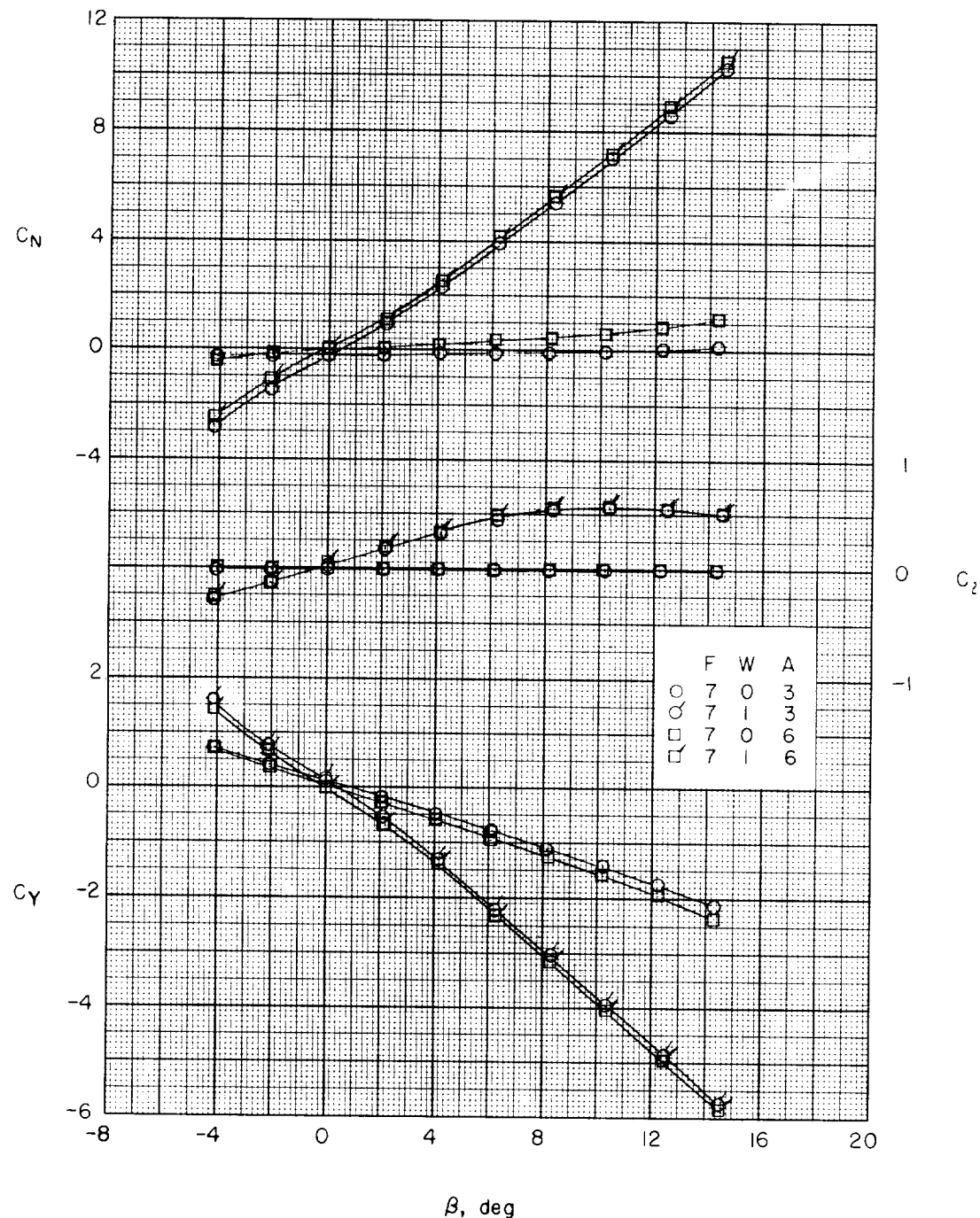
(f) $\alpha \approx 20.5^\circ$.

Figure 34.- Continued.



β , deg

(g) $\alpha \approx 24.7^\circ$.

Figure 34.- Concluded.

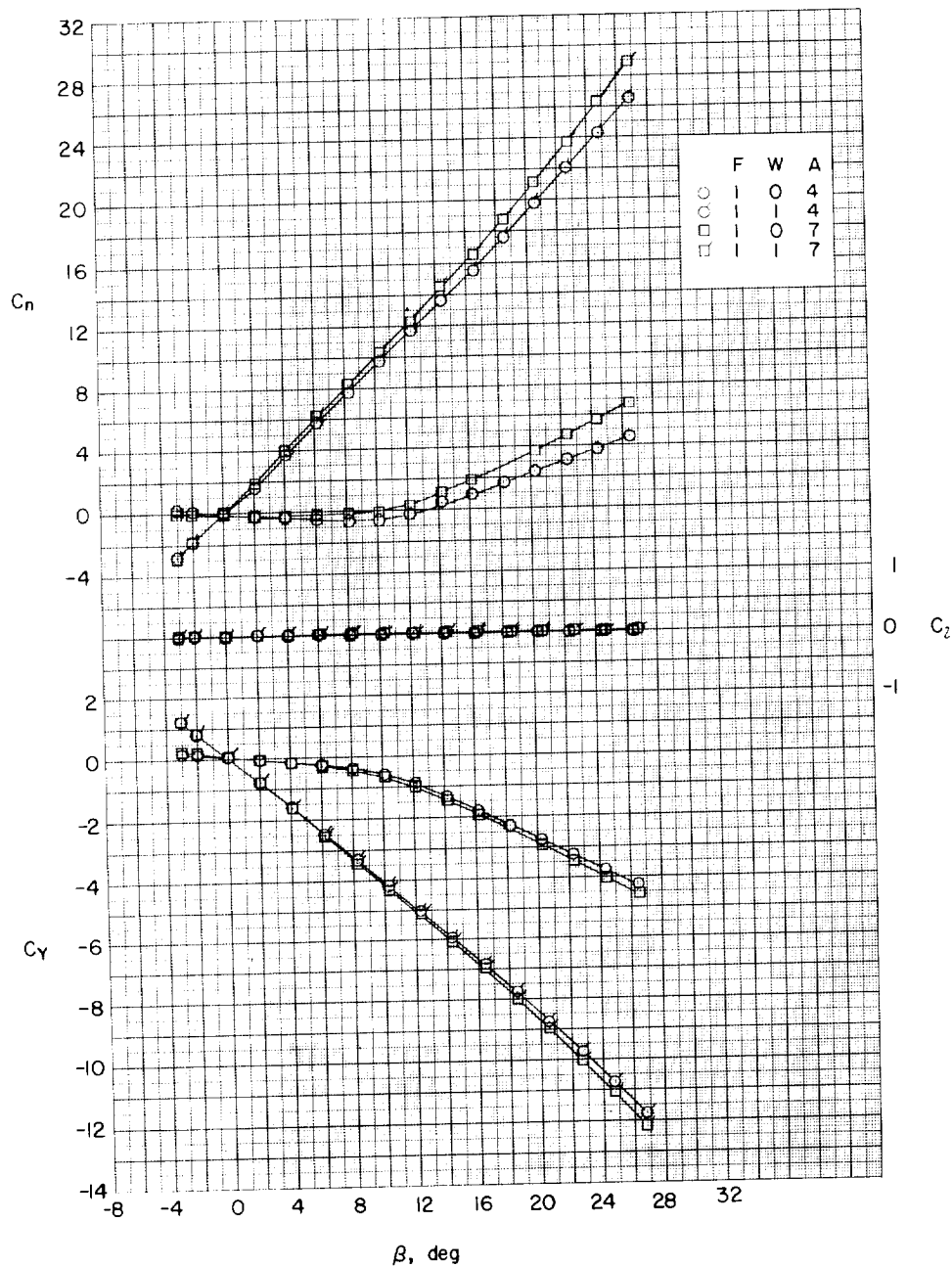
(a) $\alpha \approx 0^\circ$.

Figure 35.- Effects of 2-caliber cylinder-boattail (A₄) and 2-caliber cylinder-flare (A₆) afterbodies on aerodynamic characteristics in sideslip. Large delta wings; $l/d = 10$.

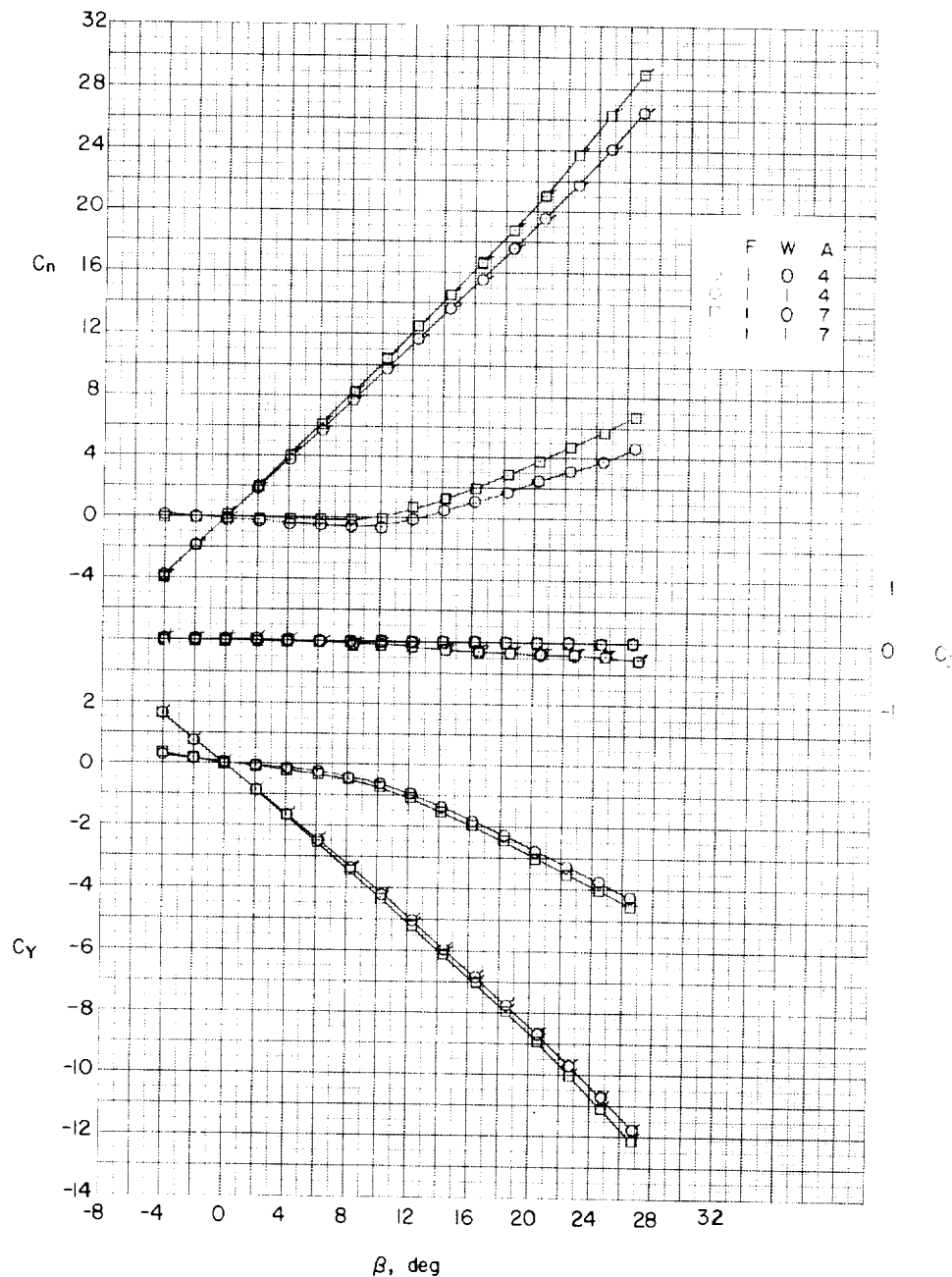
(b) $\alpha \approx 4.1^\circ$.

Figure 35.- Continued.

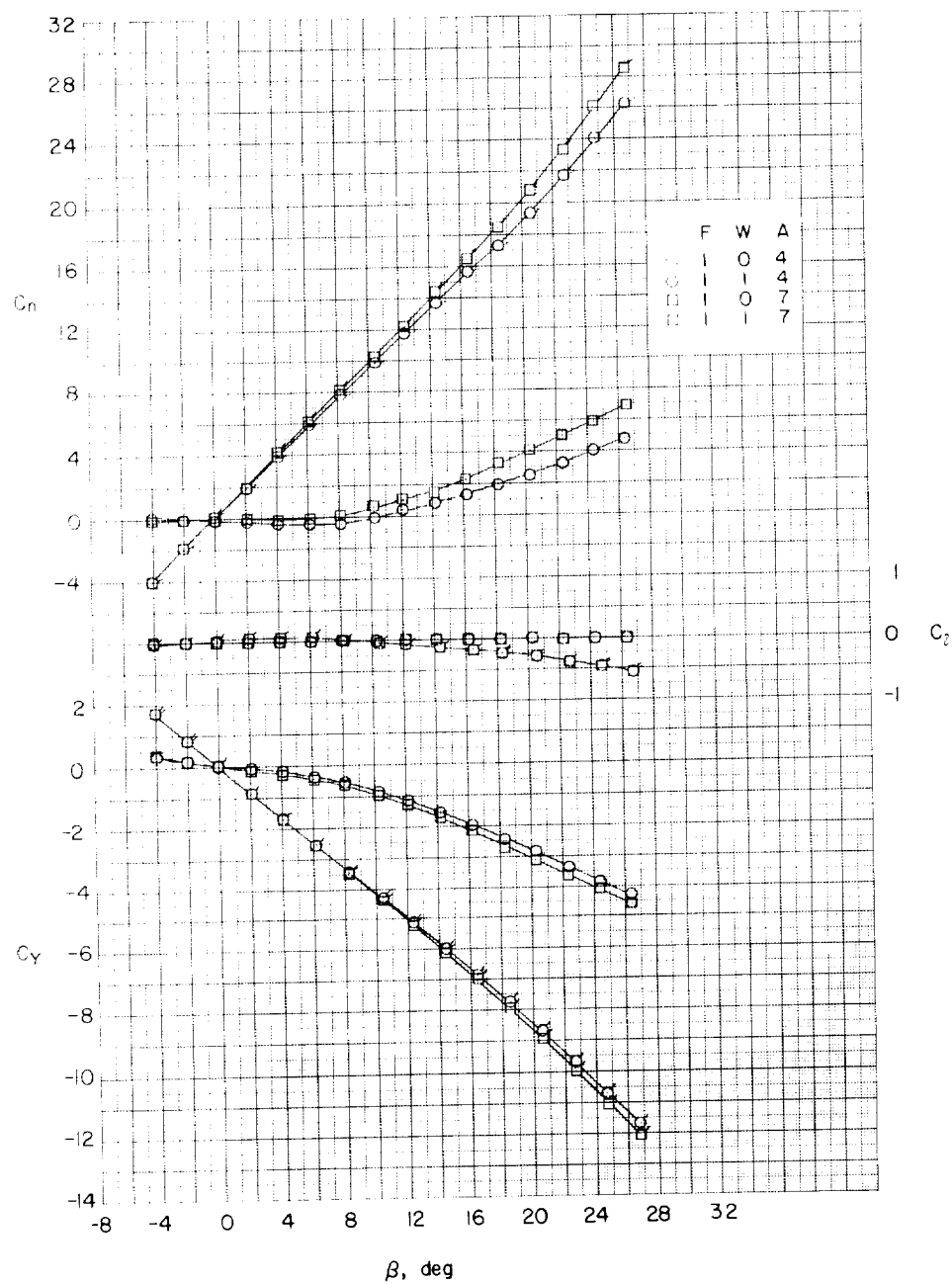
(c) $\alpha \approx 8.2^\circ$.

Figure 35--Continued.

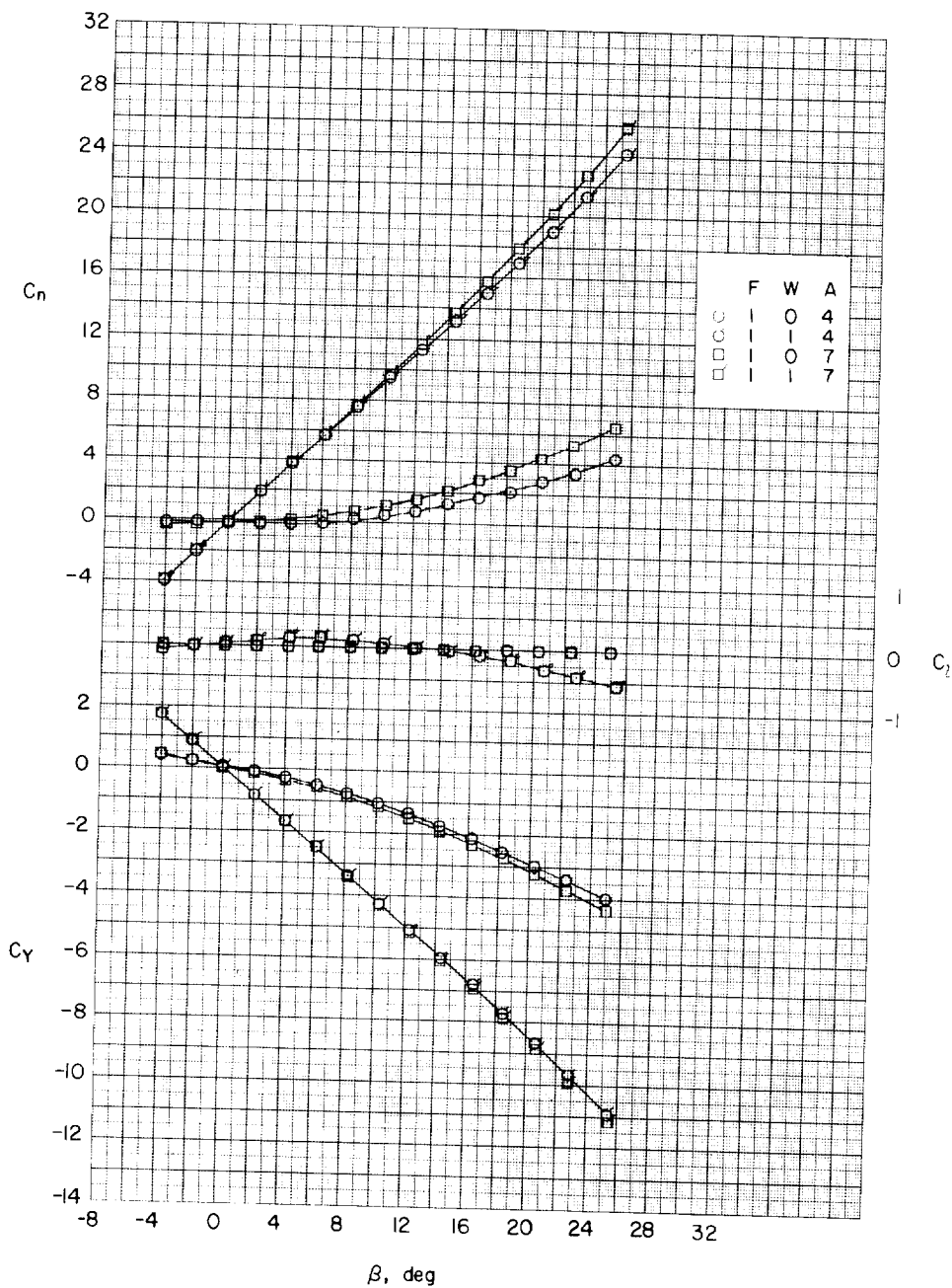
(d) $\alpha \approx 12.3^\circ$.

Figure 35.- Continued.

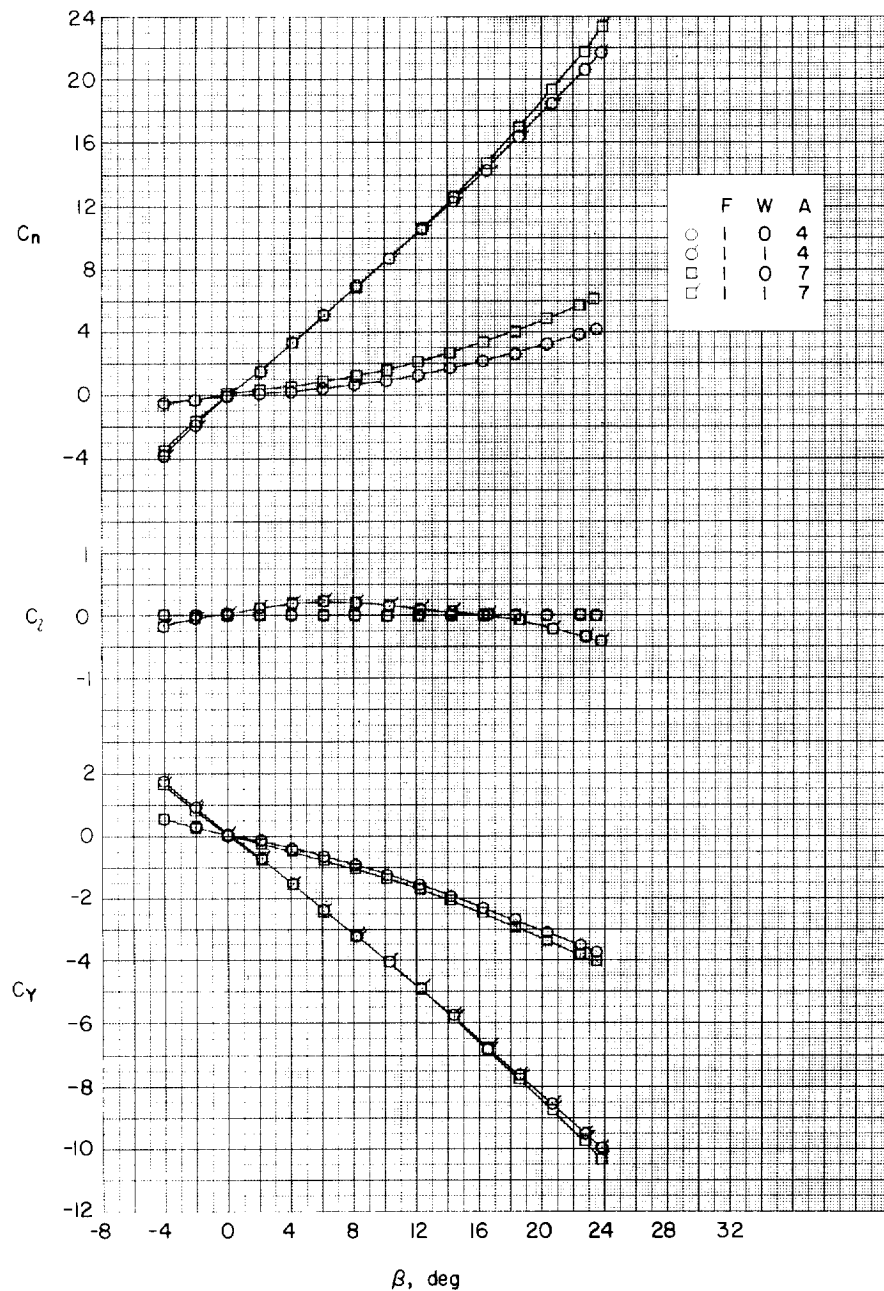
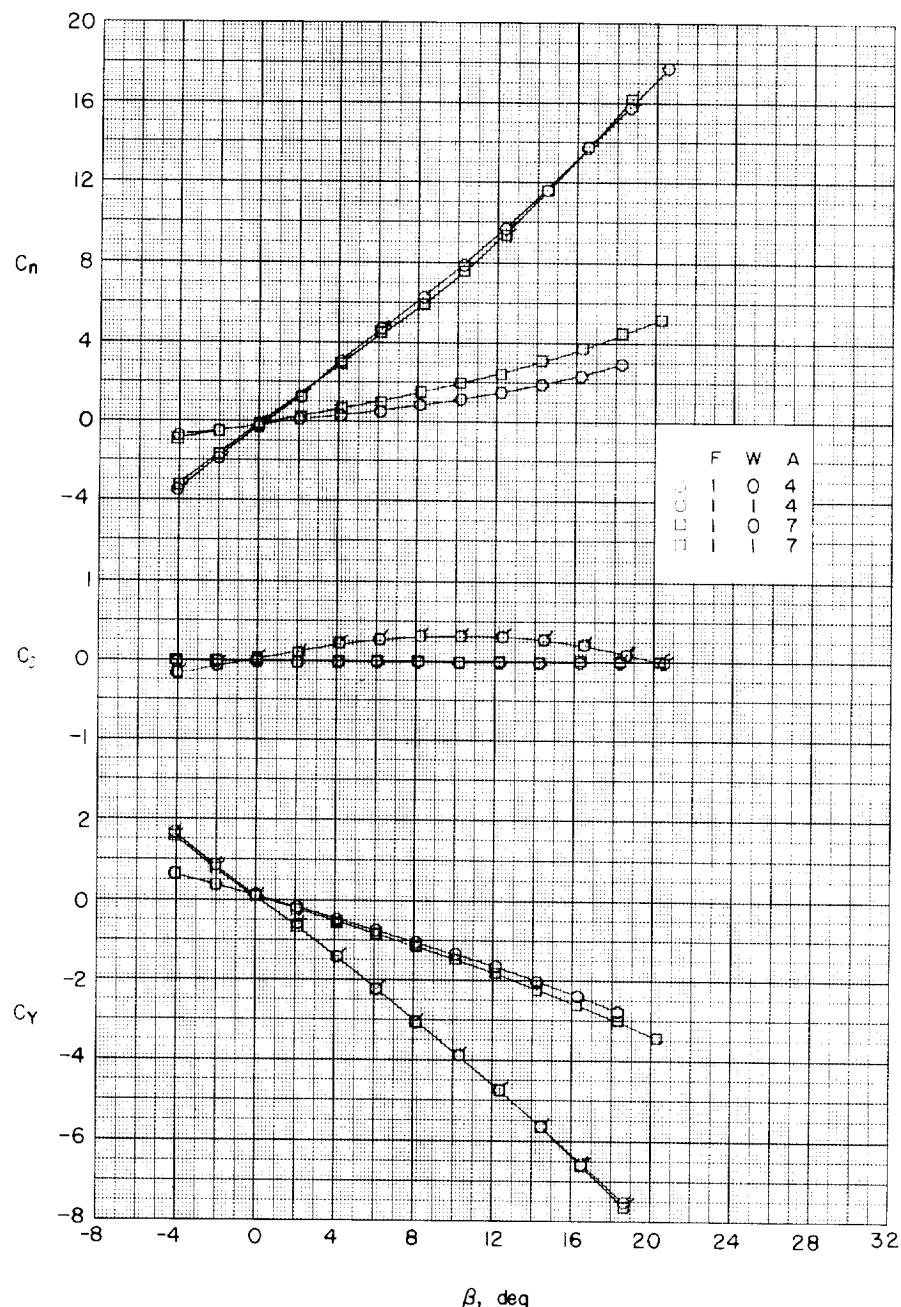
(e) $\alpha \approx 16.4^\circ$.

Figure 35.- Continued.



(f) $\alpha \approx 20.5^\circ$.

Figure 35.- Continued.

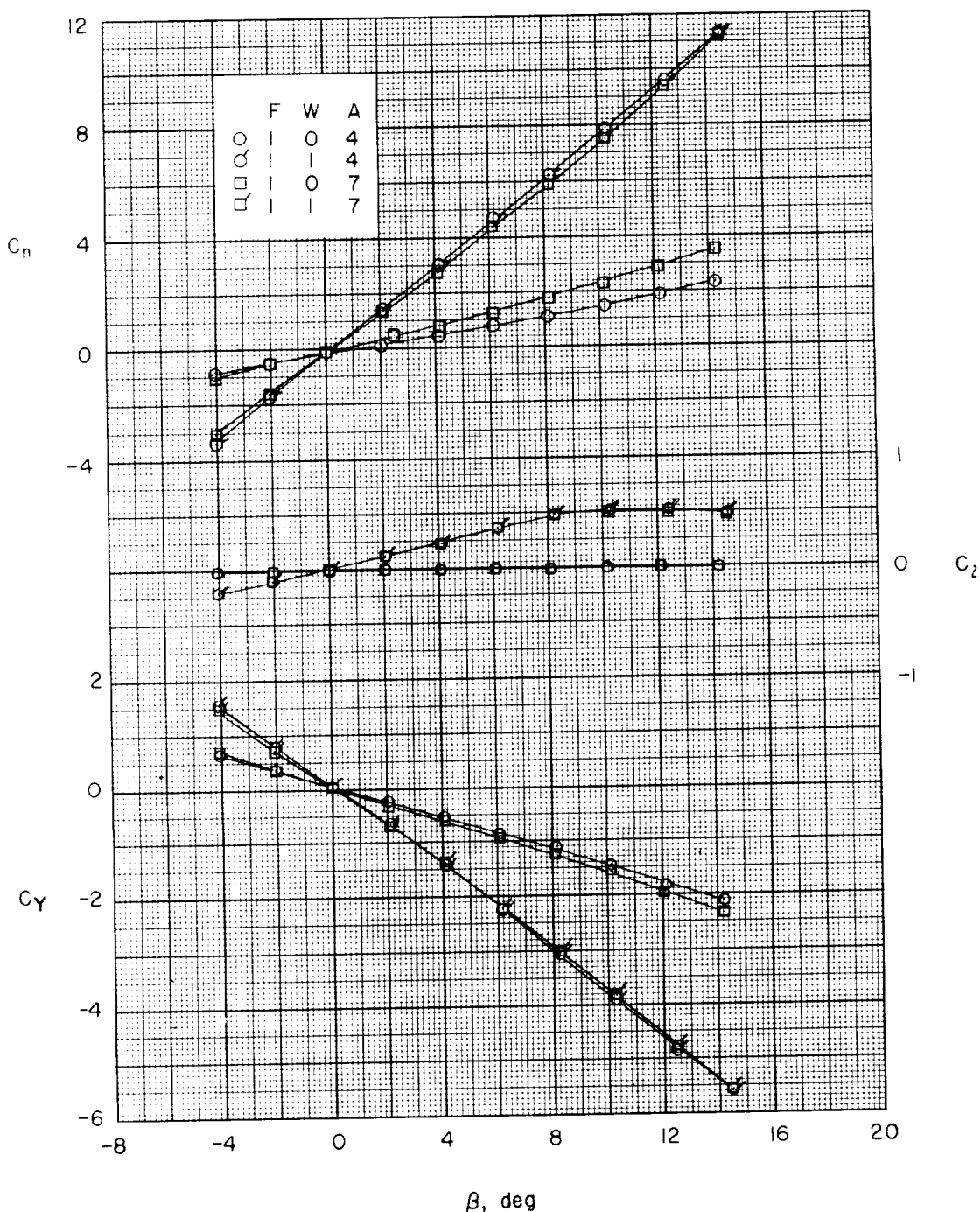
(g) $\alpha \approx 24.7^\circ$.

Figure 35.- Concluded.

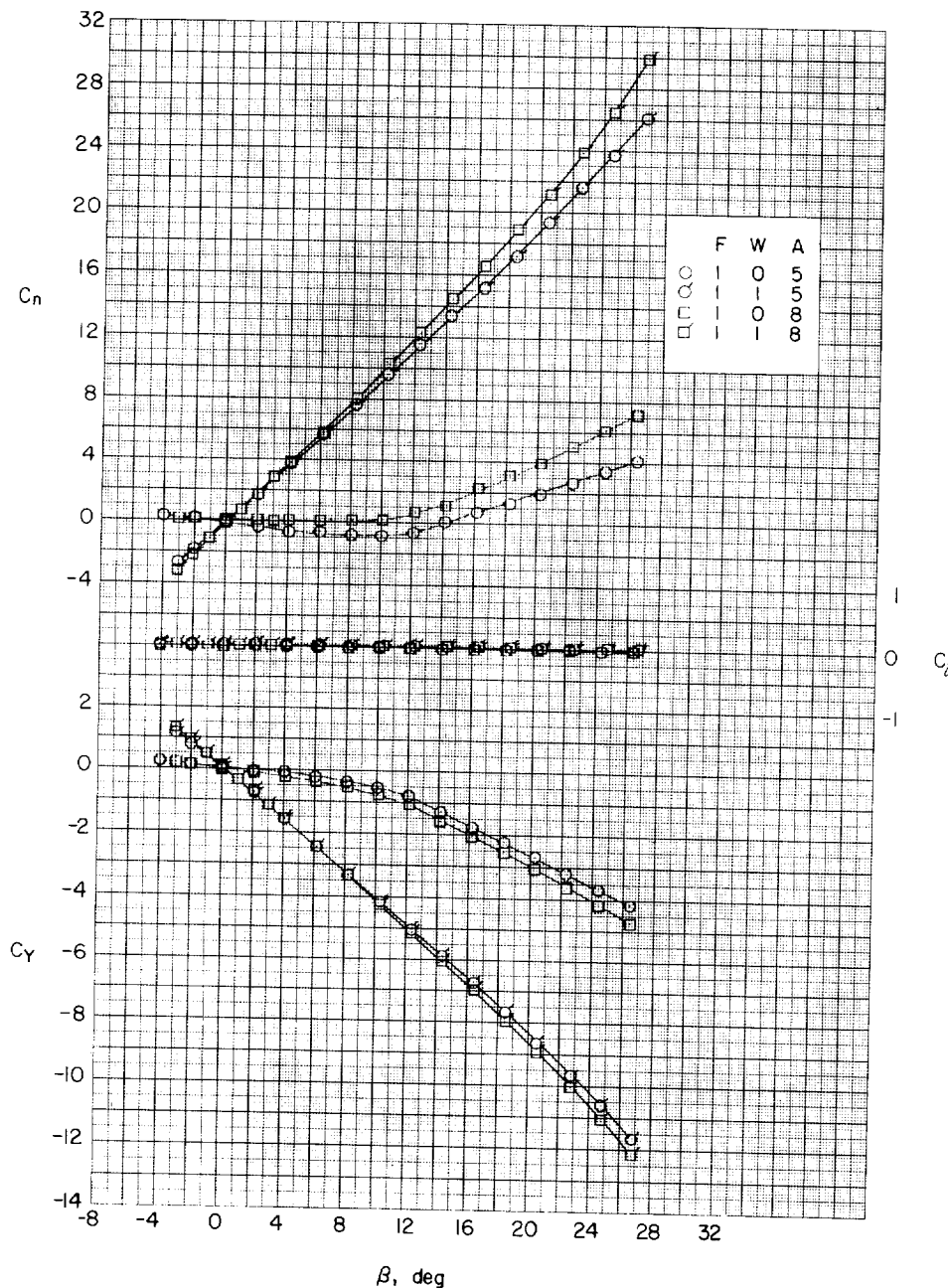
(a) $\alpha \approx 0^\circ$.

Figure 36.- Effects of 2-caliber boattail (A_5) and 2-caliber flare (A_8) afterbodies on the aerodynamic characteristics in sideslip. Large delta wings; $l/D = 10$.

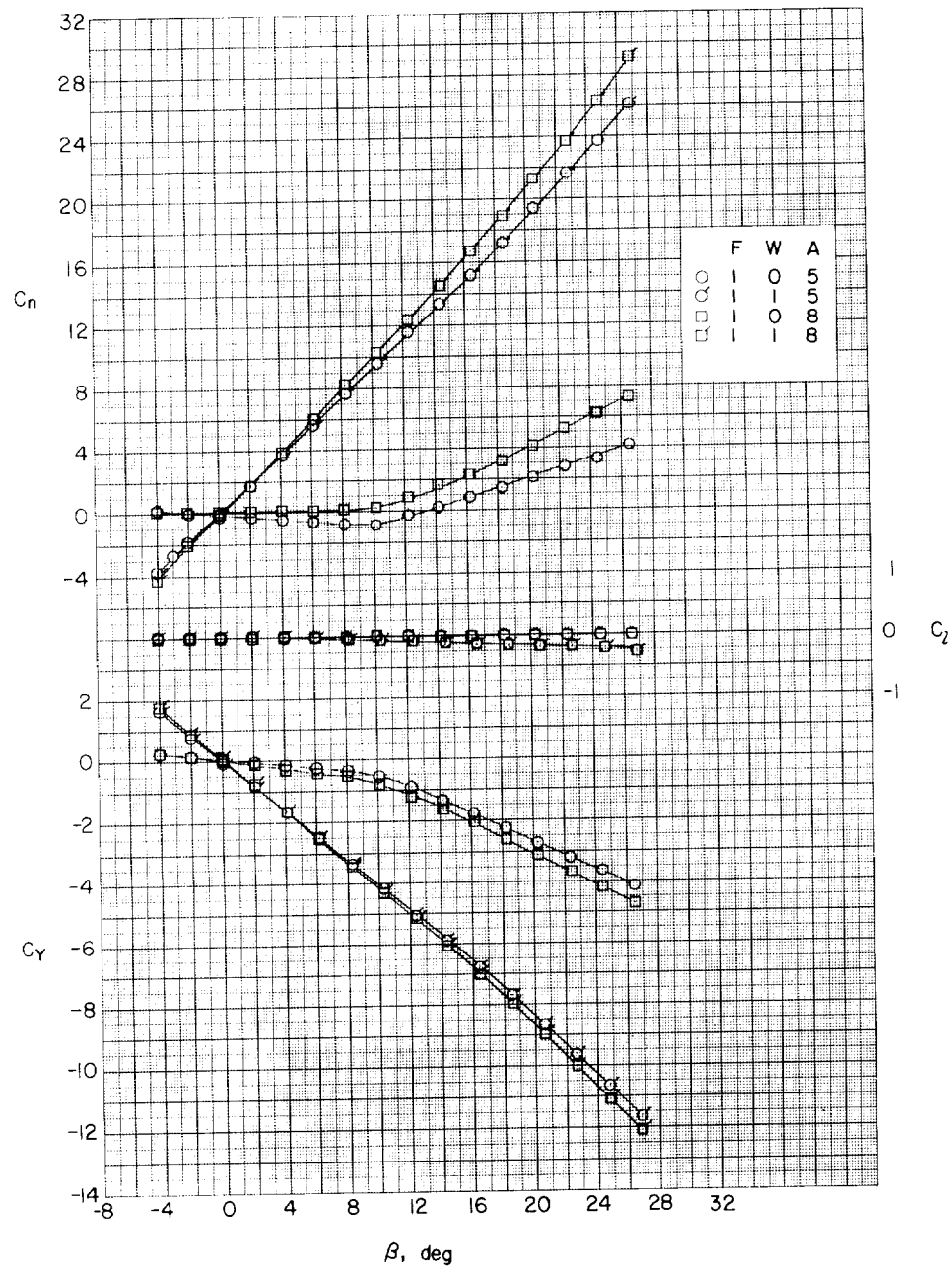
(b) $\alpha \approx 4.1^\circ$.

Figure 36.- Continued.

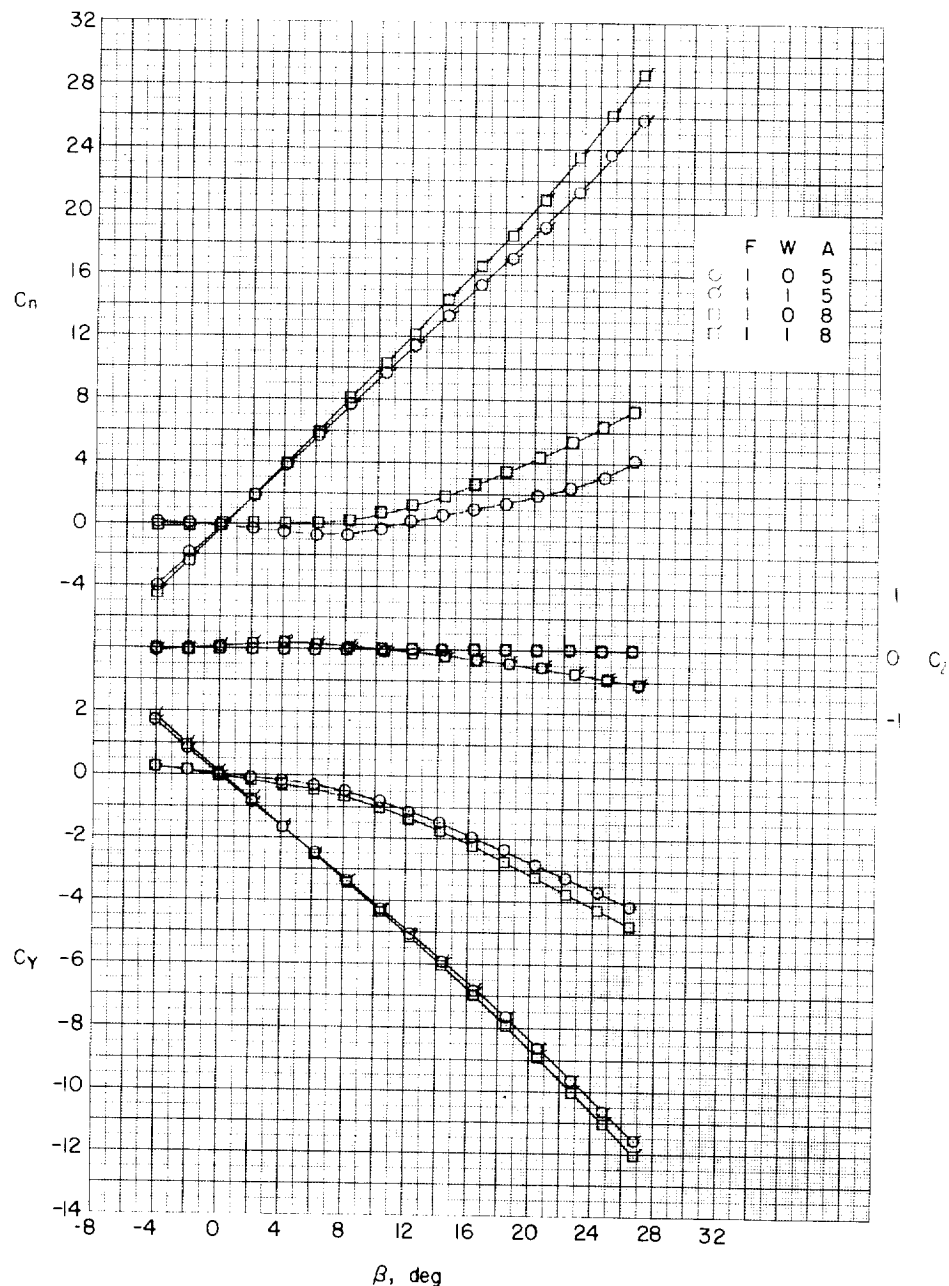
(c) $\alpha \approx 8.2^\circ$.

Figure 36.- Continued.

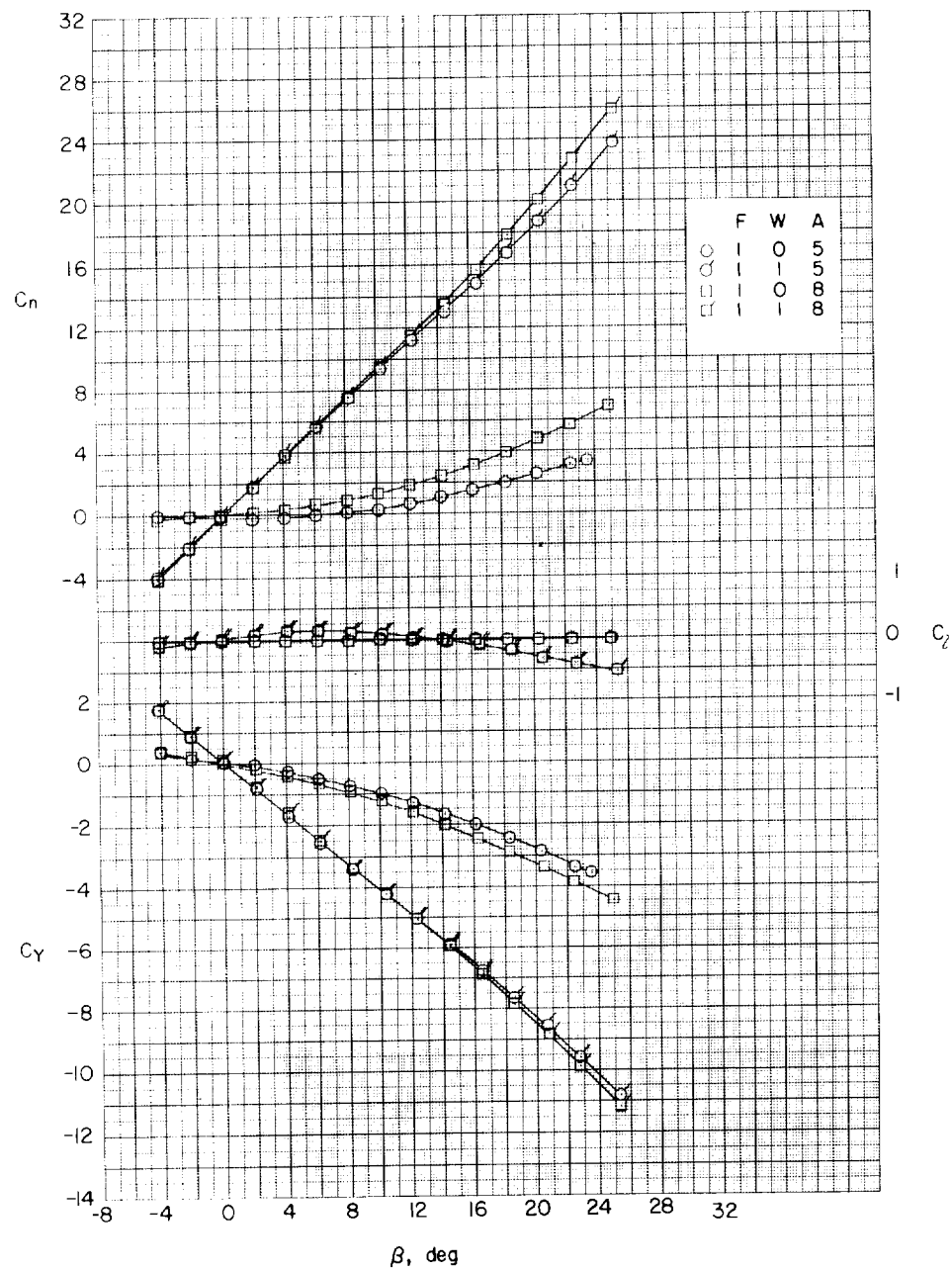
(d) $\alpha \approx 12.3^\circ$.

Figure 36.- Continued.

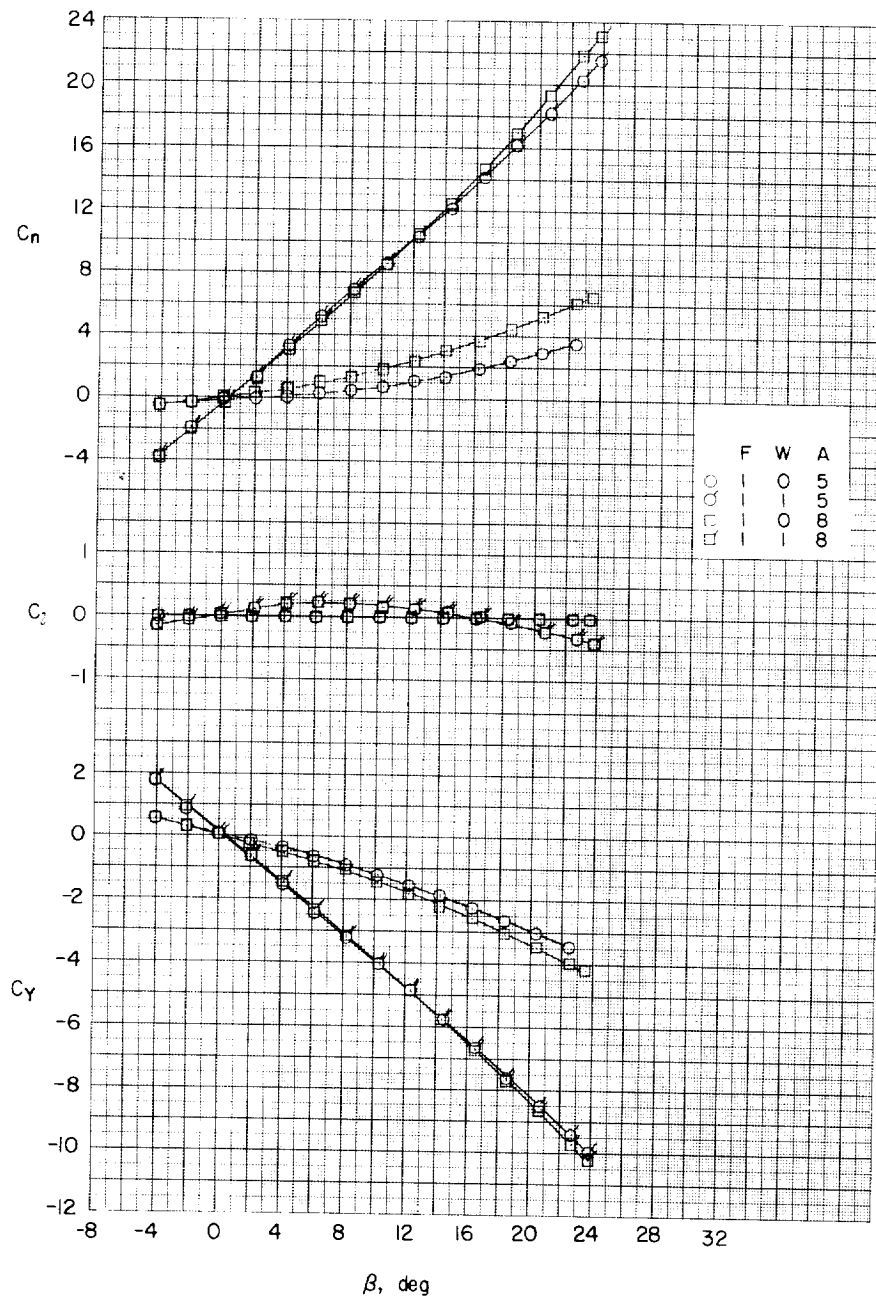
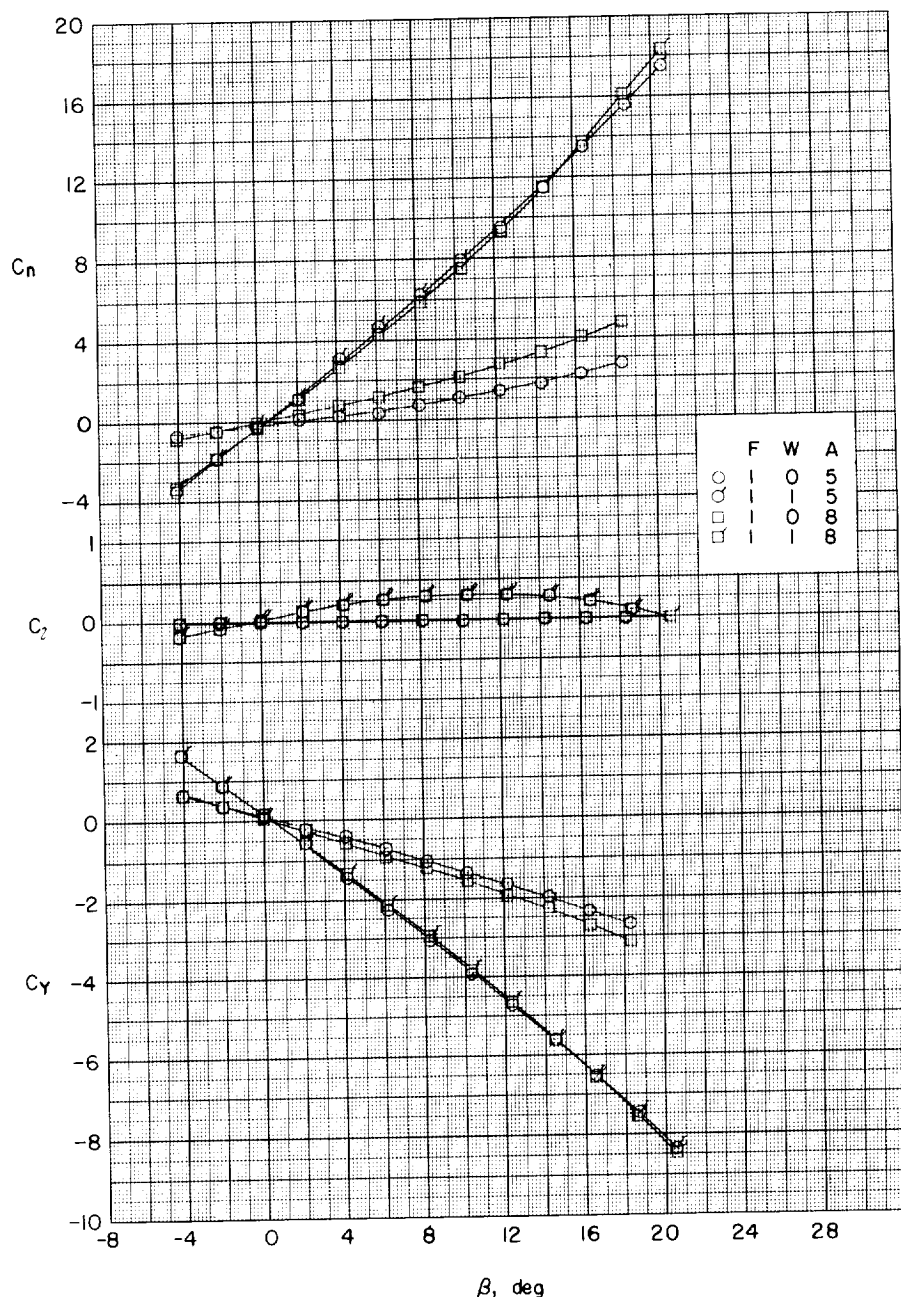
(e) $\alpha \approx 16.4^\circ$.

Figure 36.- Continued.



(f) $\alpha \approx 20.5^\circ$.

Figure 36.- Continued.

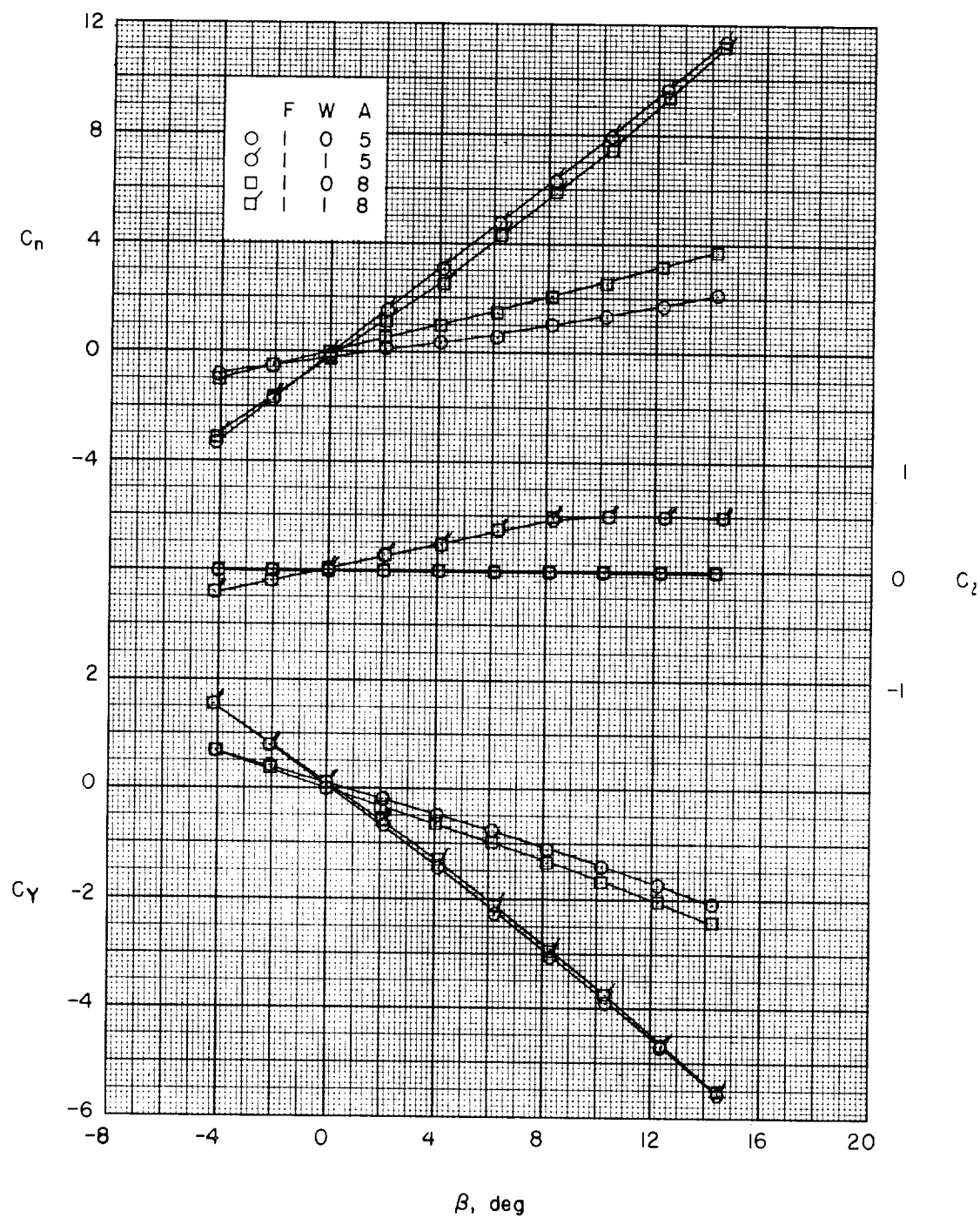
(g) $\alpha \approx 24.7^\circ$.

Figure 36.- Concluded.

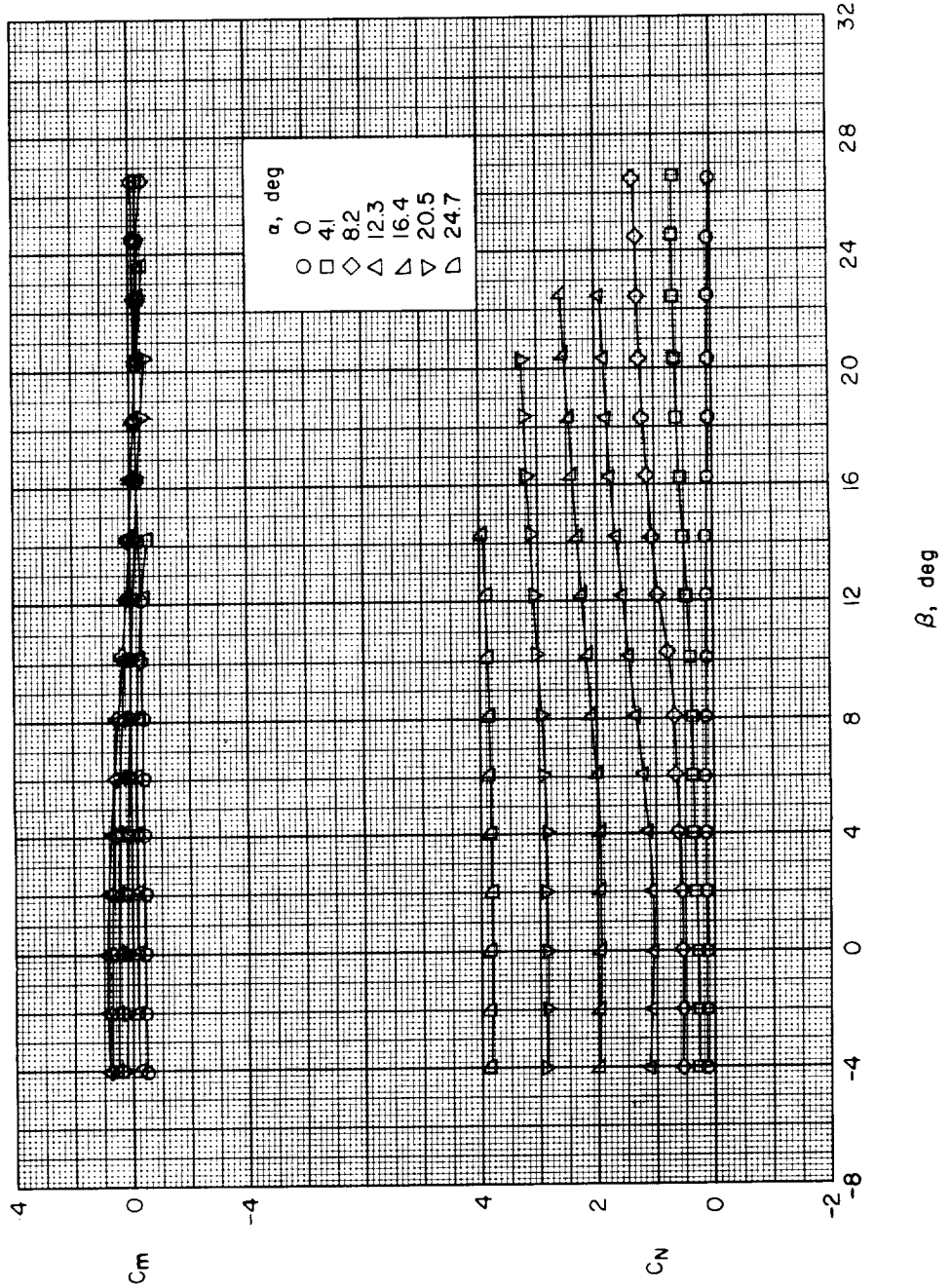
(a) Body alone, $F_7W_0A_3$.

Figure 37.- Variation of C_m and C_N with β for various angles of attack. One-caliber boattail (A_3) and 1-caliber flare (A_6) afterbodies; large delta wings; $l/d = 10$.

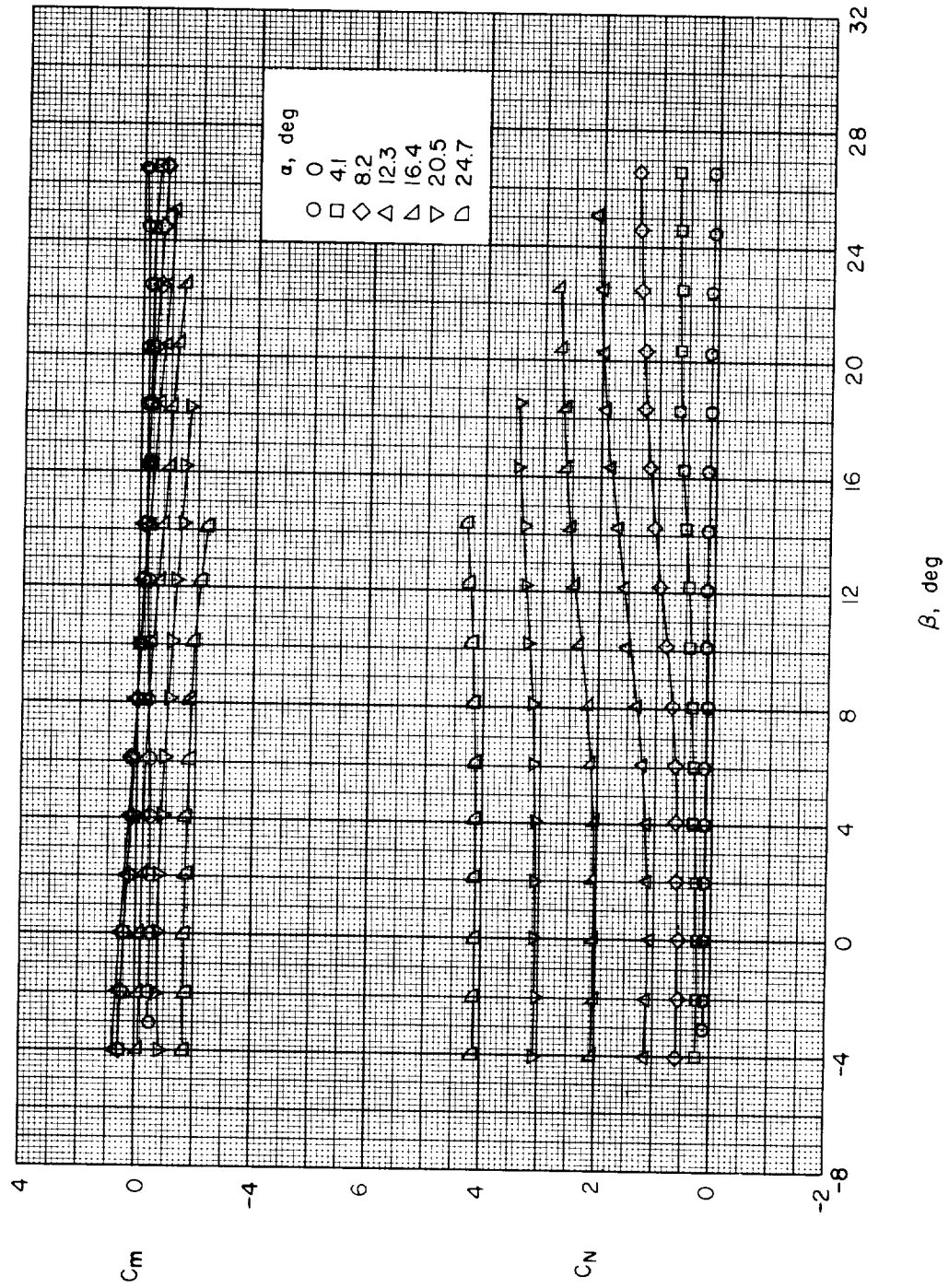
(b) Body alone, F_{7W0A6}.

Figure 37.- Continued.

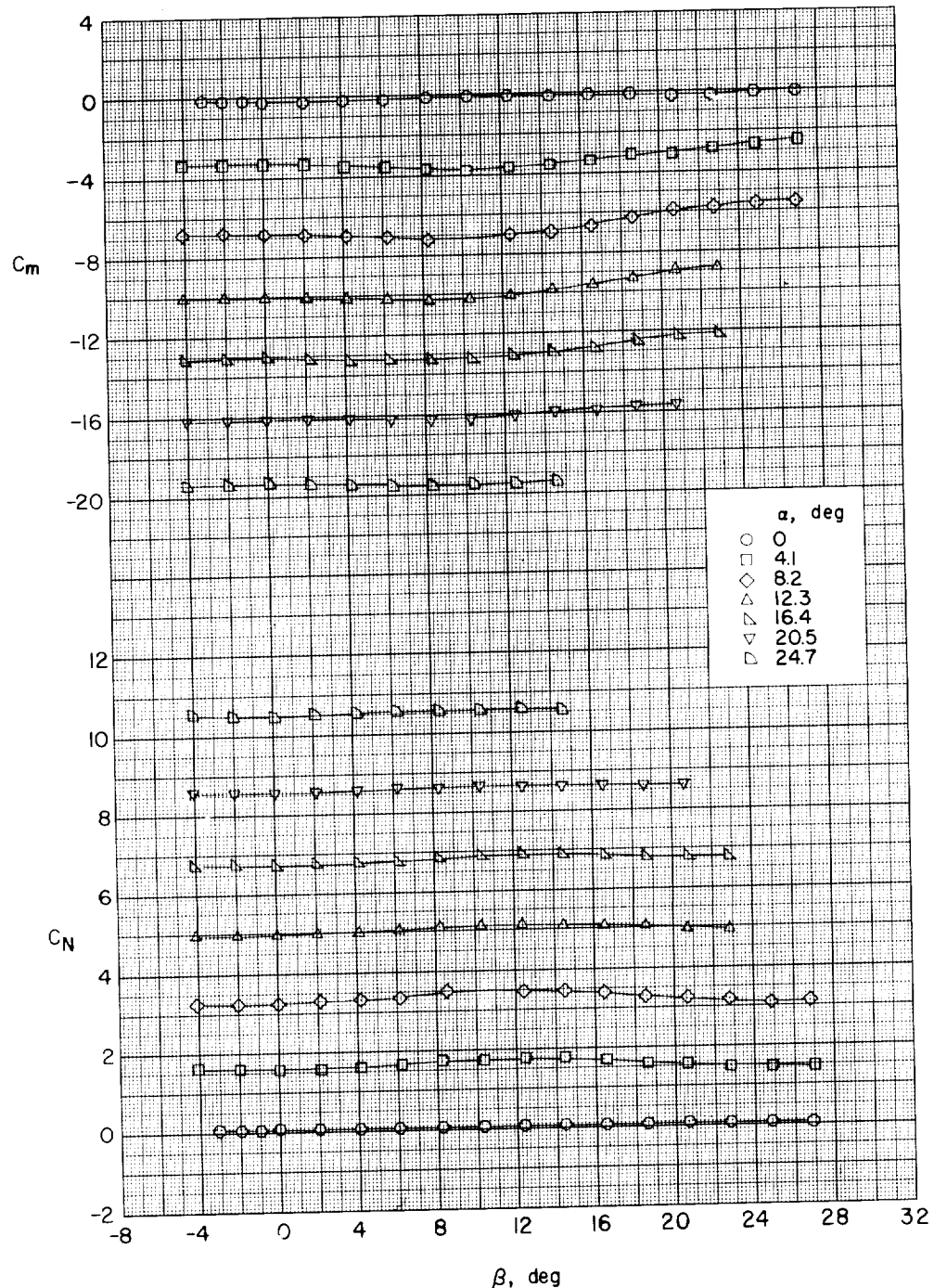
(c) Large delta wing, F₇W₀A₃.

Figure 37.- Continued.

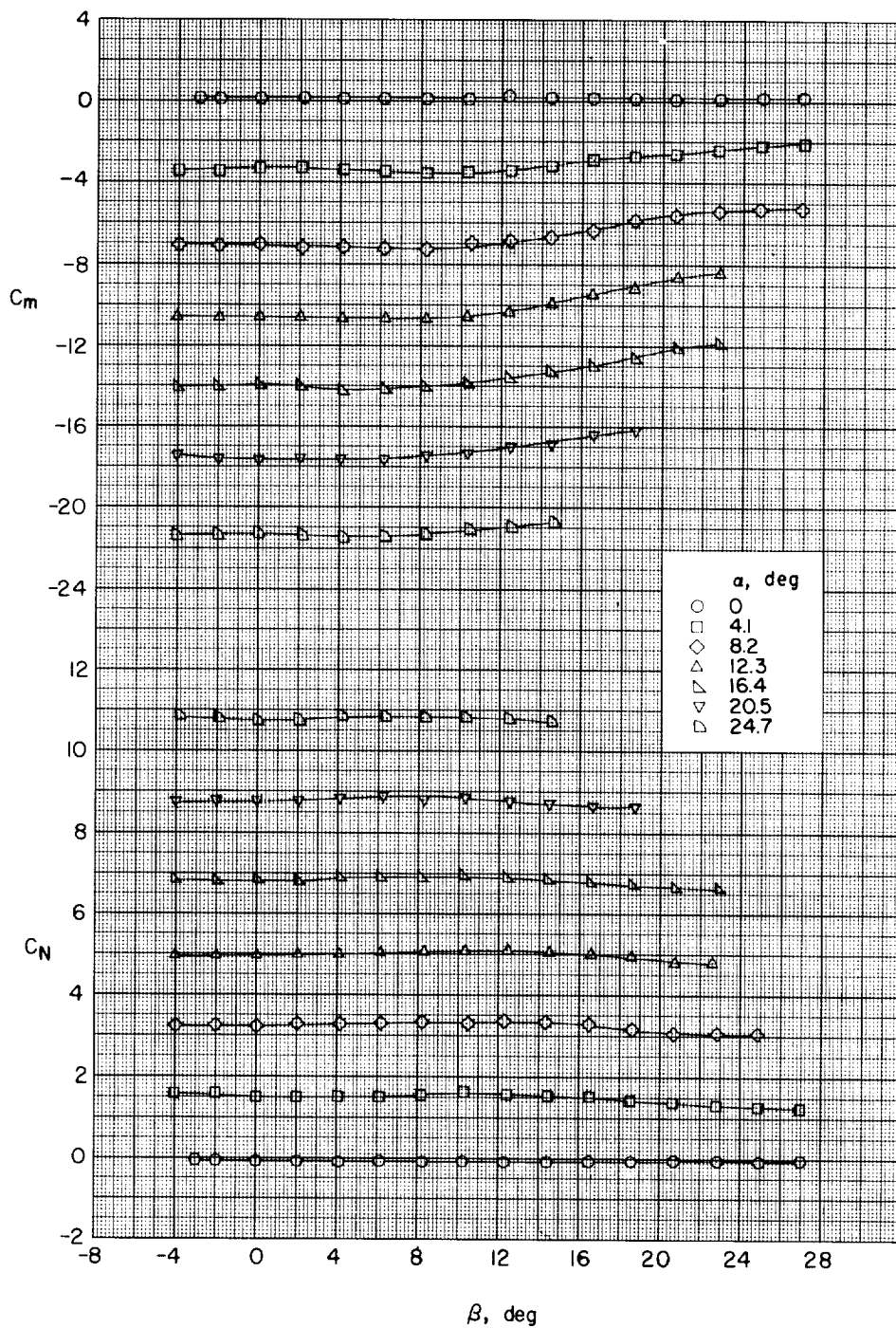
(d) Large delta wing, F₇W₁A6.

Figure 37.- Concluded.

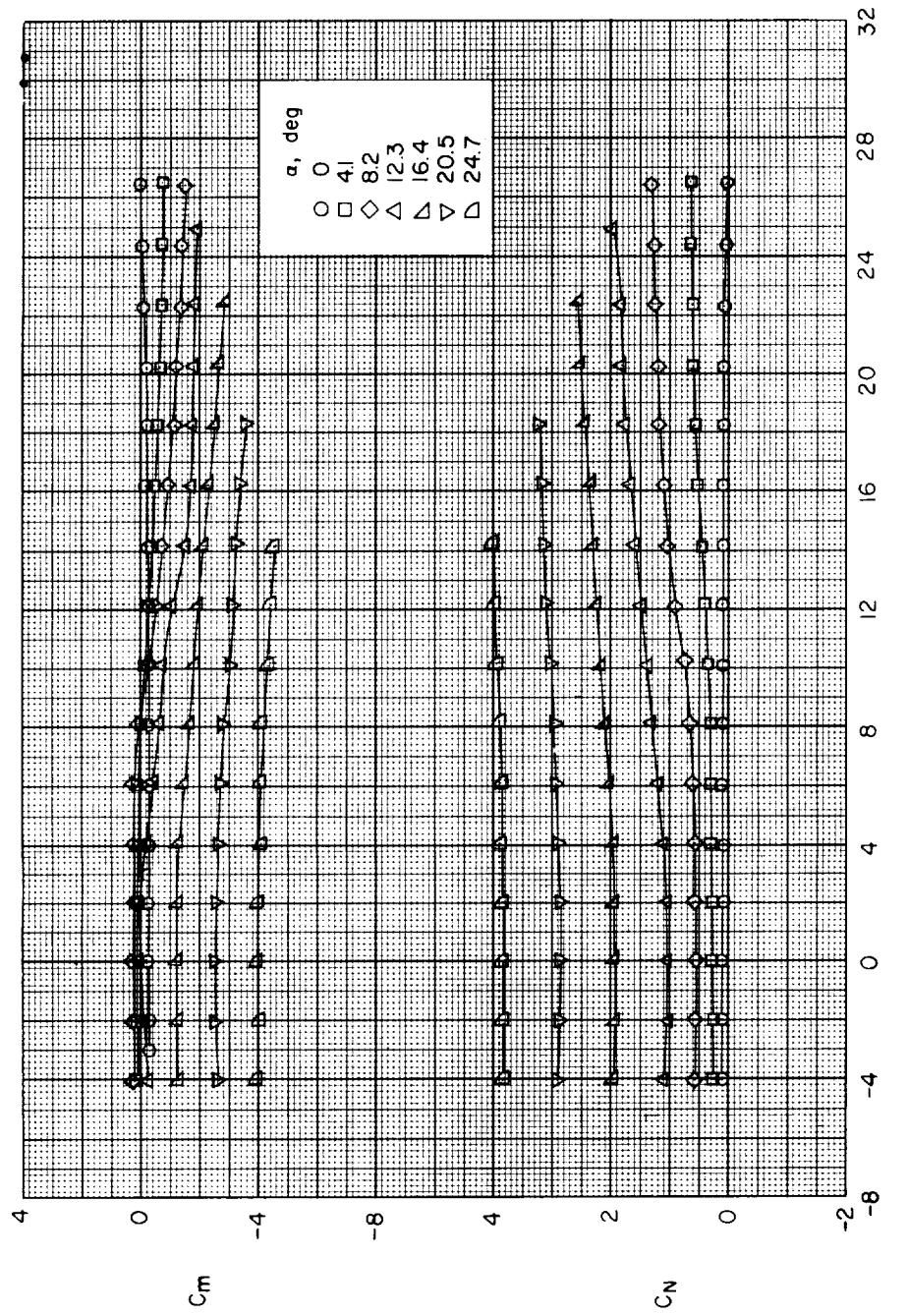
(a) Body alone, $F_1W_0A_4$.

Figure 38.- Variation of C_m and C_N with β for various angles of attack. Two-caliber cylinder-boattail (A_4) and 2-caliber cylinder-flare (A_7) afterbodies; large delta wings; $l/d = 10$.

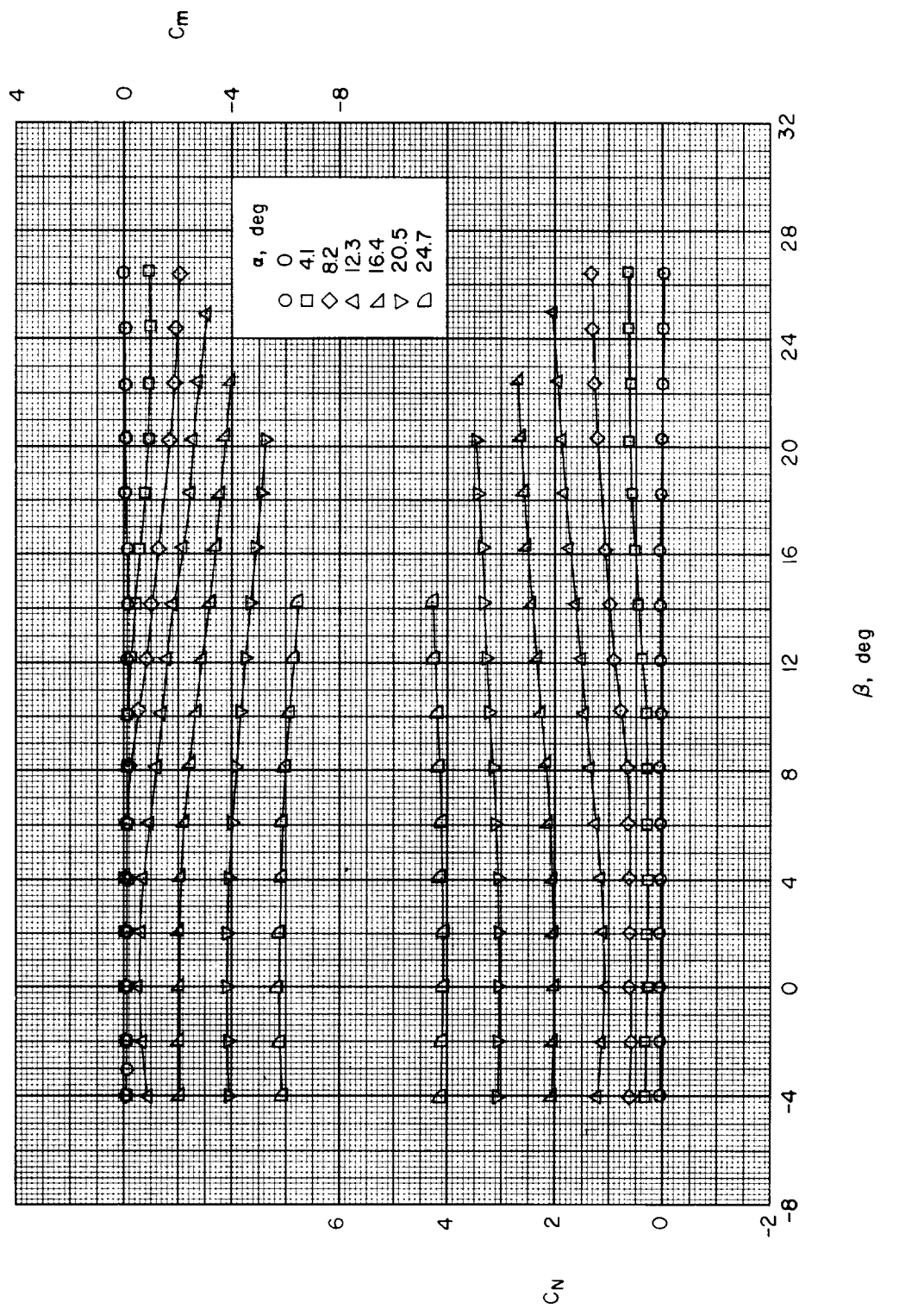
(b) Body alone, F₁WCA₇.

Figure 38.— Continued.

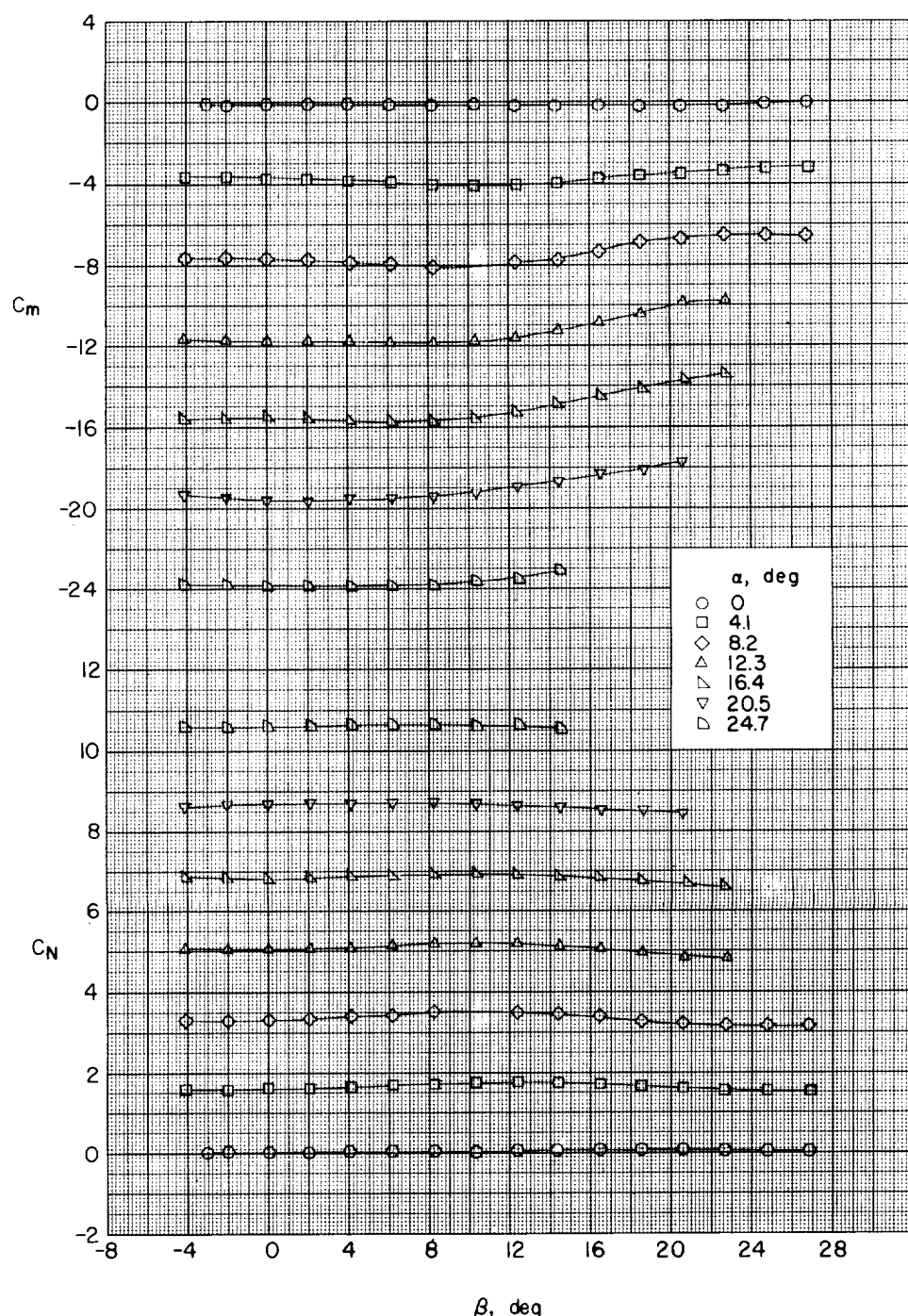
(c) Large delta wing, $F_1W_1A_4$.

Figure 38.- Continued.

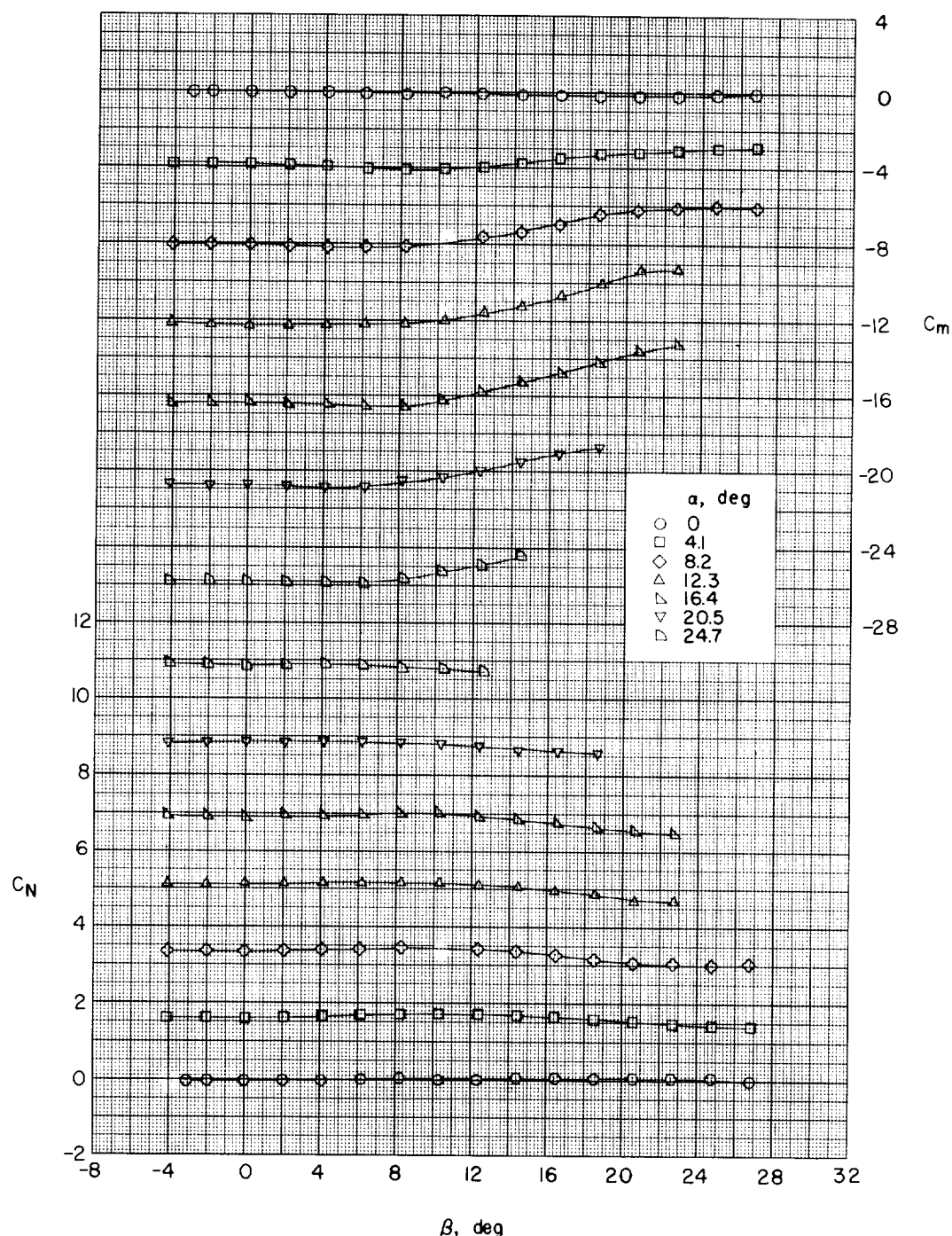
(d) Large delta wing, $F_1W_1A_7$.

Figure 38.- Concluded.

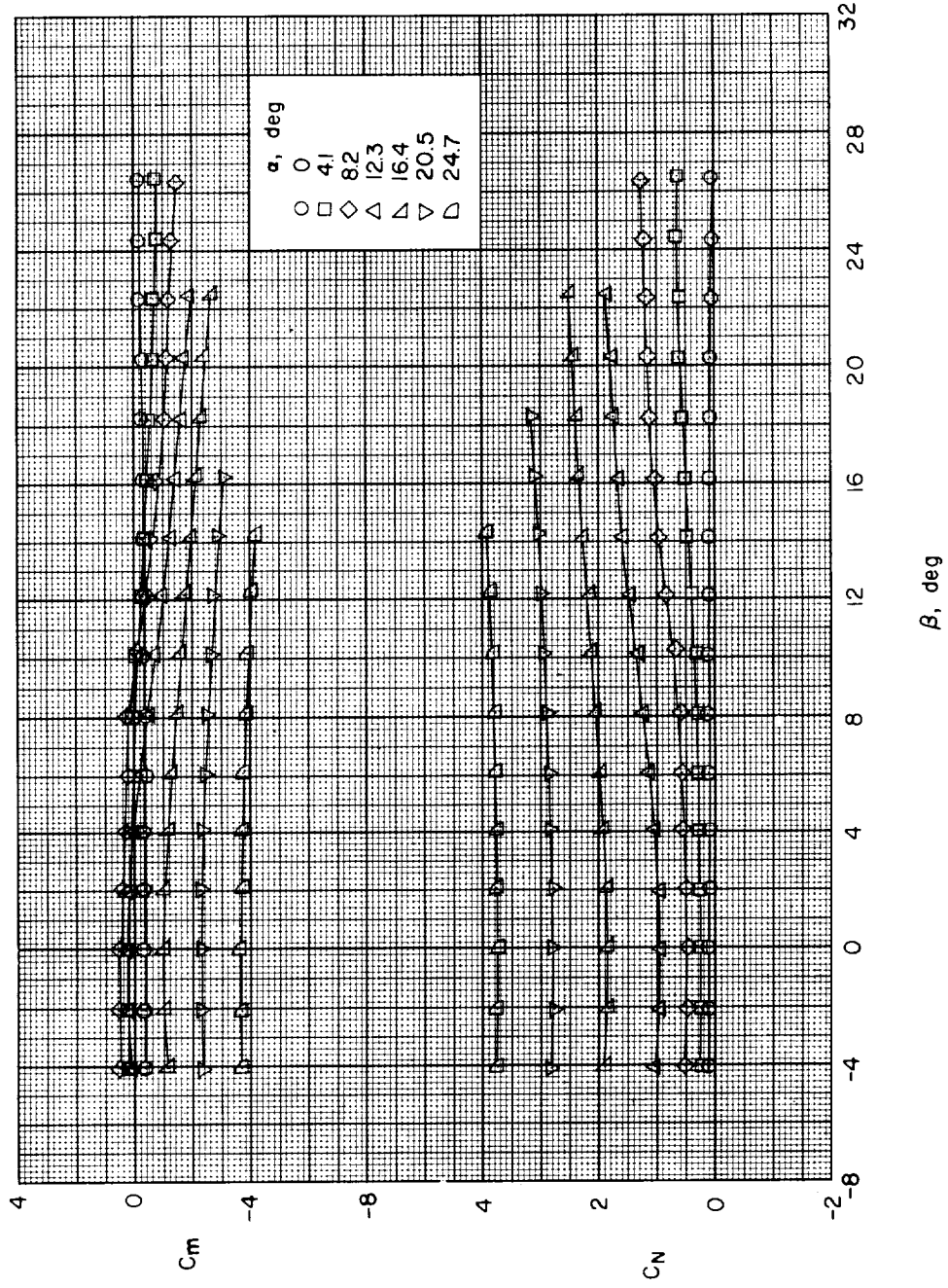
(a) Body alone, $F_{W_0 A_5}$.

Figure 39.- Variation of C_m and C_N with β for various angles of attack. Two-caliber boat-tail (A_5) and 2-caliber flare (A_8) afterbodies; large delta wings; $l/d = 10$.

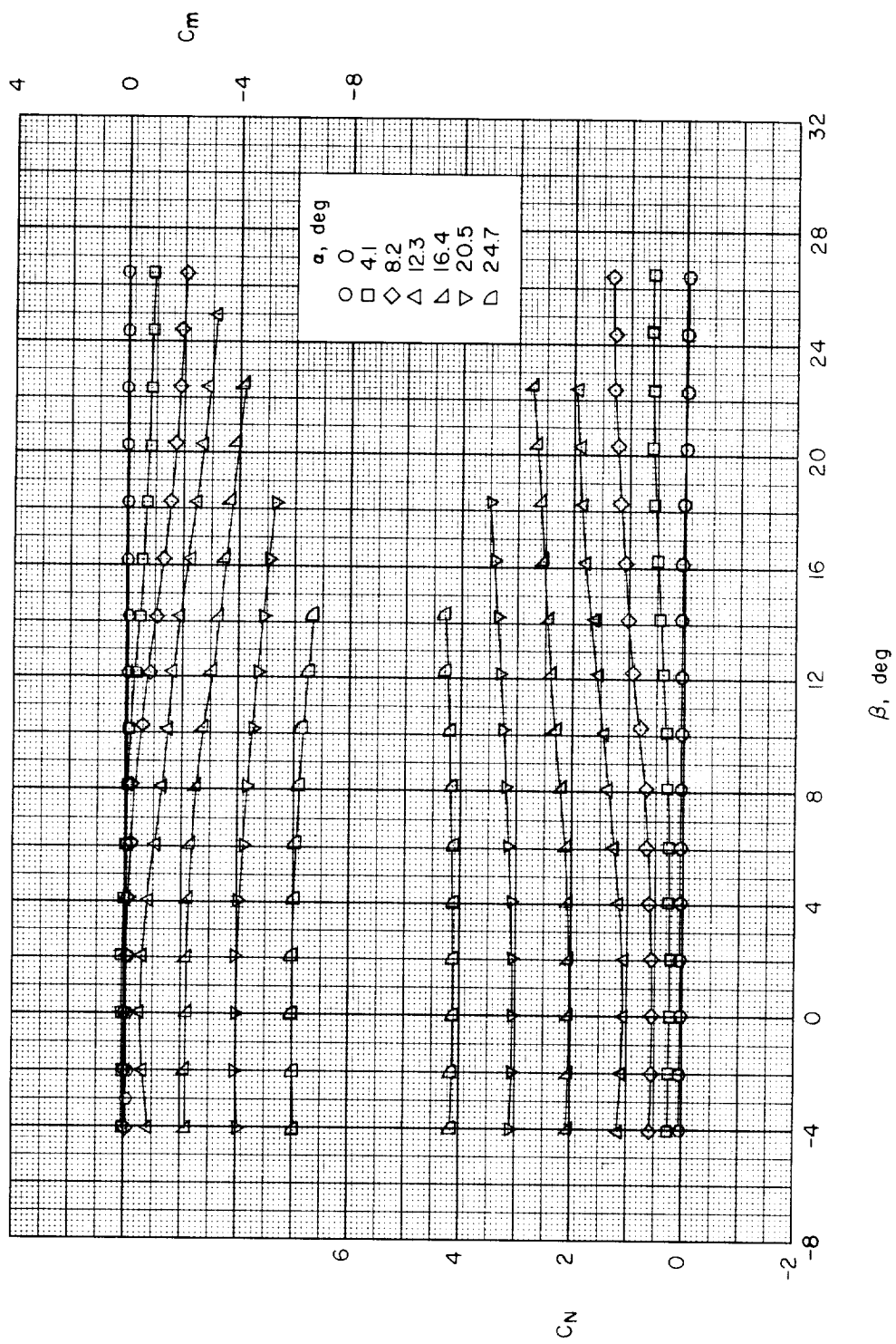
(b) Body alone, $F_1W_0A_8$.

Figure 39.- Continued.

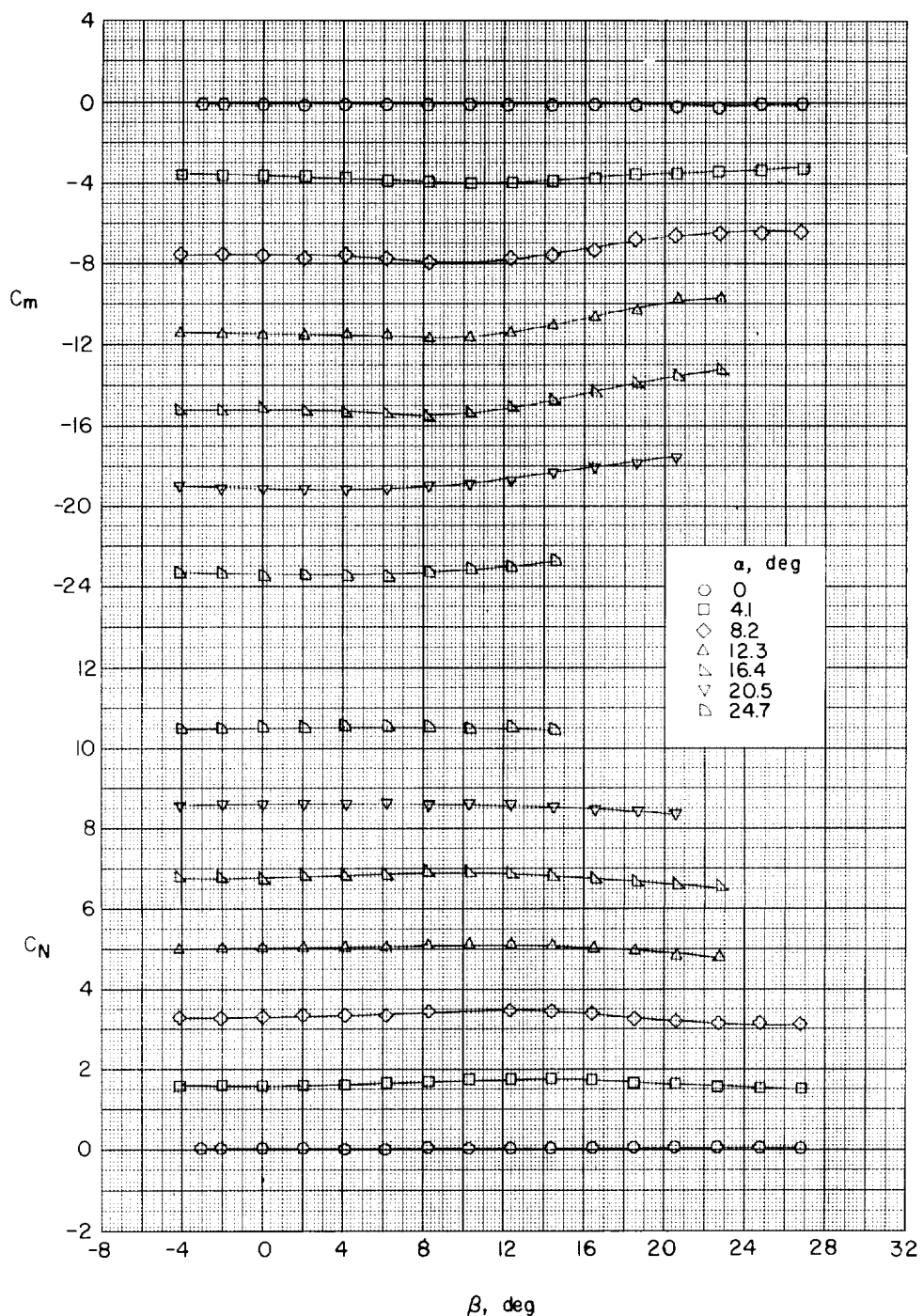
(c) Large delta wing, F₁W₁A₅.

Figure 39.- Continued.

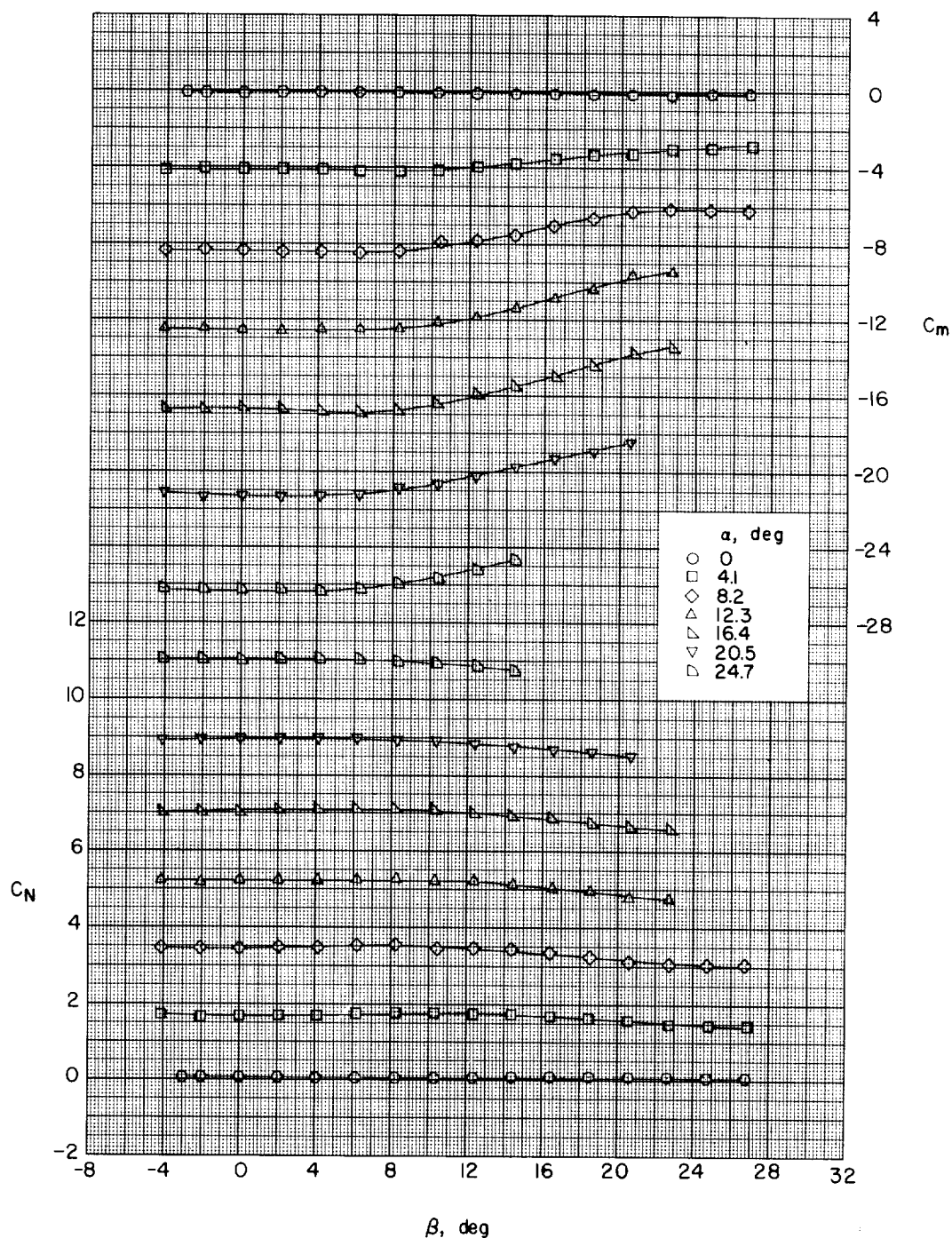
(d) Large delta wing, F₁W₁A₈.

Figure 39.- Concluded.

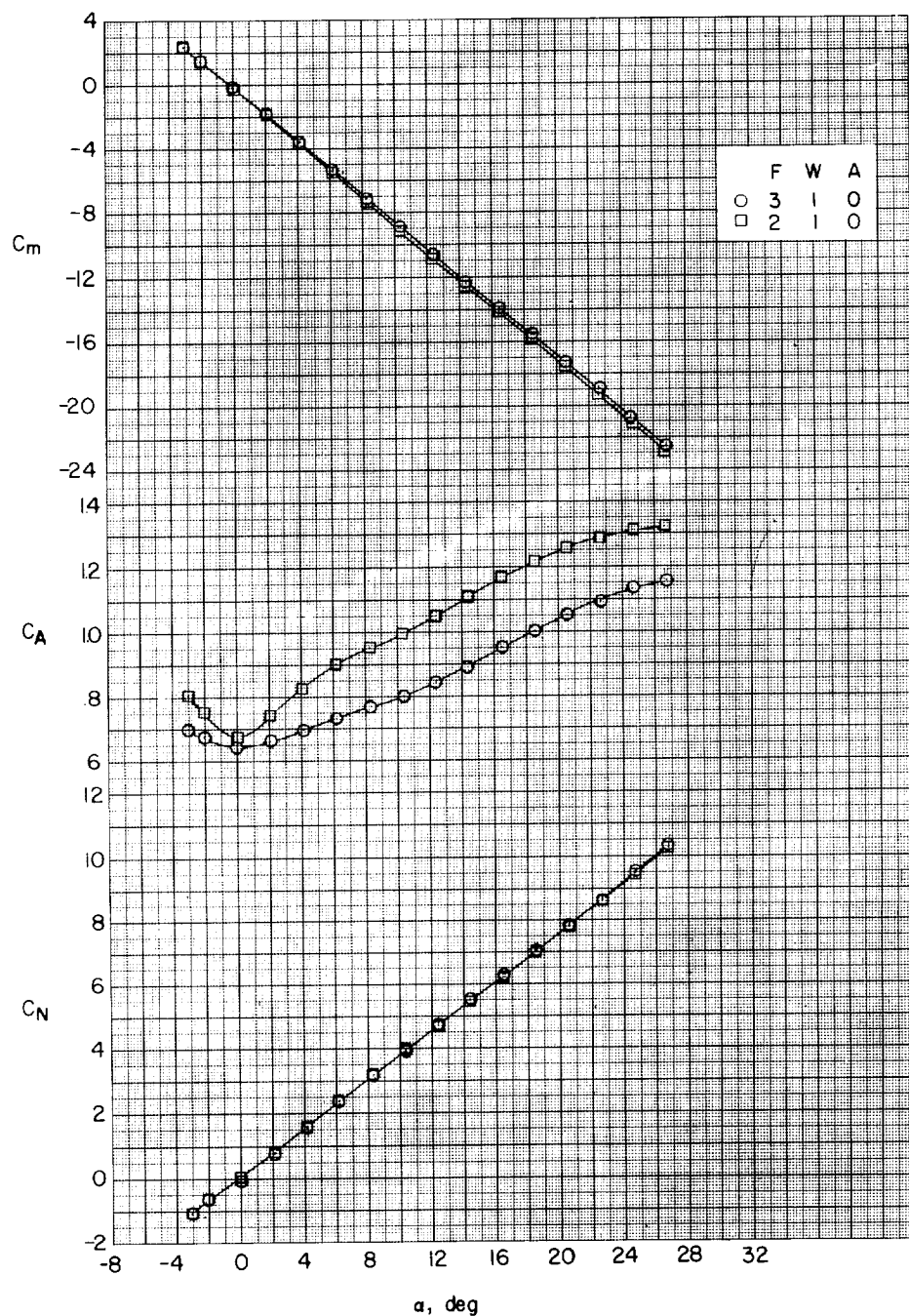


Figure 40.- Aerodynamic characteristics in pitch of tripod nose configuration with screen (F_3) and without screen (F_2). No afterbody; large delta wings.

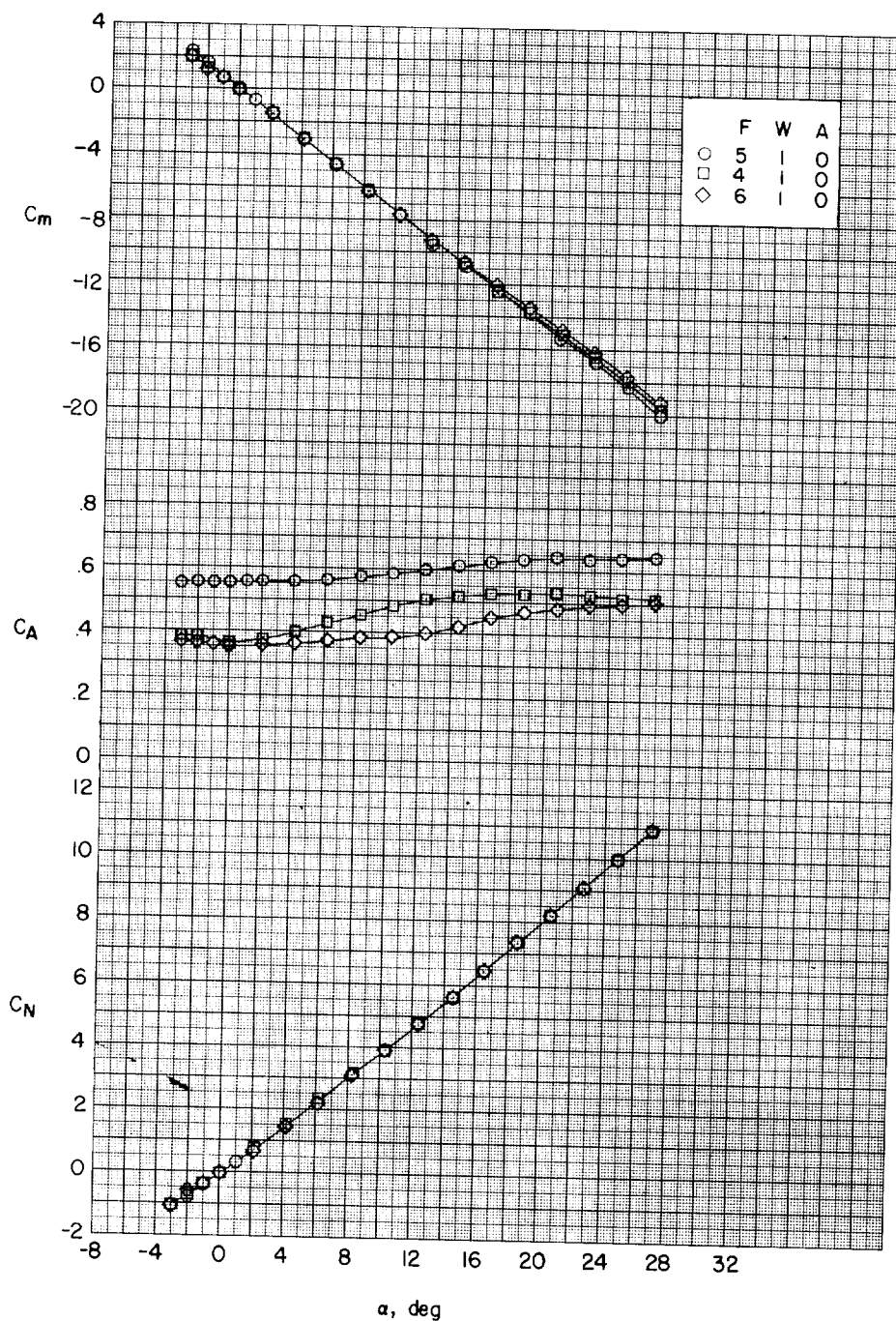


Figure 41.- Aerodynamic characteristics in pitch of rounded nose configuration (F₅) with spike (F₄) and with slotted-cone (F₆). No afterbody; large delta wings.

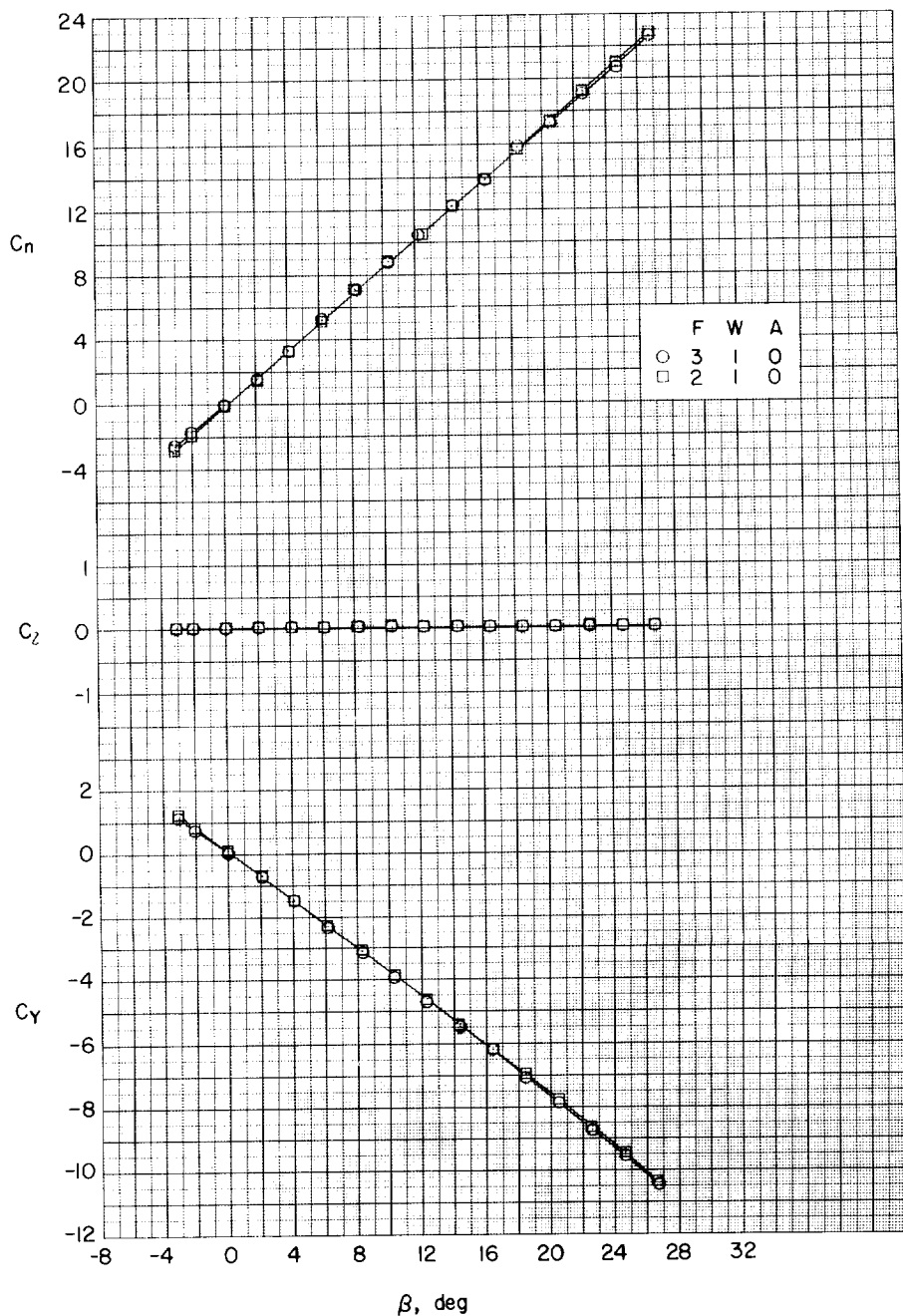
(a) $\alpha \approx 0^\circ$.

Figure 42.- Aerodynamic characteristics in sideslip of tripod nose configuration with screen (F₃) and without screen (F₂). No afterbody; large delta wings.

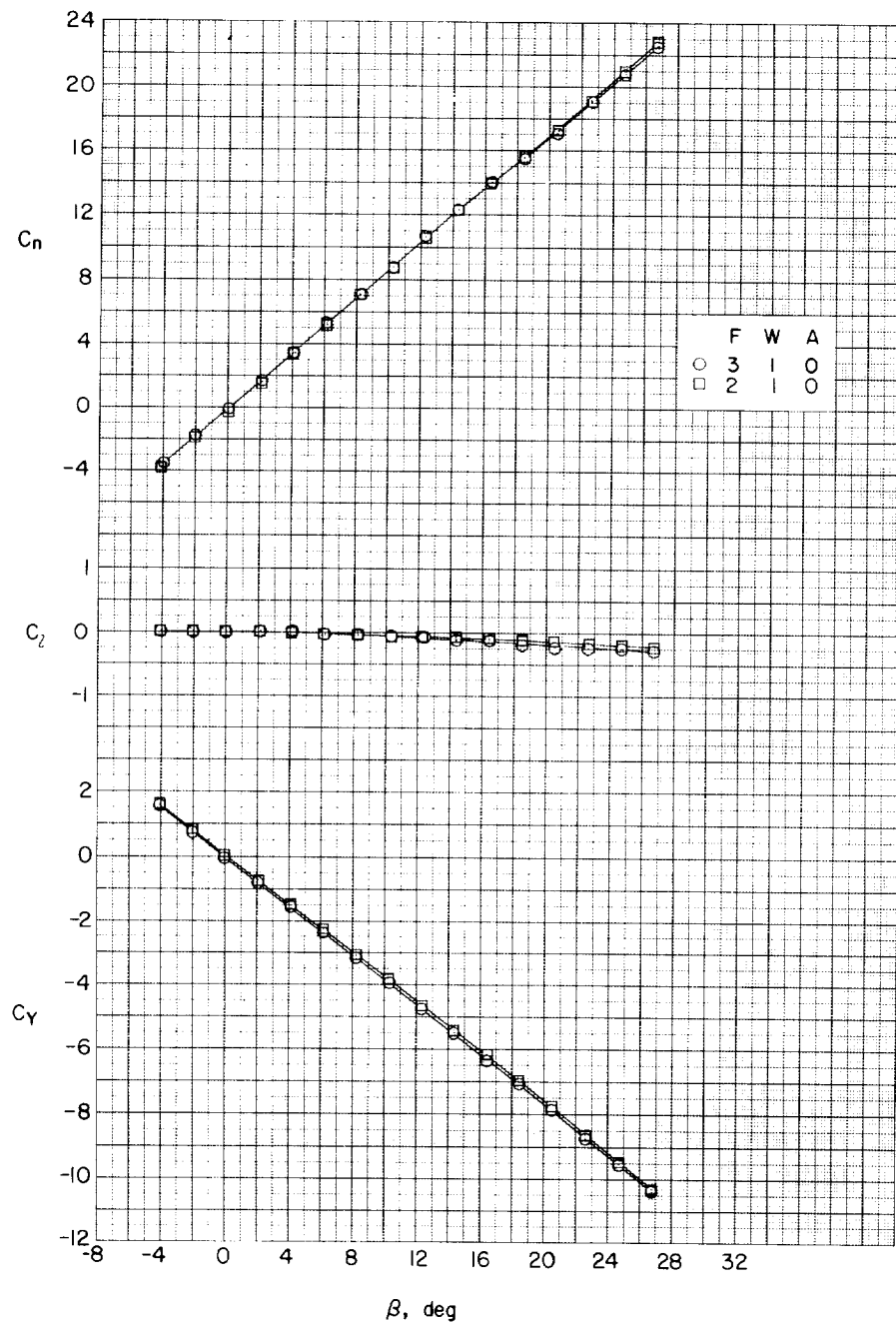
(b) $\alpha \approx 4.1^\circ$.

Figure 42.- Continued.

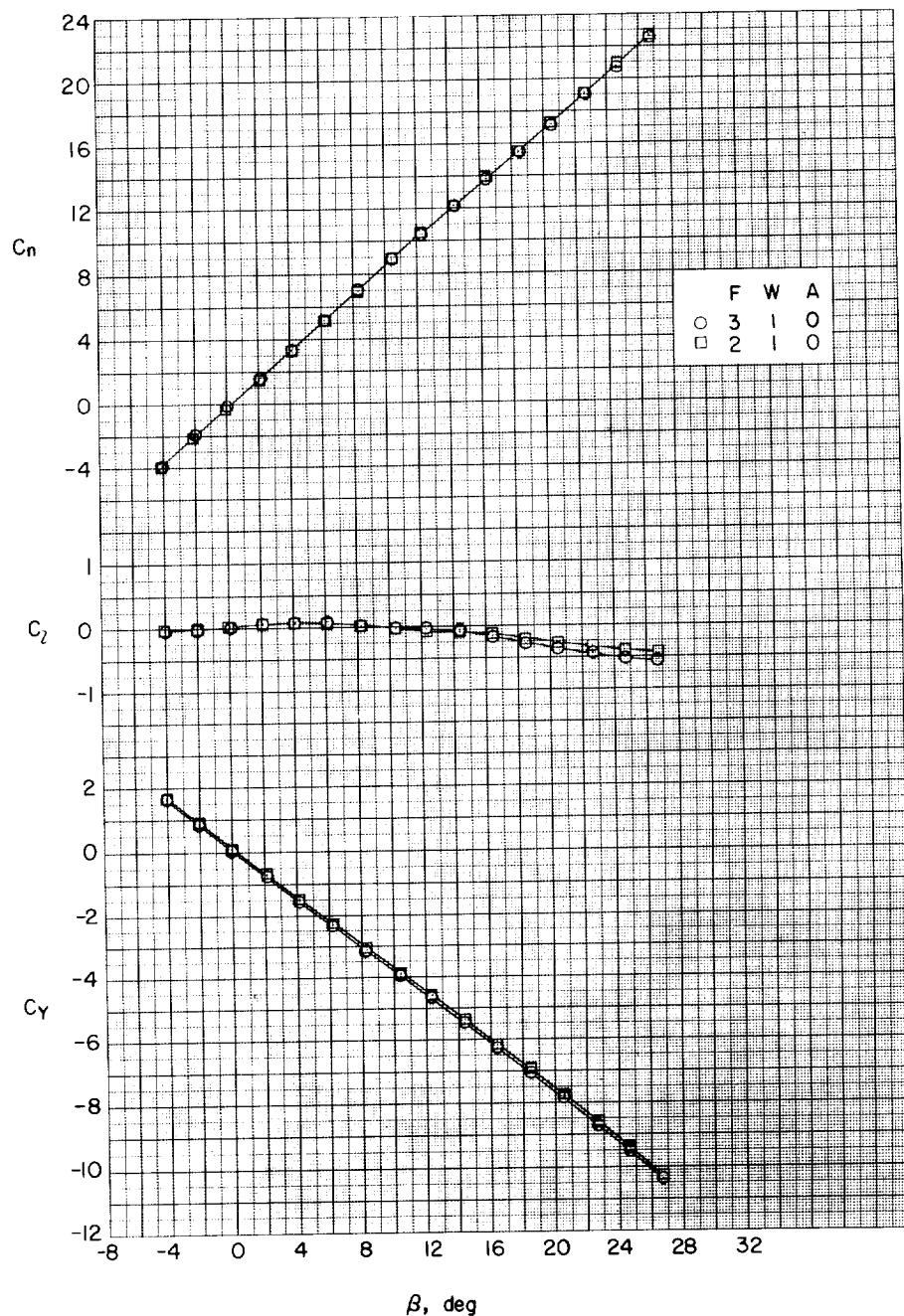
(c) $\alpha \approx 8.2^\circ$.

Figure 42.- Continued.

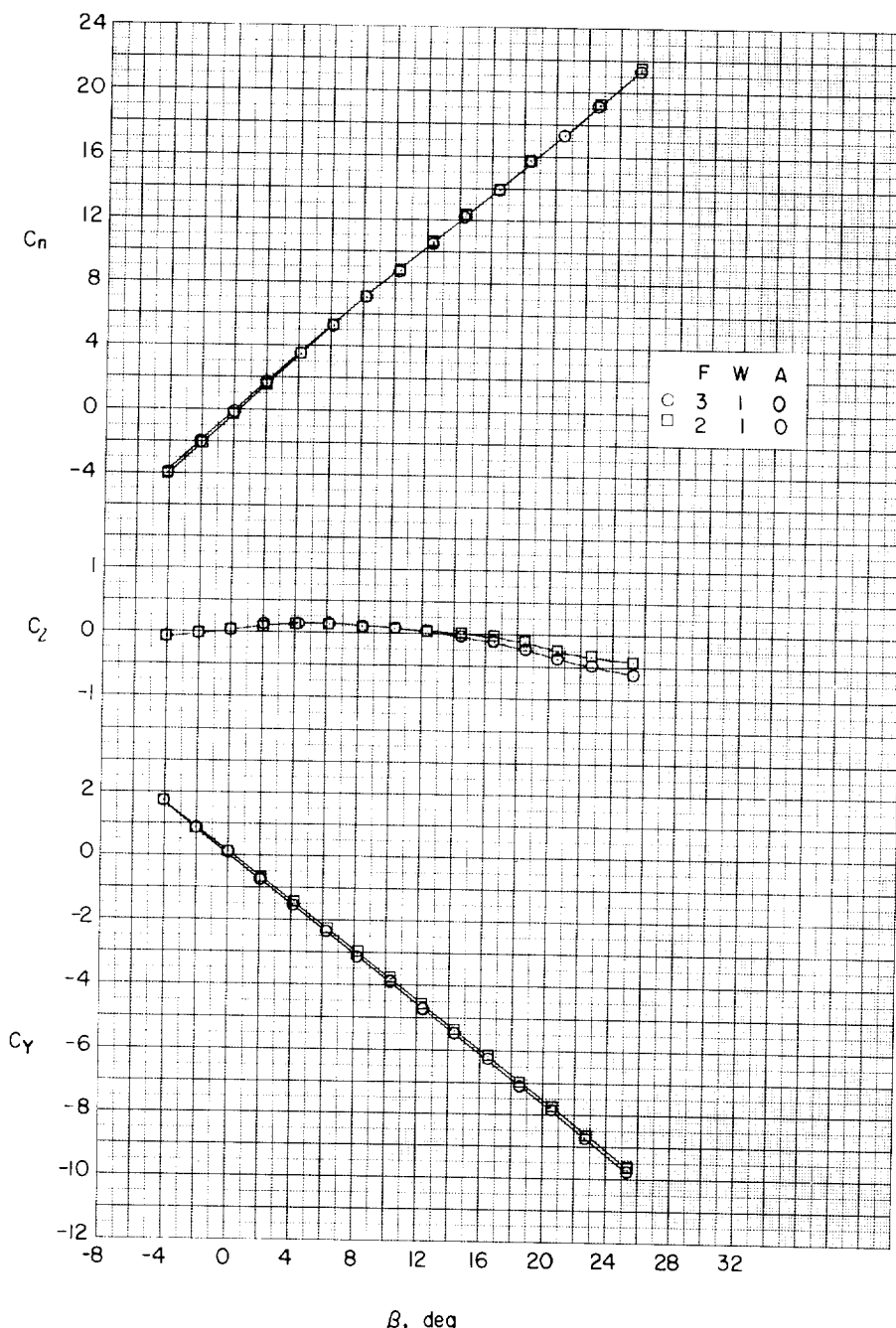
(d) $\alpha \approx 12.3^\circ$.

Figure 42.- Continued.

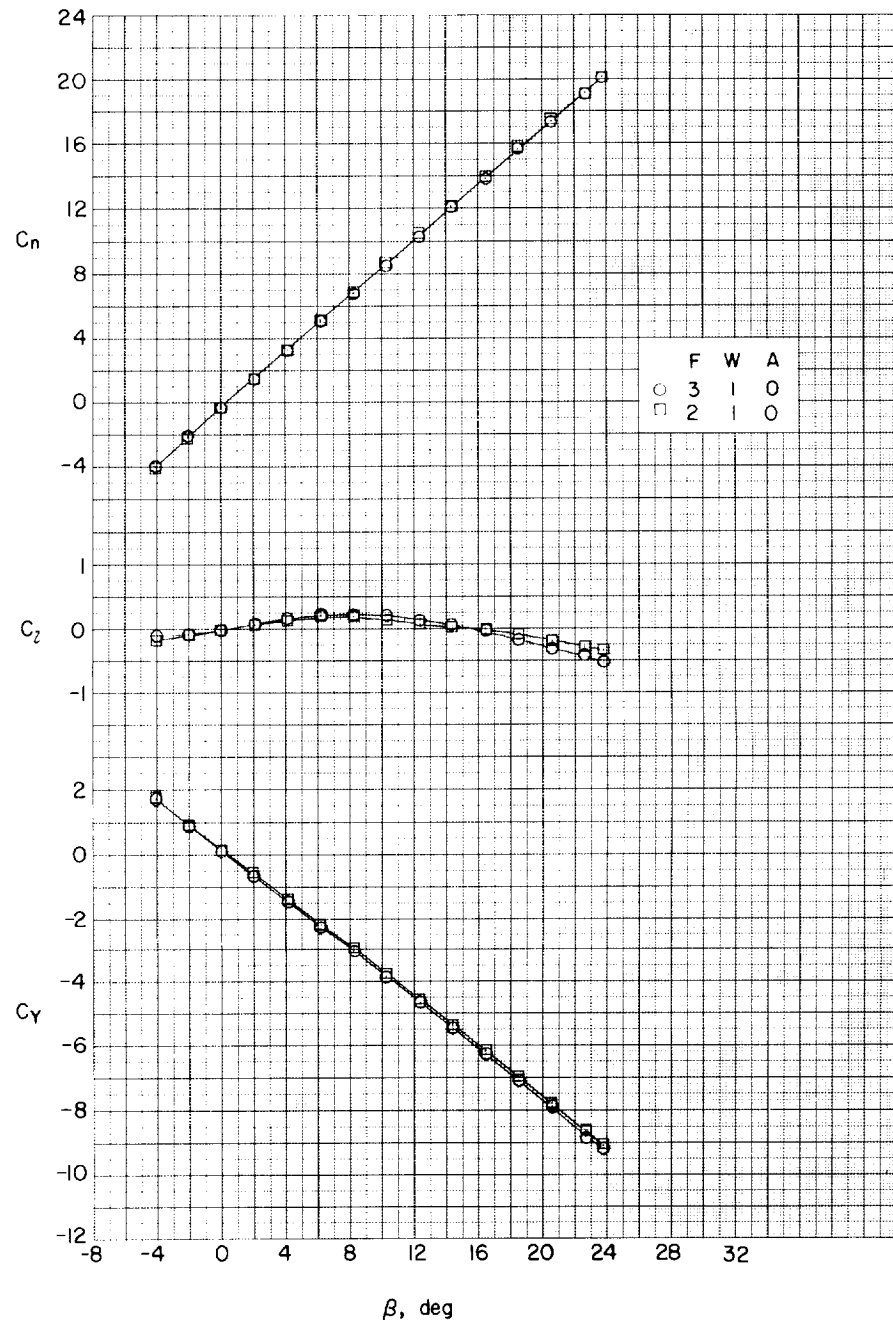
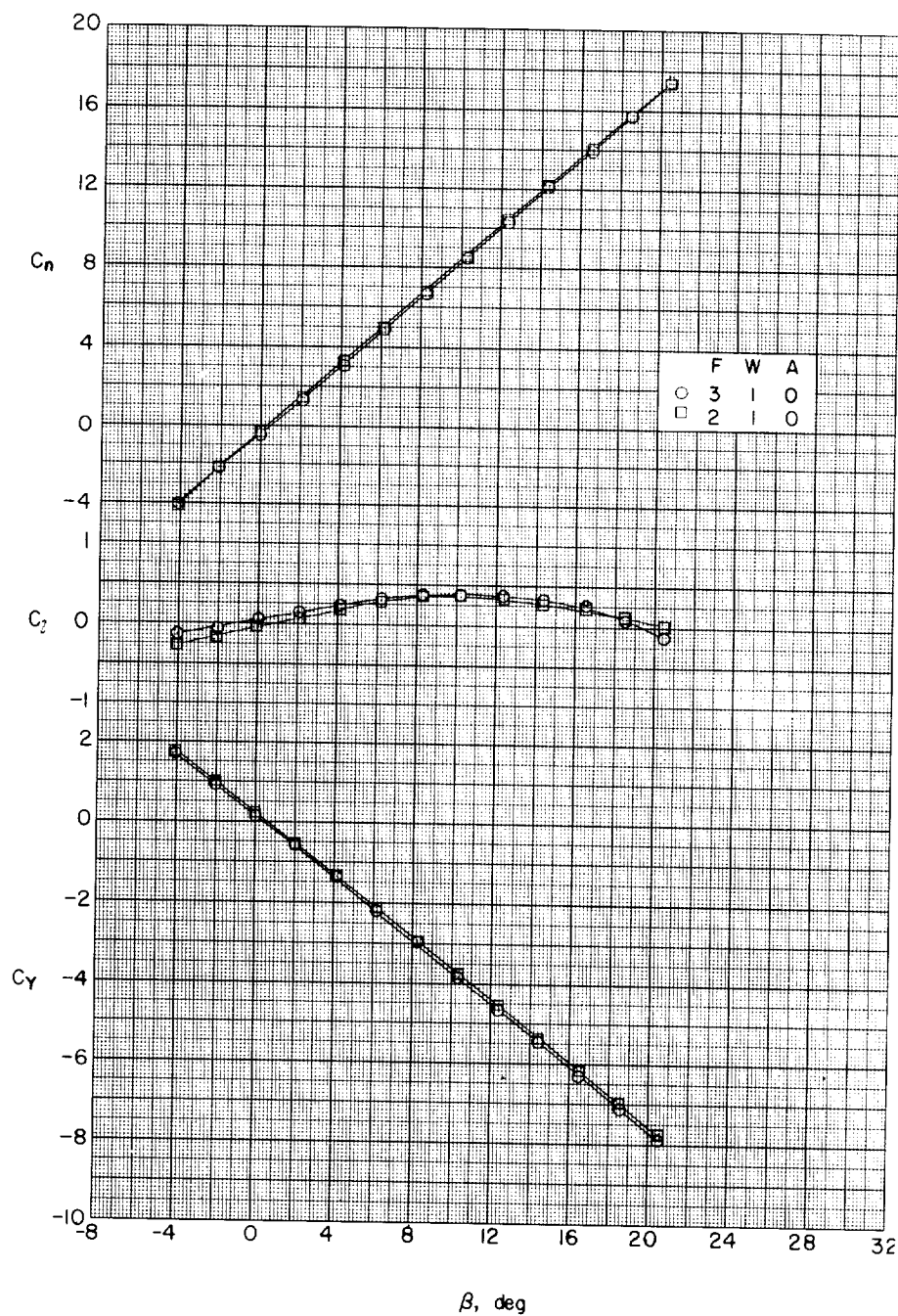
(e) $\alpha \approx 16.4^\circ$.

Figure 42.- Continued.



(f) $\alpha \approx 20.5^\circ$.

Figure 42.- Continued.

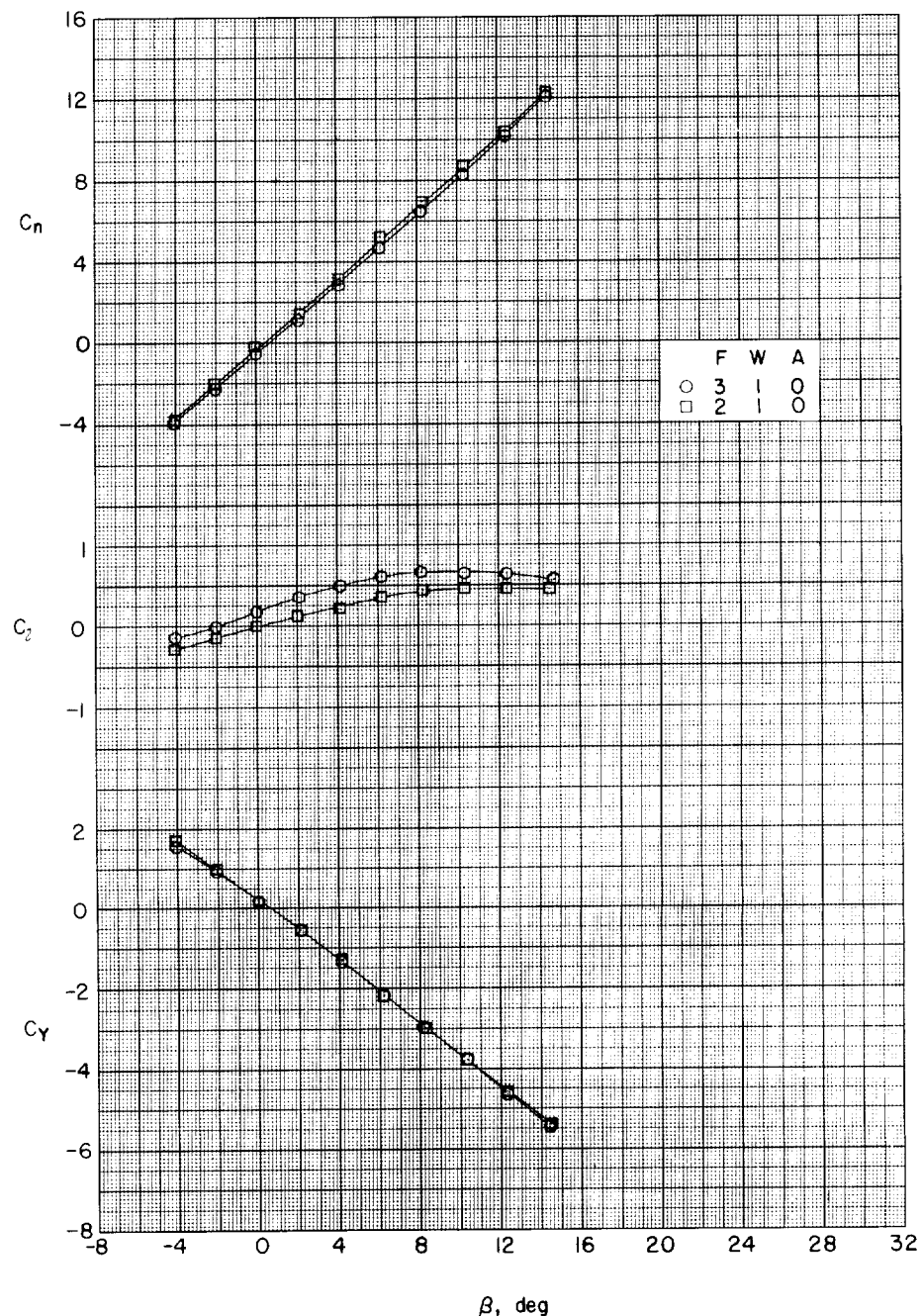
(g) $\alpha \approx 24.7^\circ$.

Figure 42.- Concluded.

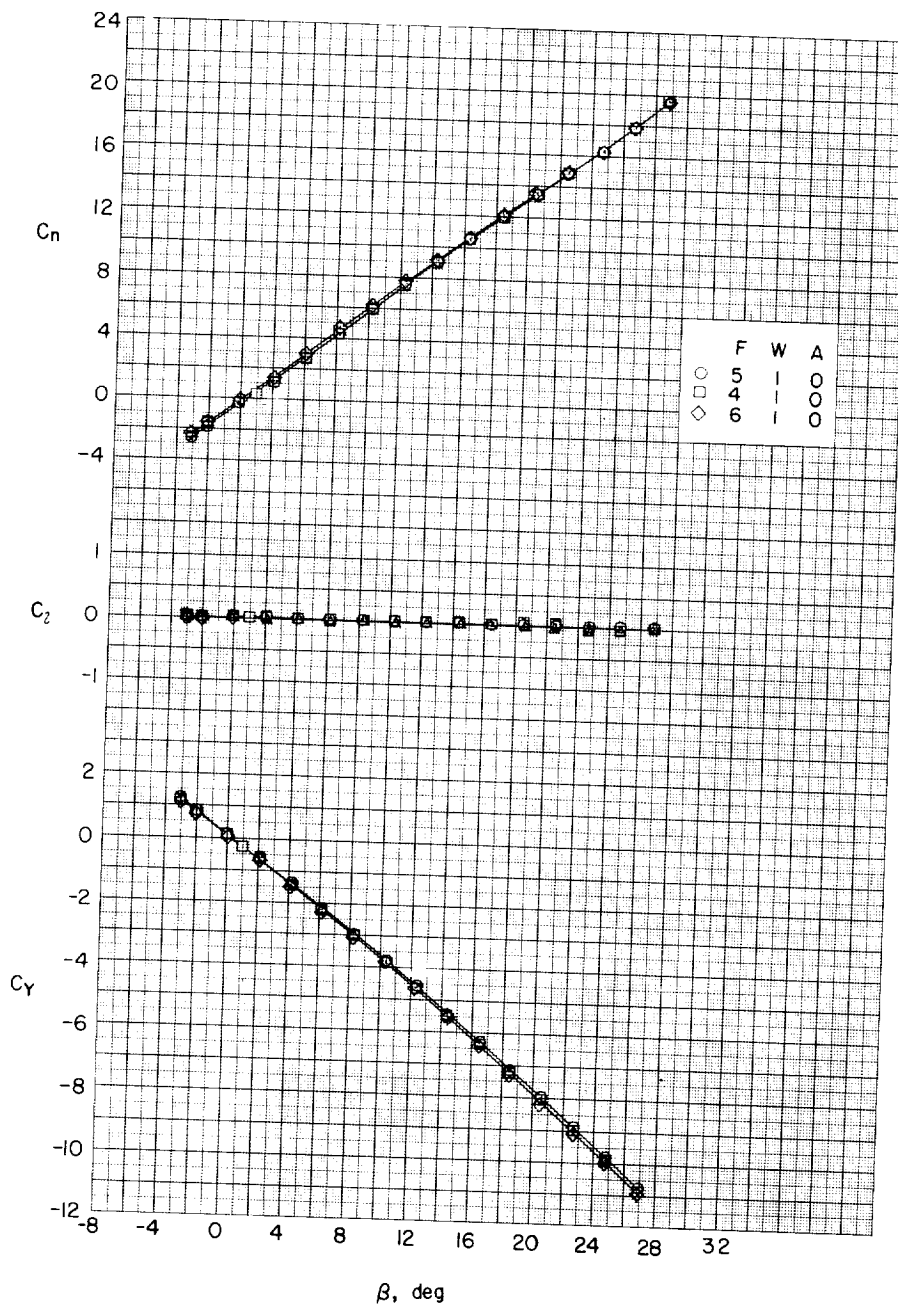
(a) $\alpha \approx 0^\circ$.

Figure 43.- Aerodynamic characteristics in sideslip of rounded-nose configuration (F₅) with spike (F₄) and with slotted cone (F₆). No afterbody; large delta wings.

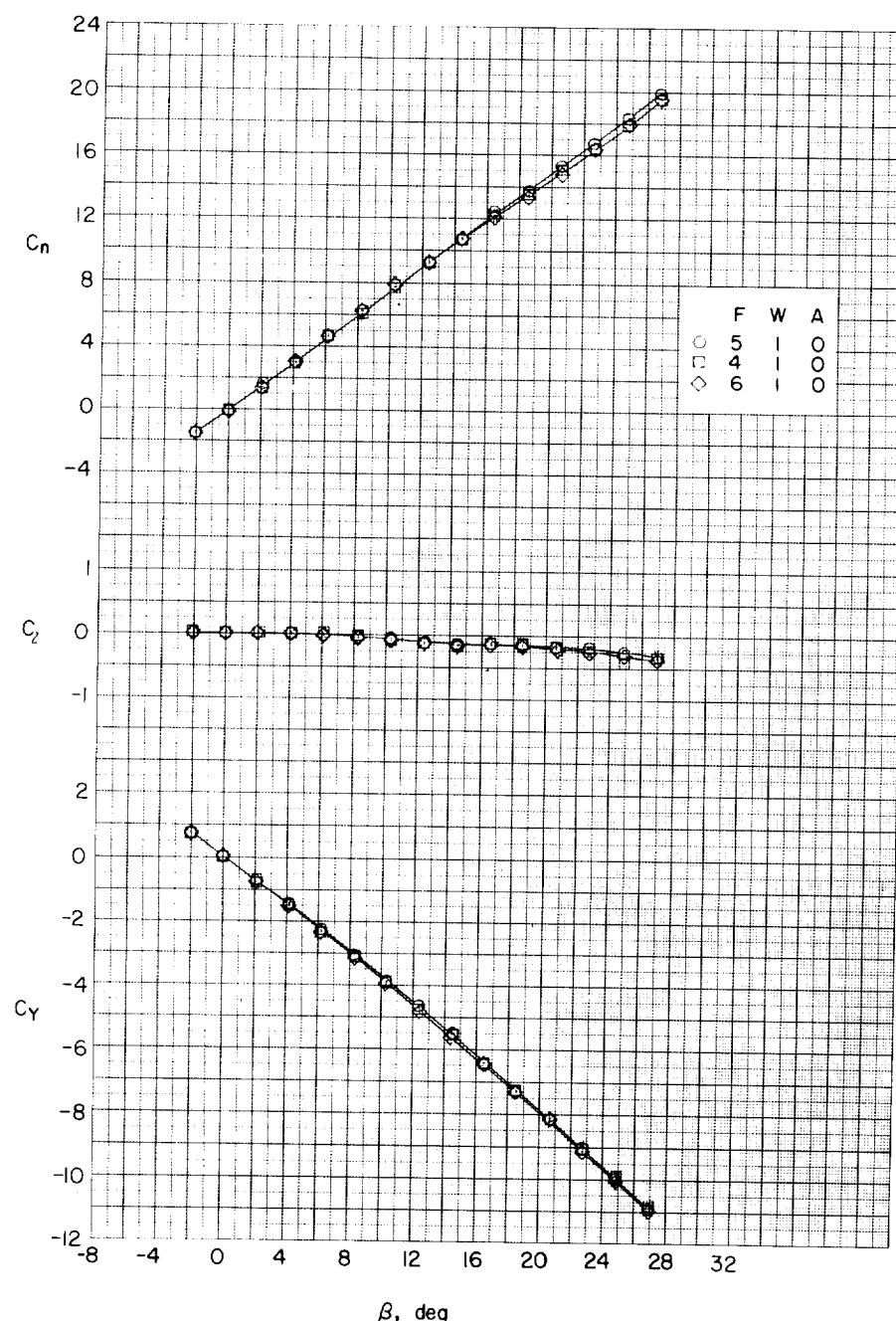
(b) $\alpha \approx 4.1^\circ$.

Figure 43.- Continued.

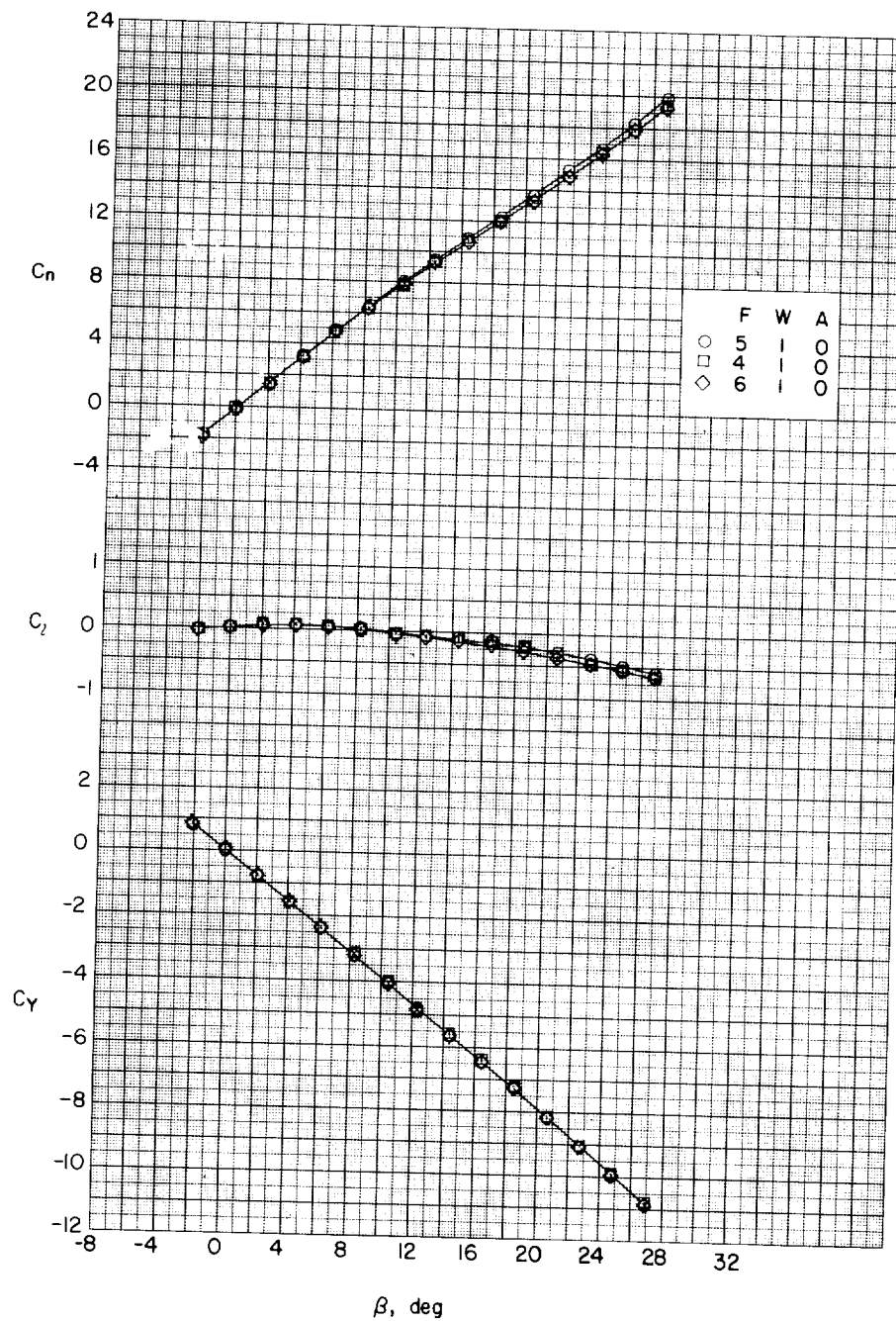
(c) $\alpha \approx 8.2^\circ$.

Figure 43.- Continued.

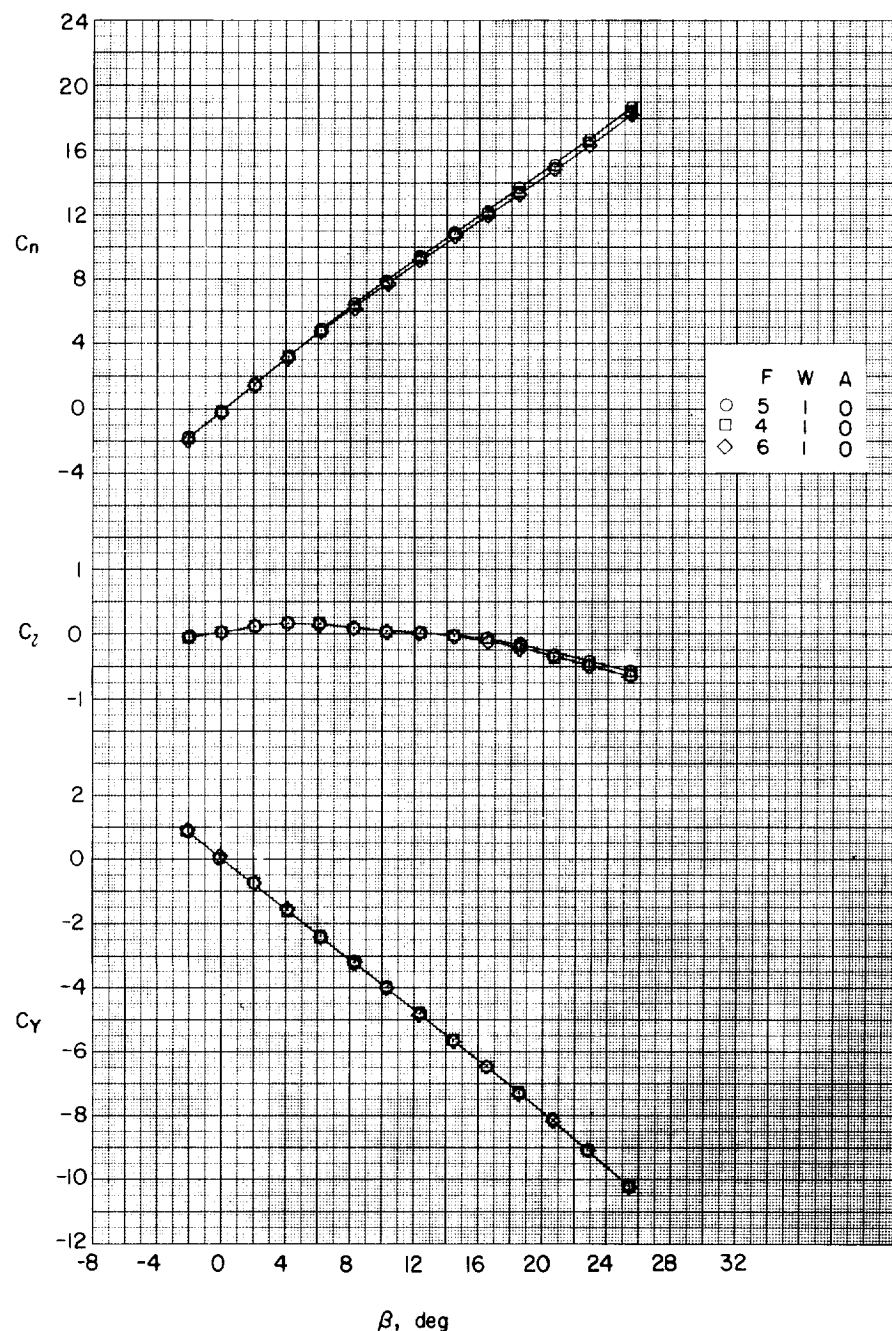
(d) $\alpha \approx 12.3^\circ$.

Figure 43.- Continued.

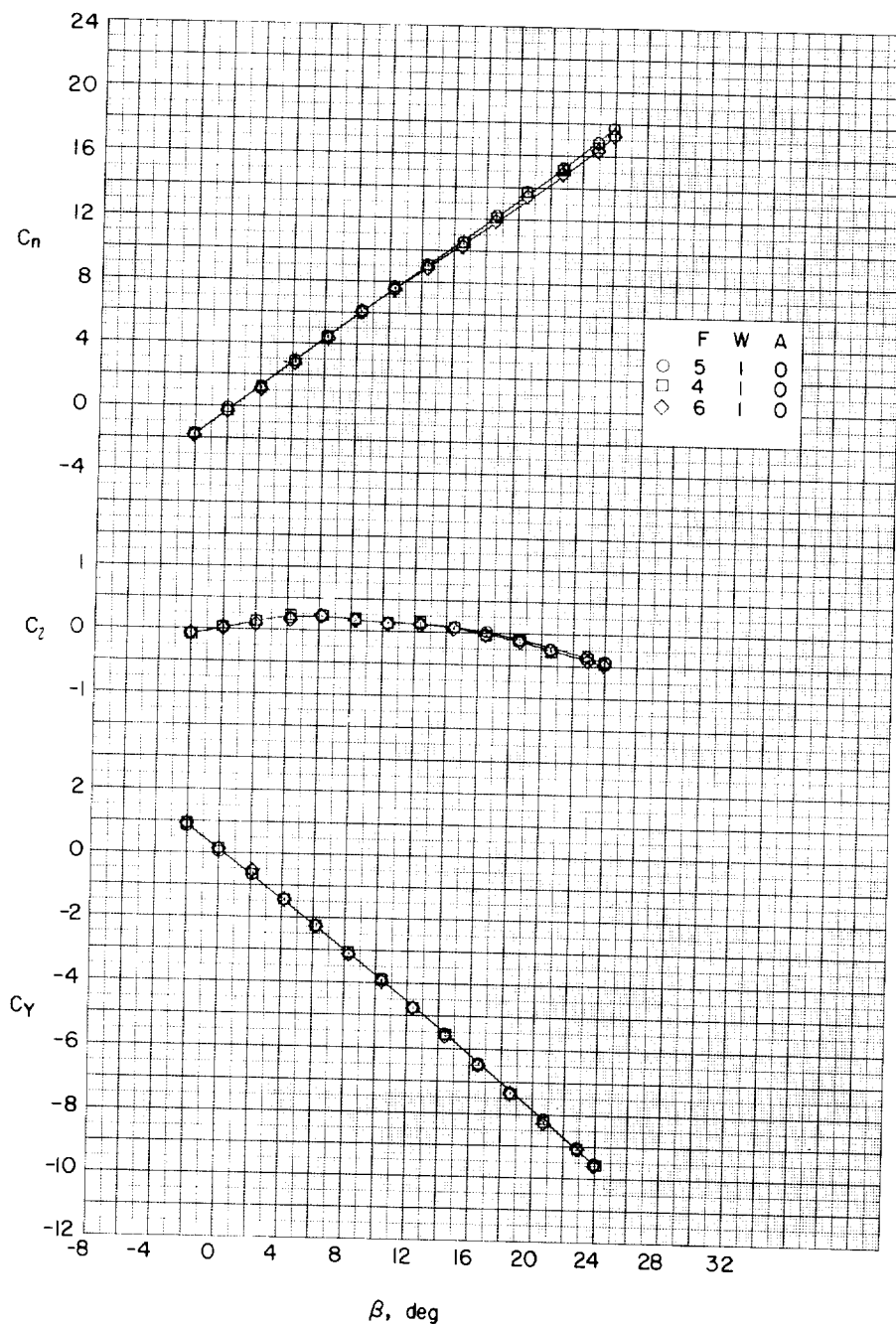
(e) $\alpha \approx 16.4^\circ$.

Figure 43.- Continued.

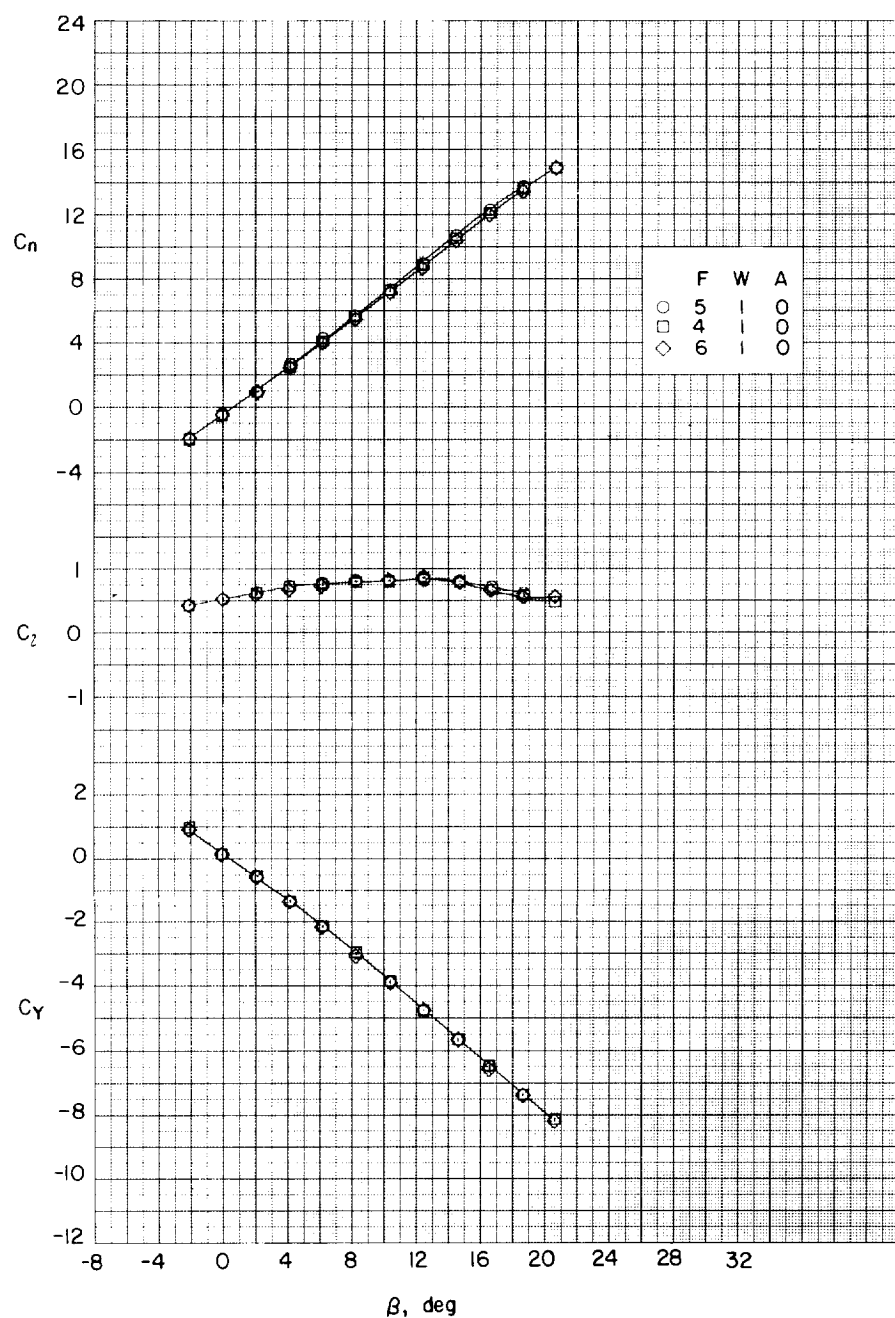
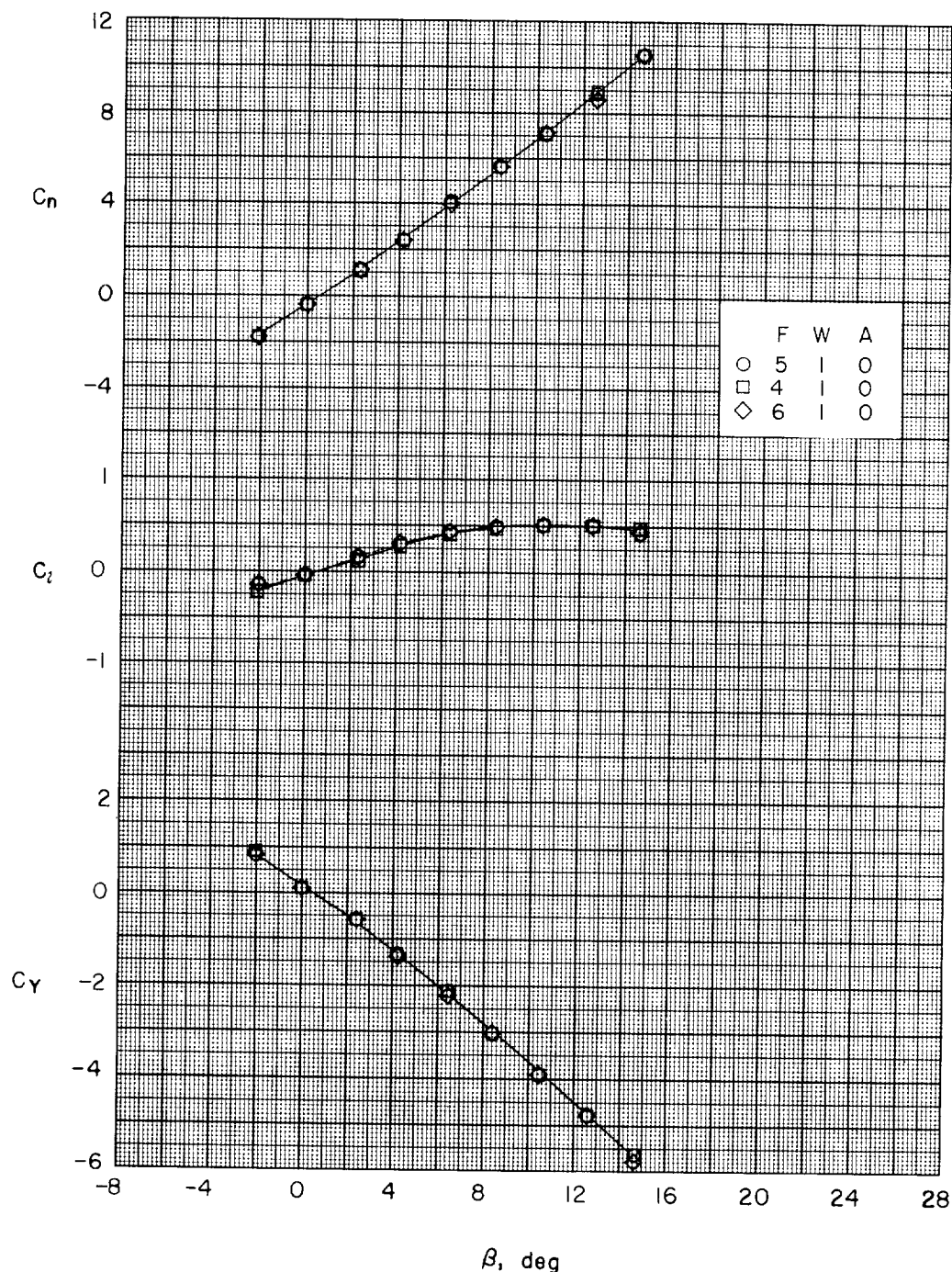
(f) $\alpha \approx 20.5^\circ$.

Figure 43.- Continued.



(g) $\alpha \approx 24.7^\circ$.

Figure 43.- Concluded.

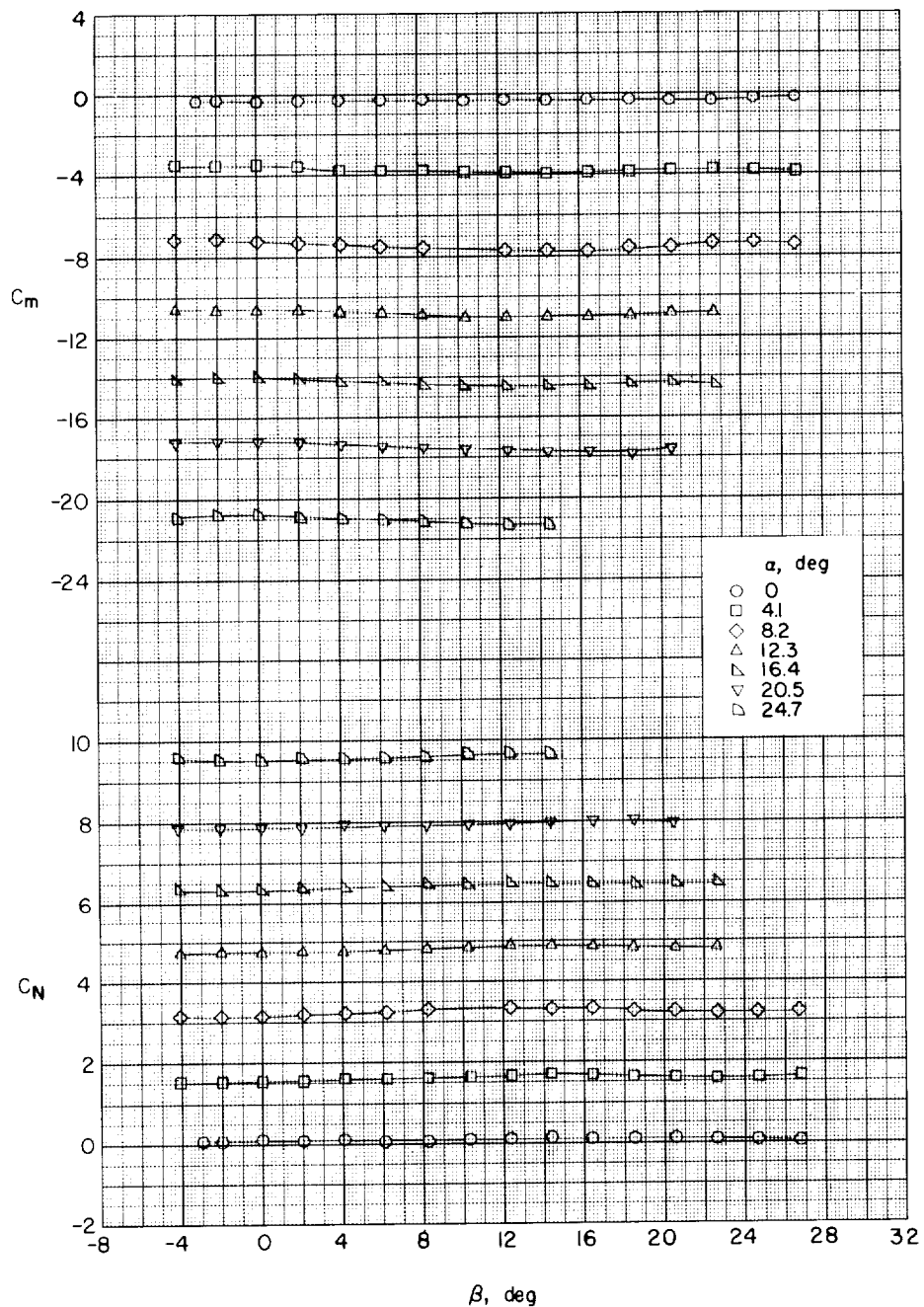
(a) Screen on, $F_3W_1A_0$.

Figure 44.- Variation of C_m and C_N with β for various angles of attack. Tripod-nose configurations; no afterbodies; large delta wings.

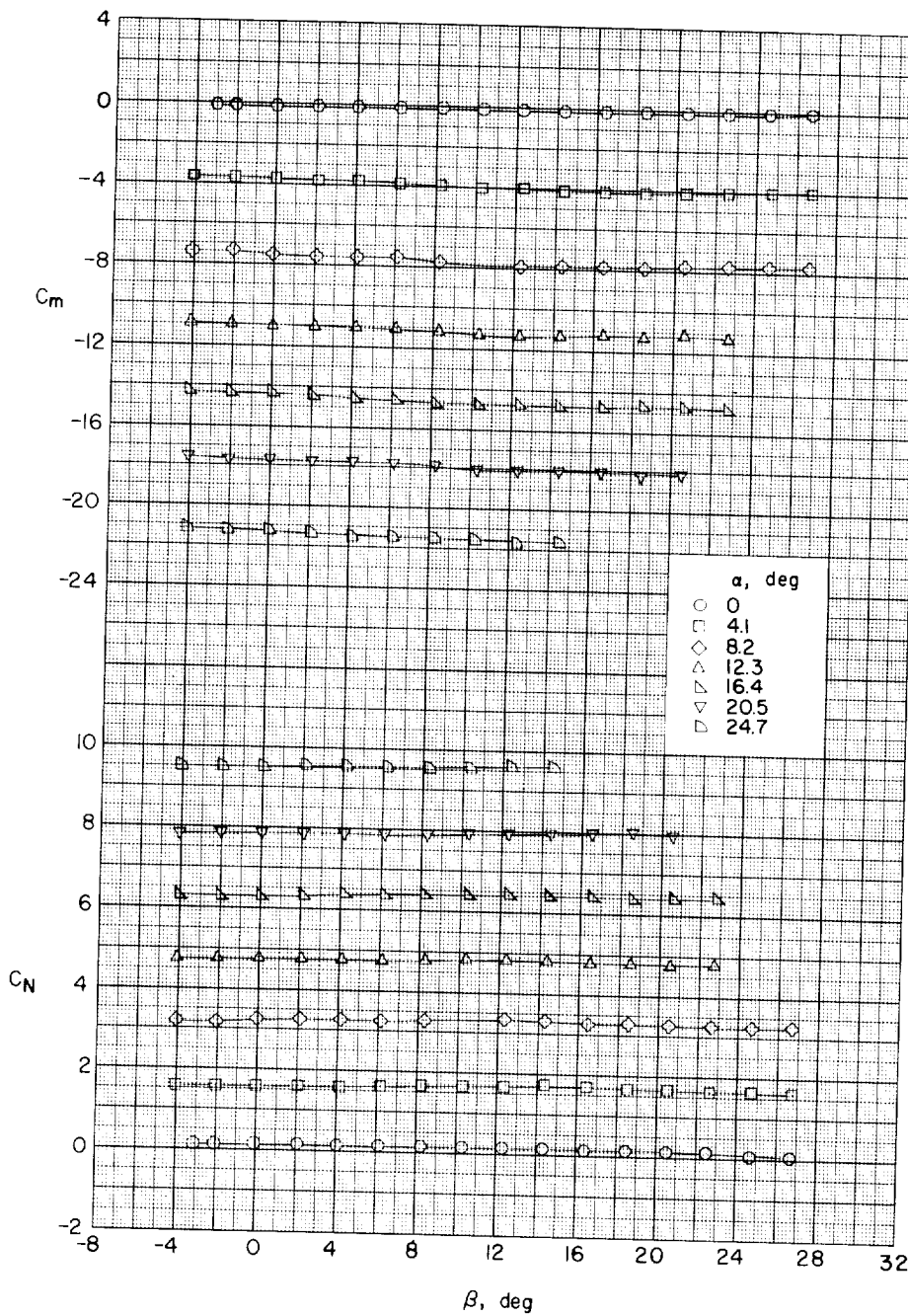
(b) Screen off, $F_2 W_1 A_0$.

Figure 44.- Concluded.

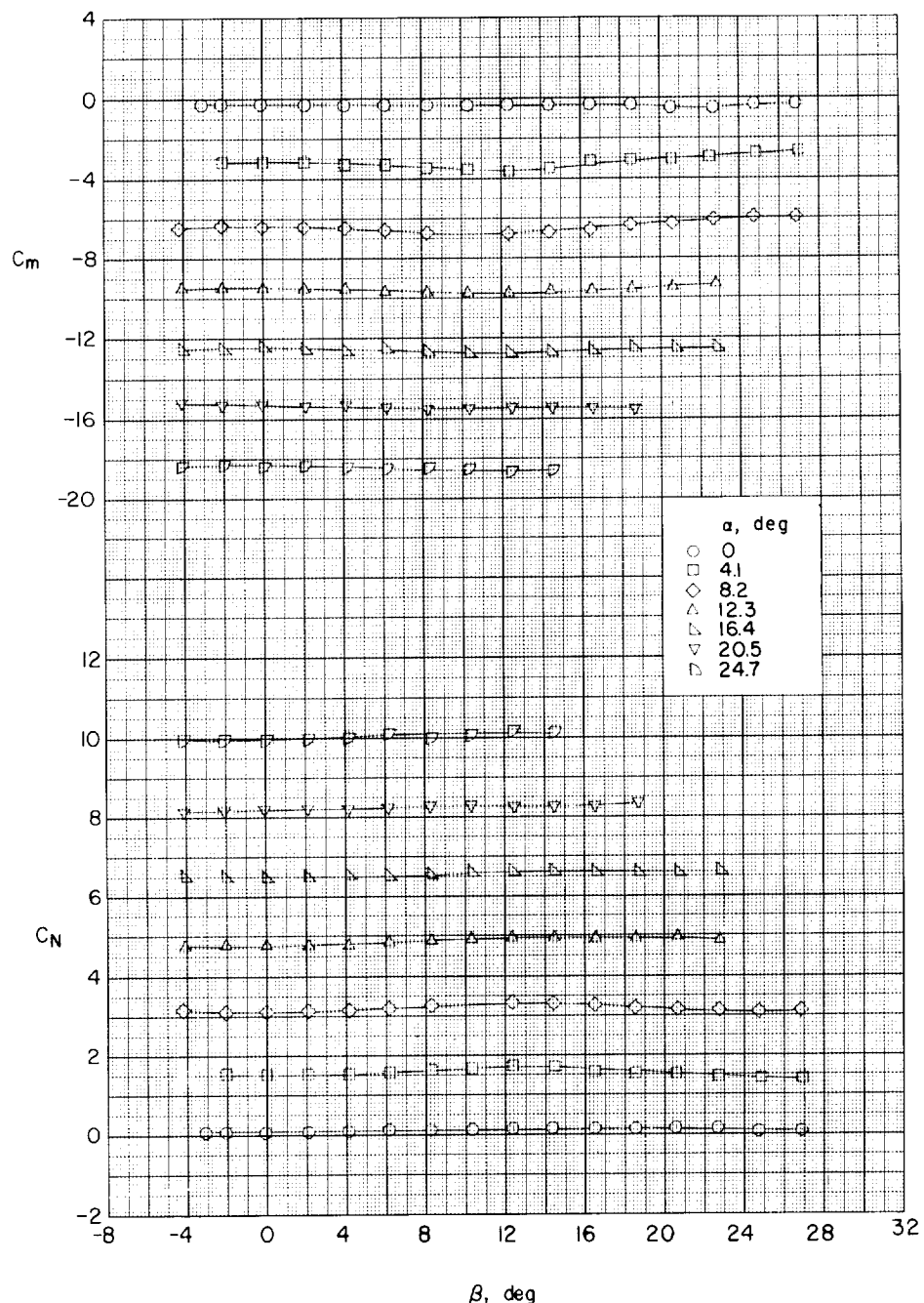
(a) Rounded-ogive nose, F₅W₁A₀.

Figure 45.- Variation of C_m and C_N with β for various angles of attack. Rounded-ogive nose; no afterbody; large delta wings.

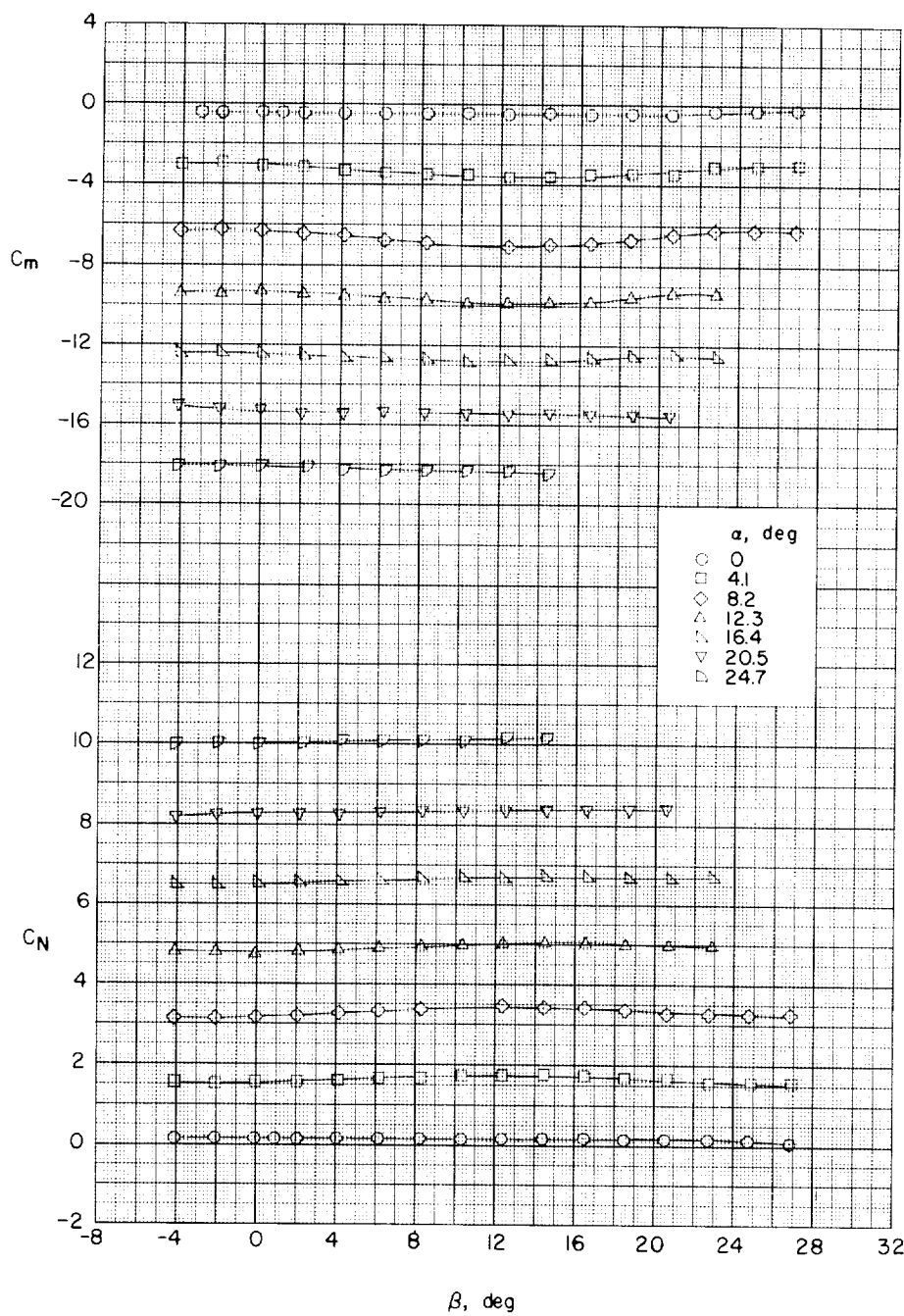
(b) Rounded-ogive nose with spike, $F_4W_1A_0$.

Figure 45.- Continued.

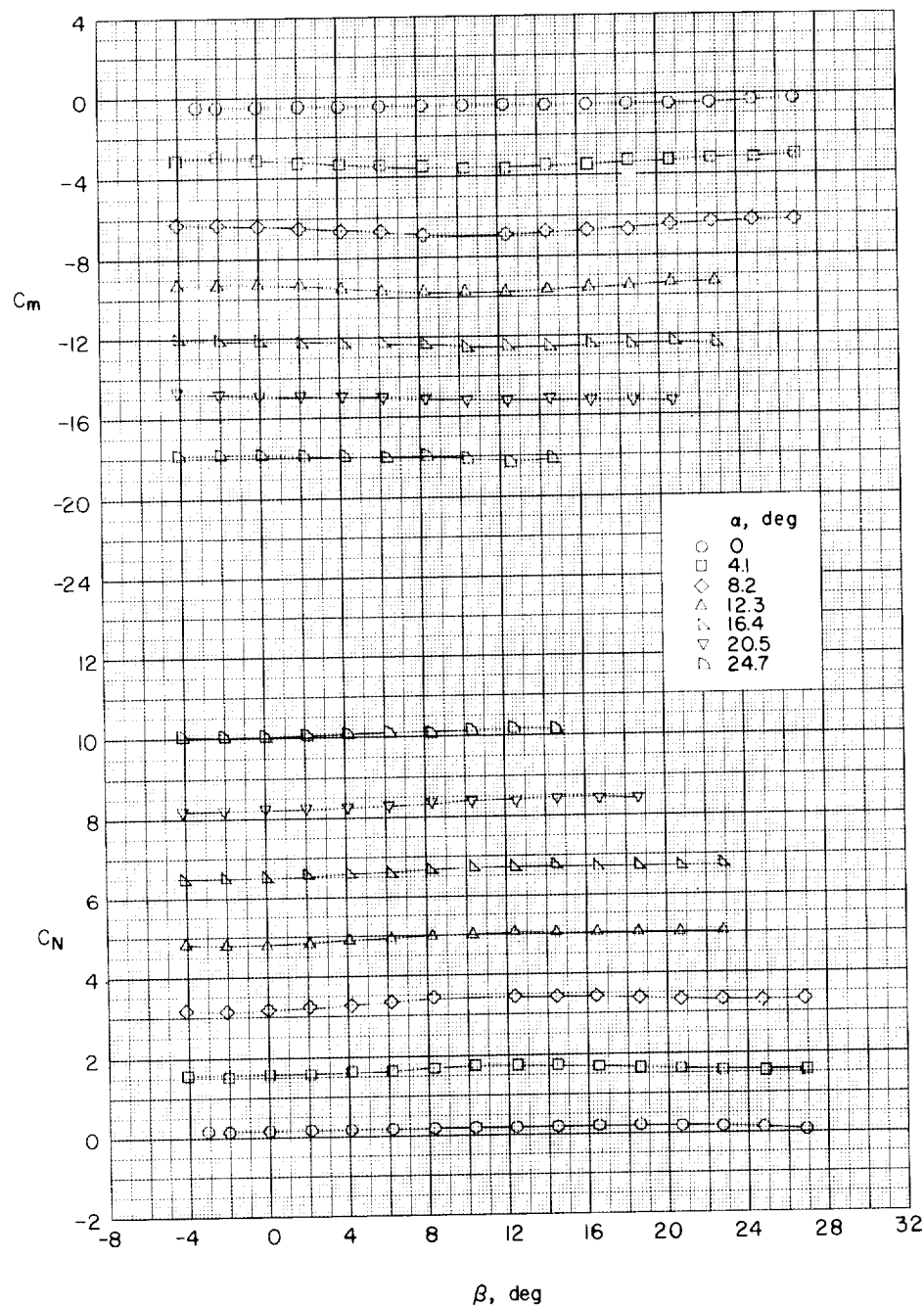
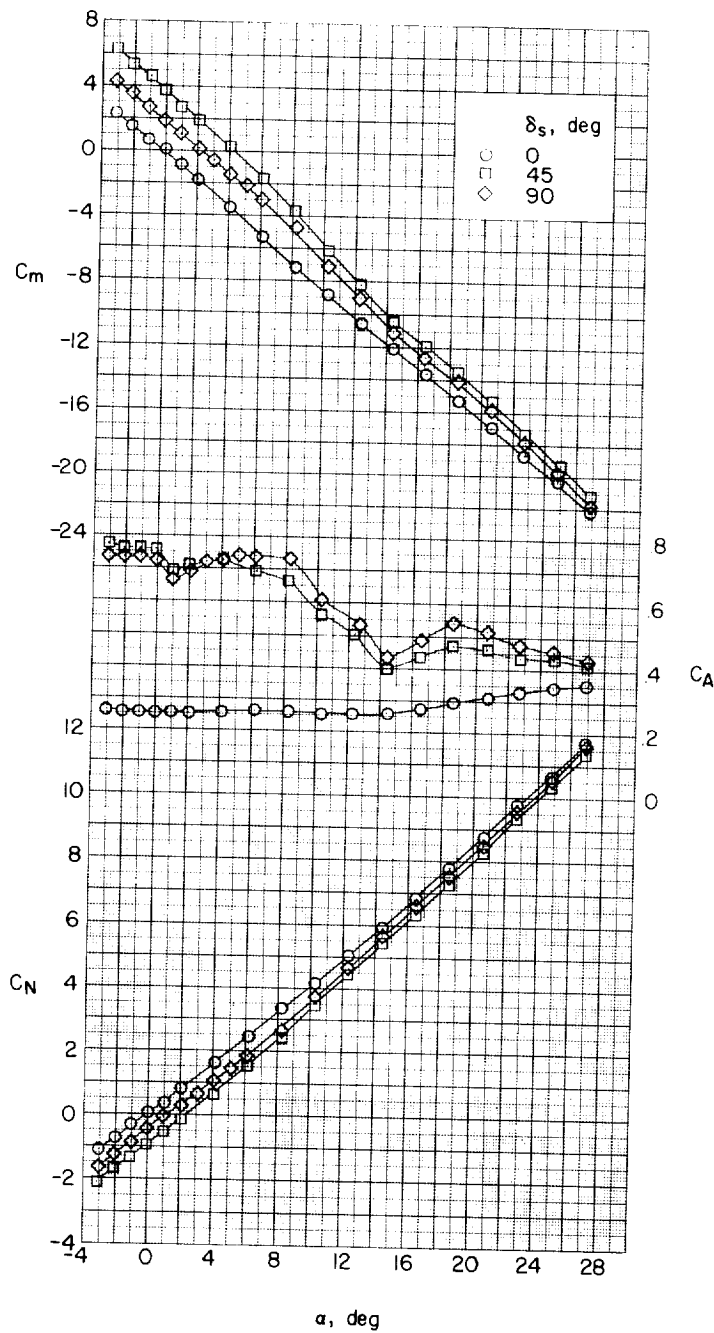
(c) Rounded-ogive nose with slotted cone, $F_6W_1A_0$.

Figure 45.- Concluded.



(a) The variation of C_m , C_A , and C_N with α . $\beta = 0^\circ$.

Figure 16.- Effects of spoiler deflection on aerodynamic characteristics ($F_7W_1A_1$). One-caliber afterbody; large delta wings; $l/d = 10$.

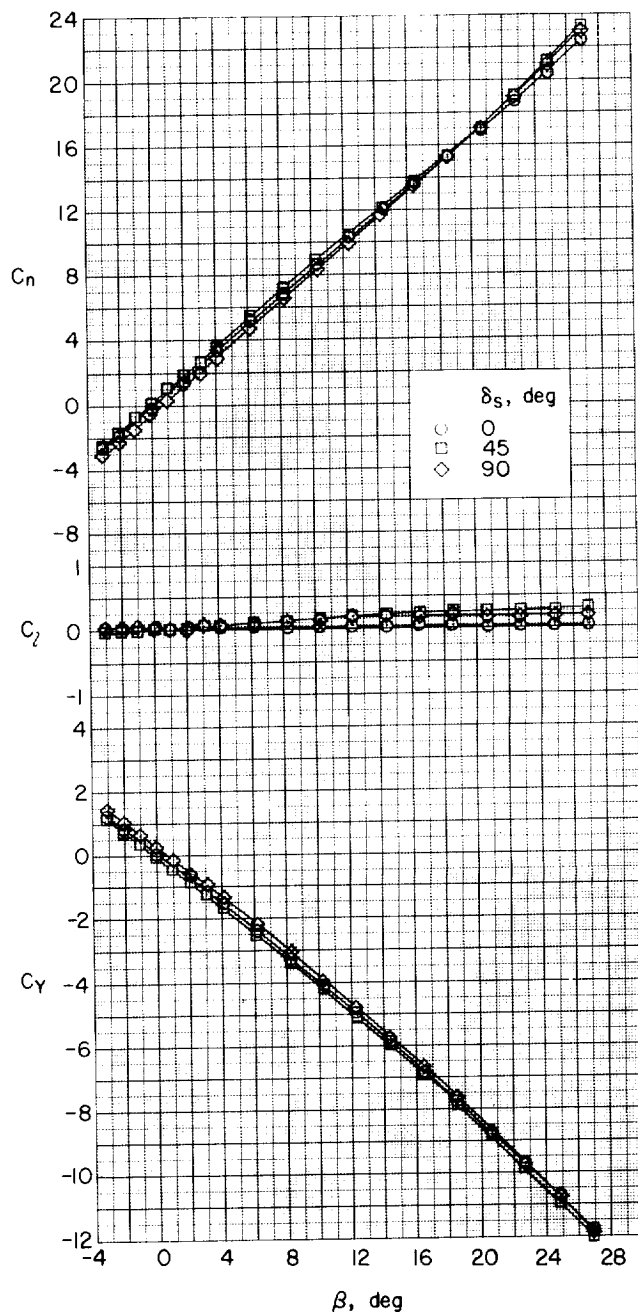
(b) The variation of C_n , C_l , and C_Y with β . $\alpha = 0^\circ$.

Figure 46.- Continued.

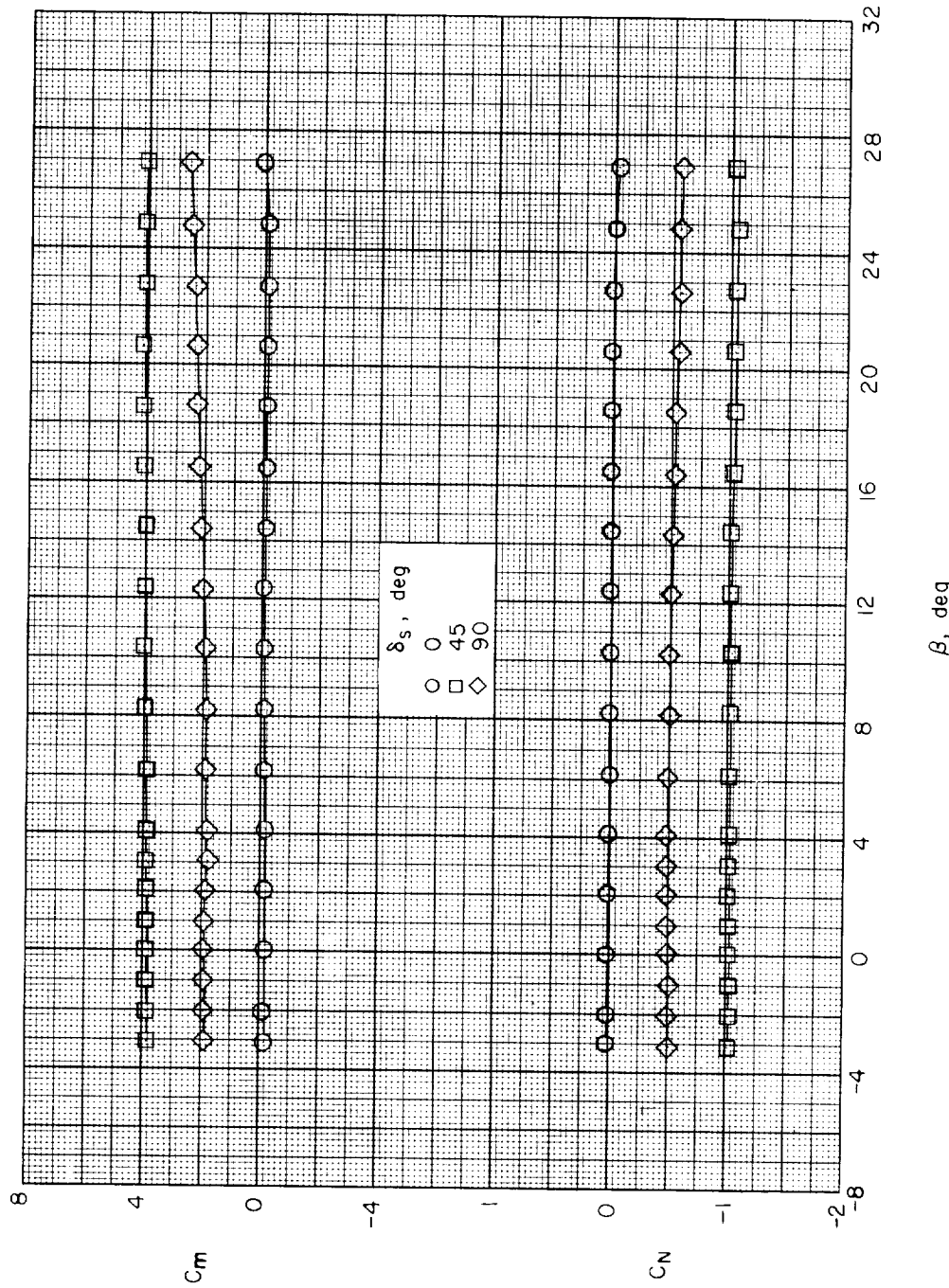
(c) The variation of C_m and C_N with β . $\alpha = 0^\circ$.

Figure 46.- Concluded.